

ASSESSING THE CHARACTERISTICS OF SELF-COMPACTING CONCRETE WITH AND WITHOUT STEEL FIBRE REINFORCEMENT

by

Abdulkarim Ahmed Mohamed Mimoun

B.Sc., M.Sc.

Thesis submitted in candidature for the degree of doctor of
Philosophy at Cardiff University



*School of Engineering
Cardiff University
United Kingdom*

March 2023

ACKNOWLEDGEMENT

First and foremost, I wish to send the most sincere and immeasurable thanks to almighty Allah (God) for his endless mercy and grace, which have helped me to complete this project successfully. I would like to express my deepest appreciation to all those who gave me the chance to complete this thesis. Foremost, I owe a debt of gratitude, which I can never repay, to my beloved country, Libya.

I would also like to thank my late father and my mother for instilling in me the values of diligence and hard work from a young age.

I also wish to send a heartfelt thank you to my supervisor, **Dr. Sivakumar Kulasegaram**. You have provided me with excellent cooperation, continuous supervision, and encouragement throughout the course of my studies. It is certainly no exaggeration to say that this thesis would have been unthinkable without his guidance and immense support. No mere words can truly express my appreciation for his assistance during this research.

It is also necessary to send my gratitude to Dr. Abhishek Kundu, Dr. Robert Davies, and Mr. Carl Wadsworth for their open-minded discussions, continuous support, and help during the laboratory work carried out for this research.

Special thanks are also extended to the Libya Cultural Attaché in London for their support.

My thanks go to the staff of the research office at the Cardiff School of Engineering.

In addition, I must thank all members of staff in the Engineering Department for their help in improving my academic knowledge. It is such a great honor for me to receive your tutoring.

A special tribute also goes to my mother, my sisters, my brothers, and the memory of my unforgettable father.

In closing, I would like to single out my dearest wife and my lovely children, for their understanding, patience, and tremendous support during this study.

SYNOPSIS

Although self-compacting concrete (SCC) with or without fibre reinforcement has been developed beyond research laboratory investigations and has now become an industrial product, its physical characteristics with respect to the fresh and hardened states behaviour and performance are not yet comprehensively understood. It is necessary to explore ways to enhance the performance of SCC (without or with fibre) to make it a more sustainable alternative to vibrated concrete (VC). This thesis focuses on the research findings related to the behaviour of SCC (without or with fibre) in fresh and hardened states. This research consists of four main parts.

In the first part, SCC, or SCC with steel fibre reinforcement (SCSFRC) was explored, and it was demonstrated that SCC and SCSFRC are extensively influenced by the characteristics of components and their proportions. Therefore, optimization of SCC mix design requires to identify robust methods for proportioning components. This study aimed to develop a simple and rational approach for designing SCC (without and with fibre) mixes based on the required target plastic viscosity and compressive strength. The plastic viscosity of an SCC (without and with fibre) mix was estimated using a micromechanical procedure to develop this rational approach. Investigational work was performed indicating the validity of this mix design method via a series of SCC mixes in term both the fresh and hardened states. The test mixes were found to meet the essential SCC and compressive strength standards, thus completely validating the adopted mix proportioning method. Therefore, this approach significantly decreases the extent of laboratory work, materials, and testing time required to achieve a mix that meets the required specifications.

The second part focused on the other important properties of fresh SCC, including SCSFRC mixes with various volume fractions of components, based on the desired target plastic viscosity and compressive strength of the mix. For SCC mixes without steel fibre, the fulfilment of flow and cohesiveness criteria was found to be satisfactory for the chosen mix design. However, for the design of SCC mixes with steel fibre, it was found that they had to additionally meet the passing and filling ability criteria.

The third part addressed the properties of hardened SCC: specific fracture energy, tensile strength, and modulus of elasticity. These were studied by detailed investigation of the role of several parameters, comprising steel fibre volume, paste to solids ratio, water to cementitious

material ratio, and strength grade of SCC mixes without or with fibre. It was found that SCC with higher volume fraction of steel fibre performs comparatively better in hardened state. Nonetheless, the amount of fibre content is restricted by workability of the SCC mix.

The fourth part introduces numerical simulation of flow of SCC with steel fibre in the slump flow and L-box tests. This simulation was performed by an incompressible mesh-less smooth particle hydrodynamics (SPH) methodology. An appropriate Bingham-type constitutive model was coupled with the Lagrangian momentum and continuity equations to simulate the flow. The numerical simulation results were compared with the actual slump flow and L-box tests carried out on several SCC with fibre mixes, and the comparison revealed that this methodology is very well suited for predicting the flow behaviour of SCC in terms of passing and filling abilities of fibre. On the other hand, the simulation of SCC mixes with steel fibre concentrated on the distribution of fibres and their orientations during the flow in three-dimensional configuration. The SPH simulation procedure can therefore substitute the time-consuming laboratory investigation of both flow and L-box tests, thereby minimizing time, effort, and material costs.

Abbreviations

SCC	Self-compacting concrete
SCSFRC	Self-compacting steel fibre reinforced concrete
FRC	Fibre reinforced concrete
SCFRC	Self-compacting fibre reinforced concrete
VMA	Viscosity modifying agents
ACMs	Additional cementitious materials
CRMs	Cement replacement materials
VC	Vibration Concrete
EFNARC	European Federation of National Trade Associations
PLC	Portland limestone cement
PC	Portland cement
CA	Coarse aggregate
FA	Fine aggregate
GGBS	Ground granulated blast-furnace slag
MS	Micro-silica
LS	Limestone
LP	Limestone powder
Cm	Mass of cementitious materials
SP	Super-plasticiser
SF	Steel fibre

w/cm	The ratio of water to cementitious materials
W	Water content
Cm	mass of cementitious materials
W/b	Water to binder ratio
W/C	Water to cement ratio
W/P	Water to powder ratio

Contents

ACKNOWLEDGEMENT	ii
SYNOPSIS.....	iii
Abbreviations	v
Contents	vii
List of Tables	xii
List of Figures	xiv
Chapter 1	xx
Introduction	xx
1.1 General background	2
1.2 Scope of the research	6
1.2.1 Aim.....	6
1.2.2 Objectives	6
1.3 Problem statements	7
1.4 Research methodology	9
1.5 Outline of the thesis	9
Chapter 2	13
Self-compacting Concrete	13
2.1 Introduction	14
2.2 Self-compacting concrete.....	14
2.2.1 Definition of SCC.....	14
2.2.2 Development of SCC.....	15
2.2.3 Theoretical background in production of SCC.....	16
2.2.4 Effect of superplasticizers and cementitious materials supplementary on the SCC production.....	19
2.3 Self-compacting fiber reinforced concrete (SCFRC).....	21
2.3.1 Type of steel fibre addition on SCC performance.....	24
2.3.2 Characterization of fibre reinforced SCC.....	25
2.3.2.1 Fibre performance in concrete.....	25
2.3.2.2 Different types of flowable fibre concrete.....	26
2.3.3 Effect of production on structural performance	26
2.3.3.1 Fibre orientation	26
2.3.3.2 Fibre distribution	27
2.3.4 Parameters influencing SCC mixture design without and with fibres	27

2.3.4.1 Fresh behaviour	27
2.3.4.2 Hardened behaviour.....	32
2.3.5 Influence of the plastic viscosity and yield stress on the SCC with and without fibres	35
2.4 Concluding remarks	40
Chapter 3	43
Modelling Fresh SCC Flow	43
3.1 Introduction.....	44
3.2 Simulating the Flow of SCC without and with fibre.....	45
3.2.1 Blocking of fresh SCC.....	45
3.3 Rheology of SCC	46
3.3.1 Rheological ‘definition’ of SCC.....	47
3.3.2 Rheological parameters of fresh SCC	47
3.3.3 Measuring the rheological parameters.....	48
3.4 Simulation of SCC flow	49
3.4.1 Methods for simulating SCC.....	50
3.4.2 Numerical solution strategy of simulation techniques	50
3.4.2.1 Description of the flow of SCC	51
3.4.2.1.1 Bingham plastic model.....	52
3.4.2.1.2 Herschel-Bulkley model	53
3.4.2.2 The governing equations used in SCC simulation	53
3.4.2.3 Fundamental methods describing the physical governing equations	54
3.4.2.4 Domain Discretization.....	56
3.5 Numerical approximation SPH	57
3.5.1 SPH concept	59
3.5.2 SPH support domain.....	59
3.5.3 Kernel approximation.....	59
3.5.4 Particle interpolation	60
3.5.5 The boundary conditions Treatment.....	61
3.5.6 Numerical solution strategies in SPH.....	61
3.6 Concluding remarks	62
Chapter 4	64
Procedure for Proportioning and Designing SCC mixes with and without steel fibres..	64
4.1 Introduction.....	65
4.2 Target compressive strength of SCC and SCSFRC mixes.....	66
4.3 Target plastic viscosity of SCC and SCSFRC mixes.....	66

4.4	Calculating the plastic viscosity of SCC and SCSFC mixes.....	67
4.4.1	An example calculation of plastic viscosity for mix with $f_{cu} = 30$ MPa	73
4.5	Examples demonstrating the use of design charts.....	77
4.6	Proposed mix-design charts method for SCC and SCSFRC.....	81
4.6.1	An example calculation for designing 50 MPa mix (without fibre) using chart.....	83
4.6.2	An example calculation for designing 70 MPa mix with 0.5% of steel fibre	87
4.6.3	An example calculation for designing 40 MPa mix with 0.5% of steel fibre (Modelling and validation).....	91
4.7	Concluding remarks	98
Chapter 5	99
Methodology	99
5.1	Raw materials of SCC.....	100
5.1.1	Cementitious components	100
5.1.1.1	Portland cement.....	100
5.1.1.2	Granulated blast furnace slag	100
5.1.1.3	Limestone powder	101
5.1.1.4	Micro-silica.....	102
5.1.2	Aggregates.....	102
5.1.3	Superplasticizers.....	103
5.2	Quantity ranges of the constituent materials for SCC.....	103
5.3	Laboratory experiments	104
5.3.1	Testing methods for self-compatibility of SCC.....	104
5.3.1.1	Fresh SCC experiments	104
5.3.1.1.1	Slump trial (Flow-ability)	104
5.3.1.1.2	J-ring trial (Flowing and passing-ability).....	105
5.3.1.1.3	L-box trial (Flowing, passing and filling-ability)	107
5.3.1.2	Hardened SCC experiments	107
5.3.1.2.1	Cubes' compressive strength trial	107
5.3.1.2.2	Tensile strengths	108
5.3.1.2.3	Modulus of elasticity.....	108
5.3.1.2.4	Fracture mechanics	109
5.4	Modelling and validation	110
5.5	Concluding remarks	111
Chapter 6	112
Understanding the effect of paste content on the performance of self-compacting concrete : Experimental validation I	112

6.1	Introduction	113
6.2	Materials.....	116
6.3	Mix design method.....	117
6.4	Experimental program.....	120
6.5	Validation of mix design method.....	121
6.5.1	Tests on fresh SCC	121
6.5.2	Tests on hardened SCC	130
6.6	Further analysis of SCC mix with target compressive strength of 50 MPa , 60 MPa and 70 MPa	132
6.7	Concluding remarks	143
Chapter 7	145
	Developing self-compacting steel fibre reinforced concrete - an investigation of flow and mechanical properties: Experimental validation II	145
7.1	Introduction	146
7.2	Experimental programme.....	148
7.3	Development of SCC mixes with and without fibre	151
7.3.1	Fresh behaviour of SCC with or without fibre	151
7.3.1.1	Flow test	151
7.3.1.2	Passing and filling test.....	154
7.3.1.3	Influence of super-plasticiser on SCC and SCSFRC mixes.....	163
7.3.1.4	Plastic viscosity of self-compacting concrete without and with steel fibre.....	164
7.3.1.5	Further analysis of SCC and SCSFRC mix with target compressive strength 40 MPa and 60 MPa.....	166
7.3.1.6	Discussion of fresh behaviour of SCC with or without fibre	169
7.3.2	Hardened behaviour of SCC with or without fibre	170
7.3.2.1	Determination of fracture parameter	173
7.3.2.2	Specimen preparation and test procedure.....	173
7.3.2.3	Discussion of Hardened behaviour of SCC with or without fibre.....	175
7.4	Concluding remarks	182
Chapter 8	184
	Simulation of SCC flow with fibre Modelling and validation	184
8.1	General Instructions	185
8.2	Development of the self-compacting normal-strength performance steel fibre reinforced concrete mixes.....	186
8.3	Modelling the flow-ability , pass—ability and fill—ability of steel fibre suspended self-compacting based on experiment	187

8.4 Modelling simulation the flowing, passing and filling ability of SCSFRC	188
8.4.1 Governing equations.....	189
8.4.2 Numerical implementation	189
8.5 Initial configuration and boundary conditions	192
8.6 Three-dimension simulation results	193
8.7 Concluding remarks	196
Chapter 9	197
Conclusions and recommendations for further study	197
9.1 Conclusions.....	198
9.2 Recommendations	200
References	203
Appendix A	237
Appendix B	246
Appendix C	251
Appendix D	265
Appendix E.....	271
Appendix F.....	276

List of Tables

Table 2.1: characteristics of steel fibres (Pająk and Ponikiewski, 2013).....	23
Table 4.1: Minimum and maximum values of plastic viscosity of the SCC base for each compressive strength (de la Rosa et al., 2018a).....	70
Table 4.2: Estimated plastic viscosity of the paste (cement +GGBS + SP + water + air).....	73
Table 4.3: Summarising the results of the plastic viscosity calculation of mix 30MPa without steel fibre	75
Table 4.4: Summarising the results of the plastic viscosity calculation of mix 30MPa with steel fibre	77
Table 4.5: Mix constituents and plastic viscosity of an SCC mix	87
Table 4.6: Mix constituents and plastic viscosity of an SCSFRC mix	90
Table 4.7: Mix constituents and plastic viscosity of an SCSFRC mix	94
Table 4.8: All the Mix constituents of an SCC mix based on target plastic viscosity and compressive strength.....	96
Table 4.9: Further details of test SCC mixes	97
Table 5.1: Typical range of SCC mix compositions according to: (EFNARC, 2005)	104
Table 5.2: Pasing ability criteria	106
Table 6.1: Typical range of SCC mix compositions according to EFNARC (EFNARC, 2005)....	118
Table 6.2 : Mix proportions of test SCC mixes (kg / m ³).....	119
Table 6.3 : Further details of test SCC mixes	119
Table 6.4: General acceptance criteria of SCC.....	120
Table 6.5: Slump flow results for SCC mixes with various compressive strengths.....	122
Table 6.6: J-ring resulting of SCC concordance with mix.....	127
Table 6.7 : J-ring test (blocking step) resulting of SCC concordance with mix	129
Table 6.8: Difference between flow and J-ring spread diameter	130
Table 6.9: Compressive strength of samples water cured at 7, 14 and 28 days.....	131
Table 6.10: Mix proportions of test SCC mixes (kg / m ³).....	134
Table 6.11: Further details of test SCC mixes	135
Table 6.12: Slump flow and J-ring test results for corresponding SCC mixes.....	136
Table 6.13: J-ring test (blocking step) and difference between flow and J-ring spread diameter results of corresponding SCC mixes.....	137
Table 6.14: Compressive strength of samples water cured at 7, 14 and 28 days.....	141
Table 7.1: Characteristics of steel fibres.....	148

Table 7.2:Mix proportions of test SCC and SCSFRC mixes (kg / m ³).....	150
Table 7.3:Further details of test SCC and SCSFRC mixes.....	151
Table 7.4: Flow, passing and filling ability test results SCC and SCSFRC concordance with mix	152
Table 7.5:Constituents and proportions for SCSFRC mixes (30 MPa) with steel fibres content (1%) and various coarse aggregate size (kg/m ³).....	159
Table 7.6 : Results of flow, pass and fill-ability for SCSFRC mixes (30 MPa) with various coarse aggregate size.....	160
Table 7.7:Constituents and proportions for SCSFRC mixes (70 MPa) with steel fibres content (1%) and without coarse aggregate size (kg/m ³)	162
Table 7.8:Results of flow, pass and fill-ability for SCSFRC mixes (70 MPa).....	163
Table 7.9:Constituents and proportions for SCC and SCSFRC mixes (40 MPa) and (60 MPa)...	167
Table 7.10 : Results of flow, pass and fill-ability for SCC and SCSFRC mixes (40 MPa) and (60 MPa).....	167
Table 7.11: Measured fracture energy, G _f (a, W) for different SCC mixes from three-point bending test (TPB)	177
Table 7.12:Results of f _{cu} , f _{st} , E, G _f of test SCC without and with steel fibre mixes	179
Table 8.1: Constituents and proportions for SCSFRC mix (kg/m ³)	186
Table 8.2 : Further details of test SCSFRC mix	187
Table 8.3:Comparison of experimental and simulations results for slump flow and L-box tests .	193
Table A-1:outline of show to usage of SCC in the literatures	238
Table A-2:Summary of mixture design methods for SCC with steel fibre.....	241
Table A-3:Influence the plastic viscosity (Pas) and yield stress (Pas) on properties of mixes with and without fibres used in SCC	243
Table A-4:Numerical simulations of SCC flow using SPH method.....	245
Table B-1:Mix constituents (kg/m ³) for SCC mixes grade 40.....	247
Table B-2:Mix constituents (kg/m ³) for SCC mixes grade 50.....	248
Table B-3:Mix constituents (kg/m ³) for SCC mixes grade 60.....	249
Table B-4:Mix constituents (kg/m ³) for SCSFRC mixes grade 40.....	250
Table D-1:Number of fibres in a vertical cross-section of 30 MPa (0.5 % of SF) based on the Lab experiment and Buffon problem	270
Table F-1:Training courses	277

List of Figures

Figure 1.1:Outline of the thesis	10
Figure 2.1:An example of congested reinforcement, an ideal application for SCC.....	14
Figure 2.2:The main functional requirements of the SCC (Repository, 2003)	15
Figure 2.3: SCC flow illustrating passing,filling and stability requirement (Vasilić, 2015)	16
Figure 2.4: Methods for achieving self-compacting ability (Brouwers and Radix, 2005).....	16
Figure 2.5:Mechanism of self-compacting ability (Okamura and Ouchi, 2003)	17
Figure 2.6: Procedure for achieving self-compacting ability (Han and Zhang, 2017).....	17
Figure 2.7:Mechanisms of achieving self-compacting ability	19
Figure 2.8:Comparison between the mixture proportion of VC and SCC	19
Figure 2.9:Different types of steel fibres used in reinforced concrete	22
Figure 2.10:Different type of fibres used in concrete reinforcement	23
Figure 2.11:Effect of increasing the fibre factor ($v_f \cdot l_f / d_f$) on the consistency of a cement paste mixed with fibres (Martinie, Rossi and Roussel, 2010).....	25
Figure 2.12:Three main differentiators of different concrete types	26
Figure 2.13: Fibre orientation caused by the flow velocity profile. Representation of a top view of fibres oriented: a) in a channel flow, and b) in a radial flow	27
Figure 2.14:Influence of the aggregate size on the fibre distribution (Johnston, 1996)	28
Figure 2.15: accumulation of coarse aggregates behind the obstacles (i.e. blocking) resulting in weak form filling and honey combing of concrete (Hosseinpoor, 2016).....	29
Figure 2.16: Two form-filling situations with SCC (Thrane, 2007)	30
Figure 2.17:Granular blocking during a L-Box test and experimental results of a J-Ring test on SCC (Roussel and Gram, 2014)	30
Figure 2.18:Slump test SCC with and without steel fibre (GÁLVEZ, 2015).....	31
Figure 2.19:The effect of fibre on free water (Centonze et al., 2016).....	31
Figure 2.20:Stress-strain curves in compression of concretes with and without fibres, ordinary concrete (OC), high strength concrete (HSC) (Boulekbache et al., 2010).....	32
Figure 2.21: Effect of the steel fibre content and concrete age on the compressive strength of SCC and SCC-FR (Grünwald and Walraven, 2020)	33
Figure 2.22: load–deflection curves from three-point bending tests performed on SCC-FR with different volume ratios of (A, left) straight steel fibres and (B, right) hooked-end steel fibres (Pająk and Ponikiewski, 2013).....	34
Figure 2.23:Effect of steel fiber hybridization on the fracture mechanisms of SCC	34

Figure 2.24:Summary of the effect of varying the proportions of concrete constituents on the Bingham constants (Domone, 2003).....	36
Figure 2.25:Relation between the slump flow and the steel fibre by the volume fraction.....	37
Figure 2.26:Proposed area in values of yield stress and plastic viscosity diagram for SCC (Flatt, 2004).....	38
Figure 2.27:Relation between the plastic viscosity and the steel fibre by the volume fraction ..	39
Figure 2.28:Effect of the fibre addition and fibre geometry on (τ_0) and ($\mu\rho$)	40
Figure 2.29:The plastic viscosity of SCC with steel fibre based on compressive strength.....	40
Figure 3.1:Flow curve of normal to high strength and SCC	47
Figure 3.2:Rheology of normal and SCC (John and Choo, 2013)	48
Figure 3.3:Methods for simulating SCC	50
Figure 3.4: The computational strategy of the simulation technique	51
Figure 3.5:non-Newtonian flow behaviour of concrete	51
Figure 3.6: Constitutive models for Newtonian and Bingham fluids	52
Figure 3.7:A bi-linear Bingham fluid constitutive model replaced by the continuous function (Ghanbari and Karihaloo, 2009).....	53
Figure 3.8:Different fluid elements at different times at a fixed location in the fluid flow	55
Figure 3.9:Fluid particle motion from time t_1 to time t_2	55
Figure 3.10:Comparison between grid method (left) and particle method (right) for the same geometry (Vesenjak and Ren, 2007)	56
Figure 3.11:SPH model (Vesenjak and Ren, 2007)	58
Figure 3.12:Smoothing kernel W and its support domain for the approximation of a current particle a (Thanh, Li and Zhang, 2020).....	59
Figure 3.13:particle approximation of function $f(x)$	60
Figure 4.1: Hierarchy of two-phase liquid-solid suspensions constituting an SCC mix.....	67
Figure 4.2:Relationship between steel fibre range and plastic viscosity of the SCC base from a plastic viscosity of SCSFRC for 30 MPa of compressive strength.....	70
Figure 4.3:Relationship between steel fibre range and plastic viscosity of the SCC base from a plastic viscosity of SCSFRC for 40 MPa of compressive strength.....	71
Figure 4.4:Relationship between steel fibre range and plastic viscosity of the SCC base from a plastic viscosity of SCSFRC for 50 MPa of compressive strength.....	71
Figure 4.5:Relationship between steel fibre range and plastic viscosity of the SCC base from a plastic viscosity of SCSFRC for 60 MPa of compressive strength.....	72

Figure 4.6:Relationship between steel fibre range and plastic viscosity of the SCC base from a plastic viscosity of SCSFRC for 70 MPa of compressive strength.....	72
Figure 4.7:Design chart for 30 MPa of the SCC base.....	78
Figure 4.8: Design chart for 40 MPa of the SCC base.....	79
Figure 4.9: Design chart for 60 MPa of the SCC base.....	80
Figure 4.10: Design chart for 70 MPa of the SCC base.....	81
Figure 4.11:Mixture design method of SCC without and with steel fibre.....	83
Figure 4.12: Design chart for 50 MPa of the SCC base.....	84
Figure 4.13:Design chart for 70 MPa of the SCSFRC base.....	89
Figure 4.14:Relationship between steel fibre range and plastic viscosity of the SCC base from a plastic viscosity of SCSFRC for 70 MPa of compressive strength.....	91
Figure 4.15:Design chart for 40 MPa of the SCSFRC base.....	93
Figure 4.16:Relationship between steel fibre range and plastic viscosity of the SCC base from a plastic viscosity of SCSFRC for 40 MPa of compressive strength.....	95
Figure 5.1: The influence of GGBS content on compressive strength of RPC (STD: Standard Curing, SC: Steam curing, AC: Autoclave curing)(Yazici et al., 2010).....	101
Figure 5.2: Role of Superplasticizers (SP) (Han and Zhang, 2017).....	103
Figure 5.3:Trial mix slump flow with study-adopted design mix.....	105
Figure 5.4:Trial mix J-ring test with study-adopted design.....	106
Figure 5.5:Trial mix L-box test with study-adopted design.....	107
Figure 6.1:Particle size distribution curves for FA and coarser fraction of LP.....	117
Figure 6.2:Schematic of experiments of study stages.....	121
Figure 6.3: Horizontal spread of SCC mixes (a) C30 (b) C40.....	122
Figure 6.4: Horizontal spread of SCC mixes (a) C50 (b) C60.....	122
Figure 6.5:Horizontal spread of SCC mix C70.....	123
Figure 6.6: Relationship between t_{500} and water to powder volume ratio of SCC mix.....	124
Figure 6.7: Relationship between amount of SP and water-to-cement (w/cm) volume ratio of SCC.....	125
Figure 6.8: Relationship between PV, t_{500} and target flow spread (650 ± 50 mm).....	126
Figure 6.9: Flow and passing ability of SCC mix (a) C30 (b) C40.....	127
Figure 6.10: Flow and passing ability of SCC mix (a) C50 (b) C60.....	127
Figure 6.11:Flow and passing ability of SCC mix (C70).....	128
Figure 6.12: t_{500} time. plastic viscosity.....	128
Figure 6.13: Plastic viscosity versus t_{500} and t_{500j} of SCC mixes.....	129

Figure 6.14: J-ring test (blocking step) SCC mix.....	130
Figure 6.15: Improvement in compressive strength of SCC mixes	131
Figure 6.16:Relationship between compressive strength (MPa) after 28days and w/cm ratios	132
Figure 6.17:Horizontal spread of SCC mix (a)C50 ⁽ⁱ⁾ (b)C50 ⁽ⁱⁱ⁾	138
Figure 6.18:Horizontal spread of SCC mix (a)C50 ⁽ⁱⁱⁱ⁾ (b)C50 ^(iv)	138
Figure 6.19:Horizontal spread of SCC mix (a)C60 ⁽ⁱ⁾ (b)C60 ⁽ⁱⁱ⁾	138
Figure 6.20:Horizontal spread of SCC mix (a)C60 ⁽ⁱⁱⁱ⁾ (b)C60 ^(iv)	139
Figure 6.21:Flow and passing ability of SCC mix (a)C50 ⁽ⁱ⁾ (b)C50 ⁽ⁱⁱ⁾	139
Figure 6.22:Flow and passing ability of SCC mix (a)C50 ⁽ⁱⁱⁱ⁾ (b)C50 ^(iv)	139
Figure 6.23:Flow and passing ability of SCC mix (a)C60 ⁽ⁱ⁾ (b)C60 ⁽ⁱⁱ⁾	140
Figure 6.24:Flow and passing ability of SCC mix (a)C60 ⁽ⁱⁱⁱ⁾ (b)C60 ^(iv)	140
Figure 6.25:Variability of the compressive strength of each mix related to the control mix C50	142
Figure 6.26:Variability of the compressive strength of each mix related to the control mix C60	142
Figure 6.27:Comparison of compressive strength between new mixes and control mix C70 ..	143
Figure 7.1: Schematic diagram detailing various stages of the experimental study	149
Figure 7.2:Relationship between the plastic viscosity and t_{500} of self-compacting concrete mixes	153
Figure 7.3:Relationship between the steel fibre volume and t_{500} for SCFRC mixes	153
Figure 7.4: Horizontal spread of SCC and SCSFRC mix:C30 (Mix 1) (Left), C50 (5) (Right)	154
Figure 7.5:Flow and pass-ability of SCSFRC mix: C50 (Mix 5) (Left), C70 (Mix 8) (Right).	154
Figure 7.6:Relationship between the plastic viscosity and t_{500} of self-compacting concrete mixes	155
Figure 7.7: Steel fibre volume against t_{500} for SCFRC mixes	155
Figure 7.8:Relationship between the plastic viscosity and T200, T400 of self-compacting concrete mixes.....	156
Figure 7.9:Relationship between the steel fibre volume and T ₂₀₀ , T ₄₀₀ of self-compacting concrete mixes.....	157
Figure 7.10: Passing and filling ability of SCSFRC mix with steel fibre (0, 0.5 and 1%) volume (C50) Mix 4, 5 and 6	157
Figure 7.11:Passing and filling ability of SCSFRC mix with steel fibre (0, 0.5 and 1%) volume (C70) Mix 7,8 and 9	158

Figure 7.12:Flow and passing ability of SCSFRC mix (1%) volume (C30) Mix 3(1)	160
Figure 7.13:Passing and filling ability of SCSFRC mix (1%) volume (C30) Mix 3(1-2-3-4) .	160
Figure 7.14:Flowing and Passing ability of SCSFRC mix (1%) volume (C30) Mix 3(4).....	161
Figure 7.15:SP /Cementitious material ratio by volume in SCC and SCSFC mixes	164
Figure 7.16:Plastic viscosity in SCC and SCSFC concrete mixes	165
Figure 7.17:Relationship between the plastic viscosity and water/cementitious materials ratio of self-compacting concrete mixes	165
Figure 7.18:Paste to solids ratio by volume in SCC and SCSFC concrete mixes.....	166
Figure 7.19:Flow and pass-ability of SCSFRC mix: C40 (a) with 16 bars, C40 (b) with 12 bars, (size of coarse aggregate with 50 % of 10mm and with 50 % of 20mm)	168
Figure 7.20:Flow, pass and fill-ability of SCSFRC mix: C40 (a) with 3 bars, C40 (b) with 2 bars, C60 (c) with 3 bars (size of coarse aggregate with 50 % of 10mm and with 50 % of 20mm)	169
Figure 7.21:Schematic representation of the three-point bending test.....	173
Figure 7.22:Shallow notch to depth ratio (0.1 mm)	174
Figure 7.23:X-Y plotters for the load-deflection curve.....	174
Figure 7.24:Beam specimen used for TPB test	175
Figure 7.25:Typical load–displacement diagrams of one notched beam (0.1 mm) from SCC mixes without and with steel fibre.	176
Figure 7.26:Variation of G_f of SCC mixes of grade with steel fibre volume fraction	177
Figure 7.27:Variation of the G_f and f_{cu} with different p/s ratios	179
Figure 7.28:Variation of the G_f and f_{st} with different p/s ratios	180
Figure 7.29: Variation of the G_f and p/s ratios	180
Figure 7.30:Variation in G_f with w/cm ratio for different steel fibre (SF) volume fractions....	182
Figure 8.1: Dimension of Flow test of SCSFRC.....	188
Figure 8.2:Dimension of L-box test of SCSFRC	188
Figure 8.3:Flow chart of truly compressible solution of the governing equations of the fluid flow.....	191
Figure 8.4:Schematic diagram of the flow of SCSFRC with rigid steel fibres.....	192
Figure 8.5:Slump flow and L-box test initial condition	192
Figure 8.6:3D numerical simulation of slump flow test for SCSFRC (0.5% vol fibre).....	193
Figure 8.7:Experiment of slump flow test for SCSFRC (0.5% vol fibre).....	194
Figure 8.8:3D numerical simulation of L-box test for SCSFRC (0.5% vol fibre).....	194
Figure 8.9:Experiment of L-box test for SCSFRC (0.5% vol fibre).....	195

Figure C-1:Flowing and passing ability of SCC mix: C30	252
Figure C-2:Flowing and passing ability of SCC mix: C40	253
Figure C-3:Flowing and passing ability of SCC mix: C50	254
Figure C-4:Flowing and passing ability of SCC mix: C60	255
Figure C-5:Flowing ability of SCC mix: C70	256
Figure C-6:Flowing and passing ability of SCSFRC mix: C30	257
Figure C-7:Flowing , passing and filling ability of SCSFRC mix: C40	258
Figure C-8:Flowing , passing and filling ability of SCSFRC mix: C40	259
Figure C-9:Flowing and passing ability of SCSFRC mix: C40	260
Figure C-10:Flowing and passing ability of SCSFRC mix: C40 *	260
Figure C-11:Flowing and passing ability of SCSFRC mix: C50	261
Figure C-12:Flowing and passing ability of SCSFRC mix: C60	262
Figure C-13:Flowing and passing ability of SCSFRC mix: C70	263
Figure C-14:Relationship between Plastic viscosity flow times (t_{500}) for target flow spread 650 ± 50 mm [C30 ,C40,C50,C60and C70].	264
Figure C-15:Plastic viscosity in SCC and SCSFRC concrete mixes	264
Figure D-1:Hardened of SCSFRC in the flow test.....	266
Figure D-2:Cut the hardened of SCSFRC in the flow test.....	266
Figure D-3:Section of Cut the hardened of SCSFRC in the flow test.....	267
Figure D-4:Color-coded steel fibre; (the 30 mm long, 0.55 mm diameter)	267
Figure D-5:Dimensions of specimen of the cast	268
Figure D-6:(a) Beam of fracture test in section (A-A). (b) One longitudinal sections of hardened slab with mix 30 MPa of SF (0.5%). (c) Red colour of account and distribution of the steel fibre clearly visible in the cut surface in two parts	269
Figure E-1:Typical load–displacement diagrams of one notched beam (0.1 mm) from SCC mixes without and with steel fibre	275

Chapter 1

Introduction

This chapter presents the general background and scope of the research by highlighting its aim and objectives. Further, the research methodology and structure of the thesis are also briefly summarised. Finally, this chapter is concluded by presenting the main research outputs from this PhD research.

1.1 General background

Concrete is created by mixing cement, fine aggregate (e.g., sand), coarse aggregate, water, and additives (additional cementitious materials), with or without admixtures, fibres, reinforcements, or pigments. Concrete is the most widespread artificial material on Earth, with a much greater volume than plastic, aluminium, and steel. Concrete is readily and easily made and used in all types of possible structural systems. Its excellent functionality, simplicity, and cost efficiency is rooted in the fact that its constituent ingredients are abundant and are readily accessible almost everywhere in the world. As a cause of its accessibility, functionality, and flexibility, it has been developed to become by far the most common and extensively utilized construction material in the world.

Concrete is employed in diverse fields of civil engineering, and over 30 billion tons of it were produced in 2013 (Bianchi, 2014). Conventional concrete has excellent characteristics as a structural material when loaded with compressive strength, but it is very brittle and weak when loaded in tensile strength (Svec, 2013). Concrete is without any doubt an attractive building material because of its ease of production and application. However, it is a relatively complicated material. Its fresh and hardened properties are still being investigated to achieve complete understanding of its behaviour. Consequently, while concrete is the most utilized and ubiquitous building material in the world, it is associated with significant complications when not accurately designed or placed.

Traditional or vibrated concrete (VC) must be compacted using external energy. This can be attained on-site from vibrating poker, and in concrete manufacturing work from vibrating tables or alternative processes. In on-site concrete casting practice, vibration is not always optimally carried out, mainly due to the drudgery of handling vibrating tools all day. On the other hand, subpar vibration is harmful to the quality of the final structure, which is much lower than that of appropriately compacted VC. The associated loss in strength may be acceptable in some situations, but the reduction in durability can often be significantly more important, leading to accelerated degradation methods, for example frost damage, sulphate attack, and reinforcement corrosion, etc.

Adequate compaction by skilled workers is mandatory to realize durable concrete structures. Nevertheless, the gradual decrease in the number of skilled workers in Japan's construction industry has indicated the decreasing quality of construction human resources. One key for the implementation of durable concrete structures independent of the quality of construction work is the employment of Self compacting concrete (SCC), which can be simply compacted into each corner of structure through its own weight, without the need for effort or vibrating compaction. The compelling practical requirement for this type of concrete was suggested by Hajime Okamura, 1986, and subsequent studies have developed SCC, including fundamental research on the workability of concrete (Okamura and Ouchi, 1996). SCC has been employed in the construction industry for more than 20 years. During this time, many studies have been performed concerning the applicability, pump-ability, durability, mix design, rheology, etc. of the SCC. In the 1990s little interest was dedicated to the mechanical characteristics of the material and its structural performance, but more recent studies have focused more on the mechanical characteristics of SCC (Desnerck *et al.*, 2016).

Since its initial use in Japan, SCC has now begun to be an alternative to VC around the world, with its ability to rationalise construction methods through offering various economic and technical benefits compared to VC (Omran, A. and Khayat, 2016). These include overcoming issues related to cast-in-situ concrete, ensuring great robustness and structural performance, decreasing construction time, and supplying a safer and healthier working environment through reducing job-site apparatus and noise levels.

SCC is a liquid particle suspension that can compact itself solely through its weight without the demand for vibration effort, and can fill the gaps in geometrically complicated structural members and highly congested reinforcement without any bleeding and segregation (EFNARC, 2005). It can achieve the major functional desiderata of flowing ability, passing ability, filling ability, and segregation resistance. To achieve such specifications, it is necessary to design suitable quantity fractions of the mixture components. Though SCC has been adopted from the investigation stage into actual application, until recently no unique mixture design process has extensively been followed for proportioning SCC mixtures, but rather various methods have been adopted based on trial-and-error via using time and material consuming laboratory trials. The construction time would be considerably decreased if practical procedures on how to choose the most suitable quantity fractions of mixture ingredients were presented in designing SCC.

The characteristics of SCC are based on the source and the kind of component materials and their characteristics. The use of SCC eliminates compacting effort, which results in reduced costs of placement, and decreased duration of construction improves productivity (Ashish, 2018). The amount of the mixture ingredients (i.e., cement, additional cementitious materials, aggregates, water, and admixtures) have a considerable influence on the rheology of SCC, which in turn influences its hardened properties. Since the SCC major properties are flowing, passing, and filling ability, its fresh characteristics cannot be thoroughly understood without understanding its rheology. An accurate prediction and quality control of SCC rheology is important for the success of its production.

The prediction and quality control of SCC flowing, passing, and filling behaviour are very challenging, especially in formworks of complex shapes, in the presence of reinforcing steel or large size of aggregate and various percentages of fibre. However, an understanding of its behaviour and flow characteristics is crucial to achieving high-quality SCC. The most cost-effective way to gain such an understanding is by performing numerical simulations, which will enable us to fully understand the flow behaviour of SCC with or without steel fibres, and to reveal the distribution of larger aggregate particles and fibres and their orientations inside the formworks. An accurate picture can only be gained by using the three-dimensional (3D) flow simulation, which shows the actual distribution of fibres and their orientations during the flow. Steel fibre reinforced concrete may provide a promising alternative to reinforcement steel in conventional mixes (Mobasher, B., Stang, H., & Shah, 1990). Conflicting with the reinforcement bars for the large continuous unidirectional, the homogeneously dispersed reinforce of the steel fibres concrete equally, consequently efficiently decreasing and influencing any micro-cracks arising in the concrete matrix. Compared to conventional steel reinforcement, steel fibres usually provide concrete with poorer strength and ductility. In several industrial applications, steel fibres can nevertheless beneficially and effectively complement or replace the conventional reinforcement steel (Sandbakk, 2011).

Self-compacting steel fibre reinforced concrete (SCSFRC) is a rational mixture of fibre reinforced concrete with SCC. Such concrete permits the simple and rapid casting of material, efficiently decreasing structural production costs. Additionally, the SCC overcomes issues because of vibration, allows for innovative architectural features, offers a better surface finish, enhances durability, produces a safer working environment, provides better reinforcement bonding, and allows for thinner concrete structures. The engagement of steel fibre (SF) with

concrete enhances resistance to freeze-thaw, explosive spalling, impact, and plastic shrinkage through curing (Grunewald, 2004).

However, SCSFRC has several significant drawbacks. The concrete is further expensive compared to vibration concrete (VC). It is regularly difficult to create the needed flow-ability characteristics of the concrete and to avoid segregation of the immersed and fibres and aggregates. As a result of the low yield stress of the concrete, formwork is required to carry reasonably high pressure. Lastly, steel fibres are not able (and will probably never be able) to transfer the same tensile loads as traditional reinforcement.

Brittle cementitious materials such as mortar and concrete can benefit from the addition of fibres to bridge cracks and retard their propagation. They provide expanded energy absorption compared with plain concrete and enhance the characteristics of cementitious materials when their fundamental brittleness boundaries enable potential application. Steel fibres have been used to replace reinforcement bars, reduce the width of cracks, and enhance post-cracking behaviour or tensile strength.

Casting concrete sections with SCSFRC simplifies the production method. The easiest approach to produce a concrete element is to make a mould, cast the concrete, demould the element; no vibration or placement of bar reinforcement is required. SCSFRC mixes the benefits of SCC in the fresh state and demonstrates enhanced performance in the hardened state due to the addition of fibres. Workability is enhanced compared with fibre reinforced concrete (FRC).

Apart from its fresh property, the states of SCC in its hardened property cannot be neglected for its successful proportioning and production. Although the literature is rich in reporting on SCC, much of the research has primarily concentrated on the fresh characteristics, rather than hardened characteristics, to produce an SCC mix that possesses the characteristics of being self-compacting. From an engineering point of view, strength remains the most important property of hardened concrete as it plays an essential part in its successful advancement and provides an indication of its overall quality (Neville, 1995). Therefore, to simultaneously achieve the sufficient fresh and hardened characteristics of an SCC mixture, the dependable method pays implied attention to its strength along with its rheological properties, i.e., strength together with rheological characteristics are mandatory design conditions to successfully make SCC without and with fibre.

Fracture behaviour is no less significant than strength among the characteristics of hardened SCC without and with fibre. An energy-based failure theory is needed for this that could be used in designing cement-based structures since it studies the response and failure of structures because of crack initiation and propagation (Karihaloo, 1995). The most crucial parameters describing the fracture behaviour of a concrete mix are its specific fracture energy and the tension softening diagram, which form a basis for the assessment of the load-carrying capacity of cracked concrete structures (Karihaloo, 1995)(Bažant and Planas, 1997).

The flow of SCC with or without fibres is best illustrated by the Bingham constitutive model, which includes two material properties: yield stress and plastic viscosity. It is known that the yield stress of SCC mixes is low in comparison with normal VC and remains nearly constant over a large range of plastic viscosities. The viscosity of a homogenous viscous fluid such as the cement paste can be measured correctly which cannot be said of any SCC (Dransfield, 2003). SCC involves comparatively large volumes of fine material and paste without and with various percentages of steel fibre content; researchers are increasingly interested in exploring ways to control its essential parameters (yield stress and plastic viscosity) in relation to fracture behaviour.

1.2 Scope of the research

1.2.1 Aim

The main aim of this research is to study the properties of SCC and its mix design. In addition, this research investigates the effect of steel fibre volume fractions on the characteristics of SCFRC. Finally, this project aims to develop a simple and rational mix design method for proportioning SCC mixes with and without steel fibres. To achieve the aforementioned goals, the fresh and hardened state properties of the developed SCC and SCSFRC mixes are explored to understand and design an accurate and reliable mix proportioning method.

1.2.2 Objectives

The research aim can be achieved via the following objectives:

- Design SCC mixes based on the desired target plastic viscosity in the range of 3 – 15 Pa s and compressive strength in the range of 30–70 MPa and investigate whether the produced SCC mixes meet the necessary self-compacting criteria in both the fresh and hardened states.

- Investigate the effects of limestone powder as a supplementary cementitious material on the performance of SCC design mix (e.g., 50, 60, and 70 MPa).
- Design SCSFRC mixes based on the desired target plastic viscosity in the range of 20 – 80 Pa s and compressive strength in the range of 30 – 70 MPa and investigate whether the produced SCSFRC mixes meet the necessary self-compacting criteria in both the fresh and hardened states.
- Assess the impacts of adding various volume fractions of steel fibre on the fresh properties of SCSFRC mixes, such as workability through a slump flow (flowing ability), J-ring (flowing ability and passing ability), and L-box (flowing, passing, and filling ability) tests.
- Examine in detail the role of several compositional parameters (steel fibre volume, paste to solid volume ratio, and strength grade) of SCC and SCSFRC mixes in their size-independent fracture energy.
- To simulate the non-Newtonian viscous flow of SCC mixes with steel fibre in a test configuration (slump flow and L-box test) using 3D meshless smooth particle hydrodynamic (SPH) methodology. This methodology aims to provide a thorough understanding of the self-compatibility standard of SCSFRC mixes designed.

1.3 Problem statements

Environmental agencies and government policies are indeed deeply concerned with the disposal of industrial by-products, and managing this waste stream is a challenging and complex task that often involves significant expenses. Industrial by-products, also known as industrial waste or residues, are materials produced during industrial processes that are not the primary intended product. Productive use is one of the preferable ways in which such materials can relieve some of the issues of sustainable waste management (SWM). If found appropriate, using these wastes for concrete production would thus be an innovative and effective solution. As these metal additives substitute part of the PC, the cost of SCC is proportionally reduced, particularly if the metal additive is an industrial by-product or waste. As a result, utilization of these kinds of metal additives in SCC has the potential to decrease the cost of SCC and to improve its long-term performance. In this context, its cost that is one of the disadvantages of SCC, connected with the consumption of high volumes of Portland cement (PC) and chemical admixtures. One alternative to decrease the cost of SCC is the use of mineral additives such as natural pozzolans, limestone powder, slag, and fly ash, which are finely divided materials supplementary to concrete as separate components, either during or before mixing (Şahmaran, Christianto and Yaman, 2006). In addition of being uneconomical,

over-reliance on cement use is environmentally undesirable, and modern construction projects are increasingly subjected to regulatory and market pressures to improve environmental performance and sustainability. Moreover, as cement manufacture is one of the most polluting industries, concrete cement should be partially or fully substituted through waste materials, such as silica fume and fly ash in order to decrease its cost and pollution.

The use of PLC (or PC+LP) as a blended SCC, incorporating powder content as a cementitious supplementary (filler), such as FA, limestone, silica fume, and GGBS, is now widely promoted, and a great deal of research relating to it has been published in international journals. For practical reasons, the impact of using PLC as a blended cement in SCC is not commonly understood, particularly in terms of the effects of incorporating LP on flow, passability, and strength in the development of concrete. Aside from technical effects, the broader associated impacts in terms of reduced carbon dioxide emissions remain unclear. These are difficult questions that have not been addressed by the construction industry. Once they are answered, broader and better-informed utilization of LP in the production of concrete can be enabled.

The issues with regard to the phenomenon of industrial by-products (Additional cementitious materials) or industrial waste in landfills, particularly the use of concrete in different percentages of these materials, has been considered from various points of view. Specifically, its strength loss has been taken into consideration in order to maintain the integrity of the whole construct. Numerous researchers have explored the deteriorative achievement and development of concrete achievement situations, but current analytical and empirical researchers are insufficient to elaborate quantitatively the impacting factors during which the aforementioned mechanisms occur.

Alongside these exciting empirical and modelling researchers, this overall methodological study collects available investigation observation and examines concrete resistance and other performance parameters relative to the deployment of diverse types of industrial by-products. This is relevant to all those involved in the use of three different types of industrial by-products to improve mechanical and physical concrete properties: and developing countries and densely populated areas with increasing cost and environmental consciousness.

1.4 Research methodology

The following are the salient points of the research methodology chosen to achieve the above objectives:

- To develop a simple and rationalistic process for designing SCC with and without steel fibre mixes based on the required target plastic viscosity and compressive strength of the mix recommended by previous researchers (Karihaloo and Ghanbari, 2012a) and (Deeb and Karihaloo, 2013a). To aid the user in producing an informed choice of mix components, a software program was established from which the design charts were created.
- To present an investigational validation of the suggested mix design method and to explore whether the produced SCC mixes with and without steel fibre (of various volume fractions) meet the necessary self-compacting criteria. All these mixes will be extensively tested in the fresh state using the slump cone (flowing ability), J-ring (flowing ability and passing ability) and L-box apparatus (flowing, passing, and filling ability) and in the hardened state using compressive strength test.
- To study the role of several compositional parameters (steel fibre volume, paste to solid volume ratio, and strength grade) of SCC mixes with and without steel fibre in their size-independent fracture energy.
- To simulate the non-Newtonian viscous flow of SCC mixes with steel fibre (of various volume fractions) in a specified test configuration (slump flow and L-box test) using the 3D meshless SPH methodology. This approach aims to present a thorough understanding of whether or not an SCC mix with and without steel fibre can satisfy the self-compacting criterion of flowing, passing, and filling ability through narrow gaps in reinforcement besides the flowability criterion.
- To examine the distribution of steel fibres in the SCFRC mixes through simulation, to check whether the fibres are homogeneously distributed after the flow has stopped.

1.5 Outline of the thesis

This thesis is organised into nine chapters, followed by a list of references and appendices. Each chapter is further divided into sections/subsections for the clarity of the presentation. An overview of the layout of the thesis is outlined in Figure 1.1 and the content of each chapter is briefly described below.

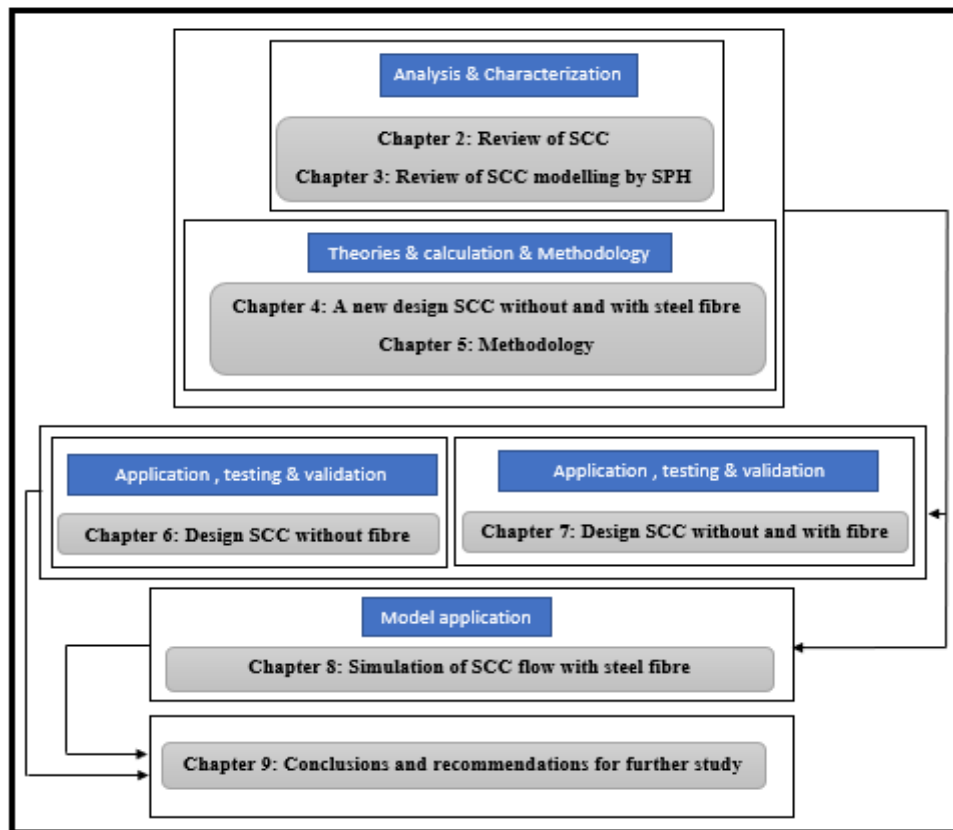


Figure 1.1: Outline of the thesis

Chapter 1 gives an overview of the research field pertaining to SCC and identifies the goals and objectives of this study. Further, it outlines the structure of the thesis and describes the chosen methodology to carry out the proposed research on SCC in both laboratory activities and numerical simulation.

Chapter 2 presents the literature review on the behaviour of SCC in general and in the case of materials used in its production, including the influence of SCC with and with steel fibre on its characteristics in the fresh and hardened performances. It looks specifically at proportioning of its components and standard tests utilized for its assessment. Moreover, this chapter summarises the present modelling emulations and empirical investigations about the impact of estimated SCC without and with steel fibre on the mechanical properties.

Chapter 3 summarizes the rheology of SCC and the approaches of simulating its flow in existing literature, according to either the heterogeneous or homogenous approaches. An overview of SPH methodology, its concept, particle interpolation, kernel functions, density, and gradient estimation is shown, together with a corrected particle interpolation. It also

presents the 3D Lagrangian form of the governing equations of the flow used to model the flow of SCC specifically. Pertinent mass and momentum conservation equations are presented in Chapter 3.

Chapter 4 explains the methodical phases undertaken to create the SCC without and with steel fibre mix design method, based on the micromechanical procedure. Here, it is worth mentioning that the micromechanical procedure enhanced this study work far beyond the range of its original intended use for the determination of SCC without and with steel fibre mix plastic viscosity; it forms the backbone of this rational mix design approach. This approach was improved by the provision of design charts as a guide for proportioning SCC without and with steel fibre mixes. Numerous examples on the use of these charts to proportion mixes with various target plastic viscosity and compressive strength are provided in this chapter.

Chapter 5 defines the advantages of raw materials used in the SCC mix design production of installations. It also presents a representation of the methods and mechanisms used in a preparation of the trial specimens, and the adopted lab experiments (fresh and hardened characteristics) and numerical simulation (fresh characteristic).

Chapter 6 is dedicated to the experimental work demonstrating the validity of the mix design procedure via a series of SCC without steel fibre mixes in both the fresh (Flow and J-ring test) and hardened (compression strength) states. Standard tests employed for SCC without steel fibres were extensively applied.

Chapter 7 is dedicated to the experimental work attesting the validity of the mix design procedure via a series of SCC without and with steel fibre mixes in both the fresh (Flow, J-ring and L-box test) and hardened (compression strength) states. To these mixes, standard tests utilized for SCC with steel fibre were comprehensively applied. Moreover, given in this chapter is the results of a combined experimental study on the fracture behaviour of SCC without and with steel fibre mixes. This combined work was conducted by investigating in detail the role of several SCC parameters (steel fibre volume, paste volume, and strength grade) without and with steel fibre mixes in their specific G_f .

Chapter 8 describes the 3D SPH method used to simulate all the developed SCC mixes in the Flow and L-box test. The results of the numerical simulation are compared with experimental tests conducted in the laboratory to validate the efficiency of the proposed methodology (SPH) to precisely predict the behaviour of SCC with steel fibre. The distribution of steel fibre in the mix is also evaluated and given in this chapter.

Chapter 9 summarizes the main outcomes of this investigation work embodied in Chapters 4 to 8. In addition, the influence of steel fibre on the fresh and hardened states of SCC is presented. It further supplies recommendations for additional work arising from the implications of this research.

Chapter 2

Self-compacting Concrete

2.1 Introduction

Reinforced concrete is widely used in construction globally due to its favourable mechanical properties. With the never-ending demand for reinforced concrete structures to meet current and future socio-economic needs, recent sophisticated developments of structural designs have emerged, including rebar reinforcement in concrete structures to increase clustering and density. However, dense, and heavy reinforcement can complicate issues of pouring and compacting concrete. Concrete must be able to flow, pass, and fill dense rebar reinforcement structures as shown in Figure 2.1, without segregation or blocking. The design of such concrete is particularly challenging due to poor casting conditions and the absence of good vibratory compaction. This can lead to the presence of voids which can in turn affect the long-term durability of concrete structures. Therefore, self-compacting concrete (SCC) seeks to ensure sufficient homogeneity and compaction of concrete cast to facilitate placement, especially in structures with congested reinforcement and limited spaces.



Figure 2.1: An example of congested reinforcement, an ideal application for SCC
(Goodier and Repository, 2003)

This chapter reviews the characteristics of SCC, production methods, materials used and their effects on its properties in fresh and hardened states, the proportioning of its components, and standard tests used for assessing its flow properties. In addition, the characteristics and performance of fibre-reinforced SCC containing steel fibres are also discussed in this chapter.

2.2 Self-compacting concrete

2.2.1 Definition of SCC

Self-compacting concrete (SCC) is a superior kind of concrete that can compact and consolidate by means of its own weight, without the need for external vibration. This characteristic of SCC can be attributed to its high deformability and cohesive strength which

enable it to flow without bleeding or segregation. These features favour the use of SCC in applications such as filling gaps in highly congested and reinforced geometrical structural members (Omran, A. and Khayat, 2016)(BS EN 206-9:2010, 2010).

2.2.2 Development of SCC

SCC was pioneered by Okamura in 1986, and then developed by Ozawa in 1988 at the University of Tokyo. It was found to have numerous benefits compared to conventional concrete; these include,

- reduced labour costs and construction time
- no need for vibration as in conventional compaction
- decreased noise pollution (particularly in urban applications)
- improved durability and reduced permeability
- improved interfacial transition zone between reinforcement or aggregate and cement paste
- good structural performance and facilitated constructability (Shi and Wu, 2005)

Performance of SCC mainly depends on the raw materials used in its mix design. Optimal proportions of materials in mix design have been explored to provide concrete with desired characteristics in terms of both fresh and hardened properties, for specific applications, (i.e. different properties may be relatively more desirable in different structural contexts) (Shi, Wu, Lv, *et al.*, 2015). SCC distinguishes itself from conventional concrete based on three main features listed below (Painuly and Uniyal, 2016) and as shown in Figure 2.2 and Figure 2.3.

- Filling ability – SCC can flow to all spaces in formwork and fully fill under its own weight.
- Passing ability – SCC can flow in constrained spaces between steel reinforcing bars without blocking or segregation.
- Segregation resistance – SCC remains homogeneous during transportation, placing, and on-site post-placing (i.e. setting) (Repository, 2003).



Figure 2.2: The main functional requirements of the SCC (Repository, 2003)

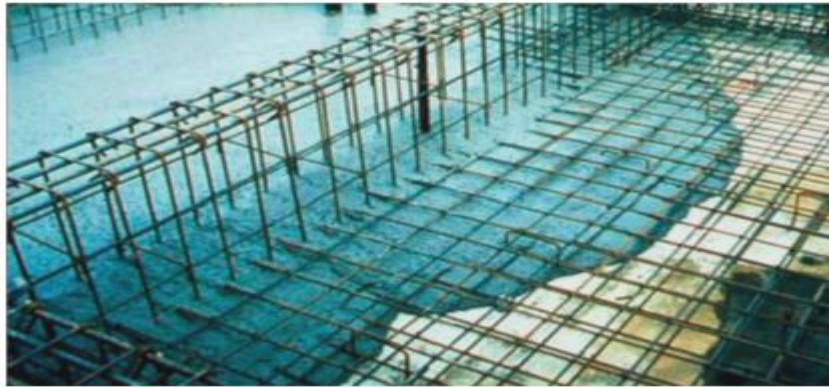


Figure 2.3: SCC flow illustrating passing, filling and stability requirement (Vasilić, 2015)

2.2.3 Theoretical background in production of SCC

As mentioned earlier, seminal work on SCC was conducted (Okamura and Ouchi, 1996) in Japan, thus it is commonly known as the *Japanese process*. The process proposes that the content of gravel in the concrete mixture equals 50% of its packed density, and that the sand content in the mortar equals approximately 50% of its filled density (see Figure 2.4). This mixture of sand and gravel results in a comparatively high paste content in SCC, thus many mixtures achieve higher strength than required, therefore sand should not exceed 42% of the mortar. In many European countries, the Japanese process has been accepted and utilized as a starting point for the growth of SCC (Brouwers and Radix, 2005). The mechanism of SCC self-compacting ability is illustrated in Figure 2.5.

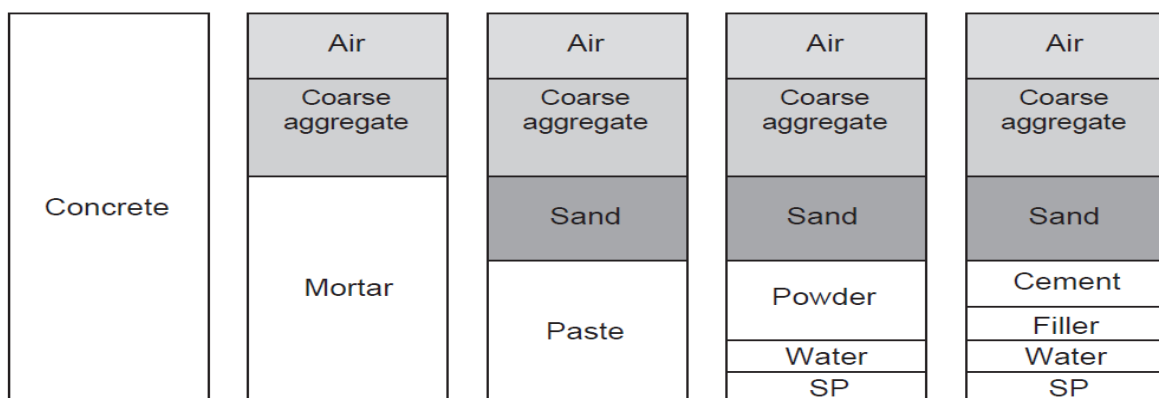


Figure 2.4: Methods for achieving self-compacting ability (Brouwers and Radix, 2005)

The occurrence of contact and collision among the particles of aggregate can grow as the comparative space between the particles reduces and at that point internal stress can grow while concrete is deformed, mostly close to obstacles. “Investigation has found that the energy required for flowing is consumed by the increased internal stress, resulting in blockage

of aggregate particles. Limiting the coarse aggregate content, whose energy consumption is particularly intense, to a level lower than normal is effective in avoiding this kind of blockage. Highly viscous paste is also required to avoid the blockage of coarse aggregate when concrete flows through obstacles. When concrete is deformed, paste with a high viscosity also prevents localized increases in internal stress due to the approach of coarse aggregate particles. High deformability can be achieved by the employment of a superplasticizer, keeping the water-powder ratio to a very low value” (Okamura and Ouchi, 2003).

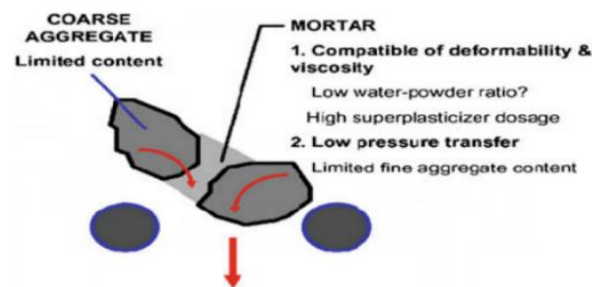


Figure 2.5: Mechanism of self-compacting ability (Okamura and Ouchi, 2003)

The European “Requirement and Strategies for SCC” provides typical parametric scales for ratios and amounts of raw materials in order to achieve self-compacting ability, with appropriate content of sand to reach equilibrium relative to the value of other composite materials (H. Okamura and Ouchi, 2003). The principles fundamentally comprise three parts, i.e., the content of limited aggregate, the lower water-to-powder ratio, and the use of superplasticizer (SP). The approach of choosing the right number of materials and admixtures is important to achieve this objective as described in Figure 2.6 and Figure 2.7.

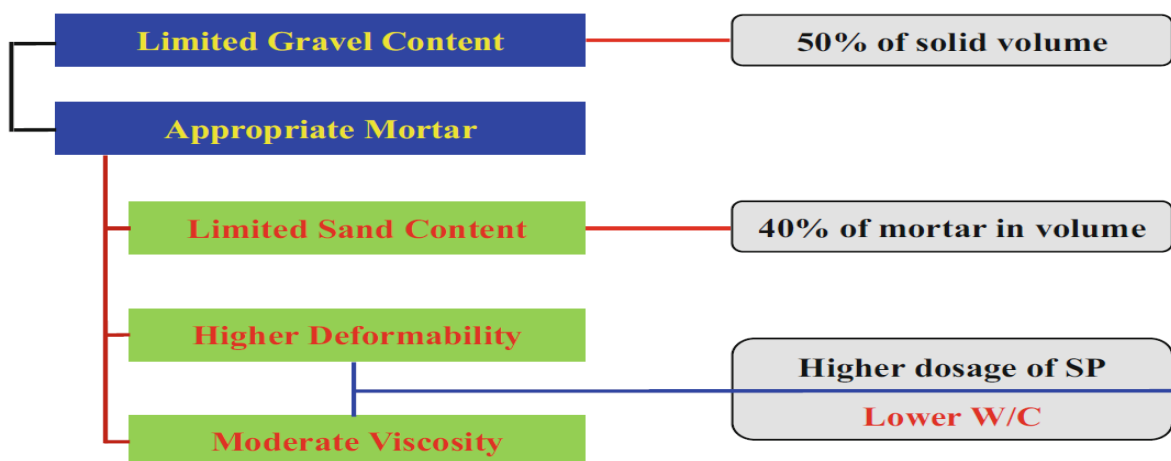


Figure 2.6: Procedure for achieving self-compacting ability (Han and Zhang, 2017)

(Okamura and Ouchi, 2003) proposed a procedure based on limiting aggregate content, using SP, and decreasing water-powder ratio (w/p).

Limiting aggregate content: This reduces friction at the boundaries of aggregates, influencing the spreading and filling ability of SCC. By decreasing the maximum size and the volume of coarse aggregates, and replacement of crushed aggregates with round ones, the passing ability of SCC in congested zones can be enhanced, thus developing the workability, and improving the packing density.

High-level volume of super-plasticiser: Obtaining a very flowable mixture faces the challenge of maintaining appropriate homogeneity. The mechanism of achieving this is by the dispersion impacts of SP on flocculated cement particles, by decreasing the attractive forces between them. An optimal amount is mandatory, as a high amount would result in segregation, while a low amount would compromise the fluidity. Achieving a good degree of cohesiveness can assure a significant improvement in the overall performance (Kwan and Ng, 2010).

High paste amount: SCC includes a high amount of paste, the role of which is to maintain aggregate separation. (Okamura and Ouchi, 2003) demonstrated that internal stresses can improve when concrete is deformed, especially nearby obstacles. The energy needed for flowing is consumed by those increased internal stresses, resulting in blockage. A high volume of fine particles increases the workability and cohesiveness while simultaneously decreasing the interlocking of coarse particles, which could result in a blocking behaviour (Khayat, 2000). The requirement of containing this large volume of fines demands that there should be cement alternative materials such as silica fume, fly ash, GGBS, etc., in order to avoid extreme heat production.

Using viscosity modifying agents (VMA): These products are commonly polysaccharides, cellulose derivatives, or colloidal suspensions. The use of VMA provides a similar impact as SP to fine particles in minimising bleeding and coarse aggregate segregation by thickening the paste and retaining the water in the skeleton. For normal strength SCC with high water to binder content, the introduction of such products seems to be justified. However, they may be less suitable for high performance SCC, with lower water to binder proportion. Viscosity modifying agents are supposed to make SCC less sensitive to water differences. Due to the small amounts of viscosity modifying agents involved, it may be difficult to attain accurate dosing.

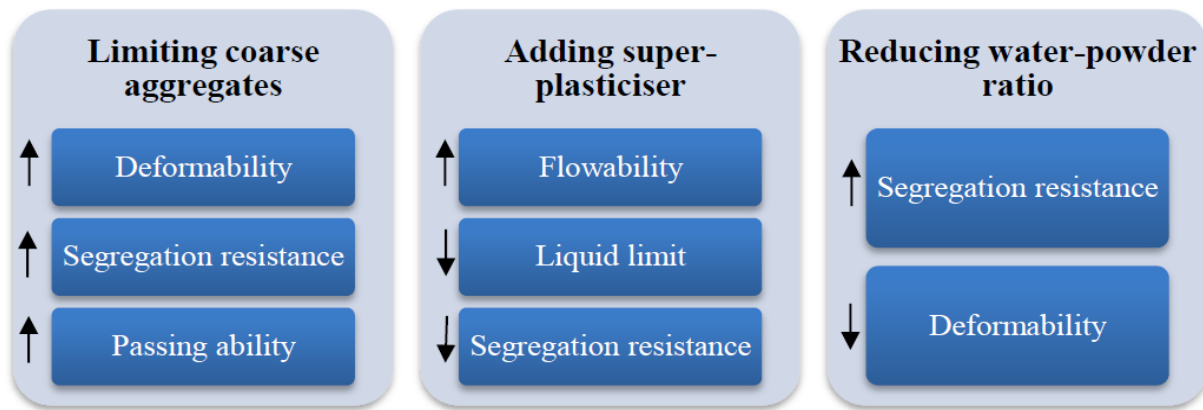


Figure 2.7: Mechanisms of achieving self-compacting ability

A comparison of percentage of mix proportions between SCC and that of conventional vibrated concrete (VC) is shown in Figure 2.8. The main difference between the SCC and VC is that the former includes more fine materials.

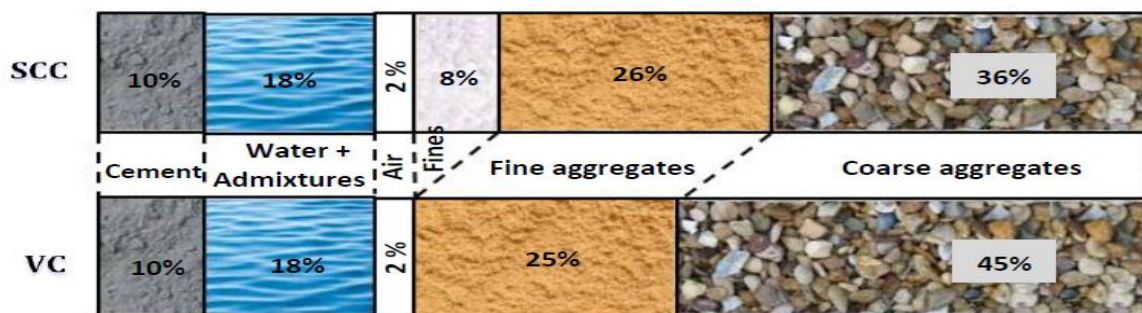


Figure 2.8: Comparison between the mixture proportion of VC and SCC

(Okamura and Ouchi, 2003)

2.2.4 Effect of superplasticizers and cementitious materials supplementary on the SCC production

SCC demands a large volume of powder content compared to concrete produced by conventional vibration to produce a cohesive and homogeneous mixture (Topçu and Uygunoğlu, 2010). Due to technical advancement, SCC has been extensively used in the construction industry (Akçay and Tasdemir, 2012), with mixtures incorporating more sand (fine aggregates) and SP to improve workability. Moreover, a smaller maximum size of aggregate is used in comparison to the conventional vibration concrete. However, the use of SP may increase shrinkage and creep cracks, which may affect structural performance of the concrete.

The use of fly ash as filler increases the paste volume of SCC, which in turn improves workability (Collepari, M. Collepari, S. Ogoumah Olagot, 2003)(H. Okamura and Ouchi, 2003)(Bouzoubaâ and Lachemi, 2001). However, SCC demands higher fine content to attain stable fresh properties, which often leads to high cement consumption (Vurst. F.V.D. S, Grünewald. S, Feys. D, 2017)(Jiao, D. Shi, C. Yuan, 2017)(Thanh.Ha, Kraus. M, 2015). In this context, its cost that is one of the disadvantages of SCC, connected with the consumption of high volumes of Portland cement (PC) and chemical admixtures. One alternative to decrease the cost of SCC is the use of mineral additives such as natural pozzolans, limestone powder, slag, and fly ash, which are finely divided materials supplementary to concrete as separate components, either during or before mixing (Şahmaran, Christianto and Yaman, 2006). In addition of being uneconomical, over-reliance on cement use is environmentally undesirable, and modern construction projects are increasingly subjected to regulatory and market pressures to improve environmental performance and sustainability.

Consequently, interest has shifted to replacement powders for content, such as silica fume, ground granulated blast furnace slag, and fly ash. The use of such materials decreases costs, and also gives supplementary performance enhancement to SCC (Bouzoubaâ and Lachemi, 2001)(Güneyisi, 2010)(Gesoglu and Özbay, 2007)(Brower, 2000). As these metal additives substitute part of the PC, the cost of SCC is proportionally reduced, particularly if the metal additive is an industrial by-product or waste. As a result, utilization of these kinds of metal additives in SCC has the potential to decrease the cost of SCC and to improve its long-term performance.

Generally using large amount of PC in production of SCC has adverse environmental impacts, including exacerbating the carbon footprint of projects and consuming natural resources. One alternative method to solve these issues is to utilize waste materials as admixtures to replace PC in SCC. The most commonly used mineral materials in SCC are industrial by-products, including fly ash (FA), artificial pozzolanic materials such as metakaolin (MK), silica fume (SF), and blast furnace slag (BFS), which can improve the durability and compressive strength of concrete due to filler influence and pozzolanic reaction (Ponikiewski and Go, 2014)(Badogiannis et al., 2015)(Behfarnia and Farshadfar, 2013). The theoretical justification for the use of SCC (H. Okamura and Ouchi, 2003) is promised on concrete design to meet the performance requirements of self-compact ability (Schutter, 2005), good durability, and high compressive strength. To meet these requirements, over recent decades self-compacting high performance concrete (SCHPC) has been developed, commonly involving higher content of

cementitious materials, smaller maximum size of aggregates, and lower water/binder ratio (Le et al., 2015). SCC has been developed replacing part of the cement by different cementitious materials, including FA (Kovler and Roussel, 2011)(Bai, Wild and Sabir, 2003)(Bai, Wild and Sabir, 2002) , GGBS (Kovler and Roussel, 2011) and MK (Ding and Li, 2002)(Siddique and Klaus, 2009)(Kovler and Roussel, 2011)(Ramezaniyanpour and Bahrami Jovein, 2012)(Bai, Wild and Sabir, 2003)(Bai, Wild and Sabir, 2002)(Bai and Wild, 2002). Gesoglu et al. (Gesoglu, Güneyisi and Özbay, 2009) found enhanced durability characteristics in SCC mixes combining ternary mixes of cement, SF and GGBS, compared to bilateral or quadrilateral mixes of binders (cement; GGBS; SF; FA). The mineral admixtures FA (Liu, 2010) and GGBS (Dinakar, Sathy and Sahoo, 2013), are often used in SCC to decrease cement content, enhance workability and improve mechanical and/or durability characteristics; as a result, this makes mixes more eco-friendly (Long, Gao and Xie, 2015). This methodology was primarily based on increasing the supplementary cementitious materials, involving fly ash, GGBS, and filler content (powder type) or silica fume. The second methodology focused on reducing powder content and combining a moderate dose of VMA to secure an acceptable stability of the mix. Furthermore, the third methodology consisted of incorporating comparatively moderate doses of VMA and supplementary cementitious materials to design SCC (Sonebi and Yahia, 2020).

2.3 Self-compacting fiber reinforced concrete (SCFRC)

Fibres can be employed for the limited replacement of conventional reinforcement (welded mesh or rebars) and, in certain structures, they can completely replace rebars. In general, these structures are distinguished by a significant level of structural redundancy, and represent functions where fibres can offer a more cost-efficient reinforcement method (Di Prisco, Plizzari and Vandewalle, 2009). Additionally, fibre reinforcement may enhance the capability of conventional reinforced concrete; reinforcing in-structure members with both fibres and rebars makes it possible to reduce re-bars (Sandbakk, 2011).

The addition of fibres affects the fresh concrete characteristics significantly by stiffening and decreasing the workability of the concrete. This influence of fibre is based on the amount of fibre content, and the type of fibre that can be consistently distributed throughout a mixture. Considering that enhanced mechanical behaviour depends largely on the addition of fibres, the selection of fibre content and type is typically based on the balance between ease of handling of fresh concrete, and maximum effectiveness in hardened properties (Sarmiento, 2015). Here fresh characteristics include flowability, passing ability, filling ability and

viscosity-related segregation resistance. The hardened characteristics are compressive strength, splitting tensile strength, modulus of elasticity, flexural strength, and fracture energy. SCFRC can use the flowing ability of concrete to enhance fibre orientation in the fresh state, and consequently it can enhance toughness and energy-absorption capacity (Btech, 2018) of hardened concrete.


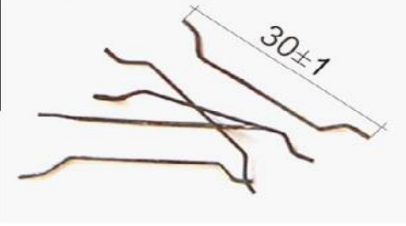
SCC is an inherently brittle material, with low strain capacity under tensile loading. By adding randomly oriented discrete fibres, SCC performance (strength and toughness) can be enhanced, and issues associated with its brittleness and poor resistance to crack growth can be addressed through preventing or controlling the initiation, spread, or coalescence of cracks (Sahmaran, et al., 2005).

Steel fibre is the most popular fibre type used in the building industry (Figure 2.9) due to its favourable characteristics. Table 2.1 illustrates some of the steel fibres commonly used in the industry. Other types of fibre are available for specific applications, but they have a much smaller market share. Since its development in its modern industrial form in the early 1960s, steel fibre reinforced concrete has been effectively used as the main material in numerous kinds of high-specification construction, including bridges, highways, tunnels, slabs, and airports.



Figure 2.9: Different types of steel fibres used in reinforced concrete

Table 2.1: characteristics of steel fibres (Pająk and Ponikiewski, 2013)

Type of Properties		
Fibre shape	Straight	Hooked end
Length (mm)	12.5 ± 1.25	30 ± 1
Wire diameter (mm)	0.40 ± 0.04	$0.8 + 0.04/- 0.03$
Aspect ratio	31.25	37.5
Tensile strength (MPa)	$>1250 \pm 15\%$	1100
Number of fibres per (kg)	81,139	7801

The concept of using fibres to reinforce concrete design is an ancient one. Fibres have been produced from a wide range of materials, in numerous shapes and characteristics (Figure 2.10), including polypropylene (Richardson and Dave, 2008), glass (Ferreira and Branco, 2007), carbon (Bayasi and Kaiser, 2003) ,Poly Vinyl Alcohol (PVA) (Bezerra, Joaquim and Savastano, 2004), and asbestos (G.Murali et al., 2012) , in addition to steel (Benson and Karihaloo, 2005).



Figure 2.10: Different type of fibres used in concrete reinforcement

2.3.1 Type of steel fibre addition on SCC performance

Steel fibre (SF) continues to carry stresses after matrix failure. The compressive strength and the modulus of elasticity of concrete do not significantly change with the addition of steel fibres, but the latter has significant impact on flexural and residual tensile strengths of concrete. Thus, in the case of steel fibre reinforced concrete (SFRC), investigating the post-peak behaviour of analysed samples is essential (Brandt, 2008)(Naaman, 2009)(Giaccio, Tobes and Zerbino, 2008) (Nataraja, Dhang and Gupta, 2000). The mechanical characteristics and post-peak behaviour of fibre reinforced concrete depend primarily on the properties of the concrete matrix, but also on the geometry, content, type, and orientation of fibres (Buratti, Mazzotti and Savoia, 2011)(Glinicki, 2010). The five most common types of steel fibres are: traditional hooked, crimped, straight, with deformed ends (coned, with end buttons or end paddles), and with deformed wire (indented, etched, or with a roughened surface) (Katzner and Domski, 2012).

In SFRC, steel fibres and the matrix are bound together through a weak interface, whose behaviour is important to comprehend and perfectly model SFRC mechanical properties, since the behaviour of this composite is significantly influenced by the fibre/matrix interface zone, and therefore by the micro-mechanical fibre reinforcement mechanisms that are mobilized in this interface. When these compounds are reinforced with a low volume of fibre proportions, the fibre contribution advantages arise mainly after crack initiation (Cunha, Barros and Sena-Cruz, 2011).

The addition of steel fibres enhances the mechanical characteristics and ductility of SCC significantly, as in VC. However, the fibres appreciably weaken the workability of SCC as a result of their large surface zone and elongated shape. The amount of fibre that can be added to an SCC mixture is consequently limited and depends on the fibre type used and the compound of the SCC mixture. The maximum possible volume of fibre demands to be established in such a way as to cause the minimum reduction in the workability, whilst keeping good flowing, passing, and filling ability. In order to make the best use of the fibres, they must be homogeneously distributed in the mixture, without clustering and blockage (Deeb, Ghanbari and Karihaloo, 2012a). There have been mixed findings of the effect of steel fibre on important mechanical characteristics for hardened SCSFRC. Adding hooked-end steel fibre (1.0% volume fraction) of RC- (65/35-BN) into the SCSFRC with water to binder proportion ($w/b = 0.3$), the cubic compressive strength and the axial compressive strength increased on average by 33% and 34%, respectively (Ding *et al.*, 2018a).

2.3.2 Characterization of fibre reinforced SCC

2.3.2.1 Fibre performance in concrete

The presence of fibre enhances the benefits of SCC by improving flexural and tensile strength and the fracture durability of hardened concrete properties, thus fibre is commonly used to prevent bridge cracks and to delay their spread. Fibres have an optimistic effect on the mechanistic characteristics of cementitious materials in terms of hardened concrete properties. This effect is based principally on the fibres (volume fraction, shape, constitutive material) and the casting method. Compared to traditional aggregates, flow in fibre-reinforced materials can encourage a prioritized fibres orientation that powerfully adjusts fresh and hardened concrete characteristics (Martinie, Rossi and Roussel, 2010)(Martinie and Roussel, 2011).

According to (Grunewald, 2004) , the main reason fibres influence the performance of the fresh concrete mix characteristics is linked to the large surface zone of fibres, which improves the fluid stage; and their elongated shape, which affects packing density and encourages interlocking between fibres, and among aggregates and fibres (Martinie, Rossi and Roussel, 2010) . High fibre content produces stiff internal composition, in which fibres tend to ball-up in the mixture, creating workability issues (Grunewald, 2004). The packing density of particles reduces with increasing fibre content, with implications for the mixture compound and fibre characteristics in terms of shape, rigidity, aspect ratio, and fibre material. (Martinie, Rossi and Roussel, 2010) stated that decreasing the aspect ratio is one approach to increase the content of fibre in a mixture. Figure 2.11 , demonstrates the impact of increasing the fibre factor, defined as the product $v_f \cdot l_f / d_f$, on the consistency of a cement paste.



Figure 2.11: Effect of increasing the fibre factor ($v_f \cdot l_f / d_f$) on the consistency of a cement paste mixed with fibres (Martinie, Rossi and Roussel, 2010)

2.3.2.2 Different types of flowable fibre concrete

SCFRC is usually designed for specific applications. It is mainly distinguished from conventional concrete (VC) through three elements: fibre dose, strength, and flowability (Figure 2.12). The level of fibre dosage is an essential aspect to distinguish various types of fibre concrete.

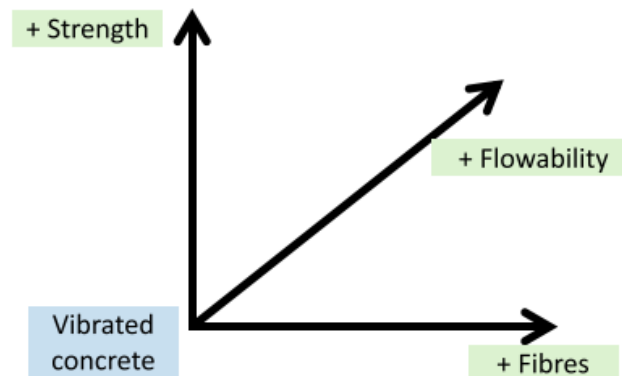


Figure 2.12: Three main differentiators of different concrete types
(Grünewald and Walraven, 2020)

2.3.3 Effect of production on structural performance

2.3.3.1 Fibre orientation

Fibres in flowable concrete rotate and change their orientation with increasing flow distance. The driving force of extensional flow is the decrease in shear stress with flow distance. Consequently, fibres align perpendicular to the flow direction. This orientation can be noted already after a flow distance of 300–400mm (e.g., from the concrete spread after the slump flow trial). Such orientation has been monitored, including in small-scale samples (i.e., round panel sample) (Abrishambaf, Barros and Cunha, 2013), (Figure 2.13 b), floors (Žirgulis, 2015), and tunnel segments (Grünewald, 2004), (Figure 2.13 a).

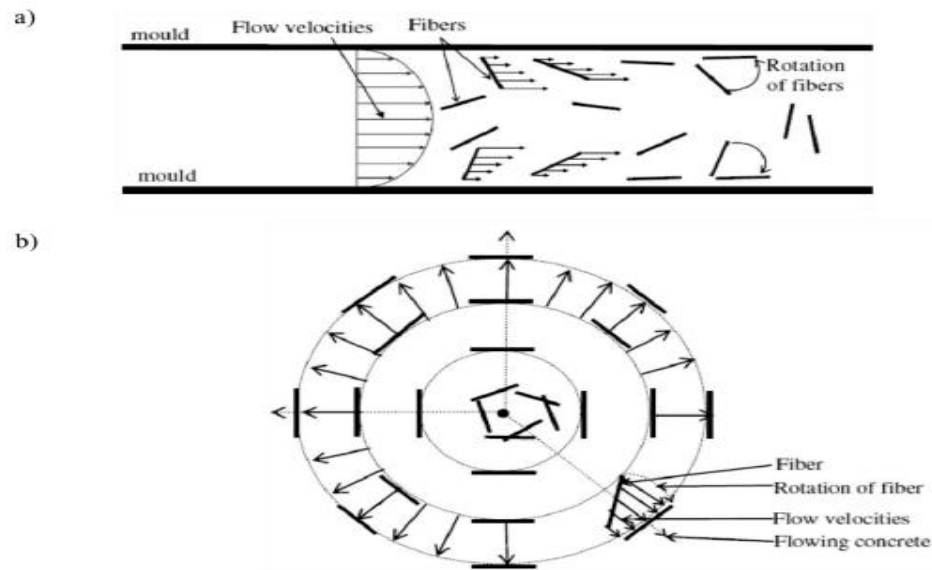


Figure 2.13: Fibre orientation caused by the flow velocity profile. Representation of a top view of fibres oriented: a) in a channel flow, and b) in a radial flow

(Boulekbache et al., 2010)

2.3.3.2 Fibre distribution

A homogenous fibre distribution requires to be achieved with: (1) production of structures with approved bar space or mould opening, (2) avoidance of extensively casting from a single point (e.g., above reinforcement), (3) avoidance of long flow distances, and (4) acceptable mixture design. Several investigations have been performed to address the distribution of fibres, leading to consensus that fibres with a high density tend to migrate downwards, whereas lighter fibres can float (Grünwald and Walraven, 2020).

2.3.4 Parameters influencing SCC mixture design without and with fibres

SCC mixture without and with fibres is influenced by size of coarse aggregate and fibre type and content in terms of fresh properties (e.g., flowing, passing, and filling ability). These parameters also have different impacts on hardened properties, as described below.

2.3.4.1 Fresh behaviour

The flowability, deformability, and segregation resistance of SCSFRC are based on the physical characteristics of the fibre and the coarse aggregate, as well to the rheological properties of the mortar (Wu and An, 2014). The mortar layer thickness is an appropriate concept to assess the segregation resistance and workability. In accordance with the excess layer thickness, there must be an adequate amount of mortar to fill in the gaps among fibres and coarse aggregate to form a film of sufficient thickness to give fluidity to the whole, and avoid blockage or segregation. (Khayat, Kassimi and Ghoddousi, 2014) suggest an SCSFRC

mixing design in which the amount of coarse aggregate is decreased as the content of fibre increases, to keep the constant of the mortar layer thickness.

Mixes containing both materials enable calculation of the percentage of aggregates for a provided fibre content and type. (Grunewald, 2004) modified the compound of the SCC mix by adding steel fibres, and replaced the volume of fibre with the same amount of coarse aggregate, then used the same amount of coarse and fine aggregates to retain a constant percentage ratio of fine aggregate to total constant of the aggregate. The findings showed that the high strength and workability of medium SCC classes is decreased by increasing the volume fraction of steel fibre, and using high ratios of fibres led to the reduction of other rheological properties indicated by the (EFNARC, 2005).

(Johnston, 1996) stated that the distribution of coarse aggregates and fibres was primarily defined by their relative size, as shown in Figure 2.14. While considering the efficiency in the hardened properties, (Vandewalle, 1993) suggested selecting the maximum aggregate size with longer fibres. (Grunewald, 2004) also recommended that the fibre length ought to be two to four times that of the maximum coarse aggregate size, and a similar recommendation was made by (Liao et al., 2006).

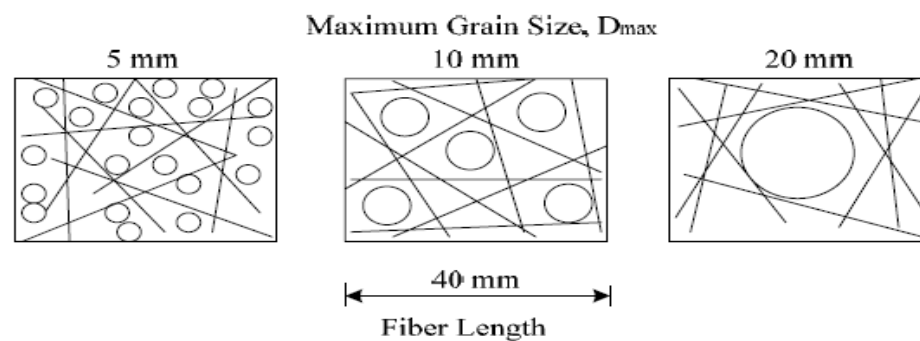


Figure 2.14: Influence of the aggregate size on the fibre distribution (Johnston, 1996)

One of the major benefits of SCC is its flowing ability through narrow gaps of the formwork, (e.g., spaces of the formwork between the walls and reinforcing bars), which are not accessible to guarantee good consolidation using conventional concrete (CV). According to published standards for SCC performance (Lanier et al., 2003). the passing ability of SCC indicates the ability of SCC to flow through openings, for example the spaces between steel reinforcing bars or fibre, without any segregation or blocking of the aggregate. As shown in

Figure 2.15, blocking is described as accumulation of coarse aggregates at the back of the bars with reinforcement, which can cause honey-combing and a weak form-filling ability (Thrane, 2007). This can lead to increased concrete permeability or porosity, which causes reduced toughness. Alternatively, it can decrease the mechanical performance of the compositions and bonding strength between the concrete and reinforcing bars.

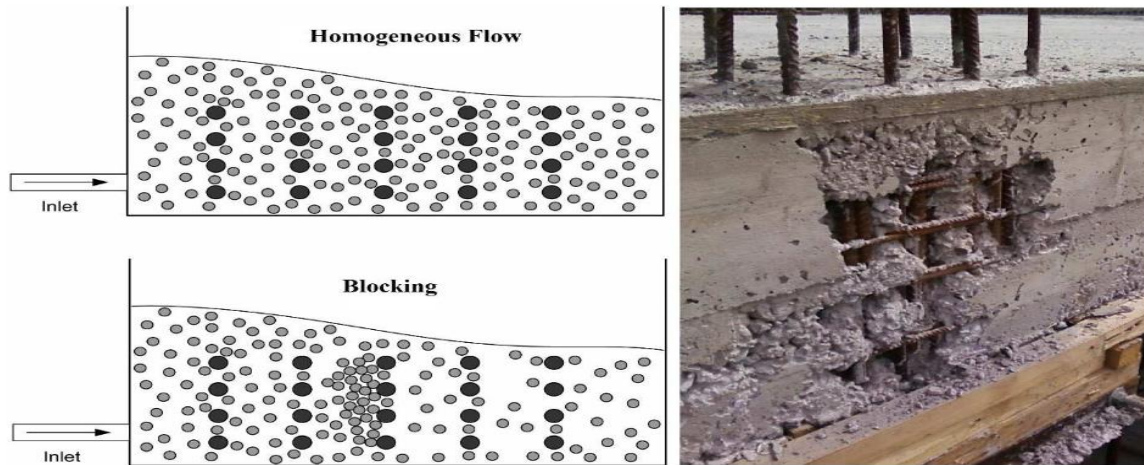


Figure 2.15: accumulation of coarse aggregates behind the obstacles (i.e. blocking) resulting in weak form filling and honey combing of concrete (Hosseinpour, 2016)

Dynamic segregation indicates the condition where particles segregate throughout flow. Compared to blocking, dynamic segregation is not affected by means of particle interactions with the boundaries of the solid. Alternatively, dynamic segregation appears to progressively develop during flow over a larger scale of time and length and is governed by the flow patterns and the intrinsic characteristics of the suspension. Dynamic segregation is illustrated in Figure 2.16, where the top layer appears to have no particles. Top layers rich in paste or mortar may lead to a lower strength, higher shrinkage, and a lack of rough surfaces in casting joints.

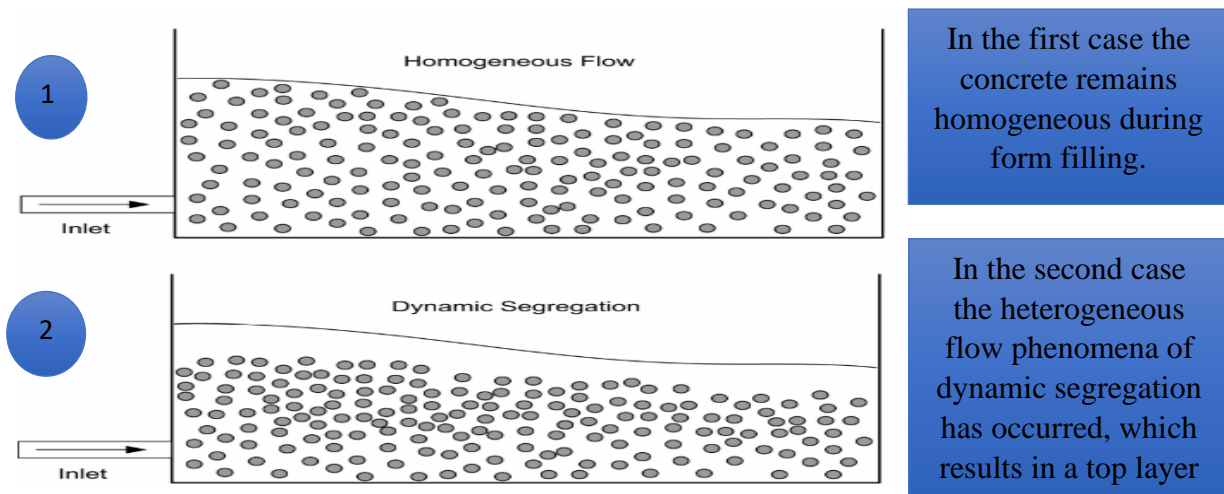


Figure 2.16: Two form-filling situations with SCC (Thrane, 2007)

Though the fluidity of a specified concrete could permit the passing and filling of formwork with complicated shapes, concrete containing coarse particles, such as the maximum size of coarse aggregate or fibre, could cause congestion in the most reinforced areas during the casting procedure (Figure 2.17). When concrete flows through an obstacle, such as steel bars, coarse aggregate, or fibre (solid stage), several phenomena occur which must be clearly understood (Roussel and Gram, 2014).

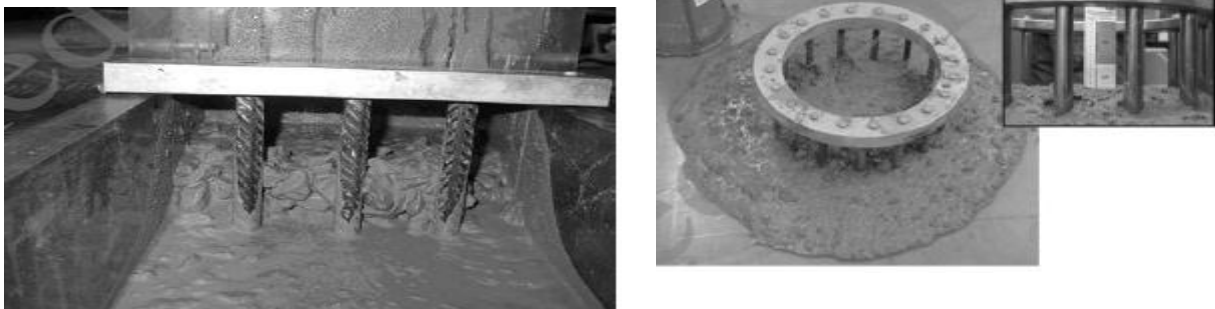


Figure 2.17: Granular blocking during a L-Box test and experimental results of a J-Ring test on SCC (Roussel and Gram, 2014)

There are no typical tests of SCC to estimate the resistance to segregation, this property may be checked from the behaviour of the material by checking that a uniform distribution of coarse aggregates should be detected and not type of segregation or exudation in the perimeter of the final trial cake performs. Considering this, it is possible to say that the sample of Figure

2.18 (A) is in compliance, but the sample of Figure 2.18 (B) cannot be deemed as SCC. It is stated in (Grunewald, 2004) that if the mix has additional fibre than critical value, the mix does not form uniform circular shape and likewise a cluster of material would appear at the centre of the flow circle, Figure 2.18 (C) (GÁLVEZ, 2015).

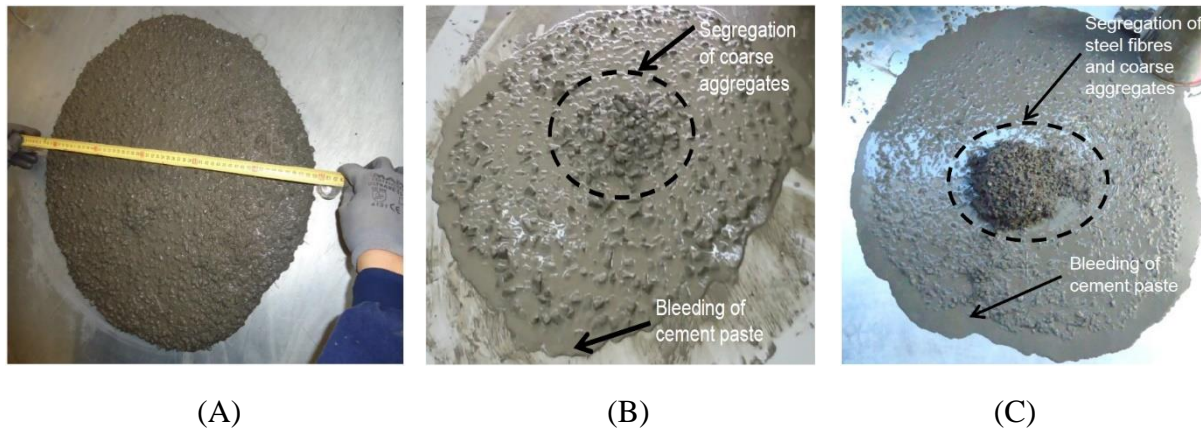


Figure 2.18:Slump test SCC with and without steel fibre (GÁLVEZ, 2015)

Regardless of the advantages of fibre reinforcement, fibres can produce a concrete mixture difficult to work in its fresh state, thus weakening the performance of the hardened state. This is because the dimensional compatibility between fibres impacts the comparative mobility of coarse aggregate particles (De Figueiredo and Ceccato, 2015). Likewise, as shown in Figure 2.19, the addition of fibres enhances the surface area that demands to be wetted, further decreasing the volume of free water to lubricate cement particles (El-Dieb and Reda Taha, 2012) (Centonze et al., 2016). Furthermore, the efficiency of the fibre depends on different factors like fibre volume, type, aspect ratio (length/diameter), and geometry, in addition to fibre orientation and dispersion (Mazaheripour et al., 2011).

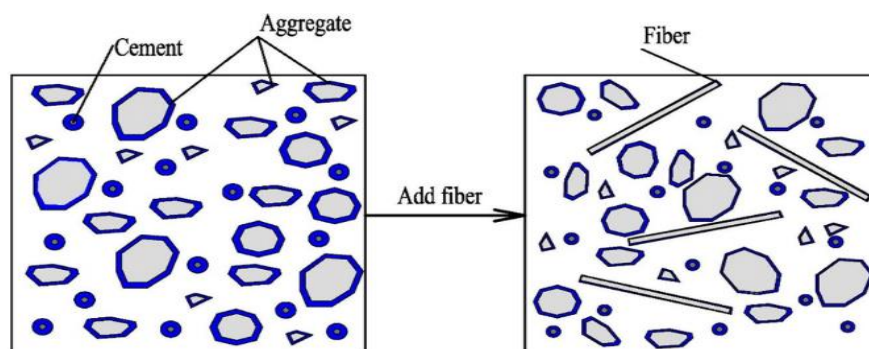


Figure 2.19:The effect of fibre on free water (Centonze et al., 2016)

2.3.4.2 Hardened behaviour

Figure 2.20 compares the compression behaviour of several types of concrete without and with fibre (Boulekbache et al., 2010). CV (OC), SCC, and HSC/HPC differ with respect to modulus of elasticity, maximum strain capacity, and maximum strength.

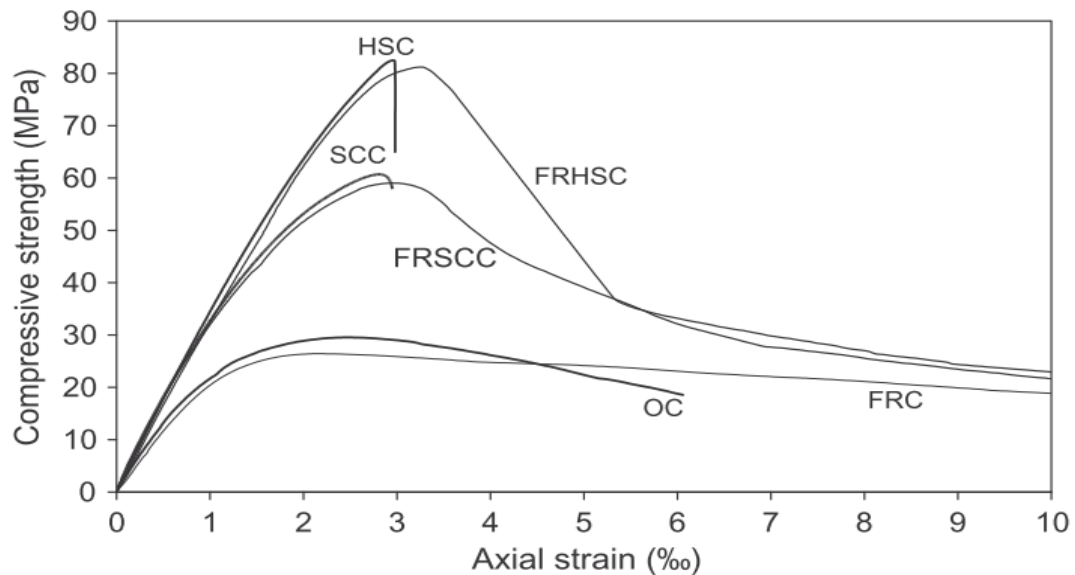


Figure 2.20: Stress-strain curves in compression of concretes with and without fibres, ordinary concrete (OC), high strength concrete (HSC) (Boulekbache et al., 2010)

The impact of steel fibres on the compressive strength of SCC is shown in Figure 2.21. A comparative reduction of compressive strength was achieved for the highest fibre dose compared to lower doses, which indicates the contradicting impacts of matrix reinforcement and inefficient fibre utilization and/or inadequate compaction. Further details are provided in (Table A-2 , Appendix A) to highlight the volume of steel fibres and the range of SCC compressive strength values achieved by previous researchers.

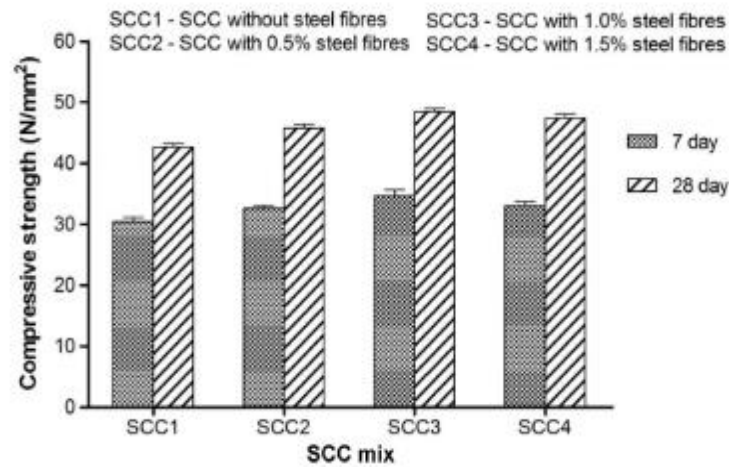


Figure 2.21: Effect of the steel fibre content and concrete age on the compressive strength of SCC and SCC-FR (Grünewald and Walraven, 2020)

In tensile stage, the fibre contribution is incredibly significant for the reason that the trial sample's structural element will fail at the weakest link, and deformations may localize in this link, which demands consideration. The maximum splitting tensile and flexural strengths increase at increasing fibre doses of steel fibres, compared to the reference SCC without fibre (Siddique, Kaur and Kunal, 2016).

(Paja and Ponikiewski, 2013) evaluated the flexural behaviour of SCFRC according to (BS EN 14651-2005) by three-point bending experimentation with notch (Figure 2.22). Investigating the impacts of various volumes of hooked-end fibres (L_f : 30.0mm, d_f : 0.8mm; L_f/d_f : 37.5) and straight fibres (L_f : 12.5mm, d_f : 0.4mm; L_f/d_f : 31.3) revealed that the maximum fibre dosage was 1.5vol.%, and the median compressive strength with (cubes of 150 mm) of SCC without fibres was 73.4MPa. With hooked-end fibres and a fibre dosage of at least 0.5vol.% the cracking strength was maintained due to the action of the fibres. A linear relationship (with a larger slope for hooked-end fibres) was achieved for both fibre types between maximum fibre dosage and flexural strength, which reflects fibre effectiveness.

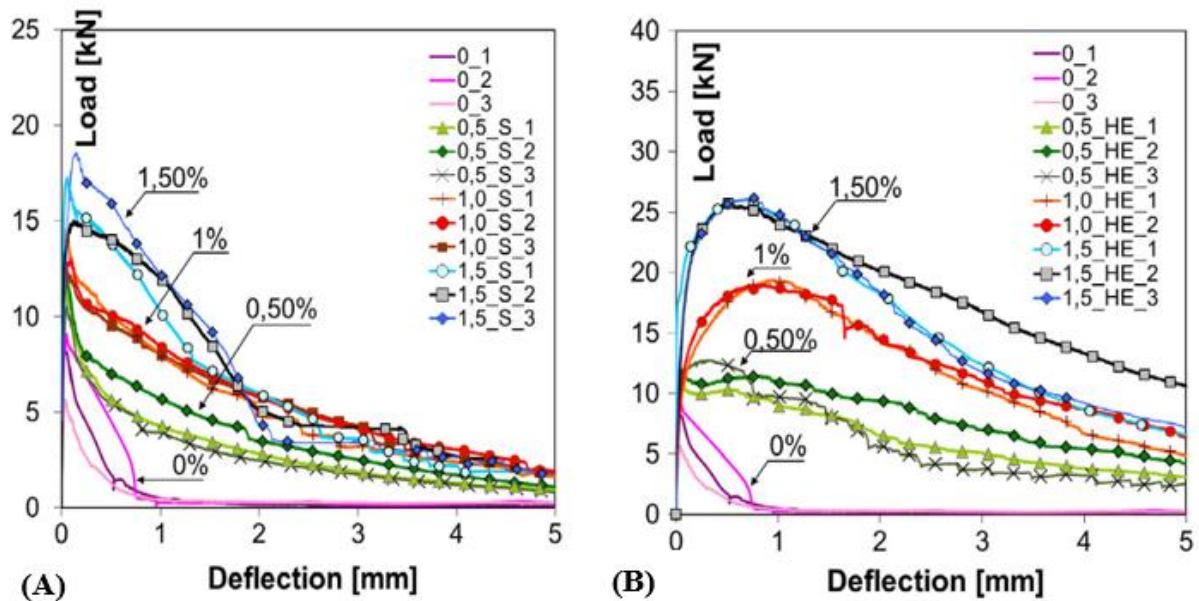


Figure 2.22: load–deflection curves from three-point bending tests performed on SCC-FR with different volume ratios of (A, left) straight steel fibres and (B, right) hooked-end steel fibres (Pająk and Ponikiewski, 2013).

Figure 2.23 illustrates the fibre bridging and arresting mechanisms for the FRCs investigated by (Rambo, Silva and Toledo Filho, 2014). Given the stiffness and higher first crack strength of the hybrid mixtures reported in the analysis, it can be said that the straight fibres were responsible for the micro-crack arrest mechanism, which also contributes to increase the energy absorption capacity of the system. Similarly, for higher levels of deformation, the crack-bridging impact given by the hooked-end fibres contributed to the post-crack mechanical performance, redistributing stresses, and controlling the crack opening.

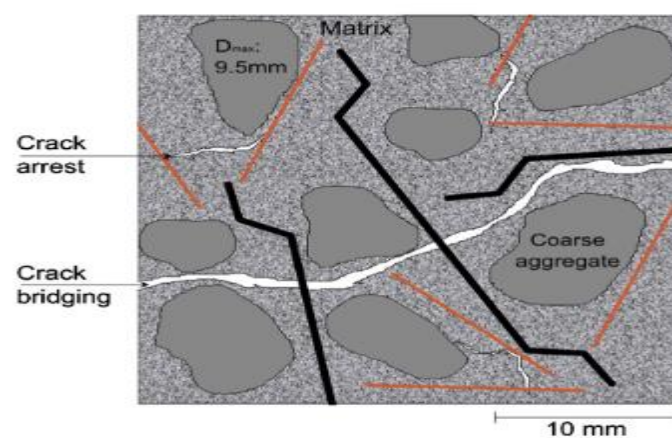


Figure 2.23: Effect of steel fiber hybridization on the fracture mechanisms of SCC (Rambo, Silva and Toledo Filho, 2014)

2.3.5 Influence of the plastic viscosity and yield stress on the SCC with and without fibres

An accurate description of the fresh characteristics of concrete can be achieved by the representation of the yield stress (τ_0) and the plastic viscosity (μ_p) of the concrete mixture. The SCC flow without or with fibres is defined by the Bingham constitutive model in terms of plastic viscosity and yield stress (Deeb, Ghanbari and Karihaloo, 2012a). It is well-known however that the yield stress of SCC mixtures is very low (around 200 Pa) in comparison with vibration or normal concretes (typically thousands of Pascals) and remains approximately constant over a large range of plastic viscosities (Dransfield J, 1967). (Ghanbari and Karihaloo, 2009) established a micromechanical process for assessing the plastic viscosity of SCC without or with steel fibres from the knowledge of the plastic viscosity of the cement paste with viscosity modifying admixture (VMA) and/or SP or of cement paste alone. This process was proposed to predict the plastic viscosity of SCC mixes without and with fibres that agree particularly good with measured values. The viscosity of SCC mixes can be accurately estimated utilizing a micromechanical method, depending on the determined viscosity of the paste of cement and the mix ratios.

Figure 2.24 shows typical impacts of differing numbers of independent parameters, compiled from several resources. The influence of superplasticizers and water content are similar to those discovered in cement paste. Decreasing or increasing the water content changes both plastic viscosity and yield stress, whereas the admixtures decrease the yield stress at largely constant plastic viscosity; large dosages of superplasticizers and plasticizers can have diverging impacts. Partial alternative of cement by ground granulated blast furnace slag (GGBS) or pulverized-fuel ash (pfa) mainly decreases yield stress, with increased viscosity in the case of GGBS, and decreased viscosity with pfa. More paste leads to a higher viscosity but lower yield stress, i.e., the concrete tends to flow more readily, but is more cohesive, a property commonly called 'fatty' or 'rich'. Mixes with less paste, although tending to flow less readily, are less viscous (known as 'bony' or 'harsh'). Air-entraining agents tend to decrease the viscosity at close-constant yield stress.

All these impacts, although typical, will not essentially occur with all mixtures, and the behaviour can vary according to the type and source of composition materials (particularly admixtures) and the characteristics of the initial mix, i.e., the starting point in Figure 2.24.

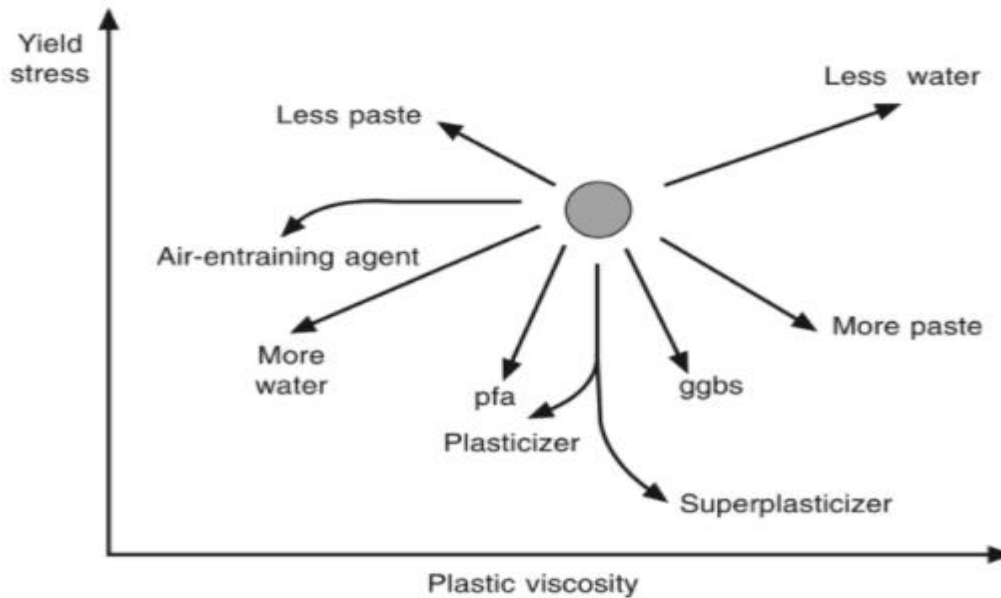


Figure 2.24: Summary of the effect of varying the proportions of concrete constituents on the Bingham constants (Domone, 2003)

The use of rheometers is appropriate in assessing the impact of fibres in SCC. No negative amounts of the yield stress were obtained if any of the materials assessed were assumed to behave like a Bingham body. Therefore, the fresh-state performance of the mixtures was demonstrated as a Bingham material by considering linear performance when specific yield stress had been exceeded and as the strain raised (Wallevik et al., 2015). Although the usage of the rheometer available did not allow the amounts of the plastic viscosity and the yield stress to be estimated, based on the proportionality among the investigational values and the physical ones the impact of the fibres has been evaluated.

Therefore, the work of (Wallevik and Wallevik, 2011) was extended to encompass the impact of fibres in the rheography. From the resultant plots it was observed that, for a given fibre, an increase of the volumetric fraction of fibres added would affect in an increase of the yield stress and in the plastic viscosity. Furthermore, a linear relationship was observed between the increase in the yield stress and the plastic viscosity with the volumetric fraction. If there is a change of the fibres' geometry, or a cocktail of fibres is created, the validity of the linear tendency observed is negotiated. For example, if a specific type of fibre with a given section is changed for the same type of fibre but with a longer geometry, a rise in the yield stress would occur, and a specific reduction of plastic viscosity might appear. The impact of the

fibre addition depends on the volumetric fraction used, the total number of fibres involved in the mixture, and the geometry of the fibres as major parameters, with the stiffness of the fibres being of minor significance.

The appropriateness of the conventional experiments as a way of finding the yield stress and plastic viscosity indirectly was investigated. It was found that while the V-funnel test demonstrates a specific relation among the results and the plastic viscosity of the mixes, no clear tendency could be seen among the slump flow patty trial results and the plastic viscosity or the yield stress (Alberti, Enfedaque and Gálvez, 2019). Furthermore, when the fibre content is increased, the relative plastic viscosity increases, while the filling ability is reduced (Khayat and Roussel, 2000). As the yield stress and plastic viscosity increase, mixtures typically have a higher consistency, which may enhance fibres' stabilizing ability, but which can also lead to worse workability for pouring or transformation (Wang *et al.*, 2017).

Figure 2.25 presents results from the literature indicating the relationship between the slump flow and steel fibre volume fraction. Ultimately, it is the combination of plastic viscosity, yield stress, and matrix density that contributes to sustaining the particles. (Flatt, 2004) reports on the most encountered combinations of plastic viscosity and yield stress values discovered in most SCC mixes. Figure 2.26 shows the proposed area in values of yield stress and plastic viscosity diagram for SCC.

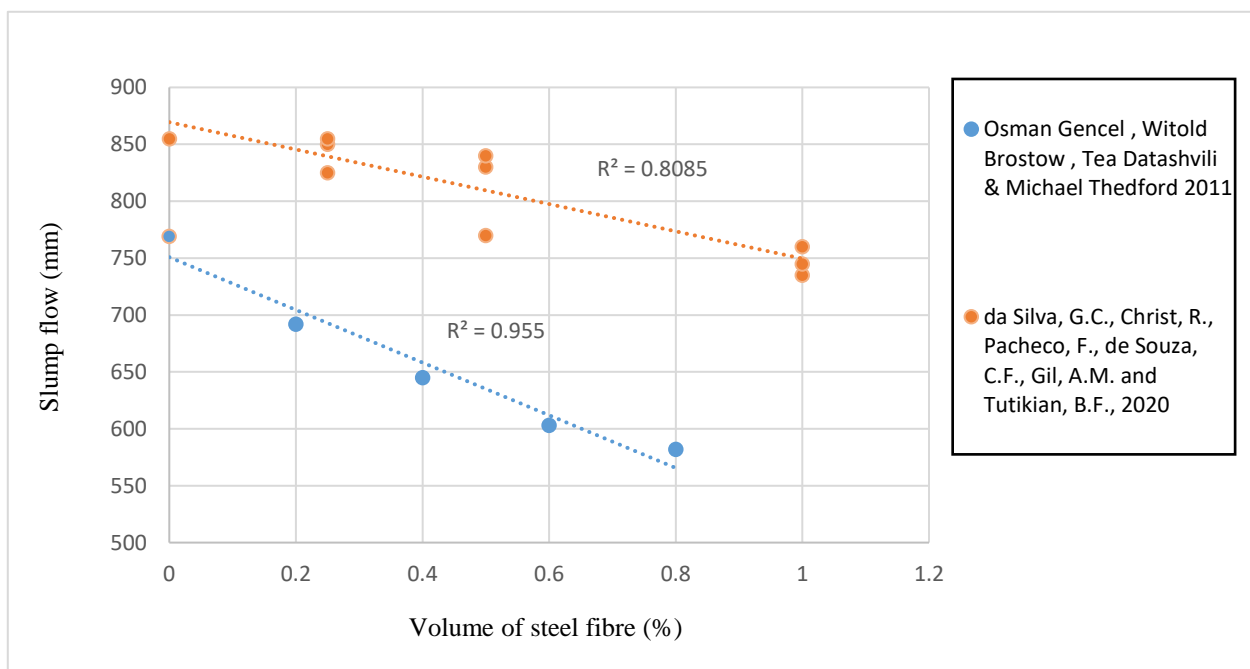


Figure 2.25: Relation between the slump flow and the steel fibre by the volume fraction

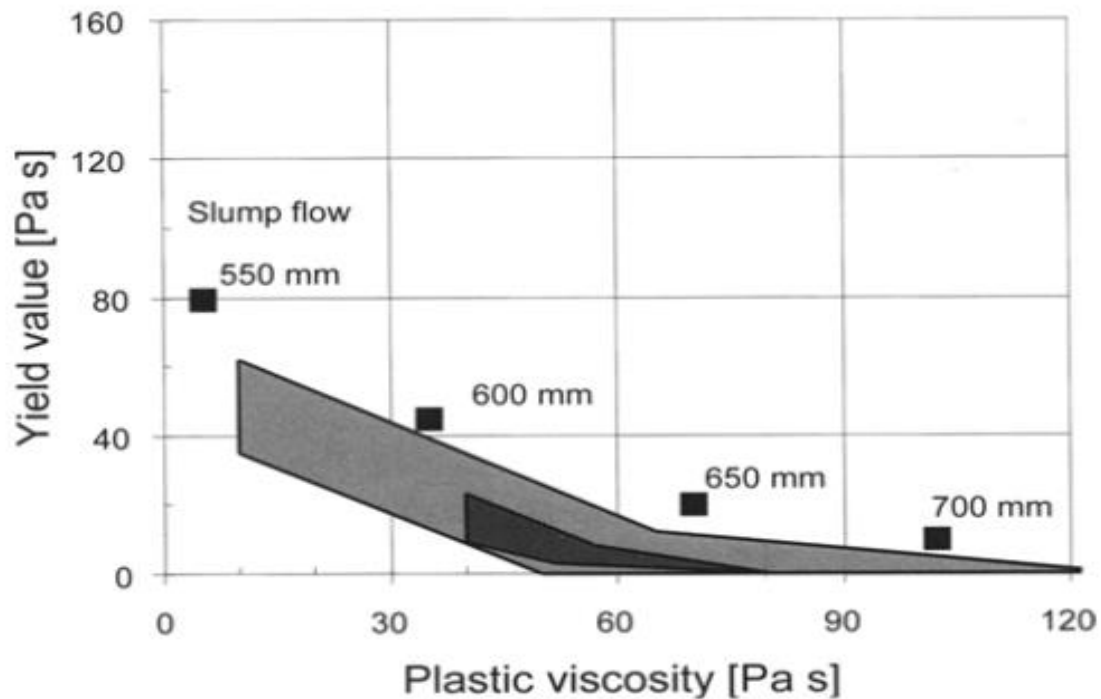


Figure 2.26: Proposed area in values of yield stress and plastic viscosity diagram for SCC
(Flatt, 2004)

(Martinie, Rossi and Roussel, 2010) observed that the increase in volume fraction of steel fibre from 0.5% to 1% slightly increased the yield stress of concrete. However, the yield stress of the mix influences distribution and orientation of fibres. With a low yield stress, the fibre is well oriented to resist the direct shear strength; conversely, for concrete with high yield stress, the orientation factor is very low. The requirements of flow confinement is also a factor influencing the orientation of fibres (Boulekbache et al., 2012). Fibres characterized as long (30 mm), with a diameter of 0.55 mm, and with crimped ends considerably increase SCSFRC mix viscosity (Ghanbari and Karihaloo, 2009). Figure 2.27 shows the relation between plastic viscosity and steel fibre volume fraction based on previous studies.

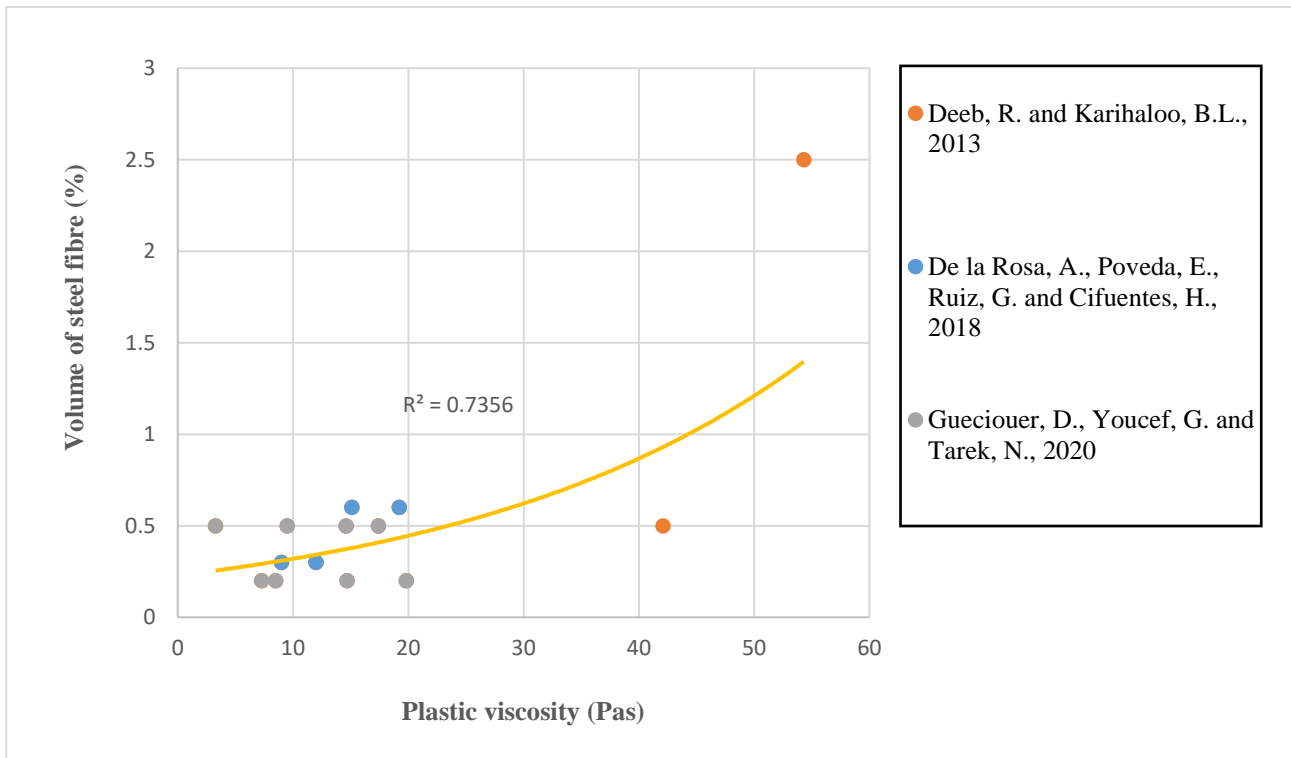


Figure 2.27:Relation between the plastic viscosity and the steel fibre by the volume fraction

The influence of the addition of several fibres to SCC mixtures is presented in Figure 2.28. Figure 2.28 (a) shows that for a given fibre an increase of the volumetric fraction of fibres added would result in an increase of the plastic viscosity and in yield stress alike. Moreover, as can be seen in Figure 2.28 (b), if a specific type of fibre with a provided part were changed for the same type of fibre but with a longer geometry, an increase in yield stress would occur, and a certain decrease of the plastic viscosity. Figure 2.29 presents the plastic viscosity of SCC with steel fibre based on compressive strength according to literature. More details are provided in (Table A-3 , Appendix A) which describes the influence the plastic viscosity (Pas) and yield stress (Pas) on properties of mixes with and without fibres used in SCC based on previous studies.

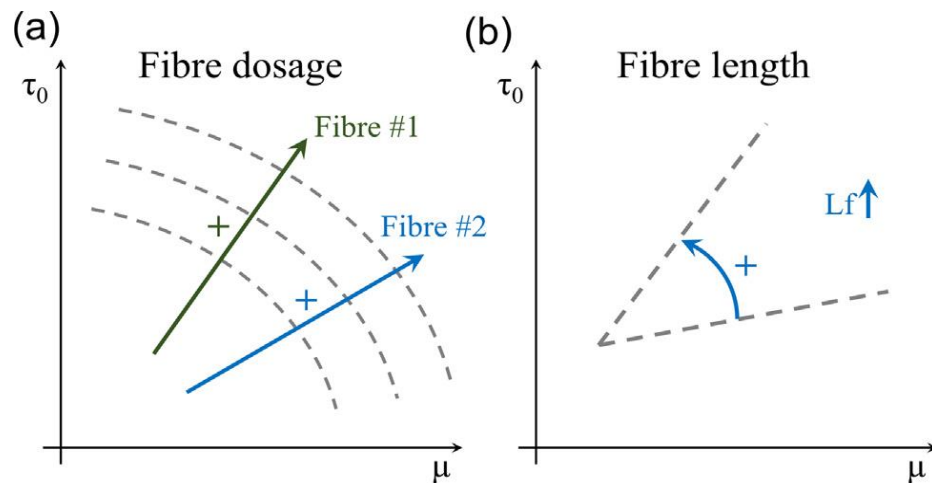


Figure 2.28: Effect of the fibre addition and fibre geometry on (τ_0) and (μ_p)
(Alberti, Enfedaque and Gálvez, 2019)

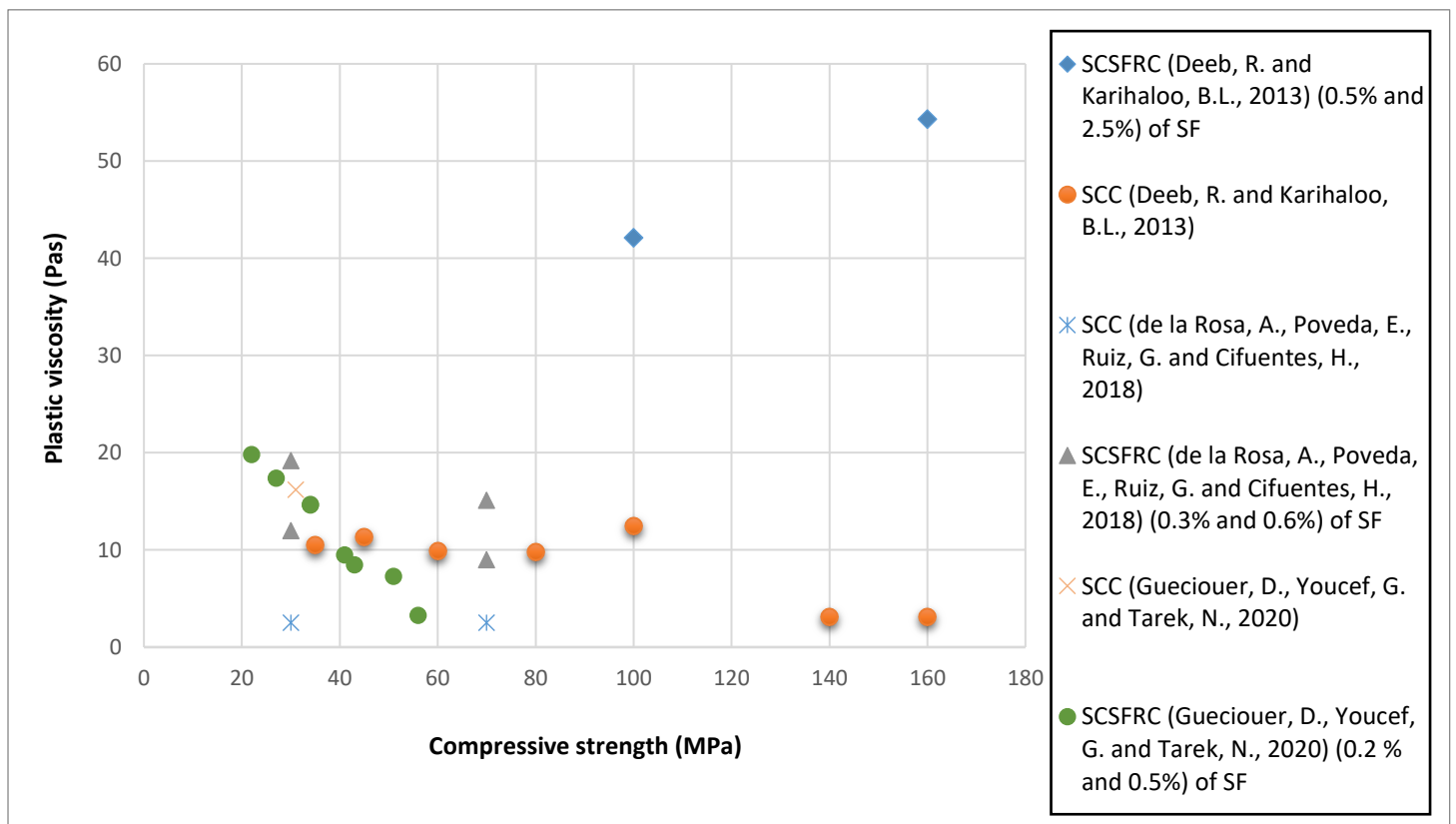


Figure 2.29: The plastic viscosity of SCC with steel fibre based on compressive strength.

2.4 Concluding remarks

SCC without and with fibre, which is characterised in its fresh properties through high rheological stability, flowability, passing ability and filling ability has excellent applicability

for components with congested reinforcement and formworks with complicated shapes. It has rationalised the construction methods by offering numerous economic and technical benefits over VC. A concrete mixture can only be categorized as SCC if its major functional conditions (passing ability, filling ability, and segregation resistance) are achieved. These are primarily completed by utilizing the advantages of SP and viscosity modifying agents (VMA) (if needed), fillers and cement replacement material (CRM).

The above three major requirements are to some extent associated and inter-connected. In other words, SCC is a trade-off among these parameters; a variation in one property will lead to a change in one or both others. Since the SCC and SCSFRC requirements are mainly affected by the fractions of the mix ingredients, it becomes crucial to develop an appropriate procedure for its proportioning. A review of the mix design methods suggests that SCC and SCSFRC can be designed using a wide range of possible constituent materials such that there is universal mix design method has generally been followed for proportioning SCC and SCSFRC mixes. To all the analysed methods, a considerable number of time and material-consuming trial mixes are inevitably required before an optimal mix proportion is achieved. Nevertheless, in most of the reviewed techniques, it should be highlighted that attention has mainly been paid to the fresh characteristics, rather than hardened characteristics, to produce an SCC and SCSFRC mix that possesses the features of being self-compacting.

Recently, a rigorous process for proportioning strength SCC and SCSFRC mixes has been developed (Dhaheer, Alyhya and Karihaloo, 2016a) (Abo Dhaheer *et al.*, 2016c) (Karihaloo and Ghanbari, 2012a), (Deeb and Karihaloo, 2013a), and (de la Rosa *et al.*, 2018b). The main consideration of this method is to exploit the expression for the plastic viscosity of an SCC and SCSFRC mix developed using micro-mechanical principles. Although this method covers a wide range of SCC mixes and reduces the need for trial mixes, it does not give practical standards on how to select the most appropriate mix. Additionally, the compressive strength was not explicitly imposed as a design criterion in this method (Abo Dhaheer *et al.*, 2016c). As a result, there is a scope in this study (Chapters 4 and 6&7) to overcome the shortcomings of this method, in which practical guidelines in the form of design charts will be developed as a guide for proportioning SCC and SCSFRC mixes.

A review of the impact of fibres on the SCSFRC was as well provided on the fresh and hardened states. Although the fibres greatly impair the workability of SCC because of their elongated shape and large surface area, the addition of fibres to SCC will lead to great

advantages and improve its performance in the hardened state. Fibres bridge cracks and retard their propagation. They contribute to an increase in energy absorption compared to VC. To make the best usage of the fibres, they want to be homogeneously distributed in the mix without blockage or segregation. However, attention has mainly been given to the passing ability and filling ability, rather than the flowing ability on the fresh characteristic, to produce an SCSFRC mix without obstacle.

An evaluation of the literature concerning the hardened characteristics indicates that SCC and SCSFRC mixes are often, but not always, accompanied with improvements in these characteristics. The compressive and tensile strengths of SCC are always higher than that of VC due to the development in mix microstructures. Several relationships have been built for VC to convert the test results of compressive and tensile strength (which is assessed by splitting, flexural and tensile strength) from one to another. However, it is not quite clear whether these conversion factors are still valid for SCC and therefore, more investigational findings are necessary to reach reliable conclusions. In this thesis, to develop relationship between the tensile strength of SCC and SCSFRC mixes of various paste to solid ratio, steel fibre volume and mix grades. This will give a better understanding of the contribution of these compositional parameters on the tensile strength of SCC and SCSFRC.

Based on the findings obtained from different studies, it is indicated that SCC and SCSFRC, with its high paste volume and fibre contents, tends to have a lower fracture energy than VC, which raises concerns among investigators. A limited number of studies has debated the parameters affecting the SCC and SCSFRC fracture behaviour such as fibre content, paste volume and strength grade. In Chapter 6, to examine in detail the role of these compositional parameters of SCC mixes in their G_f with different strength grade.

The next chapter will briefly focus on the rheology of SCC without and with fibre SCSFRC and simulation of its flow, which are the two critical issues in the range of this research. As well to examine the computational techniques and in particular, the smooth particles hydrodynamic (SPH) that are used to simulate the flow of the non-Newtonian SCSFRC in slump flow and L-box.

Chapter 3

Modelling Fresh SCC Flow

3.1 Introduction

There are numerous areas of concrete technology that use numerical or computer simulations. These simulations can be used in computer-assisted rheometric analysis, allowing improved comprehension of the material with its fresh properties. This is of great interest to current flowable concretes (e.g., 3D printable concretes or SCC) that must achieve complex requirements in terms of fresh properties, and which involve supplementary tools to monitor and measure their rheology (Bonen and Shah, 2005)(Roussel, 2018). Nowadays, computer modelling, or simulation is an indispensable tool for solving complicated engineering challenges. This can substitute costly trials or experimental evaluations in order to save time, materials, and effort (Deeb, Kulasegaram and Karihaloo, 2014a). Computational simulations of SCC flow can be useful to understand the rheological performance of SCC and can permit the classification of lower workability of the fresh concrete state to facilitate efficient filling of formwork (Roussel et al., 2007).

SCC numerical modelling is an indispensable and inexpensive methodology, not only as a tool for form filling prediction but additionally in terms of determination of fresh concrete states, mixture design, and casting optimization processes. Currently, the numerical modelling of fresh concrete flow has achieved significance, and it is becoming a significant tool for the prediction and optimization of casting methods (Qiu and Han, 2018). Any computational model of SCC flow should be able to explain correctly the behaviour of rheological SCC and follow the large deformation and Lagrangian nature of the flow. The selection of the right simulation approach is a highly significant issue, and several methods have been attempted to simulate flow.

A number of computational approaches have been proposed to simulate the SCC flow by assuming concrete as a homogeneous viscous fluid, and using either the discrete element method or the Lagrangian finite element method (Dufour and Pijaudier-Cabot, 2005). (Kulasegaram, Karihaloo* and Ghanbari., 2010) summarized different computational methods used in the past to model concrete flow and identified their disadvantages and advantages. Of these methodologies, SPH is particularly suitable because it treats SCC as a homogeneous viscous fluid, while allowing for particles of different sizes to be tracked through the flow (Alyhya, Kulasegaram and Karihaloo, 2017).

3.2 Simulating the Flow of SCC without and with fibre

Numerous tools have been developed to assess the workability of SCC with/without fibre and containing various size of coarse aggregates. These tools can be classified into three types. (Tattersall, 1991): qualitative assessment, quantitative experimental assessment, and quantitative fundamental assessment. The qualitative assessment of SCC with/without fibre was studied via its functional requirements (e.g., flowing ability, passing ability, filling ability and stability), and quantitative experimental assessment via classical trials suggested by the British and European Standards (BS EN 206-9:2010, 2010) , including slump flow (flowing ability), J-ring (flow and passing ability), L-box (passing and filling ability), and V-funnel (filling ability) experiments, as presented in the previous chapter.

This chapter quantitatively reviews SCC workability (e.g., flowing, passing and filling ability) in terms of its fundamental rheological characteristics, which is important for the success of its production. However, the prediction of SCC rheological behaviour is not a simple task, especially in the presence of reinforcement members, complex shapes of formwork, and various sizes and proportions of aggregates and fibres. In this respect, numerical simulation can be a helpful and valuable methodology for a deeper understanding of SCC mix flow behaviour, and assessment of its ability to meet the necessary self-compacting standards. Recent advances in the field of SCC technology support a systematic approach to concrete casting, where both investigational studies and numerical simulations are utilized to attain an optimal mixture design and efficient casting processes (Vasilić, 2015).

3.2.1 Blocking of fresh SCC

It is necessary to distinguish between physical jamming of aggregates of various sizes and blocking of the concrete mix due to poor workability (incomplete form in relation to flowing, passing, and filling ability). Blocking or jamming may occur simply due to the fact that the aggregate of various sizes is too large to pass an obstruction, especially in the presence of fibre. A large amount of coarse material may lead to blocking or segregation of concrete. When the coarse material is too high in relative to fine aggregates, jamming arises due to the paste layer surrounding each particle not being sufficiently thick. Blocking formed by numerous aggregates becomes visible as an arch among rebars or a narrow gap in the complex shapes of formwork, which blocks the additional aggregates of various sizes from passing and filling.

When SCC was first developed, the risk of blocking was a main worry and the demand to predict this risk emerged. Various models of blocking have been improved, and simulation is one potential tool to model this phenomenon. Methods based on distinct elements can model mixing, form filling and possible blocking difficulties. For larger amounts, a continuous methodology is to be utilized, to discover potential problem zones that can be modelled in more detail. To take benefit of the full potential of SCC, particularly when planning complicated structures, simulation may serve as a tool in the construction and formwork design in addition to determining the desired rheological parameters for the mixture design of SCC (Vignesh Kumar, Venkateswarlu and Naidu, 2019). In addition, numerical simulations can be employed to enhance the mix design, determine unknown material characteristics from rheometer measurements, predict casting behaviour, analyse defects (e.g., improper filling, blocking, or segregation), improve casting method, and predict fibre orientations (Vasilić, 2015).

The following sections in this chapter briefly describe various computational methods used in the past to model SCC or concrete flow, highlighting their advantages and disadvantages. The numerical approach used is discussed with respect to the simulation procedures. An overview of smooth particle hydrodynamics (SPH), a mesh-free computational method, is given in this chapter. SPH can take into account special features such as large deformations, large heterogeneity, and free surfaces flow of SCC with and without fibre, as these features pose big challenges to the mesh-based methods. More detailed analysis of SPH approach can be found in specific studies performed in (Deeb, 2013).

3.3 Rheology of SCC

Rheology is the science of flow and deformation of matter, which pertains to the workability and mobility of fresh cement-based materials like mortar, cement paste, or concrete in terms of material parameters (e.g., plastic viscosity and yield value) (Sheinn, A.M.M., Ho, D.W.S. and Tam, 2003). The rheology of SCC varies from normal to high strength, as illustrated in Figure 3.1. SCC has almost no yield value (about zero to 60 Pa, compared to normal concrete for which yield strength varies from a couple of hundreds to several thousand Pa). This can lead to lower plastic viscosity and yield stress values. The typical ranges of rheological parameters of SCC vary between 50 to 200 Pa for yield stress, and 20 to 100 Pa s for plastic viscosity (Banfill, 2006) (Hosseinpour, 2016).

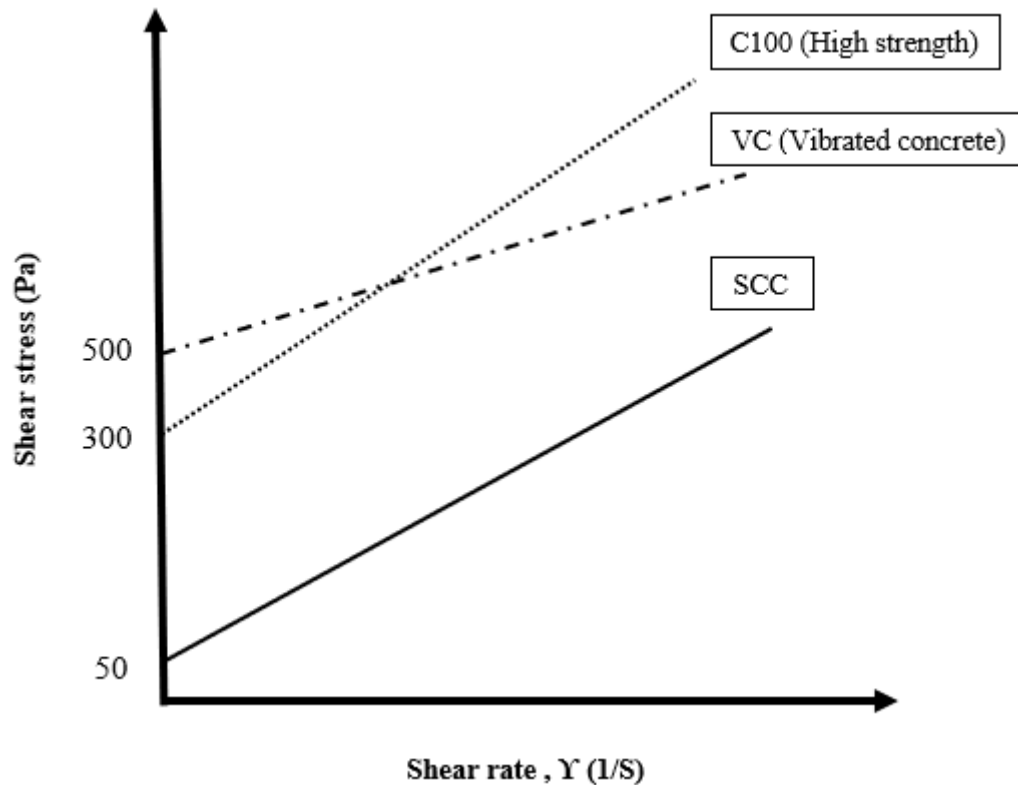


Figure 3.1: Flow curve of normal to high strength and SCC
(Sheinn, A.M.M., Ho, D.W.S. and Tam, 2003)

3.3.1 Rheological ‘definition’ of SCC

The rheology has to be identified to provide a quantitative fundamental method of characterizing its stability, flow, passing, and filling ability, which are crucial characteristics for the concrete industry, as they affect all hardened mechanical states. The rheological parameters pertinent to the fresh behaviour of SCC mix are yield stress (τ_y) (Vasilić, 2015) (Badry, Kulasegaram and Karihaloo, 2016) and plastic viscosity (η) (Vasilić, 2015) (Abo Dhaheer *et al.*, 2016c) (de la Rosa *et al.*, 2018a) (Abo Dhaheer *et al.*, 2016b).

3.3.2 Rheological parameters of fresh SCC

From a rheological perspective, SCC, which is dominated by its fluid-like behaviour, is a viscous non-Newtonian fluid, usually explained by a bi-linear Bingham-type rheological model that includes two parameters: plastic viscosity (η) and yield stress (τ_y) (Heirman *et al.*, 2008). η is the measure of the resistance to flow due to internal friction, which is mainly due to the interaction between fluid particles. SCC should have a comparatively high viscosity to reduce coarse aggregate and water sinking downwards from paste through the fresh SCC mass. τ_y is the measure of the minimum amount of energy required to make SCC flow, which

starts once the shear stress becomes higher than the yield stress (when it becomes equal or lower than the yield stress, the flow stops).

The comparative rheology required in concrete for various applications and where admixtures are typically used to achieve requirements is shown in Figure 3.2 . High-strength concrete is often cohesive (i.e., with high plastic viscosity) because of its high cement and low water content. Underwater and pump concrete also need to be cohesive to resist segregation, and admixtures are often used to achieve this. As the yield stress falls, the plastic viscosity of normal concrete also falls, unless the mix design is modified to increase cohesion and prevent segregation, as required by high slump, flowing concrete. SCC yield stress is almost zero, but a range of plastic viscosities is required to meet applications from a rapid flow wet mix to a slow creeping flow with high plastic viscosity, while retaining low yield stress. With such considerations the impacts of individual admixtures or admixture combinations can be selected to achieve the required changes in yield value and plastic viscosity for particular applications (John and Choo, 2013).

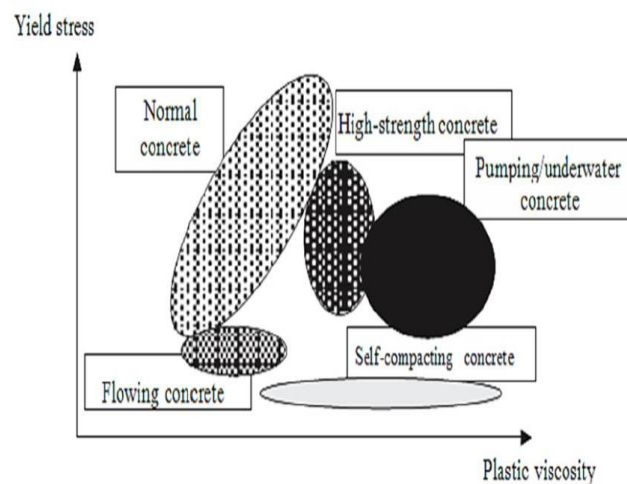


Figure 3.2: Rheology of normal and SCC (John and Choo, 2013)

3.3.3 Measuring the rheological parameters

The relationship between the shear stress and strain rate are routinely measured by rheometers. To obtain the rheological characteristics of general viscous liquids (such as cement pastes) and solid-liquid suspensions (such as SCCs), a rheometer is normally used. Several types of this instrument have been proposed to evaluate the η and τ_y of cementitious

materials (Ghanbari, 2011). The plastic viscosity of a homogeneous viscous fluid, such as a paste (mixture of cement, cement replacement material, water and super-plasticiser), can be measured accurately with a viscometer, however this is not possible for a non-homogeneous viscous fluid such as an SCC mix. The same SCC mix can exhibit diverse η values when measured with different rheometers, as reported by many researchers (Felekoğlu, Türkel and Baradan, 2007) (Wallevik and Wallevik, 2011). Vasilić (Vasilić, 2015) noted that “due to the complexity of the material behaviour and the concrete rheometer setups, it is nearly impossible to obtain the set of actual rheological parameters (plastic viscosity and yield stress) in fundamental units from rheometer measurements”.

It is therefore necessary to seek alternative methods for estimating the plastic viscosity of an SCC mix accurately and reliably. (Ghanbari and Karihaloo, 2009) proposed a micromechanical procedure for accurately estimating the plastic viscosity of SCC mixes based on knowing the plastic viscosity of the paste used in the mix (more details are given in Chapter 4). Complex material behaviour of SCC does not allow its rheological parameters from being measured accurately using rheometers, with a large scatter in the measured yield stress and plastic viscosity (Vasilić, 2015). It is therefore prudent to explore reliable methods such as numerical simulations to accurately estimate SCC mix yield stress. One of these methods is to inversely measure the t_{500} and flow spread of the mix in a cone flow test using 3D SPH method for simulating the flow of SCC (Badry, Kulasegaram and Karihaloo, 2016).

3.4 Simulation of SCC flow

The factors described above could explain the reason why the classical tests such as slump flow, L-box, J-ring, and V-funnel tests are not always sufficient to ensure the SCC self-compacting criteria and to predict its behaviour. Numerical simulation of SCC can be advantageous in this regard in terms of:

- Providing a useful tool for predicting SCC rheological parameters (plastic viscosity and yield stress).
- Examining whether or not the formwork is completely filled.
- Investigating the blocking and passing behaviour of the mix as particles migrate through narrow gaps in reinforcements, especially when large aggregates and/or fibres are present.
- Assisting in proportioning an SCC mix and optimizing its ingredients, thus improving on the traditional trial and error SCC mix design.

- Investigating the distribution of large aggregates during the flow of concrete and therefore avoiding segregation and ensuring the homogeneity of the mix.
- Examining the distribution of fibres and their orientation in the formwork, therefore optimizing the durability and strength of concrete.

3.4.1 Methods for simulating SCC

The simulation methods of concrete flow can be divided into two main groups, as shown in Figure 3.3. The first comprises methods that treat concrete as a homogeneous medium, whereby SCC is regarded as a viscous fluid without particle or fibre inclusions. It is the easiest and fastest way to simulate fresh concrete. The drawback of this method is that the aggregate blocking and segregation cannot be predicted (Roussel, 2007). The second group is methods that treat concrete as a heterogeneous medium, focussing on differences in the physical properties between the liquid and granular components used in the concrete and their effects on the flow. This method highlights the distribution of the large aggregates in this mix, allowing the actual distribution of coarse aggregates and/or fibres (and their orientations) to be revealed during the flow. However, selecting the right technique depends on the purpose of the simulation, and whether the solid components of concrete are considered as separate particles or are embedded in the mortar.

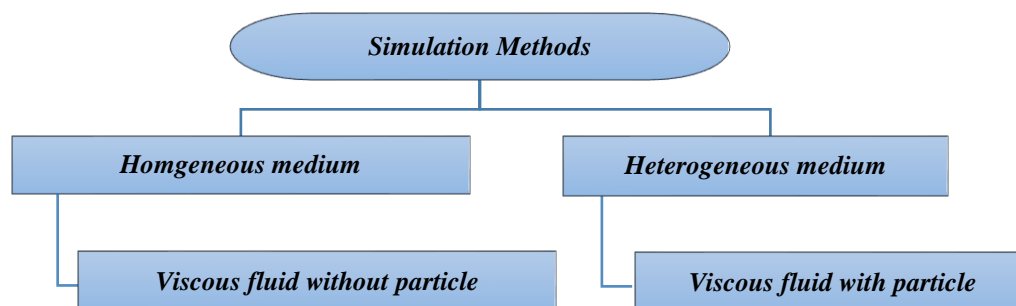


Figure 3.3: Methods for simulating SCC

3.4.2 Numerical solution strategy of simulation techniques

Numerical simulations use the basic steps shown in Figure 3.4. In the first step, the focus is on the observed physical phenomenon, which is represented by a mathematical model with a set of governing equations. To numerically solve the governing equations, the next step

involves dividing the continuum problem domain into a discrete number of elements or components. This forms the computational frame for the numerical approximation, which is based on a theory of function approximations, and includes discrete representation of the governing equations according to the discretization techniques used.

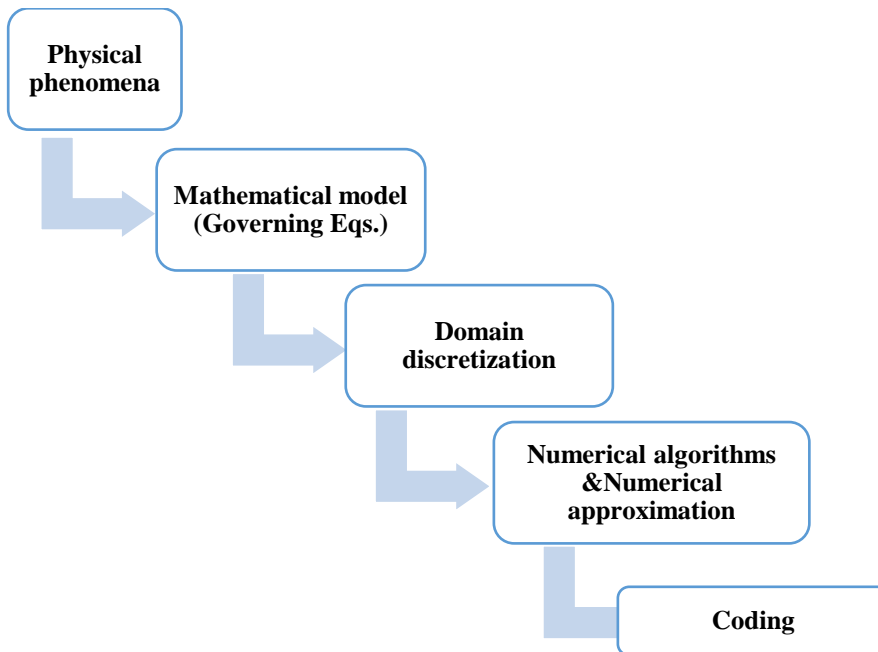


Figure 3.4: The computational strategy of the simulation technique

3.4.2.1 Description of the flow of SCC

To describe the non-Newtonian flow behaviour of concrete, the two commonly used models are those of Bingham and Herschel-Bulkley, as shown in Figure 3.5.

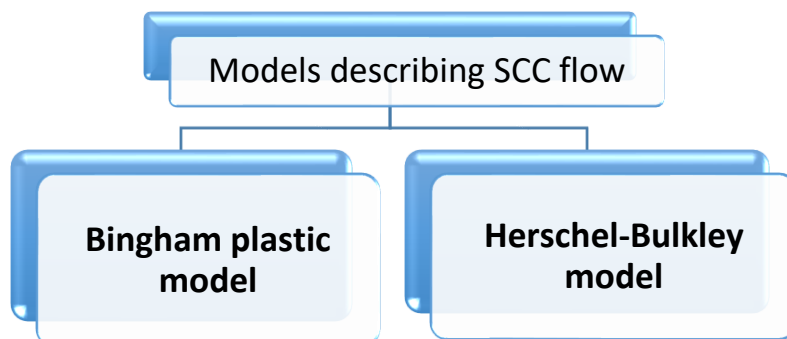


Figure 3.5: non-Newtonian flow behaviour of concrete

3.4.2.1.1 Bingham plastic model

The Bingham plastic model (commonly called the “Bingham model”) is the simplest relation to show the behaviour of a fluid having a yield stress τ_y . It is written as

$$\tau = \tau_y + \eta\dot{\gamma} \quad \tau > \tau_y \quad (3.1)$$

$$\dot{\gamma} = 0 \quad \tau \leq \tau_y \quad (3.2)$$

Where the parameters denoted by the notations are as follows; τ - shear stress (Pa), τ_y - yield value (Pa), η - plastic viscosity (Pa s), and $\dot{\gamma}$ - shear rate.

Figure 3.6. displays the curves representing Newtonian and Bingham fluids using these paramters.

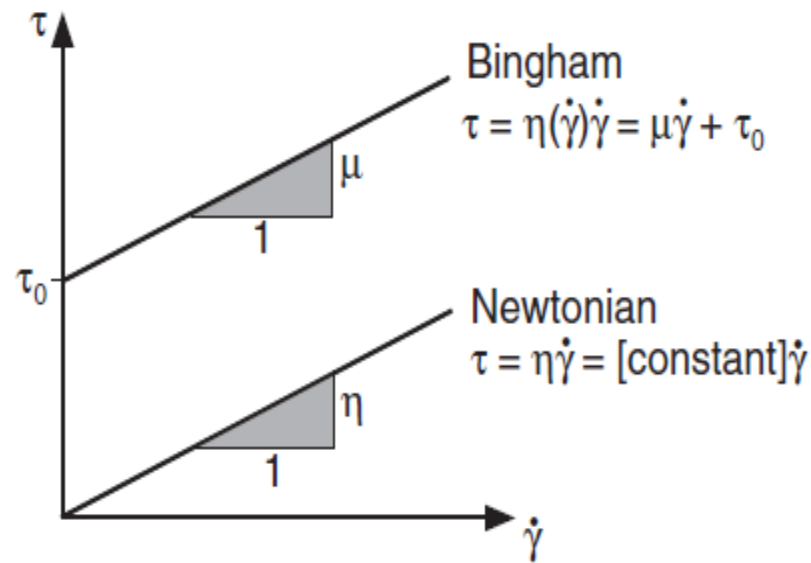


Figure 3.6: Constitutive models for Newtonian and Bingham fluids
(Wallevik and Wallevik, 2011)

From a practical point of view, it is expedient to represent the bi-linear Bingham model with its associated discontinuity at zero shear rate by a continuous function (Papanastasiou, 1987).

$$\tau = \eta\dot{\gamma} + \tau_y(1 - e^{-m\dot{\gamma}}) \quad (3.3)$$

Where m is a very large number. It can be seen from Figure 3.7 that the continuous function in Eq. (3.3) approaches the bi-linear function for large value of m . On the scale of the Figure 3.7, the discontinuity at τ_y cannot be distinguished for $m = 5000$ and 50000 .

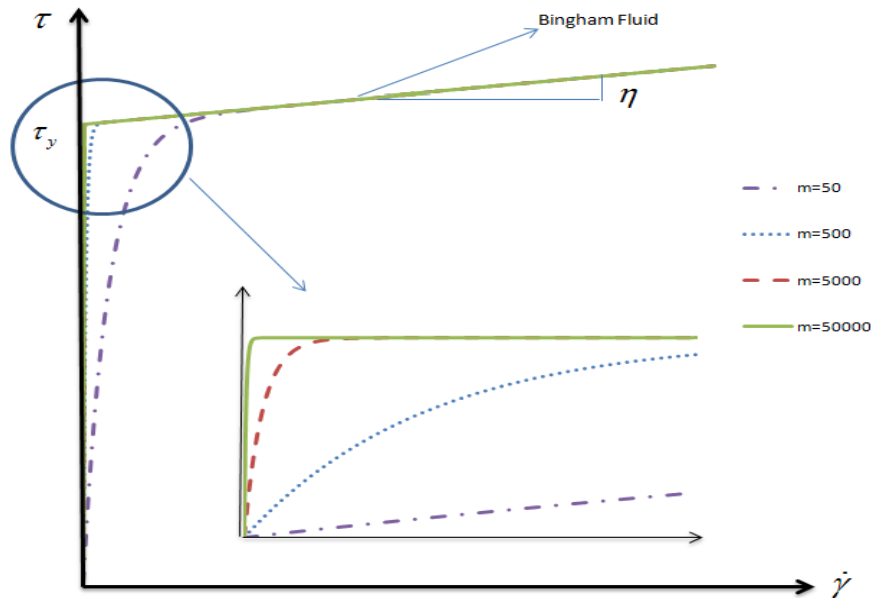


Figure 3.7: A bi-linear Bingham fluid constitutive model replaced by the continuous function (Ghanbari and Karihaloo, 2009)

3.4.2.1.2 Herschel-Bulkley model

This model is a generalization of the Bingham model such that, upon deformation, the viscosity can be shear thinning or shear thickening. The constitutive equation is given by:

$$\tau = \tau_y + \eta \dot{\gamma}^n \quad \tau > \tau_y \quad (3.4)$$

$$\dot{\gamma} = 0 \quad \tau \leq \tau_y \quad (3.5)$$

For: $n < 1$, the fluid exhibits shear thinning properties; $n = 1$, the fluid shows Bingham behaviour; and $n > 1$, the fluid shows shear thickening behaviour.

3.4.2.2 The governing equations used in SCC simulation

SCC is represented as a fluid and its flow is governed by fluid motion equations (i.e., for continuity, momentum, and energy conservation), which are based on the fundamental physical laws of conservation. However, when there is no change in the temperature during a test and the heat flux in the continuum is absent, the energy can be assumed to be identically

conserved. Since the viscosity and density are not affected by the temperature, the energy conservation equation can be ignored while modelling SCC flow. The continuity equation or the mass conservation equation in the Lagrangian form is given by:

$$\frac{D\rho}{Dt} + \rho \nabla \cdot \mathbf{v} = 0 \quad (3.6)$$

Where ρ , t , and \mathbf{v} are respectively, the fluid particle density, time, and particle velocity; $\nabla \cdot \mathbf{v}$ is the time rate of change of the volume of a moving fluid element; and D denotes the substantial or material derivative.

For an incompressible fluid, the density is constant, therefore (3.6) becomes:

$$\nabla \cdot \mathbf{v} = 0 \quad (3.7)$$

If gravity (g) is the only body force acting on the continuum, the momentum conservation equations in the Lagrangian form can be written in the compact vectorial form as:

$$\frac{D\mathbf{v}}{Dt} = -\frac{1}{\rho} \nabla P + \frac{1}{\rho} \nabla \cdot \boldsymbol{\tau} + \mathbf{g} \quad (3.8)$$

where P , g and $\boldsymbol{\tau}$ are pressure, gravitational acceleration, and shear stress, respectively.

3.4.2.3 Fundamental methods describing the physical governing equations

- **Eulerian and Lagrangian methods**

To describe the physical governing equations, there are two fundamental approaches: Eulerian and Lagrangian. The Eulerian approach is a spatial description used to track a certain fixed location in the flow field and follows the change in properties (velocity, temperature, density, mass, or concentration, etc.) as different fluid elements pass through that location. Suppose that the velocity is being followed at a location in the fluid flow through which different fluid elements pass at different times (Figure 3.8).

$$t_1 \rightarrow V_1 \quad , \quad t_2 \rightarrow V_2$$

The time rate of change of the velocity in such a measurement is denoted as $\left. \frac{\partial v}{\partial t} \right|_{(x,y,z)}$, which is the partial derivative of the velocity with respect to time. Note that the suffix (x, y, z) implies that the observer records the change in the property at the fixed location (x, y, z) . $\left(\frac{\partial v}{\partial t} \right)$ is also called the local rate of change of that property (velocity in this case).

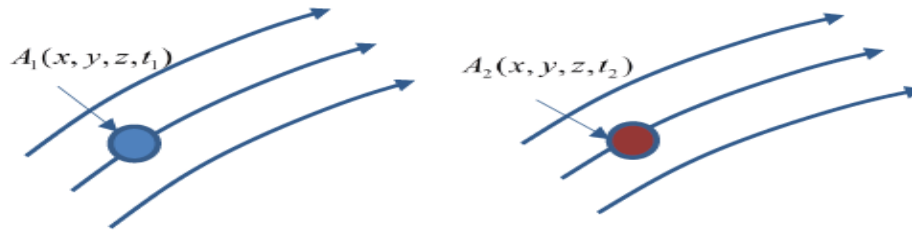


Figure 3.8: Different fluid elements at different times at a fixed location in the fluid flow

The Lagrangian approach is used to track a material element of the fluid as it moves and the changes in its properties (e.g., velocity) are monitored. Figure 3.9 illustrates that at time t_1 , the ‘material’ or ‘particle’ of the fluid ‘A’ has moved from location (x_1, y_1, z_1) to another location (x_2, y_2, z_2) at time t_2 . Its property, such as velocity, is recorded, as the material moves in the flow-field. The recorded property is associated with the same fluid particle, but at different locations and at different times.

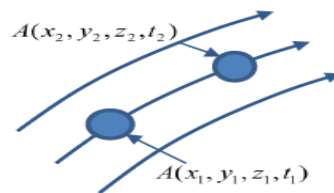


Figure 3.9: Fluid particle motion from time t_1 to time t_2

The time change of the velocity in such a measurement is denoted as $\frac{Dv}{Dt}$, which is called the material derivative or substantial derivative value. It reflects time rate of change in the velocity (or any other properties) of the tagged fluid particle as observed by an observer moving with the fluid. An example of the Lagrangian method is the SPH method.

$$t_1 \rightarrow V_1 \rightarrow (x_1, y_1, z_1)$$

$$t_2 \rightarrow V_2 \rightarrow (x_2, y_2, z_2)$$

The two derivatives, Lagrangian and Eulerian, are related to each other, e.g. for velocity:

$$\frac{Dv}{Dt} = \frac{\partial v}{\partial t} + (V \cdot \nabla) V \cdot \nabla \quad (3.9)$$

Where the term $V \cdot \nabla$ is the convective derivative, which defines the time rate of change as the fluid element moves from one location to another in the flow field.

3.4.2.4 Domain Discretization

In this step, the continuum problem domain needs to be divided into a finite number of discrete components to numerically solve the governing equations. Implementation of this procedure differs according to the numerical method used. From a graphical point of view, computational modelling can be divided into grid and particle-based methods. Figure 3.10 illustrates the two different discretization of the same geometrical domain.

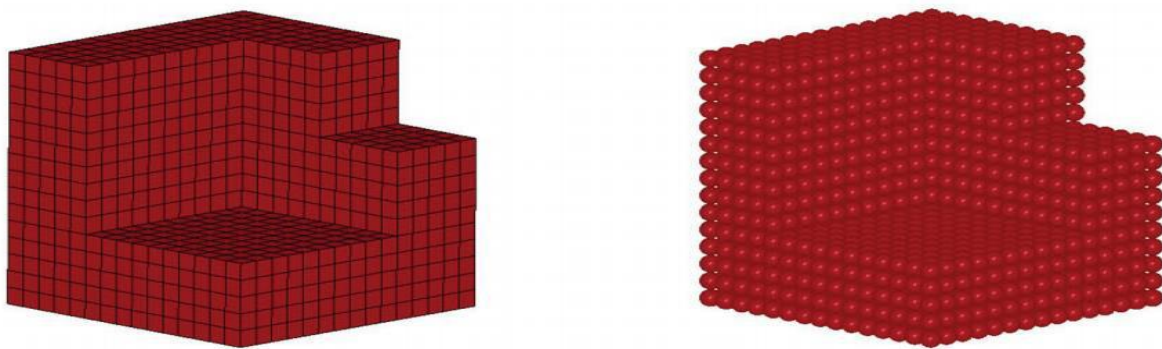


Figure 3.10: Comparison between grid method (left) and particle method (right) for the same geometry (Vesenjak and Ren, 2007)

In the grid or mesh-based method, the continuum domain is divided into small discrete domains connected to each other by nodes. The accuracy of the numerical approximation is closely related to the mesh topography (i.e., shape, size etc.). Examples of the mesh-based method include the finite element method (FEM), the finite difference method (FDM), and the finite volume method (FVM). The generation of the mesh for a grid method is a prerequisite, and for complicated problems constructing the mesh can be more difficult than solving the problem itself, since the results are based on the quality of the mesh (Vesenjak and Ren, 2007). Therefore, mesh-less methods are more attractive to treat problems where it is difficult to use grid-based methods.

In particle (or mesh-less) methods, a domain is represented by a set of nodal points or particles without using any mesh to connect those nodes. In these methods, large deformations, moving interfaces, difficult boundary conditions and complex geometries are easy to handle, since the connectivity among nodes is generated as part of the computation. A mesh-free method, smooth particle hydrodynamics (SPH) (Kulasegaram and Karihaloo,

2013) ; (Deeb, Karihaloo and Kulasegaram, 2014) and (Deeb, Kulasegaram and Karihaloo, 2014a) is used in this thesis (Chapter 8) for the analysis of SCC flow.

3.5 Numerical approximation SPH

The simplicity and Lagrangian nature of SPH have been exploited in the past to model many free-surface fluid flows and related engineering problems (Bonet and Kulasegaram, 2000) ; (Cummins and Rudman, 1999) ; (Kulasegaram et al., 2004) ; (Woolfson, 2004) (Monaghan, 1994) ; (Kulasegaram and Karihaloo, 2013). The fundamental SPH algorithm was enhanced to maintain linear and angular momentum exactly using the particle equivalent of the Lagrangian for a compressible non-dissipative fluid (Wetzstein et al., 2005). SPH was originally established for cosmological and astrophysics applications (Lucy, 1977), (Gingold and Monaghan, 1977) , where boundaries were typically either not significant, or were necessary only for very simple conditions. However, the SPH method has been expanded to deal with solid and fluid problems that include more complex boundary conditions in recent years (Kulasegaram et al., 2004).

Various numerical approaches have been established to model the flow of fresh SCC, and to explore the distribution and orientation of steel fibres reinforced SCC (SCSFRC) (Mechtcherine et al., 2014) (Švec et al., 2011)(Kulasegaram, Karihaloo and Ghanbari, 2011)(Švec et al., 2014). (Kulasegaram, Karihaloo and Ghanbari, 2011) used SPH to simulate the slump flow test and L-box test of SCC in 2D, treating SCC mixtures as non-Newtonian incompressible viscous fluids, whose rheology was described using the Bingham constitutive model. In addition, 3D Lagrangian particle-based SPH method is used to simulate the flow of SCC and SCSFRC in the L-box configuration in (Deeb, Kulasegaram and Karihaloo, 2014b).

Development in SPH method offers a glimpse of the future of fresh concrete flow simulation. Although SPH was first developed to study astrophysics problems (R. A. Gingold and J. J. Monaghan, 1977) (Lucy, 1977) , it has exceptional advantages in enabling the simulation of flow and infilling behaviour. It has been used to study wave-structure interactions for Newtonian flow (Colagrossi and Landrini, 2003) , and has been successfully used to simulate non-Newtonian flow, such as in metal forming (Bonet and Kulasegaram, 2000), the impacting droplet (Chui and Heng, 2010), blood-vessel interaction (Xu et al., 2013), and Couette flow (Zhou, Ge and Li, 2010).

Several studies have simulated the flow of cement-based materials using SPH method. Assuming that SCC is a homogeneous fluid that consists of particles of different sizes and

shapes, SPH (as a mesh-free particle method) is an ideal computational method to predict concrete flow performance accurately. This method can also assist in proportioning SCC mixes, thus improving on the traditional trial and error SCC mix design process. SPH method was used for 2D and 3D simulation of the rheological behaviour and free surface flow profile evolution of SCC in different workability tests, such as vane viscometers (Zhu et al., 2010), slump flow (Deeb, Kulasegaram and Karihaloo, 2014a) (Badry, Kulasegaram and Karihaloo, 2016), L-Box (Lashkarbolouk et al., 2013), J-Ring (Abo Dhaheer, Kulasegaram and Karihaloo, 2016), and V-funnel (Lashkarbolouk, Halabian and Chamani, 2014) set-ups. Some of these simulations considered the presence of different size of coarse particles, as well as fibres and their orientations during the flow (Deeb, Karihaloo and Kulasegaram, 2014) (Deeb, Kulasegaram and Karihaloo, 2014b) (Kulasegaram, Karihaloo and Ghanbari, 2011) (Deeb, 2013).

For example, (Deeb, Kulasegaram and Karihaloo, 2014a) presented a 3D simulation of SCC slump flow using SPH method with and without the presence of fibres. In that study, the flow of fluid was simulated using Bingham constitutive model, as well as considering distribution of coarse spherical particles larger than 8 mm. The particles smaller than 8 mm represented the viscous paste portion of the suspension. The results demonstrated the ability of SPH method to simulate particle-particle interactions, particle tracking, and prediction of flow performance of SCC as a heterogeneous material. On the other hand, (Deeb, Kulasegaram and Karihaloo, 2014a) showed that the orientation and motion of fibres suspended in an SCC matrix can be accurately predicted using SPH method.

SPH is a method for obtaining approximate numerical solutions of the equations of fluid dynamics by representing the fluid with a set of particles (Figure 3.11). From the computational point of view, the particles are just interpolation points from which properties of the fluid can be evaluated. From the physical point of view, the SPH particles are material particles which can be treated like any other particle system (Wetzstein et al., 2005).

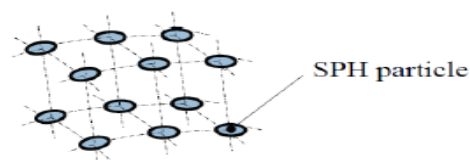


Figure 3.11:SPH model (Vesenjok and Ren, 2007)

3.5.1 SPH concept

SPH is a mesh-free Lagrangian numerical method, which was first developed to simulate astrophysical fluid dynamics in 1977. It is relatively easy to incorporate complicated physical effects into SPH formulas, thus SPH has been successfully applied in various fields, such as dynamic material response (Randles and Libersky, 1996), high velocity impact (Johnson, Stryk and Beissel, 1996) and Newtonian or non-Newtonian flows (Zainali et al., 2013). As a particle-based method, the system is discretized into several particles or points that possess material properties, such as mass, position, velocity, etc. An SPH interpolation process is then employed to approximate values and derivatives of continuous field quantities by using those domain particles (Huang, Gao and Zhang, 2019).

3.5.2 SPH support domain

In Figure 3.12, the particle i interacts with the neighbouring particles within the support domain Ω with a radius of kh (where k is a constant), formed by a smoothing function. Interpolation of any variable at any position r can be calculated using SPH approximation with the aid of a kernel or smoothing function (Huang, Gao and Zhang, 2019).

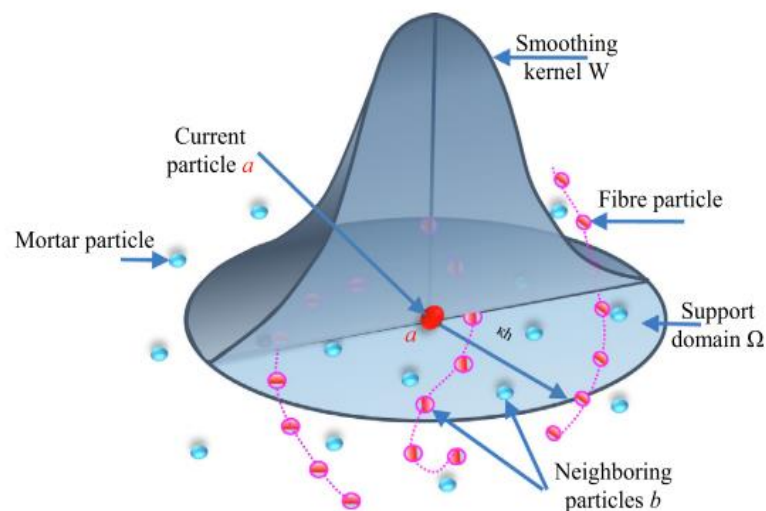


Figure 3.12: Smoothing kernel W and its support domain for the approximation of a current particle a (Thanh, Li and Zhang, 2020)

3.5.3 Kernel approximation

SPH provides a concept to approximate the spatial derivative using particles, which facilitates computation of the spatial derivatives in particle-based method, as in grid-based methods. Each particle (e.g., particle 'a' in Figure 3.12) carries the field variables such as the mass

(m_a), density (ρ_a), pressure (P_a), velocity (\mathbf{v}_a), position (\mathbf{r}_a), temperature (T_a), colour (c_a) and any other quantities, depending on the nature of the flow and of the fluid. The mass is constant through the simulations. However, the other physical quantities are updated at every time step. These field variables are represented by integral kernel or smoothing functions (Figure 3.12).

3.5.4 Particle interpolation

Particle approximation in SPH involves discretizing the entire domain problem into a limited number of particles N , and then approximating all the field variables on these particles. For example, the finite volume V_b of particle 'b' in the support domain is calculated as $V_b = \frac{m_b}{\rho_b}$, where ρ_b and m_b are the density and mass of the particle, respectively. The inclusion of these properties makes SPH the ideal numerical solution to simulate dynamic fluid flow applications, such as the flow of SCC.

$$f(x) = \sum_{b=1}^N m_b \frac{f(x_b)}{\rho_b} W(x - x_b, h) \quad (3.10)$$

A quantity $f(x)$ (Figure 3.13) at an arbitrary position x is approximated using quantities f_b positions x_b . The kernel function W realises a diminishing influence of particles at larger distances. Over all the particles N in the support domain, $f(x)$ can be expressed in the equivalent forms of discretized particle approximation (Bonet and Lok, 1999) as ,

$$f(x) = \sum_{b=1}^N V_b f(x_b) W_b(x) \quad (3.11)$$

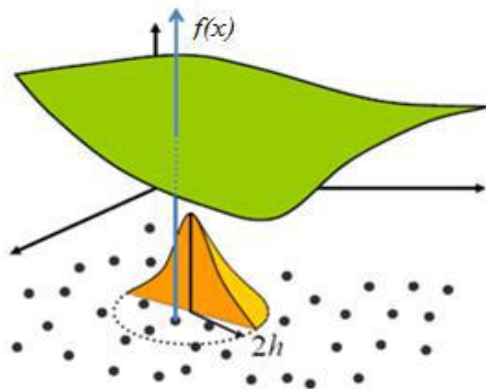


Figure 3.13:particle approximation of function $f(x)$

where $W_b(x)$ is an interpolating kernel, representing the kernel with compact support domain of radius r (Figure 3.13). There are different possibilities in selecting the kernel function W . Spline kernel functions are the most common as they can be designed to have specific characteristics and possess a compact support (Bonet and Kulasegaram, 2000).

The gradient of function $f(x)$ in Eq. (3.11) is given by,

$$\nabla f(x) = \sum_{b=1}^N V_b f(x_b) \nabla W_b(x) \quad (3.12)$$

where the quantity $\nabla W_b(x)$ denotes the gradient of the kernel, which is taken as centred on the position of particle a (Figure 3.13).

Eq. (3.11) and (3.12) state that the value of any function (or its gradient) at any position is approximated using the values of the function at all the particles within the support domain (particles $b=1,2,\dots,N$) of that particle weighted by the smoothing function, $W_b(x)$. The application of Eq. (3.11) to compute the approximate value for the density of a continuum leads to the classical SPH equation as,

$$\rho(x) = \sum_{b=1}^N m_b W_b(x) \quad (3.13)$$

3.5.5 The boundary conditions Treatment

Boundary conditions in SPH should be imposed to balance the inner particle forces to prevent them penetrating the wall. Various procedures are available for this, such as mirror particles (Takeda, Miyama and Sekiya, 1994) ; (Cummins and Rudman, 1999), dummy particles (Shao and Lo, 2003); (Lee *et al.*, 2008) ; (Amini, Emdad and Farid, 2011) , and repulsive forces (Monaghan, 1994) methods. In this thesis the dummy particle methodology was selected, as described in Chapter 8.

3.5.6 Numerical solution strategies in SPH

In SPH, enforcing incompressibility can be pursued using two different approaches - the truly incompressible SPH (ISPH) (Kulasegaram, Karihaloo and Ghanbari, 2011) and the weakly compressible SPH (WCSPH) (Monaghan, 1994) ; (Lee *et al.*, 2008) . In ISPH approach, a projection method based on the predictor-corrector time stepping scheme is used to track the flow in which the SCC incompressibility has been imposed exactly through the pressure Poisson Eq. (as explained in Chapter 8). In WCSPH approach, the incompressibility condition is imposed approximately through the so-called weakly or quasi-compressible SPH

(Monaghan, 1994). This leads to the replacement of the real incompressible fluid by an artificial quasi-compressible fluid having a small, user-defined, fluctuation in the density, by which the time-consuming solution of the Poisson equation can be avoided (Becker and Teschner, 2007) However, WCSPH requires a much smaller time step in order to keep the density fluctuation down to 1% to avoid numerical instability (Lee et al., 2008) . This can be circumvented by implementing ISPH (as discussed in Chapter 8), by which the pressure and velocity are computed separately.

3.6 Concluding remarks

This chapter has described the rheology of SCC and has provided an overview of the related rheological parameters, methods of measurement, and models describing fluid flow. In addition to its rheology, the simulation of SCC flow, highlighting the numerical strategy used in its techniques, was reviewed, justifying the selection of SPH as a suitable method to model heterogeneous SCC flow.

A review of the methods used for measuring the rheological parameters indicates that, due to the complexity of the material behaviour and the concrete rheometers' setups, it is nearly impossible to obtain these rheological properties reliably from rheometer measurements. For this reason, alternative methods have been developed to determine these parameters. Yield stress is estimated in an inverse manner from the measured t_{500} and the final flow spread diameter of the mix in a cone slump flow test using SPH simulations. The plastic viscosity can be determined using the micromechanical procedure based on the plastic viscosity of the paste (as described in next chapter). The micromechanical procedure was used in this study to determine SCC plastic viscosity, and to pave the way for developing a rational mix design method for proportioning SCC mixes with and without fibre. The steps and procedures adopted to develop this rational method are described in Chapter 4.

The literature reviewed in this chapter indicates that SPH can assist in many ways with regards to SCC applications, such as proportioning SCC mixes, providing a useful tool for predicting SCC rheological parameters, and modelling the flow and monitoring the movement of large aggregates and/or steel fibres in the cone slump flow and L-box tests. Beyond the scope of its mentioned capabilities, the SPH methodology can help to simulate SCC mixes in the slump flow and L-box tests. This will be used to examine whether or not the produced mixes meet the flowing, passing, and filling ability criterion and flow homogeneously with no blockage in complex and heavily reinforced structural members.

Chapter 8 reports on the simulation of the flow of fresh SCC in the slump flow and L-box test using the SPH approach.

Chapter 4

Procedure for Proportioning and Designing SCC mixes with and without steel fibres

4.1 Introduction

The proportioning of SCC mixes requires a balance between their flow and passing ability on the one hand, and the resistance to segregation on the other (Corinaldesi and Moriconi, 2004) (Wu and An, 2014) (H. Okamura and Ouchi, 2003). In early 20th century, mix proportioning approaches were all heuristic in nature, requiring many trial mixes, but extensive research work carried out on the rheological properties of SCC has greatly improved the proportioning of SCC mixes (Roussel, 2006) (Tregger et al., 2012) (Chidiac and Mahmoodzadeh, 2009) (Figueiras et al., 2014) (Wallevik and Wallevik, 2011) (Li and Kwan, 2011). A summary of different mix proportioning approaches can be found in previous reviews (Shi, Wu, Lv, *et al.*, 2015) (Ashish and Verma, 2018). The European Federation of National Trade Associations (EFNARC) guidelines (EFNARC, 2005) give typical ranges of primary ingredients (Table 5.1 in chapter 5). The actual amounts depend on the desired strength and other performance requirements; consequently, despite improvements, mix proportioning still involves considerable trial and error.

A rigorous method for proportioning normal and high strength SCC mixes based on their plastic viscosity has been developed by (Karihaloo and Ghanbari, 2012b) and (Deeb and Karihaloo, 2013b) that exploits the expression for the plastic viscosity of an SCC mix developed by (Ghanbari and Karihaloo, 2009) using micro-mechanical principles. This expression shows how the known plastic viscosity of the paste is increased by the addition of solid phase particles (i.e., filler, fine, and coarse aggregates). The contribution of each of the solid phases to the overall increase depends on its volume fraction and the shape of its particles. As a result, the final expression for the plastic viscosity of an SCC mix is the product of the known plastic viscosity of the paste, and the contributions of each of the solid phases. While the method for proportioning SCC mixes proposed by previous studies (Karihaloo and Ghanbari, 2012b) (Deeb and Karihaloo, 2013b) is rigorous and based on sound physical principles, it produces a number of mixes that reach the target plastic viscosity, without any practical guidelines on how to choose the most appropriate mix. Moreover, the method was developed on the basis of reference mixes of a range of known cube compressive strength, but the latter was not explicitly imposed as a design criterion.

The aim of this chapter is to address the above shortcomings of this method for proportioning SCC and SCSFRC mixes. Practical guidelines in the form of design charts are provided to enable the selection of appropriate mix proportions to achieve the target plastic viscosity in the range of 5 - 85 Pa.s, and the target cube compressive strength in the range of 30 - 70 MPa. Several mixes with varying paste to solid ratios by volume were selected using these

guidelines and were prepared in the laboratory in order to confirm the simplicity and usefulness of this method.

4.2 Target compressive strength of SCC and SCSFRC mixes

The compressive strength of a concrete mix is mostly determined by the ratio of water to cementitious material (w/cm) under given curing conditions. The addition of steel fibres up to 1% by volume to vibrated or self-consolidated concrete has a negligible effect on the compressive strength (Ezeldin, Member and Balaguru, 1993) (Bencardino *et al.*, 2008)(Banthia and Dubey, 2000) (Poveda *et al.*, 2017) .

There are various empirical equations to calculate the compressive strength from w/cm ratio based on the widely recognized Abram's rule (de la Rosa *et al.*, 2018a). The differences among them are due to the geometry of the specimen and other factors. (Abo Dhaheer *et al.*, 2016c) proposed an equation in order to determine the compressive strength on $100 \times 100 \times 100 \text{ mm}^3$ cubes, from a regression analysis of numerous experimental tests for SCC with or without fibre in the range 30 and 70 MPa:

$$f_{cu} = \frac{195}{12.65^{(w/cm)}} \quad (4.1)$$

Where f_{cu} is the 28-day equivalent cube compressive strength (MPa), and w/cm is the ratio of water to cementitious materials (i.e., cement + cement replacement material, e.g., GGBS).

4.3 Target plastic viscosity of SCC and SCSFRC mixes

Fresh SCC or SCSFRC is best described by the Bingham constitutive model, which is governed by two material properties: yield stress and plastic viscosity. The yield stress of SCC mixes is very low (around 200 Pa) in comparison with normal concretes (thousands of Pascals), and remains nearly constant over a large range of plastic viscosities (John and Choo, 2013). Thus, the most crucial parameter is the plastic viscosity, which changes with the plastic viscosity of the paste and the mix composition. The viscosity of a homogenous viscous fluid such as cement paste (a mixture of cement, cement replacement material, water and super-plasticiser) can be measured accurately, unlike non-homogeneous viscous fluids such as SCC or SCSFRC. (Ghanbari and Karihaloo, 2009) developed a micromechanical procedure for estimating the plastic viscosity of SCC with or without fibres from the knowledge of the plastic viscosity of cement paste alone, or of the cement paste with SP and/or VMA. This procedure has been shown to predict the plastic viscosity of SCC (with or without fibres) mixes with a reasonable accuracy related to the measured values.

4.4 Calculating the plastic viscosity of SCC and SCSFC mixes

In this procedure, SCC is regarded as a two-phase suspension, in which the solid phase is suspended in a viscous liquid phase. The increase in the plastic viscosity of the liquid phase as a result of the addition of the solid phase (filler, fine, and coarse aggregates) is estimated in stepwise manner from the two-phase suspension model. In the first step, the solid phase is the finest solid material, for example the filler in the viscous fluid (i.e., paste) phase. In the next step, the finest solid (i.e., fine aggregate) is the solid phase suspended in the viscous fluid phase now formed by the two-phase suspension from the first step. This procedure is continued until all the solid phase ingredients have been added. The plastic viscosity of the i^{th} liquid–solid suspension can be estimated from the plastic viscosity of the preceding $(i-1)^{\text{th}}$ phase as:

$$\eta_{ci} = \eta_{c(i-1)} * f_i(\phi_i) \quad (4.2)$$

Where η_{ci} is the plastic viscosity of the i^{th} liquid–solid suspension, and $\eta_{c(i-1)}$ is the plastic viscosity of the preceding $(i - 1)^{\text{th}}$ phase.

In the first step $i = 1$, η_{c0} is the known plastic viscosity of the paste; and $f_i(\phi_i)$ is a factor larger than unity that predicts the increase in the plastic viscosity induced by the solid phase with a volume fraction ϕ_i . Figure 4.1 shows the hierarchy of these two-phase liquid-solid suspensions used in the estimation of the plastic viscosity of all mixes developed, based on the viscosity of their constituent cement paste.

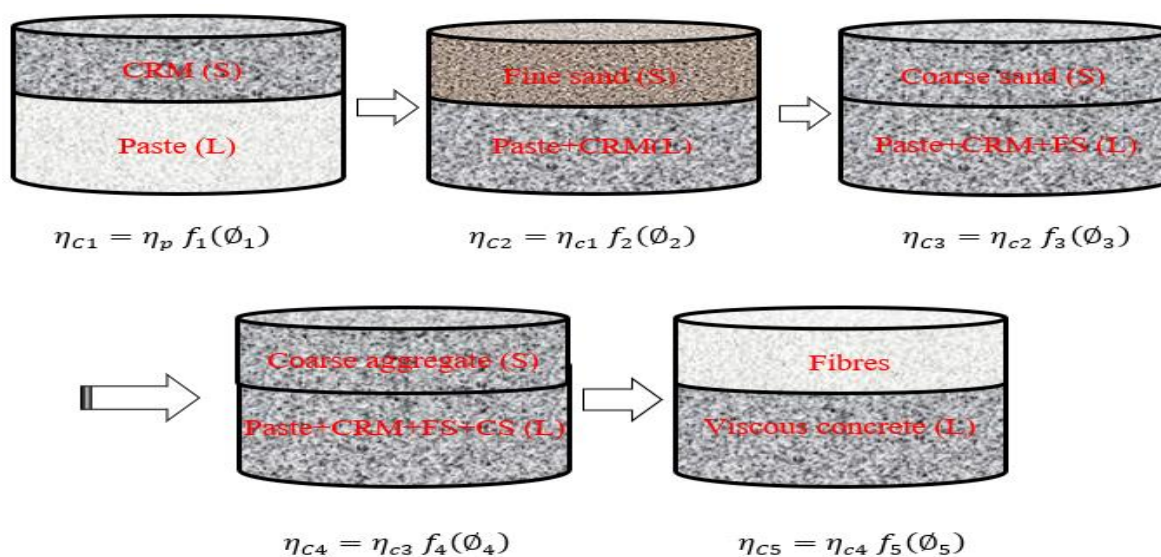


Figure 4.1: Hierarchy of two-phase liquid-solid suspensions constituting an SCC mix

According to this procedure, the plastic viscosity of an SCC mix is given by:

$$\eta_{mix} = \eta_{paste} \times f_1(\phi_1) * f_2(\phi_2) \dots \dots \dots f_n(\phi_n) \quad (4.3)$$

Where n is the total number of solid phases in the mix.

Besides the filler, fine, and coarse aggregates, air voids can also be treated as a second phase in a viscous suspension. Einstein was the first to develop an expression $f_i(\phi_i)$ for dilute suspensions (second phase volume fraction less than 10%) containing randomly distributed rigid or hollow spheres with no hydrodynamic interactions:

$$f_i(\phi_i) = 1 + [\eta]\phi_i \quad (4.4)$$

The numerical factor $[\eta]$ is equal to 2.5 for rigid spherical particles and to 1 for spherical air bubbles that are packed randomly in a hexagonal arrangement. Subsequent investigations have proved that the numerical factor 2.5 is quite accurate even for rigid ellipsoidal particles with an aspect ratio less than 3.

However, at higher concentrations of the solid phase (volume fraction $> 10\%$ up to the maximum possible volume fraction, ϕ_m), the hydrodynamic interactions between the particles and the Brownian motions cannot be ignored. In this situation, a formula proposed by (Krieger, 1959) has been found to be appropriate for cement-based suspensions :

$$f_i(\phi_i) = \left(1 - \frac{\phi_i}{\phi_m}\right)^{-[\eta]\phi_m} \quad (4.5)$$

The values of ϕ_m are 0.74 for hexagonal close packing, 0.63 for random hexagonal packing, and 0.524 for cubic packing. The particle size distribution significantly affects ϕ_m . Additionally, the numerical factor $[\eta]$ and ϕ_m depend upon the shear rate; the former tends to decrease with increasing shear rate, whereas the latter shows the opposite trend. However, $[\eta]$ and ϕ_m change in such a way that a decrease in the first leads to an increase in the second, but the product of both changes remains practically the same and equal, on average, to 1.9 (De Kruif et al., 1985).

In most SCC mixes, the volume fractions of the filler, fine, and coarse aggregates generally exceed 10%, so that their contribution to the increase in the known plastic viscosity of the paste is given by Eq. 4.5. The volume fraction of the trapped air bubbles is however low, around 2%, such that Eq. 4.4 with the numerical factor equal to 1 is appropriate. For simplicity, this 2% increase due to trapped air is included in the plastic viscosity of the paste, as in the following:

$$\eta_{eb} = \eta_{paste} \times \left(1 - \frac{\phi_{Filler}}{\phi_m}\right)^{-1.9} \times \left(1 - \frac{\phi_{Fine Agg.}}{\phi_m}\right)^{-1.9} \times \left(1 - \frac{\phi_{Coarse Agg.}}{\phi_m}\right)^{-1.9} \quad (4.6)$$

$$\eta_e = \eta_{eb} \times \left(1 + \frac{\pi\phi_f l_d^2}{3\ln(2l_d)}\right) \quad (4.7)$$

Where η_{eb} is the plastic viscosity of the viscous concrete mix without fibres given by Eq. (4.6), ϕ_f is the fibre volume fraction, and l_d is the length to diameter ratio (or aspect ratio) of the fibre.

In the final fluid-solid suspension, the increase in the viscosity induced by a dilute concentration of long steel fibres is estimated. In this context, the fibres are regarded as rigid slender bodies whose free translation and rotation are restrained by the viscous concrete mix (Ghanbari and Karihaloo, 2009). The plastic viscosity of SCC with fibres is given by:

$$\eta_e = \eta_{paste} \times \left(1 - \frac{\phi_{Filler}}{\phi_m}\right)^{-1.9} \times \left(1 - \frac{\phi_{Fine Agg.}}{\phi_m}\right)^{-1.9} \times \left(1 - \frac{\phi_{Coarse Agg.}}{\phi_m}\right)^{-1.9} \left(1 + \frac{\phi_f}{\phi_\lambda}\right) \quad (4.8)$$

Here, $\frac{3\ln(2l_d)}{\pi l_d^2}$. Note that the packing density (i.e., the maximum volume fraction, ϕ_m) increases with the addition of solid phases. When the first solid phase is added to the paste, the packing is loose so that it is appropriate to assume cubic packing. However, when the last solid phase is added to the suspension, the packing is very dense, and it is appropriate to assume hexagonal close packing. In addition, the target f_{cu} sets limits on permissible plastic viscosity range of the base SCC, η_{eb} , that complies with the imposed conditions (Dhaheer, Alyhya and Karihaloo, 2016b). In this respect, with the data of η_e and λ known, the maximum ($\eta_{eb\ max}$) and the minimum ($\eta_{eb\ min}$) values of plastic viscosity of the base SCC are obtained, from which the fibre volume fraction interval can be established, as observed by previous researchers (Grünewald and Walraven, 2001). This can be easily established by solving for ϕ_f in Eq. (4.7) and entering the two limits for η_{eb} :

The permissible interval for the fibre volume can also be estimated graphically. Figure 4.2 to Figure 4.6 presents the permissible range of the fibre content for a specific value of plastic viscosity of the SCSFRC for the compressive strengths of 30, 40, 50, 60 and 70 MPa.

$$\phi_{f \min} = \phi_{\lambda} \left(\frac{\eta_e}{\eta_{eb \min}} - 1 \right) \quad (4.9)$$

and

$$\phi_{f \max} = \phi_{\lambda} \left(\frac{\eta_e}{\eta_{eb \max}} - 1 \right) \quad (4.10)$$

Table 4.1: Minimum and maximum values of plastic viscosity of the SCC base for each compressive strength (de la Rosa et al., 2018a)

f_{cu} (MPa)	$\eta_{paste (min)}$ (Pa s)	$\eta_{paste (max)}$ (Pa s)
30	1.4	11.4
40	1.1	11.1
50	2	12
60	1.1	12.1
70	1.4	12.5

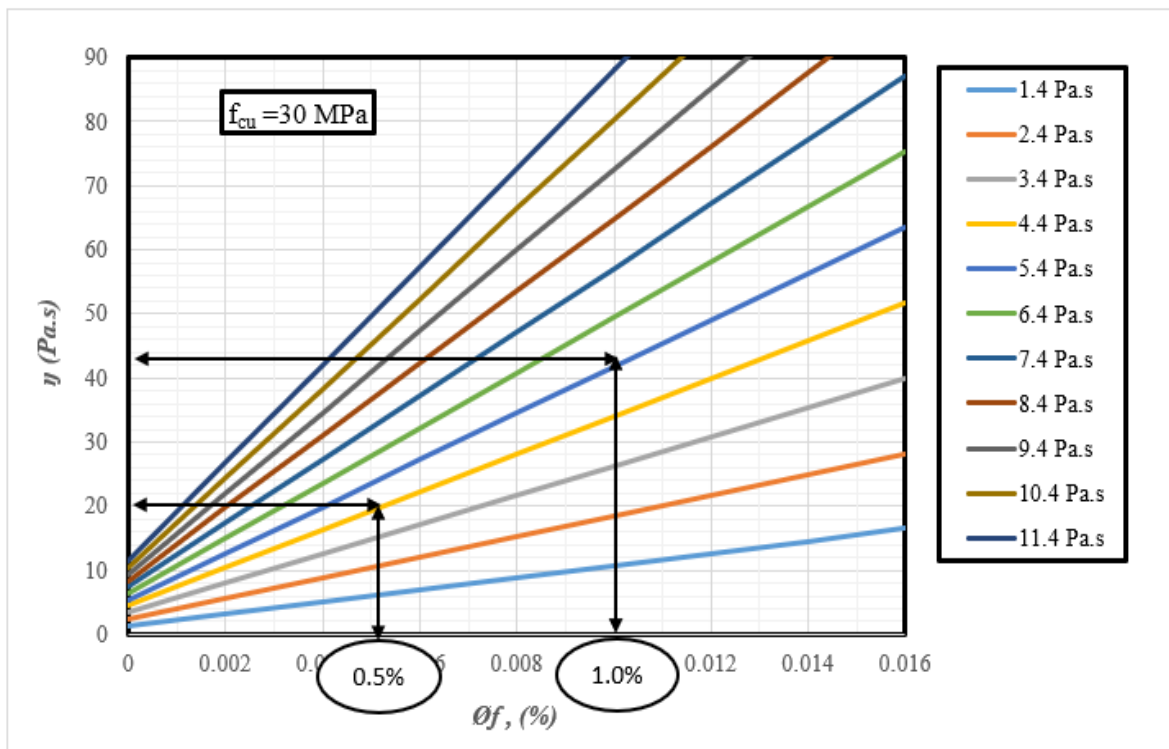


Figure 4.2: Relationship between steel fibre range and plastic viscosity of the SCC base from a plastic viscosity of SCSFRC for 30 MPa of compressive strength

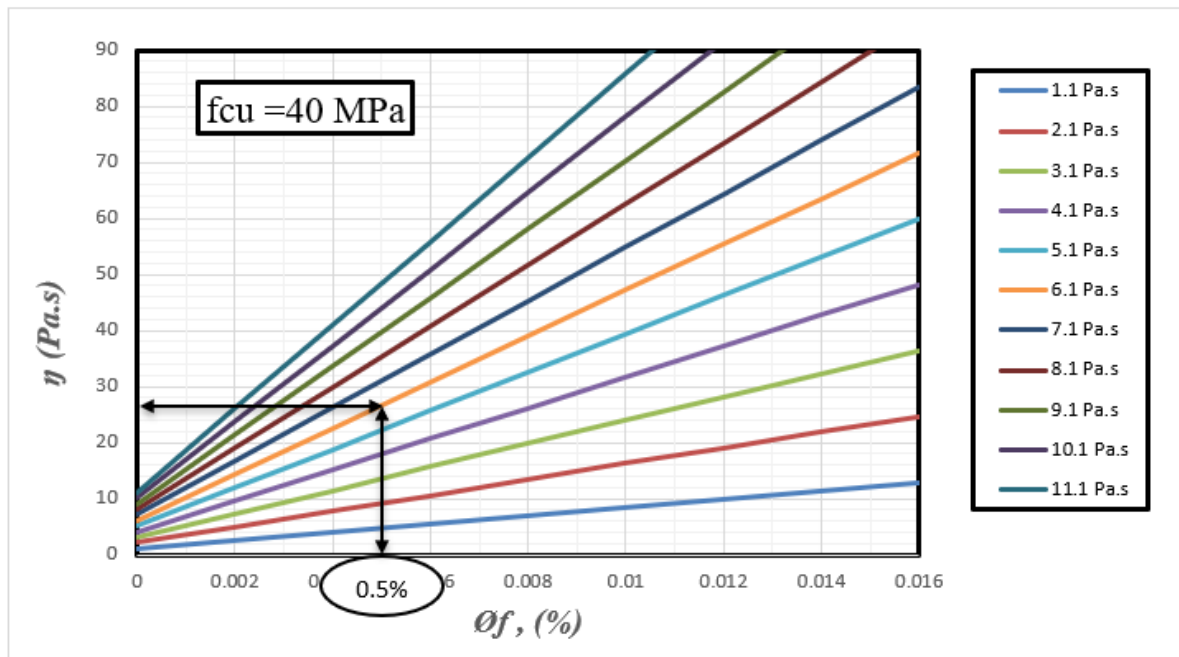


Figure 4.3: Relationship between steel fibre range and plastic viscosity of the SCC base from a plastic viscosity of SCSFRC for 40 MPa of compressive strength

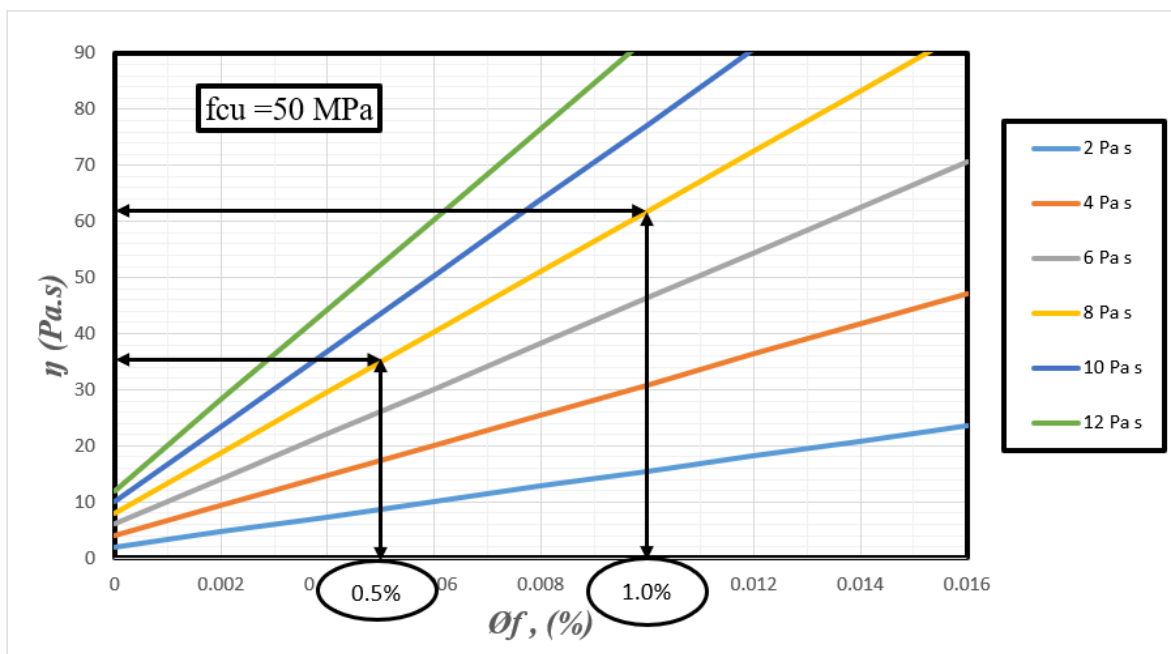


Figure 4.4: Relationship between steel fibre range and plastic viscosity of the SCC base from a plastic viscosity of SCSFRC for 50 MPa of compressive strength

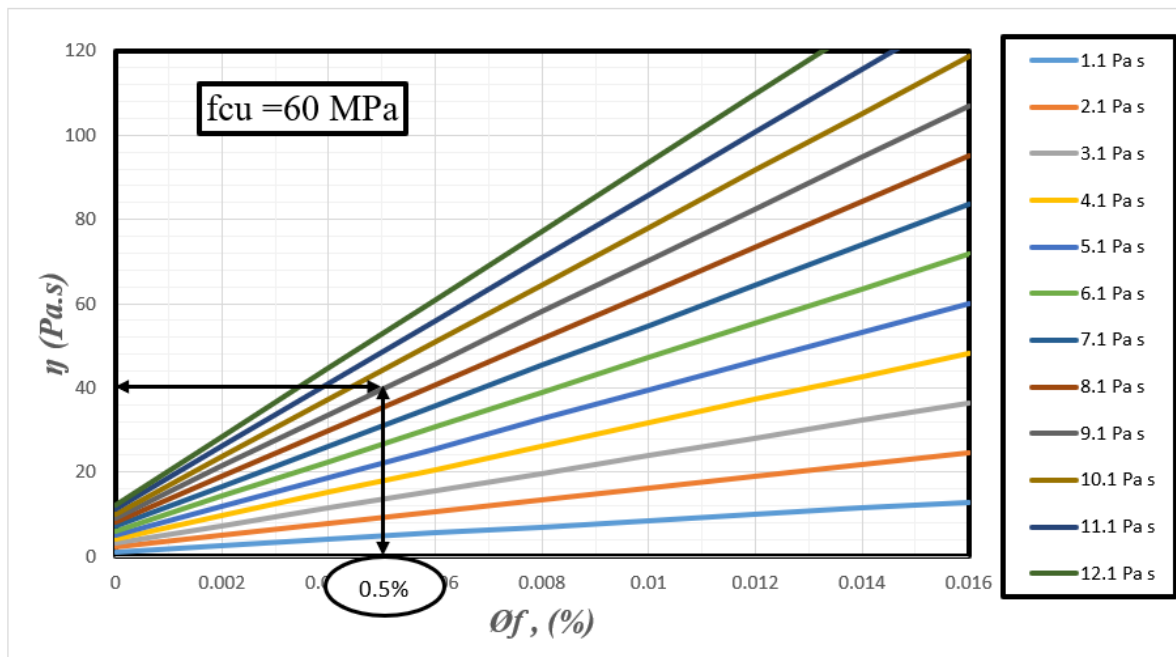


Figure 4.5: Relationship between steel fibre range and plastic viscosity of the SCC base from a plastic viscosity of SCSFRC for 60 MPa of compressive strength

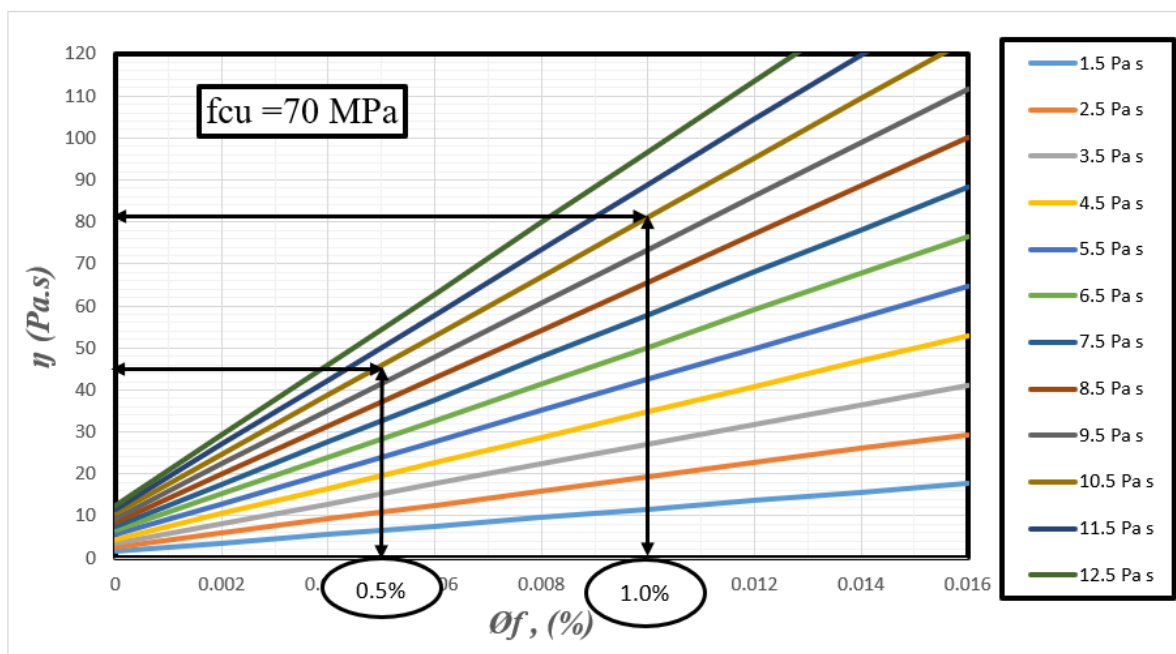


Figure 4.6: Relationship between steel fibre range and plastic viscosity of the SCC base from a plastic viscosity of SCSFRC for 70 MPa of compressive strength

4.4.1 An example calculation of plastic viscosity for mix with $f_{cu} = 30$ MPa

The calculation of the plastic viscosity will be demonstrated on a mix 30MPa without or with steel fibre (as it is designed in Chapter 6 & 7) as an example and it is the same procedure for all developed SCC without or with steel fibre mixes.

- **Plastic viscosity for 30 MPa (without steel fibre) mix**

Step 1: Estimating the plastic viscosity of the liquid phase (η_{paste})

The plastic viscosity of the cement paste (cement + ggbs + SP + water + air) is estimated by using the literature (Sun, Voigt and Shah, 2006) ; (Nehdi and Rahman, 2004) and it equals to 0.11 Pa s (see Table 4.2).

Table 4.2: Estimated plastic viscosity of the paste (cement +GGBS + SP + water + air)

f_{cu} (MPa)	w/cm	η_{paste} (Pa s)	$\eta_{paste+airvoids}$ (Pa s)
30	0.63	0.104	0.11
40	0.57	0.176	0.18
50	0.53	0.224	0.23
60	0.47	0.286	0.29
70	0.40	0.330	0.34

Step 2: Adding the first solid phase i.e., limestone powder (LP)

In this case, limestone powder (LP) is considered the solid phase and cement paste (cement + ggbs + SP + water + air) is the liquid phase. The volume fraction of the solid phase is determined using Eq. (4.11):

$$\phi_{LP} = \frac{v_{LP}}{v_{LP} + v_p} \quad (4.11)$$

Here, v_{LP} : is the volume fraction of the solid phase (limestone powder), v_p : is the volume of the continuous matrix phase (paste volume) in which the solid phase is suspended. After calculating the volume of each ingredient in the mix, the volume of paste is $v_p = 0.337 \text{ m}^3$, limestone powder is considered the solid phase and the components within the container are the liquid phase. The volume fraction of LP is:

$$\phi_{LP} = \frac{v_{LP}}{v_{LP} + v_p}$$

$$\phi_{LP} = \frac{0.066}{0.066 + 0.337} = 0.165 > 0.10$$

Using Eq. (4.5); $-[\eta]\phi_m = 1.9$, $\phi_m = 0.524$, gives;

$$f_{LP}(\phi_{LP}) = \left(1 - \frac{\phi_{LP}}{\phi_m}\right)^{-1.9} = \left(1 - \frac{0.165}{0.524}\right)^{-1.9} = 2.051$$

Based on Eq. (4.2); the plastic viscosity of the suspension is:

$$\eta_{(\phi_{LP+air+p})} = \eta_{paste} \times f_{LP}(\phi_{LP}) = 0.11 \times 2.051 = 0.226 \text{ Pa s}$$

Step 3: Adding the fine aggregate (FA)

Fine aggregate (FA) is now considered as the solid phase and the ingredients in the container as the liquid phase. The volume fraction of FA is

$$\phi_{FA} = 0.419 > 0.10$$

Using Eq. (4.5); $-[\eta]\phi_m = 1.9$, $\phi_m = 0.63$, gives;

$$f_{FA}(\phi_{FA}) = \left(1 - \frac{\phi_{FA}}{\phi_m}\right)^{-1.9} = \left(1 - \frac{0.419}{0.63}\right)^{-1.9} = 7.97$$

Based on Eq. (4.2); the plastic viscosity of the suspension is:

$$\eta_{(\phi_{FA+\phi_{LP+air+p}})} = \eta_{paste} \times f_{LP}(\phi_{LP}) \times f_{FA}(\phi_{FA}) = 0.11 \times 2.051 \times 7.97 = 1.80 \text{ Pa s}$$

Step 4: Adding the coarse aggregates (CA)

Coarse aggregates are now considered as the solid phase and the ingredients in the container as the liquid phase. The volume fraction of CA is

$$\phi_{CA} = 0.304 > 0.10$$

Using Eq. (4.5); $-[\eta]\phi_m = 1.9$, $\phi_m = 0.74$, gives;

$$f_{CA}(\phi_{CA}) = \left(1 - \frac{\phi_{CA}}{\phi_m}\right)^{-1.9} = \left(1 - \frac{0.304}{0.74}\right)^{-1.9} = 2.73$$

Based on Eq. (4.2); the plastic viscosity of the suspension is:

$$\begin{aligned} \eta_{(\phi_{CA+\phi_{FA+\phi_{LP+air+p}}})} &= \eta_{paste} \times f_{LP}(\phi_{LP}) \times f_{FA}(\phi_{FA}) \times f_{CA}(\phi_{CA}) \\ &= 0.11 \times 2.051 \times 7.97 \times 2.73 = 4.92 \text{ Pa s} \end{aligned}$$

The results of the plastic viscosity calculation of mix 30 MPa are summarised in Table 4.3.

Table 4.3: Summarising the results of the plastic viscosity calculation of mix 30MPa without steel fibre

Ingredients	Mass, kg/m ³	Volume, m ³	ϕ	f(ϕ)
Paste	--	0.337	--	--
Limestone powder	160	0.066	0.165	2.05
Fine Aggregate	772	0.291	0.419	7.97
Coarse Aggregate	851	0.304	0.304	2.73

- **Plastic viscosity for 30 MPa mix with steel fibre**

Step 1: Estimating the plastic viscosity of the liquid phase (η_{paste})

$$(\eta_{paste}) = 0.11$$

Step 2: Adding the first solid phase i.e., limestone powder (LP)

In this case, limestone powder (LP) is considered the solid phase and cement paste (cement + ggbs + SP + water + air) is the liquid phase. The volume fraction of the solid phase is determined using Eq. (4.11):

$$\phi_{LP} = \frac{v_{LP}}{v_{LP} + v_p}$$

Here, v_{LP} : is the volume fraction of the solid phase (limestone powder), v_p : is the volume of the continuous matrix phase (paste volume) in which the solid phase is suspended. After calculating the volume of each ingredient in the mix, the volume of paste is $v_p = 0.344 \text{ m}^3$, limestone powder is considered the solid phase and the components within the container are the liquid phase. The volume fraction of LP is:

$$\phi_{LP} = \frac{v_{LP}}{v_{LP} + v_p}$$

$$\phi_{LP} = \frac{0.066}{0.066+0.344} = 0.161 > 0.10$$

Using Eq. (4.5); $-[\eta]\phi_m = 1.9$, $\phi_m = 0.524$, gives;

$$f_{LP}(\phi_{LP}) = \left(1 - \frac{\phi_{LP}}{\phi_m}\right)^{-1.9} = \left(1 - \frac{0.161}{0.524}\right)^{-1.9} = 2.008$$

Based on Eq. (4.2); the plastic viscosity of the suspension is:

$$\eta_{(\phi_{LP+air+p})} = \eta_{paste} \times f_{LP}(\phi_{LP}) = 0.11 \times 2.008 = 0.221 \text{ Pa s}$$

Step 3: Adding the fine aggregate (FA)

Fine aggregate (FA) is now considered as the solid phase and the ingredients in the container as the liquid phase. The volume fraction of FA is

$$\phi_{FA} = 0.414 > 0.10$$

Using Eq. (4.5); $-[\eta]\phi_m = 1.9$, $\phi_m = 0.63$, gives;

$$f_{FA}(\phi_{FA}) = \left(1 - \frac{\phi_{FA}}{\phi_m}\right)^{-1.9} = \left(1 - \frac{0.414}{0.63}\right)^{-1.9} = 7.67$$

Based on Eq. (4.2); the plastic viscosity of the suspension is:

$$\eta_{(\phi_{FA}+\phi_{LP+air+p})} = \eta_{paste} \times f_{LP}(\phi_{LP}) \times f_{FA}(\phi_{FA}) = 0.11 \times 2.008 \times 7.67 = 1.69 \text{ Pa s}$$

Step 4: Adding the coarse aggregates (CA)

Coarse aggregates are now considered as the solid phase and the ingredients in the container as the liquid phase. The volume fraction of CA is

$$\phi_{CA} = 0.297 > 0.10$$

Using Eq. (4.5); $-[\eta]\phi_m = 1.9$, $\phi_m = 0.74$, gives;

$$f_{CA}(\phi_{CA}) = \left(1 - \frac{\phi_{CA}}{\phi_m}\right)^{-1.9} = \left(1 - \frac{0.304}{0.74}\right)^{-1.9} = 2.64$$

Based on Eq. (4.2); the plastic viscosity of the suspension is:

$$\begin{aligned} \eta_{(\phi_{CA}+\phi_{FA}+\phi_{LP+air+p})} &= \eta_{paste} \times f_{LP}(\phi_{LP}) \times f_{FA}(\phi_{FA}) \times f_{CA}(\phi_{CA}) \\ &= 0.11 \times 2.051 \times 7.97 \times 2.73 = 4.49 \text{ Pa s} \end{aligned}$$

Step 5: Adding the steel fibre (SF)

The formula used to determine the plastic viscosity of a mix containing fibres represented in the Equation (4.7) as proposed by (Ghanbari and Karihaloo, 2009).

$$\eta_{scsf}(\text{max}) = \eta_{SCC}(\text{max}) \times \left(1 + \frac{\pi\phi_f l_d^2}{3 \ln(2l_d)}\right)$$

Using Eq. (4.5); $[\eta]\phi_\lambda$, $\phi_\lambda = \frac{3 \ln(2\lambda)}{\pi\lambda^2} = \frac{3 \ln(2*55)}{\pi*55^2} = 0.0015$, gives;

$$f_{SF}(\phi_{SF}) = \left(1 + \frac{\phi_{sf}}{\phi_{\lambda}}\right) = \left(1 + \frac{\pi\phi_{sf}l_d^2}{3\ln(2l_d)}\right) = 4.42$$

Based on Eq. (4.2); the plastic viscosity of the suspension is:

$$\eta_{(\phi_{SF}+\phi_{CA}+\phi_{FA}+\phi_{LP}+air+p)} = \eta_{paste} \times f_{LP}(\phi_{LP}) \times f_{FA}(\phi_{FA}) \times f_{CA}(\phi_{CA}) \times f_{SF}(\phi_{SF}) = 0.11 \times 2.008 \times 7.67 \times 2.64 \times 4.42 = 19.67 Pa s \text{ (Figure 4.2)}$$

The results of the plastic viscosity calculation of mix 30 are summarised in Table 4.4.

Table 4.4: Summarising the results of the plastic viscosity calculation of mix 30MPa with steel fibre

Ingredients	Mass, kg/m ³	Volume, m ³	ϕ	$f(\phi)$
Paste	--	0.344	--	--
Limestone powder	158	0.066	0.165	2.05
Fine Aggregate	768	0.290	0.419	7.97
Coarse Aggregate	827	0.295	0.304	2.73
Steel fibre	40	0.005	--	--

4.5 Examples demonstrating the use of design charts

Thousands of solid phase volume fraction combinations were produced using a software program. These combinations covered wide ranges of target cube compressive strength and mix plastic viscosity. They have been collected in groups according to the target strength for ease of SCC mixture proportioning. It was found convenient for presentation of a huge body of data to normalize the amount of dry phases by the plastic viscosity and to present the amounts in separate plots, beginning with the cementitious materials (cm), and ending with the content of all dry phases (cm + LP + FA + CA). These design charts are given in Figure 4.7 - Figure 4.10. The scatter reflects the multiplicity of combinations. It is, however, interesting to note that the scatter is the least in the bottom (cm) and the top (cm + LP + FA + CA) curves. This is because the amount of cm calculated from the target compressive strength is according to the water content which varies in the narrow range of 150–210 l/m³, (EFNARC, 2005) and the amounts of all dry ingredients contribute to the target plastic viscosity of the mix.

In order to demonstrate how easy it is to use the design charts (Figure 4.7 - Figure 4.10) , assume we wish to design an SCC without and with steel fibre mix with a target cube compressive strength of 70 MPa - 30 MPa.

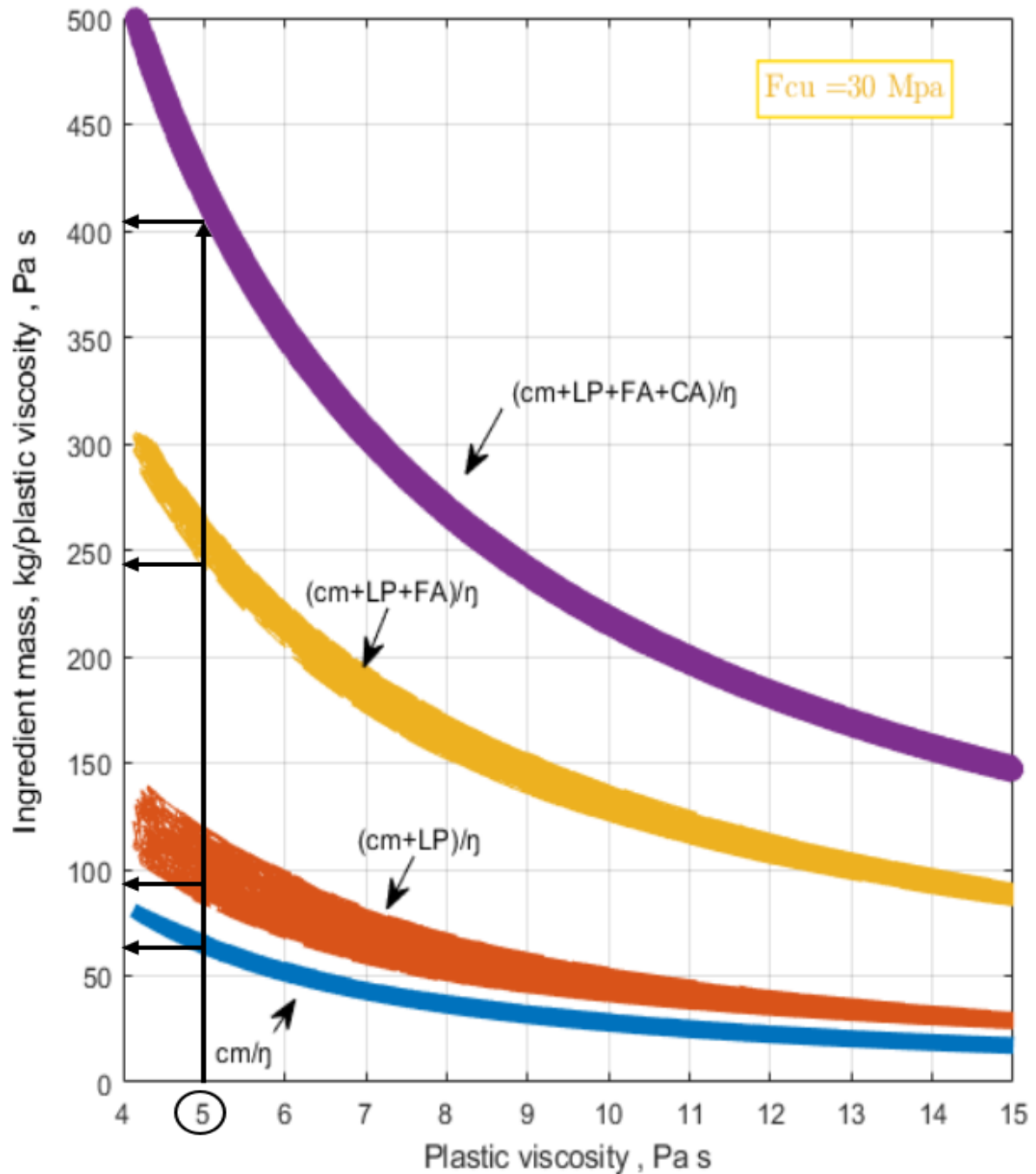


Figure 4.7: Design chart for 30 MPa of the SCC base

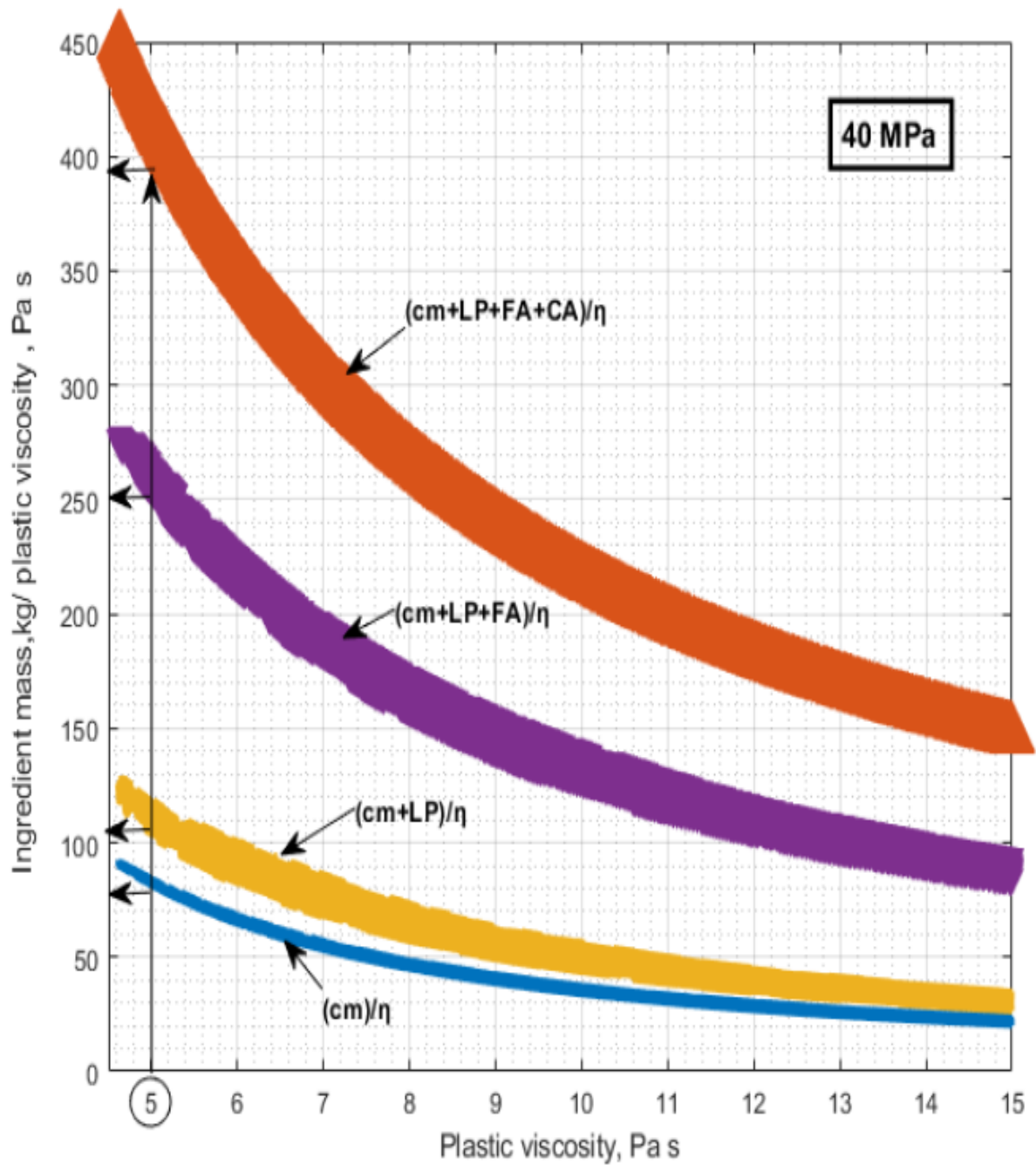


Figure 4.8: Design chart for 40 MPa of the SCC base

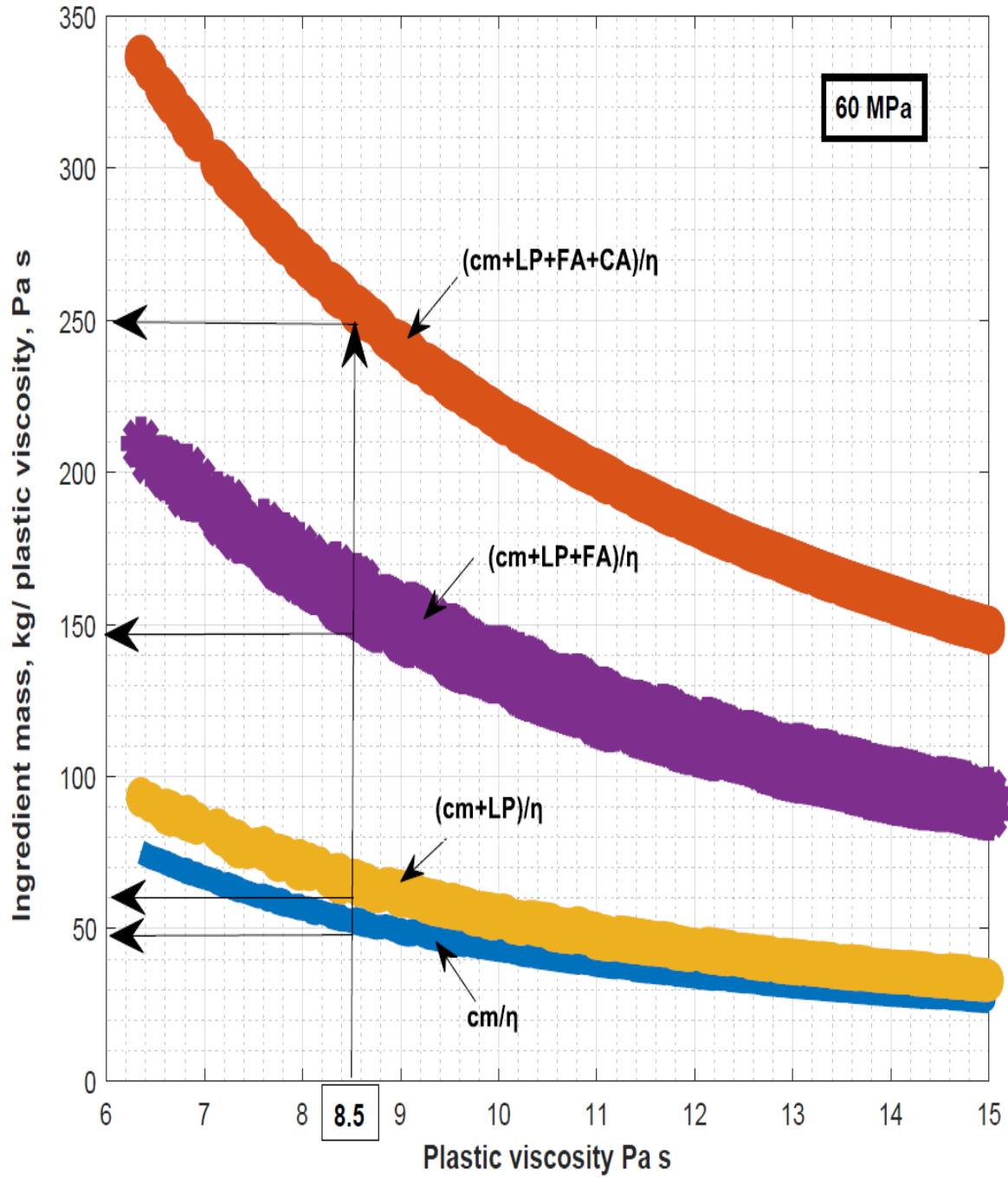


Figure 4.9: Design chart for 60 MPa of the SCC base

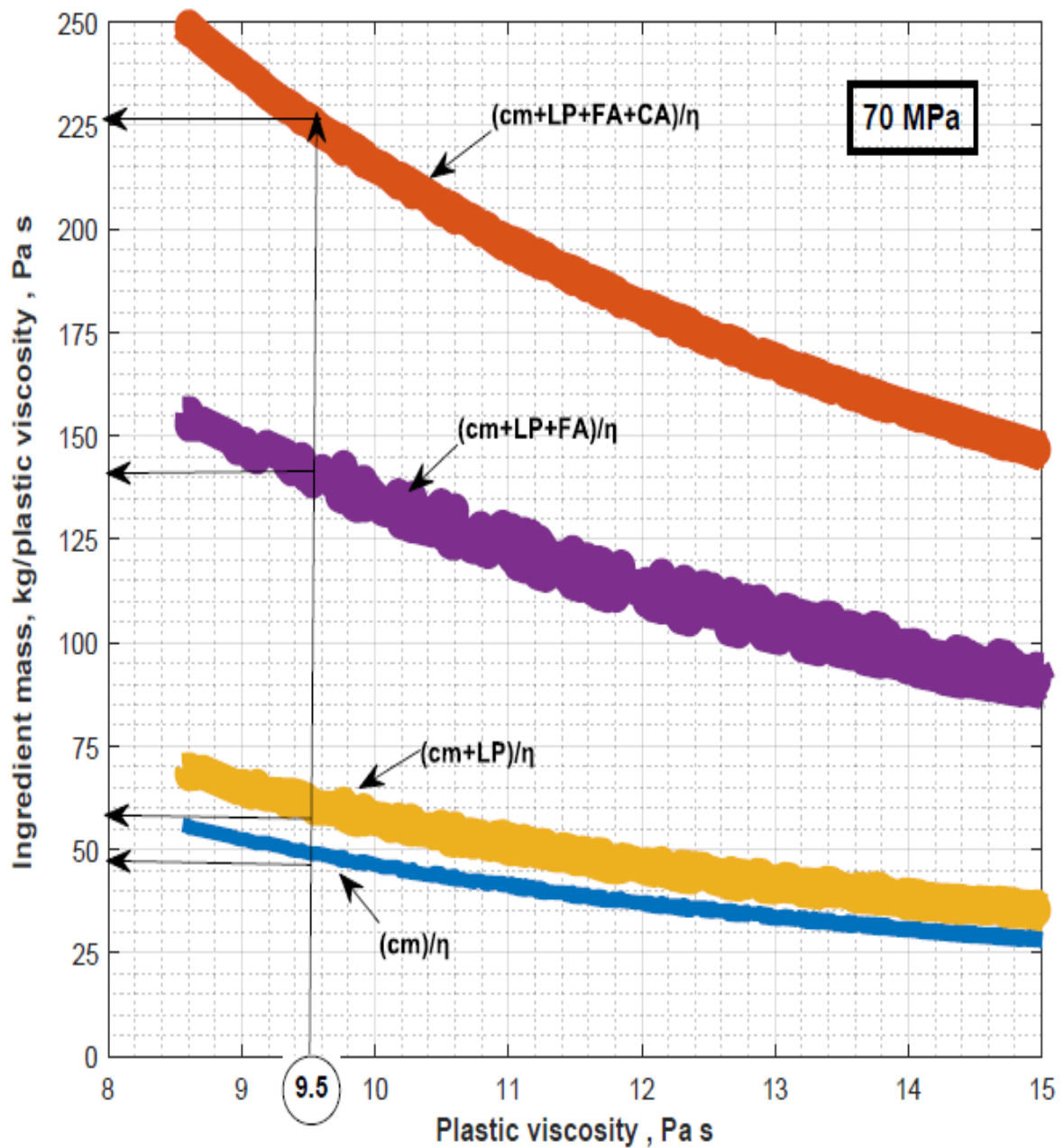


Figure 4.10: Design chart for 70 MPa of the SCC base

4.6 Proposed mix-design charts method for SCC and SCSFRC

The basic steps of the proposed mix design method are summarized below.

- 1- Select the desired plastic viscosity of the SCC and SCSFRC mix within the range of 5–85 Pa s, remembering that the slump flow t_{500} time increases with increasing plastic viscosity

- of the mix. The EFNARC guidelines (EFNARC, 2005) will be helpful in the choice of the desired plastic viscosity depending on the application.
- 2- Calculate the ratio of water to cementitious materials (w/cm) that produces the target cube characteristic strength from Eq. (4.1).
 - 3- Choose the water content in the range of 150–210 kg/m³, following EFNARC guidelines,(EFNARC, 2005) and calculate the mass of cementitious materials (cm) in kg/m³. The amount of ggbs is assumed to be 25% of cementitious material (cm). It is known that the replacement of 25% cement (c) by ggbs has little or no effect on the paste viscosity (Nehdi and Rahman, 2004).
 - 4- Assume a trial super-plasticizer (SP) dosage as a percent of the cementitious material mass in the range of 0.4–0.8% for the MasterGlenium super-plasticizer used in this work. For this super-plasticizer, the manufacturer’s recommended dosage is 0.2–1.2 kg per 100 kg of cementitious material (Solutions, 2016);
 - 5- Estimate the plastic viscosity of the paste from the w/cm and SP/ cm ratios (Sun, Voigt and Shah, 2006) (see Table 4.2). It is known that SP/cm has little impact on the paste viscosity; the major impact is on the yield stress (Dransfield J, 1967) ;
 - 6- Calculate the mass of the solid phase ingredients (filler, fine aggregate, and coarse aggregate) according to their volume fractions, as explained in the examples below.
 - 7- Choose a fibre content, ϕ_f , within the permissible range for the desired SCSFRC. From the values of the η_{\max} and η_{\min} and Eqs. (4.9) and (4.10), calculate the permissible limits for ϕ_f , $\phi_{f\min}$ and $\phi_{f\max}$, respectively. Table 4.1 gives the values for η_{\max} and η_{\min} . They vary in accordance with the plastic viscosity of the cement paste and the compressive strength. The values of η_{\min} in Table 4.1 are the same from 30 to 70 MPa, because the values of the plastic viscosity of the cement paste are very close.
 - 8- Check if the total volume of the produced mix is equal to 1 m³. If not, scale the ingredient masses to achieve a total volume of 1 m³.
 - 9- Calculate the plastic viscosity of the SCC or SCSFC mix using Eq. (4.6 or 4.8) and compare it with the desired one (step 1). If the difference is within $\pm 5\%$, adopt the mix proportions. If not, choose a different combination of the volume fractions of the solid phase ingredients (step 6), and repeat steps 7–8.

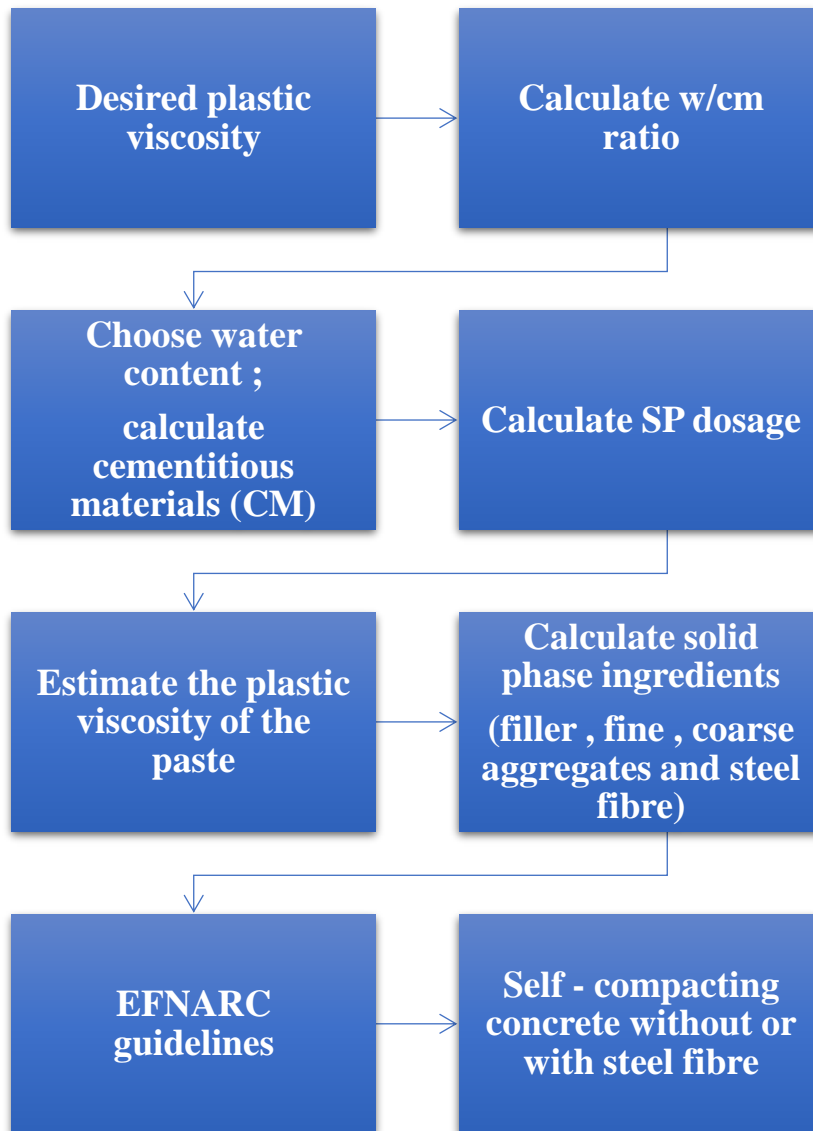


Figure 4.11: Mixture design method of SCC without and with steel fibre

4.6.1 An example calculation for designing 50 MPa mix (without fibre) using chart

- Suppose the desired target plastic viscosity of mix is 7 Pa s.
- For the desired target strength = 50 MPa \rightarrow w/cm = 0.53 (Equation 4.1);
- Calculate the cementitious material content (cm); (Figure 4.12)

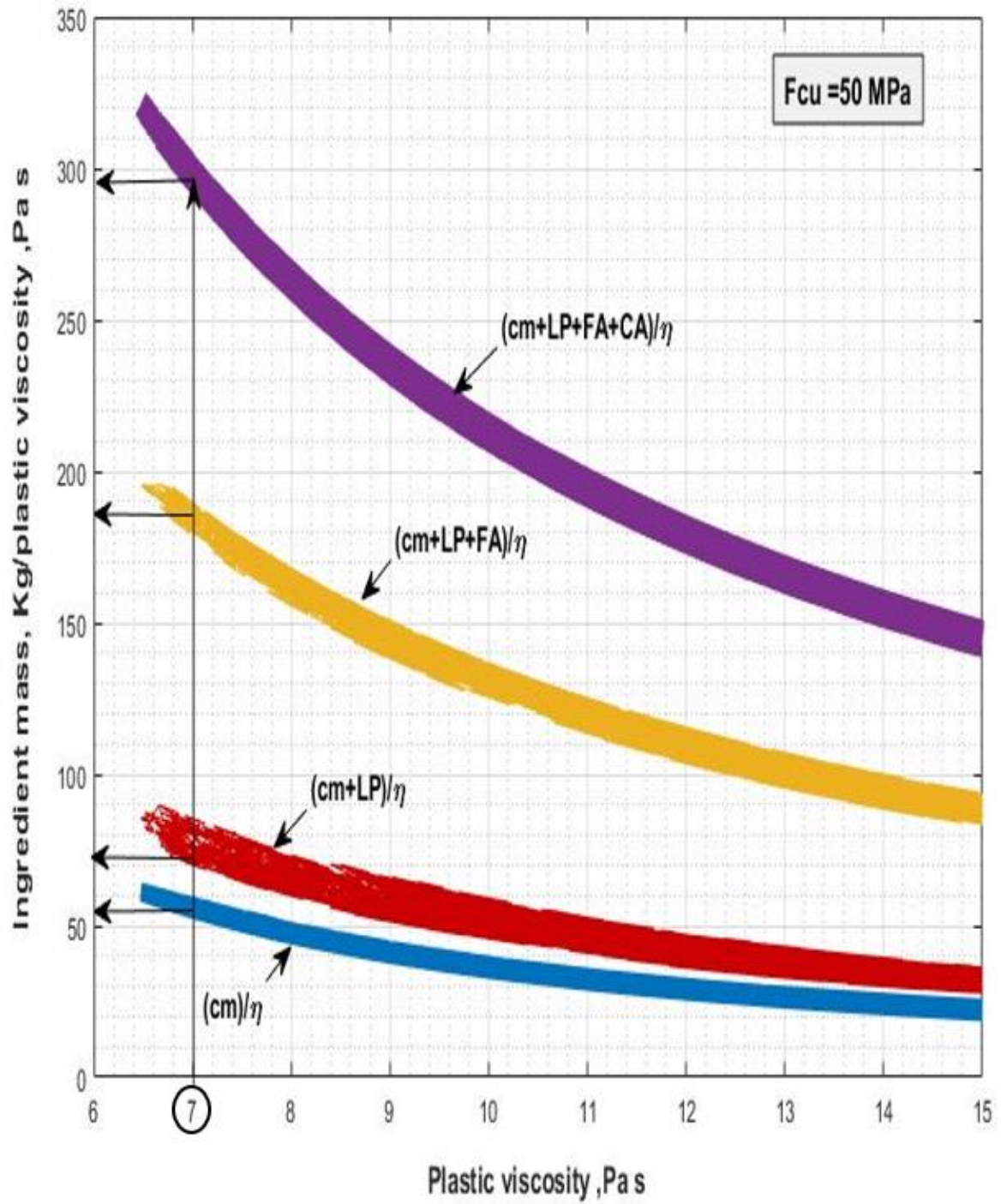


Figure 4.12: Design chart for 50 MPa of the SCC base

$$\text{For } \eta_{mix} = 7 \text{ Pa s} \rightarrow \frac{cm}{\eta} = 55.5 \text{ (bottom curve)} \rightarrow cm = 55.5 \times 7$$

$$= 388.5 \text{ Kg/m}^3$$

$$C = 0.75 \times 388.5 = 291.375 \text{ Kg/m}^3$$

$$GGBS = 0.25 \times 388.5 = 97.125 \text{ Kg/m}^3$$

$$\text{As } \frac{w}{cm} = 0.53 \rightarrow w = 0.53 \times 388.5 = 205.91 \text{ kg/m}^3$$

- Assume a trial super-plasticizer dosage (super-plasticizer mass, SP) as a percent of mass of cementitious materials (say 0.65%), which equals to 3 kg/m^3 .
- The plastic viscosity of the paste according to its w/cm and SP/cm ratios is equal to 0.23 (Table 4.2);
- Calculate the solid phase ingredient contents (LP, FA, and CA);

$$\text{For } \eta_{mix} = 7 \text{ Pa s} \rightarrow \frac{cm + LP}{\eta} = 75 \text{ (second curve from bottom)} \rightarrow (cm + LP)$$

$$= 75 \times 7 = 525 \text{ Kg/m}^3 \rightarrow LP = 525 - 388.5 = 136.5 \text{ Kg/m}^3$$

$$\frac{cm + LP + FA}{\eta} = 180 \text{ (second curve from top)} \rightarrow (cm + LP + FA) = 180 \times 7$$

$$= 1260 \text{ Kg/m}^3 \rightarrow FA = 1260 - 388.5 - 136.5 = 735 \text{ Kg/m}^3$$

$$\frac{cm + LP + FA + CA}{\eta} = 305 \text{ (top curve)} \rightarrow (cm + LP + FA + CA) = 305 \times 7$$

$$= 2135 \text{ Kg/m}^3 \rightarrow CA = 2135 - 735 - 388.5 - 136.5$$

$$= 875 \text{ Kg/m}^3$$

- Calculate the total volume of the mix.

$$C = 388.5 * 0.75 = 291.37 \text{ Kg/m}^3 \rightarrow 291.37 * \frac{100}{85} = 342.78 \text{ Kg/m}^3$$

$$\rightarrow 342.78 - 291.37 = 51.41 \text{ Kg/m}^3$$

$$LP = 136.5 - 51.41 = 85.08 \text{ Kg/m}^3$$

$$GGBS = 388.5 * 0.25 = 97.125 \text{ Kg/m}^3$$

$$\text{Total volume} = \left(\frac{c}{\rho_C} + \frac{ggbs}{\rho_{ggbs}} + \frac{w}{\rho_w} + \frac{SP}{\rho_{sp}} + \frac{LP}{\rho_{LP}} + \frac{FA}{\rho_{FA}} + \frac{CA}{\rho_{CA}} + 0.02 \right)$$

$$\text{Total volume} = \left(\frac{291.37}{2950} + \frac{97.125}{2400} + \frac{205.91}{1000} + \frac{3}{1070} + \frac{85.08}{2400} + \frac{735}{2650} + \frac{875}{2800} \right.$$

$$\left. + 0.02 \right) = 0.9933 \text{ m}^3$$

As the yield does not equal 1 m³, the amounts of material are adjusted, and the mix plastic viscosity is recalculated using Equation (4.6).

$$cm = 291.375 / 0.9933 = 293.35 \text{ kg/m}^3$$

$$GGBS = 97.125 / 0.9933 = 97.78 \text{ kg/m}^3$$

$$w = 205.91 / 0.9933 = 207.30 \text{ kg/m}^3$$

$$SP = 3 / 0.9933 = 3.02 \text{ kg/m}^3$$

$$LP = 85.08 / 0.9933 = 85.65 \text{ kg/m}^3$$

$$FA = 735 / 0.9933 = 739.98 \text{ kg/m}^3$$

$$CA = 875 / 0.9933 = 880.94 \text{ kg/m}^3$$

$$\text{Total volume} = \left(\frac{c}{\rho_c} + \frac{ggbs}{\rho_{ggbs}} + \frac{w}{\rho_w} + \frac{SP}{\rho_{sp}} + \frac{LP}{\rho_{LP}} + \frac{FA}{\rho_{FA}} + \frac{CA}{\rho_{CA}} + 0.02 \right) = 1.000 \text{ m}^3$$

$$\begin{aligned} \text{Total volume} = & \left(\frac{293.35}{2950} + \frac{97.78}{2400} + \frac{207.30}{1000} + \frac{3.02}{1070} + \frac{85.65}{2400} + \frac{739.98}{2650} + \frac{880.94}{2800} \right. \\ & \left. + 0.02 \right) = 1.000 \text{ m}^3 \end{aligned}$$

- Calculate the volume fractions of solid phases; 2950, 2400, 1000, 1070, 2400, 2650, and 2800 kg/m³

$$\phi_{LP} = \frac{\frac{85.65}{2400}}{\left(\frac{293.35}{2950} + \frac{97.78}{2400} + \frac{207.30}{1000} + \frac{3.02}{1070} + 0.02 \right) + \frac{85.65}{2400}} = 0.087$$

$$\phi_{FA} = \frac{\frac{739.98}{2650}}{\left(\frac{293.35}{2950} + \frac{97.78}{2400} + \frac{207.30}{1000} + \frac{3.02}{1070} + \frac{85.65}{2400} + 0.02 \right) + \frac{739.98}{2650}} = 0.407$$

$$\begin{aligned} \phi_{CA} &= \frac{\frac{880.94}{2800}}{\left(\frac{293.35}{2950} + \frac{97.78}{2400} + \frac{207.30}{1000} + \frac{3.02}{1070} + \frac{85.65}{2400} + \frac{739.98}{2650} + 0.02 \right) + \frac{880.94}{2800}} \\ &= 0.314 \end{aligned}$$

- Check the plastic viscosity using Equation (4.6).

$$\eta_{mix} = \eta_{paste} \times \left(1 - \frac{\phi_{LP}}{\phi_m} \right)^{-1.9} \times \left(1 - \frac{\phi_{FA}}{\phi_m} \right)^{-1.9} \times \left(1 - \frac{\phi_{CA}}{\phi_m} \right)^{-1.9}$$

$$\eta_{mix} = 0.23 \times \left(1 - \frac{0.087}{0.524} \right)^{-1.9} \times \left(1 - \frac{0.407}{0.63} \right)^{-1.9} \times \left(1 - \frac{0.314}{0.74} \right)^{-1.9} = 6.75 \text{ Pa.s}$$

$$\text{Viscosity diff.} = \frac{(\text{Calculated } \eta_{mix} - \text{Target } \eta_{mix})}{\text{Target } \eta_{mix}} \times 100$$

$$\text{Viscosity diff.} = \frac{(6.75 - 7)}{7} \times 100 = -3.6 \%$$

The actual mix plastic viscosity is within $\pm 5\%$, the mix proportions are acceptable.

Table 4.5: Mix constituents and plastic viscosity of an SCC mix

Ingredient (kg/m ³)									
	Cement	ggs	w	SP	LP	FA	CA	η (pa s)	Difference
Design Mix	293	98	207	3	86	740	881	6.75 Pa.s	-3.6%
Density	2950	2400	1000	1070	2400	2650	2800	-	

4.6.2 An example calculation for designing 70 MPa mix with 0.5% of steel fibre

- Suppose further that the desired target plastic viscosity of the SCSFRC is 45 Pa s.
- For the desired target strength = 70 MPa \rightarrow w/cm = 0.40 (Equation 4.1);
- Calculate the cementitious material content (cm); (Figure 4.13)

$$\text{For } \eta_{mix} = 10.5 \text{ Pa s} \rightarrow \frac{cm}{\eta} = 44 \text{ (bottom curve)} \rightarrow cm = 44 \times 10.5$$

$$= 462 \text{ Kg/m}^3$$

$$C = 0.75 \times 462 = 346.5 \text{ Kg/m}^3$$

$$GGBS = 0.25 \times 462 = 115.5 \text{ Kg/m}^3$$

$$\text{As } \frac{w}{cm} = 0.40 \rightarrow w = 0.40 \times 462 = 184.8 \text{ kg/m}^3$$

- Assume a trial super-plasticizer dosage (super-plasticizer mass, SP) as a percent of mass of cementitious materials (say 0.65%), which equals to 3 kg/m³;
- The plastic viscosity of the paste according to its w/cm and SP/cm ratios is equal to 0.34 (Table 4.2);
- Calculate the solid phase ingredient contents (LP, FA, and CA) ;

$$\text{For } \eta_{mix} = 10.5 \text{ Pa s} \rightarrow \frac{cm + LP}{\eta} = 60 \text{ (second curve from bottom)}$$

$$\rightarrow (cm + LP) = 60 \times 10.5 = 630 \text{ Kg/m}^3 \rightarrow LP = 630 - 462$$

$$= 168 \text{ Kg/m}^3$$

$$\frac{cm + LP + FA}{\eta} = 130 \text{ (second curve from top)} \rightarrow (cm + LP + FA) = 130 \times 10.5$$

$$= 1365 \text{ Kg/m}^3 \rightarrow FA = 1365 - 462 - 168 = 735 \text{ Kg/m}^3$$

$$\frac{cm + LP + FA + CA}{\eta} = 210 \text{ (top curve)} \rightarrow (cm + LP + FA + CA) = 210 \times 10.5$$

$$= 2205 \text{ Kg/m}^3 \rightarrow FA = 2205 - 462 - 735 - 168 = 840 \text{ Kg/m}^3$$

- Calculate the steel fibre contents (SF).

$$m_f = \rho_f \phi_f = 7850 \times 0.005 = 39.25 \text{ kg / m}^3$$

- Calculate the total volume of the mix.

$$\text{Total volume} = \left(\frac{c}{\rho_c} + \frac{ggbs}{\rho_{ggbs}} + \frac{w}{\rho_w} + \frac{SP}{\rho_{sp}} + \frac{LP}{\rho_{LP}} + \frac{FA}{\rho_{FA}} + \frac{CA}{\rho_{CA}} + \frac{SF}{\rho_{sf}} + 0.02 \right)$$

$$\text{Total volume} =$$

$$= \left(\frac{346.5}{2950} + \frac{115.5}{2400} + \frac{184.8}{1000} + \frac{3.003}{1070} + \frac{168}{2400} + \frac{735}{2650} + \frac{840}{2800} + \frac{39.25}{7850} + 0.02 \right)$$

$$= 1.026 \text{ m}^3$$

As the yield does not equal 1 m³, the amounts of material are adjusted, and the mix plastic viscosity is recalculated using Equation (4.6).

$$cm = 346.5 * 1.026 = 338 \text{ kg/m}^3$$

$$GGBS = 115.5 * 1.026 = 112.55 \text{ kg/m}^3$$

$$w = 184.8 * 1.026 = 180 \text{ kg/m}^3$$

$$SP = 3.003 * 1.026 = 2.9 \text{ kg/m}^3$$

$$LP = 168 * 1.026 = 164 \text{ kg/m}^3$$

$$FA = 735 * 1.026 = 716 \text{ kg/m}^3$$

$$CA = 840 * 1.026 = 819 \text{ kg/m}^3$$

$$SF = 39.25 * 1.026 = 38 \text{ kg/m}^3$$

$$\text{Total volume} = \left(\frac{338}{2950} + \frac{112.55}{2400} + \frac{180}{1000} + \frac{2.9}{1070} + \frac{164}{2400} + \frac{716}{2650} + \frac{819}{2800} + \frac{38}{7850} \right.$$

$$\left. + 0.02 \right) = 1.000 \text{ m}^3$$

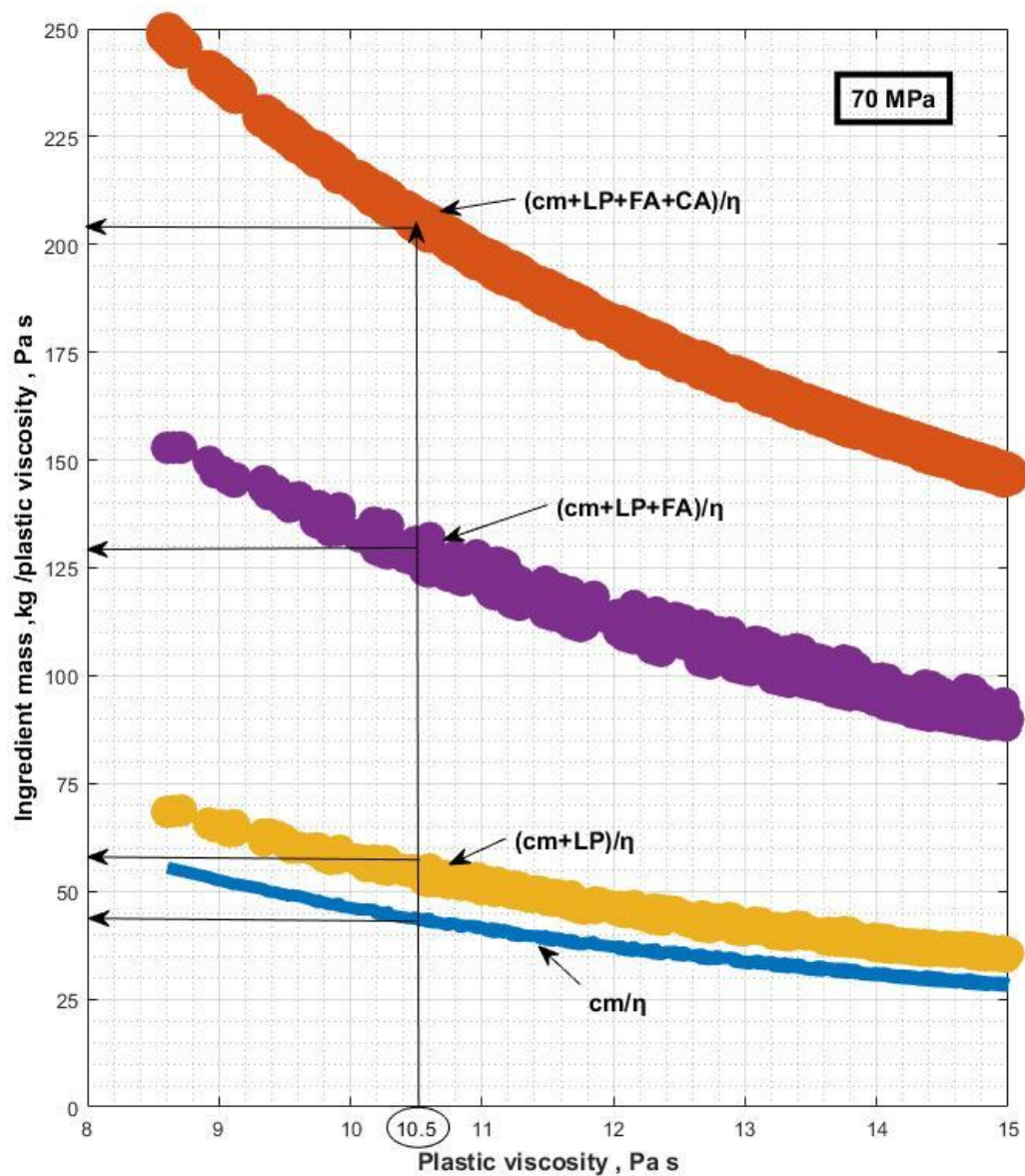


Figure 4.13: Design chart for 70 MPa of the SCSFRC base

- Check the plastic viscosity using Equation (4.6); For this purpose, the volume fractions of solid phases that are suspended in a viscous phase should be calculated.

$$\phi_{LP} = \frac{\frac{LP}{\rho_{LP}}}{\left(\frac{c}{\rho_C} + \frac{w}{\rho_w} + \frac{SP}{\rho_{SP}} + \frac{LP}{\rho_{LP}} + \frac{m_f}{\rho_{CA}} + 0.02\right)} = 0.158$$

$$\Phi_{FA} = \frac{\frac{FA}{\rho_{FA}}}{\left(\frac{c}{\rho_C} + \frac{w}{\rho_w} + \frac{SP}{\rho_{sp}} + \frac{LP}{\rho_{LP}} + \frac{FA}{\rho_{FA}} + 0.02\right)} = 0.385$$

$$\Phi_{CA} = \frac{\frac{CA}{\rho_{CA}}}{\left(\frac{c}{\rho_C} + \frac{w}{\rho_w} + \frac{SP}{\rho_{sp}} + \frac{LP}{\rho_{LP}} + \frac{FA}{\rho_{FA}} + \frac{CA}{\rho_{CA}} + 0.02\right)} = 0.294$$

$$\Phi_{sf} = \frac{\frac{SF}{\rho_{SF}}}{\left(\frac{c}{\rho_C} + \frac{w}{\rho_w} + \frac{SP}{\rho_{sp}} + \frac{LP}{\rho_{LP}} + \frac{FA}{\rho_{FA}} + \frac{CA}{\rho_{CA}} + \frac{SF}{\rho_{SF}} + 0.02\right)} = 0.0049$$

The calculated plastic viscosity η_{eb} according to Eq. (4.6) is η_{eb}

$$\eta_{max (SCC)} = \eta_{paste} \times \left(1 - \frac{\Phi_{LP}}{\Phi_m}\right)^{-1.9} \times \left(1 - \frac{\Phi_{FA}}{\Phi_m}\right)^{-1.9} \times \left(1 - \frac{\Phi_{CA}}{\Phi_m}\right)^{-1.9}$$

$$\eta_{max (SCC)} = 0.34 \times \left(1 - \frac{0.158}{0.524}\right)^{-1.9} \times \left(1 - \frac{0.385}{0.63}\right)^{-1.9} \times \left(1 - \frac{0.294}{0.74}\right)^{-1.9} = 10.5 Pa.s$$

$$\eta_{max (SCSFRC)} = \eta_{max (SCC)} \times \left(1 + \frac{\Phi_{sf}}{\Phi_\lambda}\right) = 10.5 \times \left(1 + \frac{0.0049}{0.0015}\right) = 44.76 Pa.s$$

Finally, calculate the plastic viscosity of the SCSFRC, η_e , according to Eq. (4.8), which gives $\eta_e = 44.76 Pa.s$. The error with respect to the target value (Figure 4.14):

$$Viscosity\ diff. = \frac{(Calculated\ \eta_{mix} - Target\ \eta_{mix})}{Target\ \eta_{mix}} \times 100$$

$$Viscosity\ diff. = \frac{(44.76 - 45)}{45} \times 100 = -0.531\ %$$

The actual mix plastic viscosity is within $\pm 5\ %$, the mix proportions are acceptable.

Table 4.6: Mix constituents and plastic viscosity of an SCSFRC mix

Ingredient (kg/m ³)										
Design Mix	Cement	ggbs	W	SP	LP	FA	CA	SF	η (pa s)	Difference
	338	113	180	2.9 (3.8)	164	716	819	38	44.76 Pa.s	-0.531 %
Density	2950	2400	1000	1070	2400	2650	2800	7850	-	--

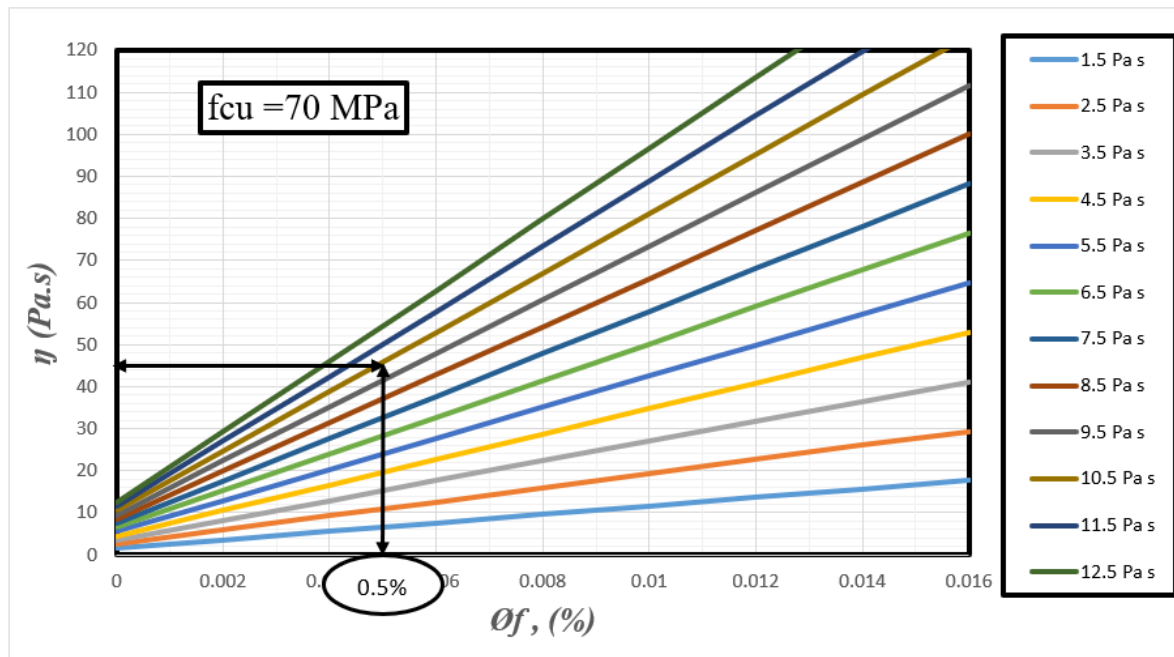


Figure 4.14: Relationship between steel fibre range and plastic viscosity of the SCC base from a plastic viscosity of SCSFRC for 70 MPa of compressive strength

4.6.3 An example calculation for designing 40 MPa mix with 0.5% of steel fibre (Modelling and validation)

Note: designing 40 MPa mix with 0.5% was achieved for simulation of SCSFRC as to seen in Table 8.1 in the Chapter 8.

- Suppose further that the desired target plastic viscosity of the SCSFRC is 27 Pa s.
- For the desired target strength = 40 MPa $\rightarrow w/cm = 0.57$ (Equation 4.1);
- Calculate the cementitious material content (cm); (Figure 4.15)

$$\text{For } \eta_{mix} = 6.1 \text{ Pa s} \rightarrow \frac{cm}{\eta} = 58 \text{ (bottom curve)} \rightarrow cm = 58 \times 6.1 \\ = 353.8 \text{ Kg/m}^3$$

$$C = 0.75 \times 353.8 = 265.35 \text{ Kg/m}^3$$

$$GGBS = 0.25 \times 353.8 = 88.45 \text{ Kg/m}^3$$

$$\text{As } \frac{W}{cm} = 0.57 \rightarrow w = 0.57 \times 353.8 = 201.66 \text{ kg/m}^3$$

- Assume a trial super-plasticizer dosage (super-plasticizer mass, SP) as a percent of mass of cementitious materials (say 0.65%), which equals to 3 kg/m^3 ;
- The plastic viscosity of the paste according to its w/cm and SP/cm ratios is equal to 0.18 (Table 4.2);

- Calculate the solid phase ingredient contents (LP, FA, and CA) ;

$$\text{For } \eta_{mix} = 6.1 \text{ Pa s} \rightarrow \frac{cm + LP}{\eta} = 81 \text{ (second curve from bottom)}$$

$$\rightarrow (cm + LP) = 81 \times 6.1 = 494.1 \text{ Kg/m}^3 \rightarrow LP = 494.1 - 353.8 = 140.3 \text{ Kg/m}^3$$

$$\frac{cm + LP + FA}{\eta} = 200 \text{ (second curve from top)} \rightarrow (cm + LP + FA) = 200 \times 6.1$$

$$= 1220 \text{ Kg/m}^3 \rightarrow FA = 1220 - 353.8 - 140.3 = 725.9 \text{ Kg/m}^3$$

$$\frac{cm + LP + FA + CA}{\eta} = 335 \text{ (top curve)} \rightarrow (cm + LP + FA + CA) = 335 \times 6.1$$

$$= 2043.5 \text{ Kg/m}^3 \rightarrow CA = 2043.5 - 353.8 - 725.9 - 140.3 = 823.50 \text{ Kg/m}^3$$

- Calculate the steel fibre contents (SF).

$$m_f = \rho_f \phi_f = 7850 \times 0.005 = 39.25 \text{ kg / m}^3$$

- Calculate the total volume of the mix.

$$\text{Total volume} = \left(\frac{c}{\rho_c} + \frac{ggbs}{\rho_{ggbs}} + \frac{w}{\rho_w} + \frac{SP}{\rho_{sp}} + \frac{LP}{\rho_{LP}} + \frac{FA}{\rho_{FA}} + \frac{CA}{\rho_{CA}} + \frac{SF}{\rho_{sf}} + 0.02 \right)$$

$$\text{Total volume} =$$

$$= \left(\frac{265.35}{2950} + \frac{88.45}{2400} + \frac{201.67}{1000} + \frac{2.29}{1070} + \frac{140.3}{2400} + \frac{725.9}{2650} + \frac{823.5}{2800} + \frac{39.25}{7850} + 0.02 \right) = 0.982 \text{ m}^3$$

As the yield does not equal 1 m³, the amounts of material are adjusted, and the mix plastic viscosity is recalculated using Equation (4.6).

$$cm = 265.35/0.982 = 270 \text{ kg/m}^3$$

$$GGBS = 88.45/0.982 = 90 \text{ kg/m}^3$$

$$w = 201.67/0.982 = 205 \text{ kg/m}^3$$

$$SP = 2.29/0.982 = 2.3 \text{ kg/m}^3$$

$$LP = 140.3/0.982 = 143 \text{ kg/m}^3$$

$$FA = 725.9/0.982 = 740 \text{ kg/m}^3$$

$$CA = 823.50/0.982 = 839 \text{ kg/m}^3$$

$$SF = 39.25/0.982 = 40 \text{ kg/m}^3$$

$$\begin{aligned} \text{Total volume} &= \left(\frac{270}{2950} + \frac{90.11}{2400} + \frac{180}{1000} + \frac{2.9}{1070} + \frac{164}{2400} + \frac{740}{2650} + \frac{839}{2800} + \frac{40}{7850} \right. \\ &\quad \left. + 0.02 \right) = 1.000 \text{ m}^3 \end{aligned}$$

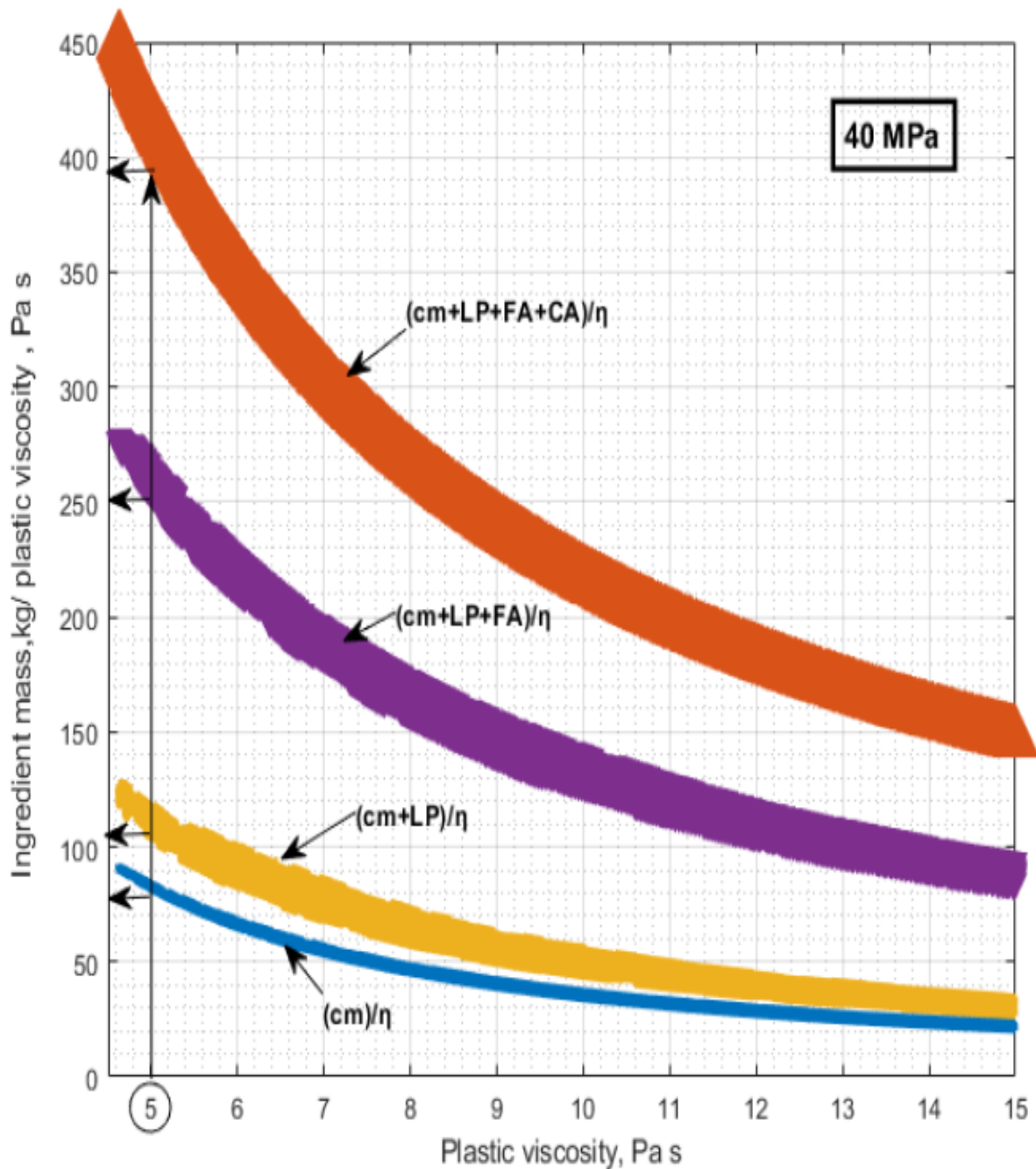


Figure 4.15: Design chart for 40 MPa of the SCSFRC base

- Check the plastic viscosity using Equation (4.6); For this purpose, the volume fractions of solid phases that are suspended in a viscous phase should be calculated.

$$\phi_{LP} = \frac{\frac{LP}{\rho_{LP}}}{\left(\frac{c}{\rho_C} + \frac{w}{\rho_w} + \frac{SP}{\rho_{sp}} + \frac{LP}{\rho_{LP}} + \frac{m_f}{\rho_{CA}} + 0.02\right)} = 0.143$$

$$\phi_{FA} = \frac{\frac{FA}{\rho_{FA}}}{\left(\frac{c}{\rho_C} + \frac{w}{\rho_w} + \frac{SP}{\rho_{sp}} + \frac{LP}{\rho_{LP}} + \frac{FA}{\rho_{FA}} + 0.02\right)} = 0.401$$

$$\phi_{CA} = \frac{\frac{CA}{\rho_{CA}}}{\left(\frac{c}{\rho_C} + \frac{w}{\rho_w} + \frac{SP}{\rho_{sp}} + \frac{LP}{\rho_{LP}} + \frac{FA}{\rho_{FA}} + \frac{CA}{\rho_{CA}} + 0.02\right)} = 0.301$$

$$\phi_{sf} = \frac{\frac{SF}{\rho_{SF}}}{\left(\frac{c}{\rho_C} + \frac{w}{\rho_w} + \frac{SP}{\rho_{sp}} + \frac{LP}{\rho_{LP}} + \frac{FA}{\rho_{FA}} + \frac{CA}{\rho_{CA}} + \frac{SF}{\rho_{SF}} + 0.02\right)} = 0.0050$$

The calculated plastic viscosity η_{eb} according to Eq. (4.6) is η_{eb}

$$\eta_{max(SCC)} = \eta_{paste} \times \left(1 - \frac{\phi_{LP}}{\phi_m}\right)^{-1.9} \times \left(1 - \frac{\phi_{FA}}{\phi_m}\right)^{-1.9} \times \left(1 - \frac{\phi_{CA}}{\phi_m}\right)^{-1.9}$$

$$\eta_{max(SCC)} = 0.34 \times \left(1 - \frac{0.158}{0.524}\right)^{-1.9} \times \left(1 - \frac{0.385}{0.63}\right)^{-1.9} \times \left(1 - \frac{0.294}{0.74}\right)^{-1.9} = 6.1 Pa.s$$

$$\eta_{max(SCSFRC)} = \eta_{max(SCC)} \times \left(1 + \frac{\phi_{sf}}{\phi_\lambda}\right) = 6.1 \times \left(1 + \frac{0.005}{0.0015}\right) = 26.81 Pa.s$$

Finally, calculate the plastic viscosity of the SCSFRC, η_e , according to Eq. (4.8), which gives $\eta_e = 44.76 Pa.s$. The error with respect to the target value (Figure 4.16):

$$Viscosity\ diff. = \frac{(Calculated\ \eta_{mix} - Target\ \eta_{mix})}{Target\ \eta_{mix}} \times 100$$

$$Viscosity\ diff. = \frac{(26.81 - 27)}{27} \times 100 = -0.68\ %$$

The actual mix plastic viscosity is within $\pm 5\ %$, the mix proportions are acceptable.

Table 4.7: Mix constituents and plastic viscosity of an SCSFRC mix

Ingredient (kg/m ³)										
Design Mix	Cement	ggbs	W	SP	LP	FA	CA	SF	η (pa s)	Difference
	270	90	205	2.3	143	739	839	40	26.81 Pa.s	-0.68 %
Density	2950	2400	1000	1070	2400	2650	2800	7850	-	--

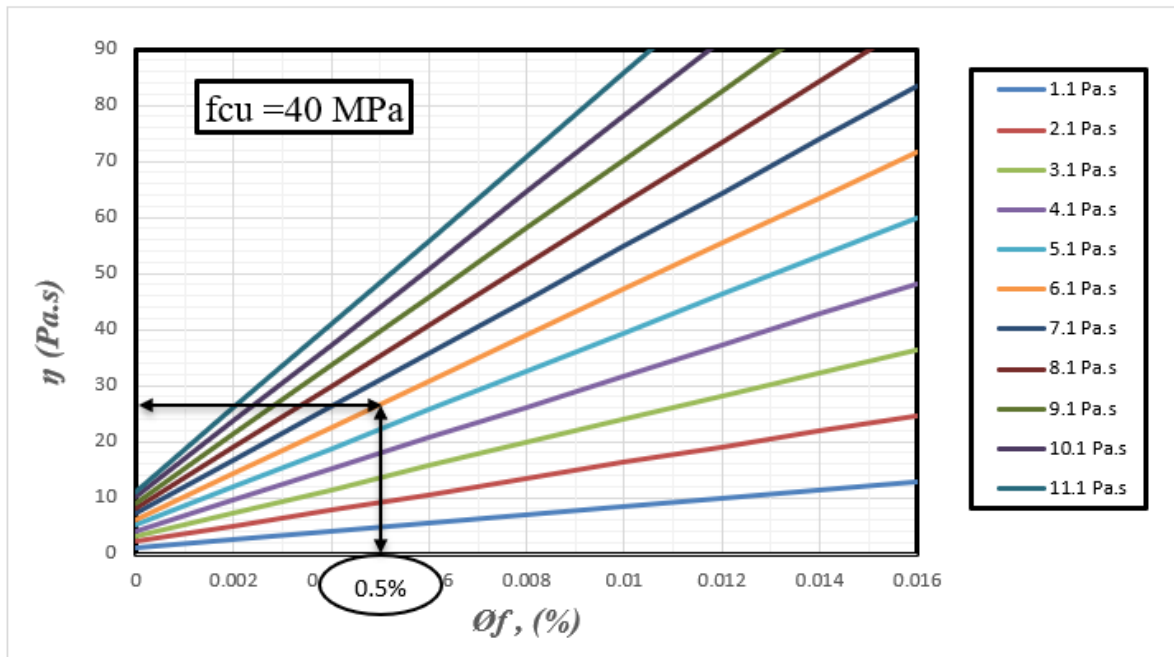


Figure 4.16: Relationship between steel fibre range and plastic viscosity of the SCC base from a plastic viscosity of SCSFRC for 40 MPa of compressive strength

Table 4.8: All the Mix constituents of an SCC mix based on target plastic viscosity and compressive strength

Design Mix	cm ^a			w	SP	LP	FA		CA	SF
	Cement	ggs ^b	ms ^c				FA**	FA***		
30MPa (0) % of SF	239	78	--	201	1.8	160	222	550	851	0
30MPa (0.5) % of SF	244	81	--	205	2.1	158	218	550	827	40
30MPa (1.0) % of SF	328	--	58	243	4.75	366	446	700	--	103
40MPa (0) % of SF	288	95	--	219	2.5	130	200	544	770	0
40MPa (0.5) % of SF	270	90	--	205	3	143	240	500	839	40
50MPa (0) % of SF	293	98	--	207	³ (2.3)	86	240	500	881	0
50MPa (0.5) % of SF	275	92	--	195	2.8	207	189	600	842	38
50MPa (1.0) % of SF	400	--	71	244	8.25	376	346	700	--	115
60MPa (0) % of SF	315	105	--	198	2.6	140	198	500	862	0
60MPa (0.5) % of SF	303	101	--	190	3.5	129	210	500	887	39
70MPa (0) % of SF	351	117	--	187	2.8	49	261	500	879	0
70 MPa (0.5) % of SF	338	113	--	180	^{2.9} (3.8)	164	216	500	819	38
70 MPa (1.0) % of SF	473	--	84	223	11.5	331	369	700	--	112

Table 4.9: Further details of test SCC mixes

Design Mix	w/cm	SP/cm %	η (pa s)	Plastic viscosity (Target)	Difference
30MPa (0) % of SF	0.63	0.56	5	4.92	-1.69
30MPa (0.5) % of SF	0.63	0.65	20	19.78	-1.10
30MPa (1.0) % of SF	0.63	1.23	41	39.66	-3.27
40MPa (0) % of SF	0.57	0.78	5	4.91	-1.76
40MPa (0.5) % of SF	0.57	0.83	27	26.82	-0.67
50MPa (0) % of SF	0.52	0.59	7	6.75	-3.63
50MPa (0.5) % of SF	0.52	0.76	35	33.85	-3.28
50MPa (1.0) % of SF	0.52	1.75	62	63.53	+2.46
60MPa (0) % of SF	0.47	0.62	8.5	8.32	-2.07
60MPa (0.5) % of SF	0.47	0.86	40	40.59	+1.47
70MPa (0) % of SF	0.40	0.70	9.5	9.42	-0.79
70 MPa (0.5) % of SF	0.40	0.84	45	44.76	-0.53
70 MPa (1.0) % of SF	0.40	2.1	81	81.21	+0.26

4.7 Concluding remarks

Methods for proportioning (SCC) without and with steel fibre (SCSFRC) mixes have not kept pace with their production techniques. This chapter developed a mix design method for SCC and SCSFRC based on the target plastic viscosity and the compressive strength required for the mix and accounted for steel fibre parameters such as volume fraction and aspect ratio. The simplicity and usefulness of this method are enhanced by the provision of design charts as a guide for mix proportioning. The target plastic viscosity of these mixes varied between 5 and 85 Pa s, and the characteristic cube strength between 30 and 70 MPa after curing 28 days. Selected examples on the use of the design charts were presented.

Methodology validation of the mix design procedure will be provided on SCC mixes in the next Chapter.

Chapter 5

Methodology

5.1 Raw materials of SCC

The main raw materials of SCC include cementitious component, aggregates and SP. The materials used in this research are Portland limestone cement (PLC), sand (fine aggregate), coarse aggregate. Further, a chemical admixture (i.e., SP) was used, in addition to other supplementary cementitious materials, such as ground granulated blast-furnace slag (GGBS) and limestone powder (LP). The following sections further describe these raw materials including their roles in optimising the performance of SCC.

5.1.1 Cementitious components

Cementitious content in SSC is generally about 380–600 kg/m³ (EFNARC, 2005). The following sections will discuss the common cementitious components and their effects on the performance of SCC.

5.1.1.1 Portland cement

The European (BS EN 197-1:2000, 2007) standard code classifies four varieties of Portland limestone cement (PLC); specifically; II/ A-L and II/A-LL comprising 6 – 20 % of limestone and II/B-L and II/B-LL comprising 21– 35% of limestone. The cement used in this study was Portland limestone cement (PLC) with strength class of II/ A-L 32, 5R. The PLC is produced by mixing limestone with ordinary Portland Cement (OPC) or cement clinker and inter-grinding limestone. The increase in the use of Portland limestone cement (PLC) is fundamentally due to reduction in consumption of raw materials, reduction of CO₂ emissions, provision of energy in clinker production (Damtoft et al., 2008).

5.1.1.2 Granulated blast furnace slag

Granulated blast furnace slag (GGBS) has been used in concrete as an additional cementitious material for many years (Shi, Wu, Xiao, et al., 2015). Yazici et al (Yazici et al., 2010) replaced Portland cement with 20%, 40%, and 60% of GGBS respectively. The compressive strength of the reactive powder concrete (RPC) with higher value of GGBS after autoclaving was over 250 MPa, as illustrated in Figure 5.1.

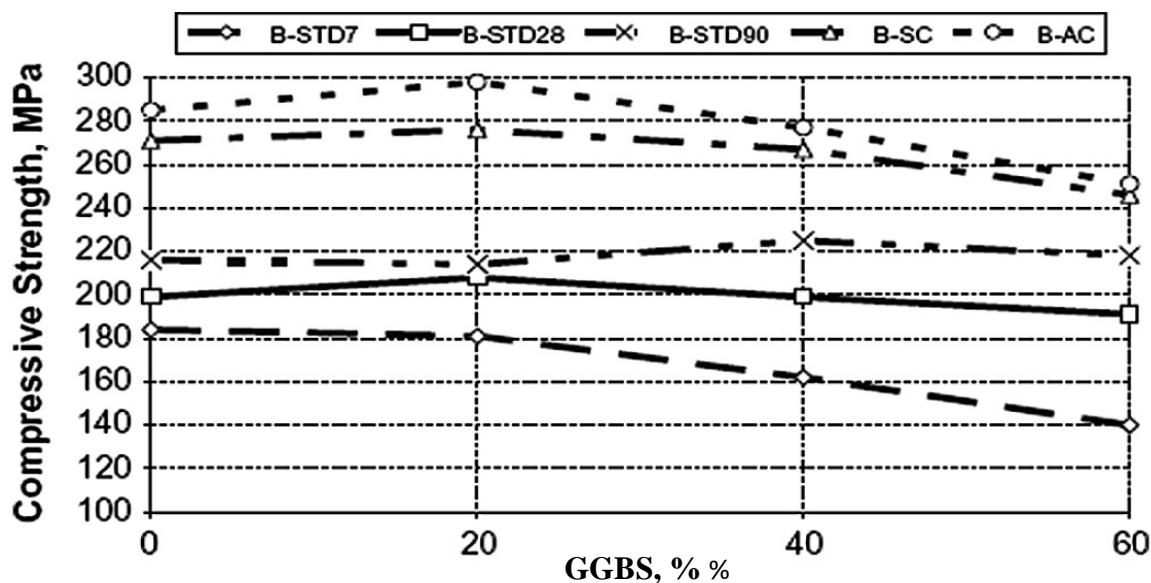


Figure 5.1: The influence of GGBS content on compressive strength of RPC (STD: Standard Curing, SC: Steam curing, AC: Autoclave curing)(Yazici et al., 2010)

The tensile and compressive strength of SCC made with 20% to 30% of GGBS (wet cured), gave higher level of strength. Demonstrating a higher effectiveness and better use of materials. This is due to the fineness of GGBS. It is noted that the GGBS has finer powder than cement (Shibani *et al.*, 2021).

5.1.1.3 Limestone powder

As a non-pozzolanic metal mixture, use of Limestone powder (LP) can improve the liquidity of concrete (Shi, Matsui and Feng, 2002)(Zhu and Gibbs, 2005). LP with two different particle sizes; the nominal particle size ($<125\ \mu\text{m}$) and maximum size ($125\ \mu\text{m}-2\ \text{mm}$) were used in this research. It was found that the concrete had higher strength with 20% LP, 10% SF, and 20% GGBS than that without LP after 28 days of curing because of quickened hydration of silica fume and cement (Shi, Matsui and Feng, 2002)(Zhu and Gibbs, 2005), which favoured the enhanced performance and structure of concrete (Svermova, Sonebi and Bartos, 2003). Additionally, LP had a favourable influence on the production of Calcium Silicate Hydrate(C-S-H) gel (Hodges and Richardson, 1996)(Schachinger, Schubert and Mazanec, 2004). The addition of LP decreases the setting times of initial and final concrete while increasing the overall shrinkage only slightly compared to conventional vibration concrete. LP filler also enhances viscosity, thus improving workability (Sua-iam and Makul, 2013).

5.1.1.4 Micro-silica

The terms micro-silica (MS) and silica fume (SF) are frequently used to describe by-products extracted from the exhaust gases of ferrosilicon, silicon, and other metal alloy smelting furnaces. Nevertheless, the terms of micro-silica and silica fume are used for condensed silica fumes that are of high quality for use in the concrete industry and cement. To enhance the microstructure of concrete mixes, MS is used as a partial replacement of cement at different weight ratios. The quality of interfacial transition zone (ITZ) is enhanced by fine particles through micro-filling effect and producing additional calcium silicate hydrate (CSH) gel reacting with calcium hydroxide. MS consists of fine particles with an average size of 0.1 –0.2 μm , and specific gravity of 2.20 (Bahrami et al., 2020). MS mainly comprises amorphous (non-crystalline) silicon dioxide (SiO_2); when added to Portland cement concrete it enhances its characteristics, specifically its bond strength, abrasion resistance, and compressive strength. The individual particles are extremely small, at around 1/100 the size of an average cement particle. Due to its fine particles, high SiO_2 content, and large surface area, SF is a very reactive pozzolan when used in concrete.

5.1.2 Aggregates

Various kinds of aggregates have been used to produce of SCC, and their optimum volume content has been studied. Two different particle criterions of coarse aggregate were used in this research in accordance with the standard codes (BS EN 12620:2002 +A1:2008, 2004) (PD 6682-1:2009+A1:2013, 2013). They comprised a gravel with 10 mm nominal particle size and 20 mm maximum size. According to (BS EN 933-1:2012, 2012) the course aggregate 10 mm, and 20 mm were obtained by the process of sieve analysis, and were appropriate for the general classifying requirements of standard code (BS EN 12620:2002 +A1:2008, 2004).

Fine aggregate (river sand) refers to a particular type of aggregate (natural crushed stone) with particle sizes of less than 4mm, and according to the BS EN 12620:2002(BS EN, 2008) can be produced naturally through the disintegration of rocks or gravel or by manufacturing aggregates. (Su, Hsu and Chai, 2001) made of SCC with 30, 31, 32, 33, and 34 percent volume fraction of coarse aggregates and investigated the influence of the coarse aggregate content on the fresh properties of SCC by measuring parameters such as slump flow T_{500} time, U-box filling height and V-funnel flowing time. It was found that both the V-funnel flowing time and the T_{500} time reduced, while the U-box filling is a height grew, with the decrease in coarse aggregates content.

5.1.3 Superplasticizers

Superplasticizer (SP) is always crucial to improve the flowing ability with a slight alteration in viscosity. If needed, a low dose of viscosity-modifying admixture can be used to eliminate the undesirable bleeding and segregation occurrence (Han and Zhang, 2017) as shown in Figure 5.2. Dispersion of massed cement particles is known to constitute the major process by which SP enhances the workability properties of concrete without increasing water content (Boukendakdji, Kadri and Kenai, 2012).

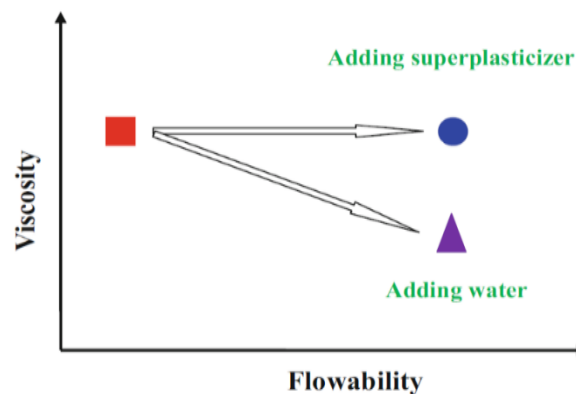


Figure 5.2: Role of Superplasticizers (SP) (Han and Zhang, 2017)

5.2 Quantity ranges of the constituent materials for SCC

The mix design of SCC is typically done using trial and error methods based on previous researchers' work. The most effective materials for SCC in terms of structural design strength use filler materials such as limestone, ground granulated blast-furnace slag (GGBS), and silica fume, alongside standard cement, and aggregates. One of the most important materials in the design mix of SCC is the use of SP, which helps develop the workability of SCC mix. The best proportioning of design mixes in SCC have been achieved through changing the percentage of filler materials in the mix. The fundamental materials and secondary materials for the mix in SCC are produced following the European Federation of National Trade Associations (EFNARC) guidelines (EFNARC, 2005), where the specified typical ranges of primary constituent materials include powder (cementitious materials + filler), water, and aggregate as shown in Table 5.1. A rigorous process for proportioning materials for normal and high strength SCC is dependent on the plastic viscosity of the SCC mixes (Abo Dhaheer *et al.*, 2016a).

Table 5.1: Typical range of SCC mix compositions according to: (EFNARC, 2005)

Ingredients	Typical range by mass (kg/m ³)	Typical range by volume (liters/m ³)
Powder (cementitious materials + filler)	380–600	-
Water	150–210	150–210
Coarse aggregate	750–1000	270–360
Water to powder ratio by volume	0.85–1.10	
Fine aggregate	Typically, 48–55% of the total aggregate	

Among 56 case studies of SCC applications, (Domone, 2006) reported that SCC can be produced using a wide range of possible constituent materials, such that there are still no clear rules for proportioning SCC mixes. These case studies revealed that coarse aggregate contents ranged from 28 to 38% of concrete volume, fine aggregate content varied from 38 to 54% of mortar volume, w/p ratio (by weight) ranged from 0.26 to 0.48, paste content varied from 30 to 42% of concrete volume, and powder content ranged from 445 to 605 kg/m³.

5.3 Laboratory experiments

5.3.1 Testing methods for self-compatibility of SCC

The unique properties of SCC do not allow the specification experiments used for VC to be employed to correctly monitor the fresh characteristics of the produced SCC. The self-compatibility tests generally employed on SCC without and with fibre mixtures are briefly explained below.

5.3.1.1 Fresh SCC experiments

5.3.1.1.1 Slump trial (Flow-ability)

Slump test, which is a process to measure the consistency, workability, and flow advantages of SCC, was carried out in accordance with (BS EN 12350-8, 2010). A non-absorbent steel surface and a rod and metal mould cone were used. This cone was in the shape of a hollow frustum, 300 mm in height, 200 mm in depth, and 100 mm in width. This experiment measures three various aspects: filling ability, viscosity, and resistance to segregation. Two horizontal perpendicular diameters (d_1 and d_2) were recorded, as illustrated in Figure 5.3, and the average flow spread diameter (SF) was calculated using the following equation:

$$SF = \frac{(d_1 + d_2)}{2} \quad (5.1)$$

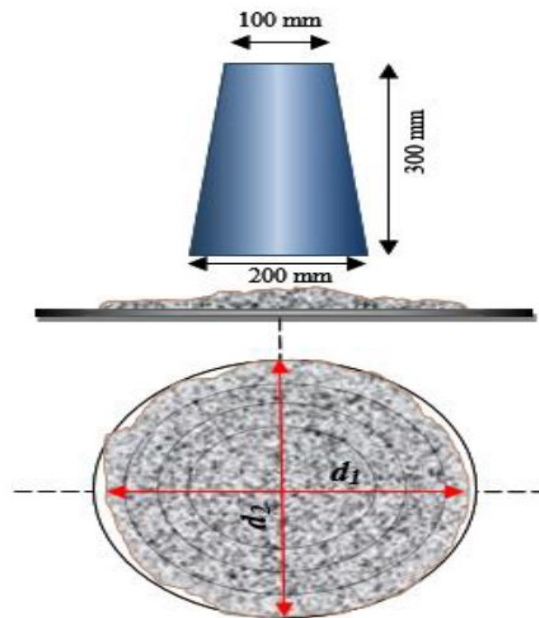


Figure 5.3: Trial mix slump flow with study-adopted design mix

The mixture viscosity is assessed by measuring the time needed for SCC to reach 500 mm flow diameter (t_{500}); the longer the t_{500} , the higher the mixture viscosity will be.

5.3.1.1.2 J-ring trial (Flowing and passing-ability)

The J-ring trial in combination with a slump trial was used to assess the passing ability of SCC through gaps in the reinforcement. The device comprises a ring with different numbers of vertical reinforcing bars, a slump cone, and a rigid plate (BS EN 12350-8, 2010) as shown in Figure 5.4. The flow spread of the J-ring (S_{FJ}) shows the restricted deformability of SCC, and can be expressed utilizing the following:

$$S_{FJ} = \frac{(d_1 + d_2)}{2} \quad (5.2)$$

$$P_j = \frac{\Delta h_{x1} + \Delta h_{x2} + \Delta h_{y1} + \Delta h_{y2}}{4} - \Delta h_0 \quad (5.3)$$

Where:

P_j is the blocking step

$\Delta h_{x1} + \Delta h_{x2} + \Delta h_{y1} + \Delta h_{y2}$ are the four measurement heights at positions just outside the J-ring

Δh_0 is the height measurement at the centre of flow.

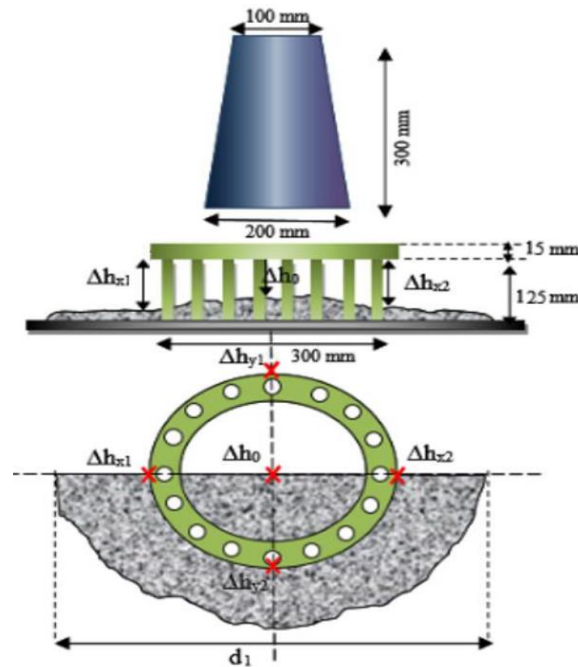


Figure 5.4: Trial mix J-ring test with study-adopted design

Criteria of acceptance.

According to (Chan, Ong and G, Tan, 2010) , the flow spread (SF_J) of SCC, with or without steel fibres using the J-ring can be assessed relative to the flow spread (SF) of the same mix using the slump test as described in .

Table 5.2: Pasing ability criteria

$(SF-SF_J)$	Passing ability rate	Notes
< 25mm	0	No visible blocking
25 mm-50 mm	1	Minimal to noticeable blocking
> 50 mm	2	Noticeable to extreme blocking

- ❖ The blocking step P_j should be less than 10 mm based on (EFNARC, 2005).
- ❖ t_{500J} which is the time needed for SCC to reach a diameter of 500 mm should be recorded.
- ❖ This test is not acceptable when the largest aggregate size in more than 40mm.

- ❖ The difference between d_1 and d_2 should be less than 50 mm otherwise the test should be repeated.
- ❖ Segregation can be detected by visually inspecting a ring of cement paste/mortar in the edge of flow, and /or ensuring that no coarse aggregates or fibres have lifted in the centre.

5.3.1.1.3 L-box trial (Flowing, passing and filling-ability)

The L-box trial is used to measure the filling and passing ability of SCC. The test is carried out in accordance with (BS EN 12350-8, 2010) and (EFNARC, 2005). The dimensions of the L-box are shown in Figure 5.5. The times for the SCC to reach a distance of 200 mm (t_{200}) and 400 mm (t_{400}) along the horizontal part were measured, along with the height of concrete at the two ends of the horizontal section of box (H_1 and H_2) after the concrete stopped flowing. The ratio H_2/H_1 represents the filling ability, which typically should be 0.8~1. The passing ability can be detected visually by inspecting the area around the rebars (steel bars).

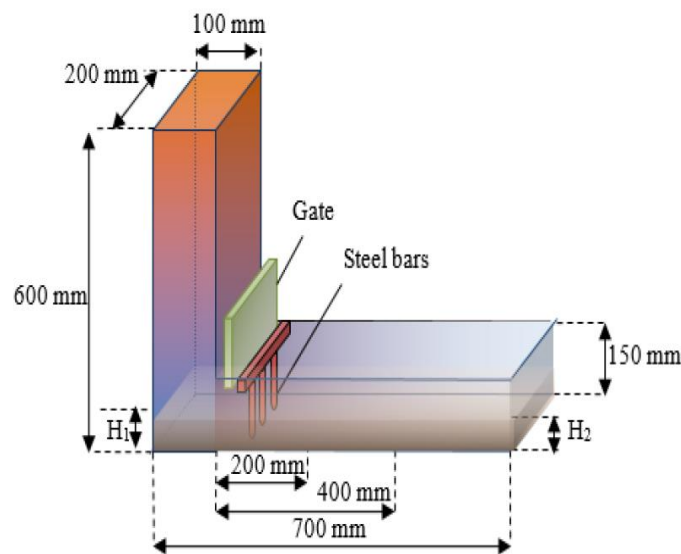


Figure 5.5: Trial mix L-box test with study-adopted design mix

5.3.1.2 Hardened SCC experiments

5.3.1.2.1 Cubes' compressive strength trial

The unconfined compression strength test for the cubical specimens (100mm length, 100 mm width, and 100mm height) was carried out in the laboratory following the guidelines of (BS EN 12390-3, 2009). The compressive strength is regarded as representative of all mechanical

properties, and it is the general characteristic material parameter used for the classification of concrete in national and international standard codes. The compressive strength of SCC and VC of similar composition does not differ significantly in the majority of published test results. Additionally, the comparison of hardening processes indicates that the strength development of SCC and VC is similar (Dehn, Holschemacher and Weiße, 2000)(Domone, 2007)(Sonebi and Bartos, 2002). Three cubical concrete specimens per mix were tested at various curing ages (7, 14, and 28 days respectively). The average, ignoring any specimens that failed, was recorded and taken as the representative value of the compression strength of that mix composition.

5.3.1.2.2 Tensile strengths

A tensile strength test for the cylindrical specimens (100mm diameter and 200mm height) was carried out after 7, 14, and 28 days (respectively) , in accordance with the indirect method proposed in (BS EN 12390-6, 2009). The tensile strength is one of the key properties that affects the safety, durability, and serviceability of concrete structures (Parra, Valcuende and Gómez, 2011). The tensile strength of SCC is superior relative to VC (Domone, 2007)(Persson, 2001). This is attributed to the high paste content in SCC and better homogeneity resulting from vibration free production compared to VC (Nikbin *et al.*, 2014).

All factors that affect the characteristics of cement matrix microstructure and interfacial transition zone (ITZ) are of decisive importance in tensile behaviour. When the water to powder (W/P) ratios are similar, the splitting tensile strength of SCC will be higher than that of VC (Holschmacher and Klug, 2002) (Zhu, Sonebi and Bartos, 2004).

5.3.1.2.3 Modulus of elasticity

A modulus of elasticity test for the cylindrical specimens (100mm diameter and 200mm height) was carried out after 7, 14, and 28 days (respectively) , in accordance with the indirect method proposed in (BS EN 12390-13:2013, 2019) . The modulus of elasticity of concrete depends on the modulus of elasticity of the individual mix ingredients, and it increases with higher aggregate content, whereas it decreases with increasing paste volume and porosity (Neville, 1995) . However, the increase in the SCC modulus of elasticity due to the decrease in porosity cannot compensate for the reduction induced by the lowering of coarse aggregate content and/or increasing paste volume. Accordingly, lower values of modulus of elasticity can be expected for SCC, as it has relatively higher content of paste and lower content of coarse aggregate than VC.

5.3.1.2.4 Fracture mechanics

Concrete structure, because of its heterogeneity, can be prone to flaws such as irregularly distributed pockets of entrapped air voids, lenses of bleed water, and shrinkage cracks, even prior to the application of load. These flaws grow stable under external load, and coalesce with existing or newly formed small cracks, until large fractures are formed, which ultimately cause the collapse of the structure. When a load is applied there will be high stress concentrations around these cracks (higher than those at other points within the structure). These cracks propagate during service and can be a serious problem in such structures. Studies of the response and failure of structures as a consequence of crack initiation and propagation have developed fracture mechanics, including an energy-based failure theory that could be used in designing cement-based structures (Karihaloo, 1995).

Fracture mechanics, in a broad sense, is a theory of failure and the propagation of that failure through the structure, based on energy criteria in conjunction with strength criteria. Physically, the fracture is the local separation of material into at least two pieces when sufficient stress is applied at the atomic level to break the bonds that hold atoms together. Fracture failure can result from many reasons, including uncertainties in the loading or environment, imperfections in materials, and deficiencies in design, construction, or maintenance.

Fracture researchers now have no doubt that the introduction of fracture mechanics into the criteria of design for all brittle failures of reinforced concrete structures (such as punching shear, diagonal shear, pull out or torsion, or for concrete dams) can achieve considerable advantages. It can help to increase uniform safety margins for structures of various sizes. This, in turn, enhances the economy and efficiency of assessment procedures, thereby improving the reliability of structures. It will also make it possible to present innovative designs and utilise new concrete materials to improve structural durability and integrity.

Furthermore, fracture mechanics can provide rational explanations for the many empirical provisions in current design codes, with particular use for high-strength, fibre-reinforced, unusually large, and pre-stressed concrete structures. Indeed, fracture mechanics is of urgent necessity for concrete dams and nuclear reactor containment vessels, for which safety concerns are particularly important, as consequences of structural failure are catastrophic (Karihaloo, 1995).

5.4 Modelling and validation

SCC workability (e.g., flowing, passing and filling ability) in terms of its fundamental rheological characteristics, which is important for the success of its production. However, the prediction of SCC rheological behaviour is not a simple task, especially in the presence of reinforcement members, complex shapes of formwork, and various sizes and proportions of aggregates and fibres. In this respect, numerical simulation can be a helpful and valuable methodology for a deeper understanding of SCC mix flow behaviour, and assessment of its ability to meet the necessary self-compacting standards.

Enforcing incompressibility in SPH can be pursued using two different approaches - the weakly or quasi-compressible SPH will be referred to as WCSPH (Monaghan, 1994) ; (Lee et al., 2008) and the truly incompressible SPH as ISPH (Kulasegaram, Karihaloo and Ghanbari, 2011) . Although both strategies achieve the incompressibility, each one has got advantages and drawbacks. Further details will be provided in Chapter 3.

The problems associated with the use of WCSPH can be circumvented by implementing ISPH. In ISPH, the pressure and velocity will be computed separately. Pressure can be solved implicitly using the Poisson equation (Kulasegaram and Karihaloo, 2013). Further details will be provided in Chapter 8.

5.5 Concluding remarks

This chapter gave a general overview of raw materials of SCC including influence of cement replacement materials and admixtures on the characteristics of SCC in the fresh state. It was concluded that in the fresh state, ACMs enhance self-compacting ability, fluidity and cohesiveness while improving its performance in the hardened state. As well, the proposed method of proportioning SCC is simple as guideline by the ranges of the constituent materials for SCC (EFNARC, 2005). This method was based on the rheological characteristics represented by plastic viscosity of the mix and the target compressive strength. Guidelines have been provided by way of design charts for choosing the mix proportions, Further details will be provided in Chapter 4. The procedure and design mix also be reviewed on the tests of SCC in both fresh and hardened state.

Investigational validation of the mix design procedure will be presented in the following chapters, on a series of SCC and SCSFRC mixes with different volumes of paste to solid ratio and fibre percentage in both fresh and hardened states.

Chapter 6

**Understanding the effect of paste content
on the performance of self-compacting
concrete : Experimental validation I**

6.1 Introduction

SCC has been developed due to several advantages associated with its properties and its application. These advantages include; economic benefits, excellent performance in terms of fresh properties, less energy requirement, increased speed of construction, no vibration necessary; easy to produce buildings and structures with complicated form work and can contain highly congested steel reinforcements (Corinaldesi, Moriconi and Ash, 2011). The key features of SCC properties are the effective filling and passing ability under its own weight and the stability without segregation to obtain thorough compaction (Ghalehnovi *et al.*, 2019). For highly desirable performance, SCC should have satisfactory plastic viscosity and low yield stress (EFNARC, 2005). Generally, SCC requires higher volume of powder content (compared to concrete produced by conventional vibration) to produce a cohesive and homogeneous mixture (Topçu and Uygunoğlu, 2010). While an adequate amount of powder does provide sufficient deformability and flowing ability to fresh SCC, additional powder can be counter-productive in increasing the viscosity or the yield strength of a mixture (Girish, Ranganath and Vengala, 2010).

To obtain appropriate viscosity levels, SCC can be produced using a viscosity-modifying admixture (VMA) or, more generally, using a large quantity of powder materials such as cement and mineral add mixtures. A super-plasticizer (SP) is effectively used to control shear stress (Nepomuceno, Oliveira and Lopes, 2012) of SCC mix. To achieve these aims, besides utilizing a strong SP, a large amount of fine powder is required (Ho, D. W.S.Sheinn, A. M.M.Ng, 2002). LP, fly ash (FA) and ground granulated blast furnace slag (GGBS) are commonly utilized in SCC mixtures to maintain consistency and segregation resistance (EFNARC, 2005).

The use of fly ash (FA) and filler increases the paste volume of SCC, which in turn develops workability (Collepari, M. Collepari, S. Ogoumah Olagot, 2003)(H. Okamura and Ouchi, 2003)(Bouzoubaâ and Lachemi, 2001). However, SCC demands large amount fine content to attain stable fresh properties, which often leads to high cement consumption (Vurst. F.V.D. S, Grünewald. S, Feys. D, 2017)(Jiao, D. Shi, C. Yuan, 2017)(Thanh.Ha, Kraus. M, 2015). In this context, its cost is one of the disadvantages of SCC, linked with the use of high volume of Portland cement (PC) and chemical admixtures. One alternative to decrease the cost of SCC is the use of mineral additives such as natural pozzolans, LP, slag, and fly ash, which are finely divided materials supplementary to concrete as separate components, either during or before

mixing (Şahmaran, Christianto and Yaman, 2006). The production of SCC normally involves the use of additional cementitious materials, such as limestone powder (LP). The LP has a very similar particle size distribution to that of cement, which suggests that the LP can be used to partially replace cement without significantly altering the particle packing of the solid matrix (Yu, 2015).

LP has been used as a major raw material in the production of PC clinker since 1824, and has been used in ground form as a filler aggregate in addition to PC to achieve cement mixtures and Portland compound cements such as PLCs, in accordance with (BS EN 197-1, 2011) , over recent decades (Elgalhud, Dhir and Ghataora, 2018) (BSI Standards Publication, 2011). The use of PLC incorporating LP as a filler is widespread in European countries, particularly in France (Bonavetti *et al.*, 2003). The earliest attempt at the use of LP as an addition in PC was in Germany in 1965 (Elgalhud, Dhir and Ghataora, 2018). PLC has many benefits in terms of both economics and technology (Tsvivilis, Voglis and Photou, 1999). The European Standard (BS EN 197-1, 2011) has allowed up to 5% LP as a minor supplementary constituent and classified four varieties of PLC: types II/ A-L and II/A-LL, comprising (6–20%) limestone; and types II/B-L and II/B-LL, comprising (21–35%) limestone. In addition, it is possible to use LP in concrete mixes with supplementary cementitious materials. The maximum allowable LP addition tends to vary in accordance with international and national standards, ranging from 6% to 35% by volume. Accordingly, a thorough understanding and investigation of the behaviour of LP used in combination with PLC for SCC production is important, not only to understand the general performance of PLC as per (BS EN 197-1, 2011), but also to comprehend the strength of SCC made with PLC. In order to decrease energy consumption and CO₂ emissions, and to promote more efficient production, cement industries increasingly produce mixed cements, composed of additional cementitious materials such as natural pozzolan, slag, limestone and fly ash (Ramezianpour *et al.*, 2009).

When LP is added to PC, it influences its characteristics in terms of fresh and hardened properties, in addition to durability (Elgalhud, Dhir and Ghataora, 2017). LP is a valuable resource generated through stone crushing processes, and it is the most general additive used for enhancing the flowing ability of SCC (Domone, 2006)(Domone, 2007). Adding limestone decreases the initial and final setting times of concrete, while only slightly increasing the total shrinkage compared to traditional concrete (Valcuende *et al.*, 2012) . The limestone acts as a filler for improving viscosity, increasing the flowing ability (Felekoglu, 2007)(Yahia,

Tanimura and Shimoyama, 2005) and ensuring stability (Yahia, Tanimura and Shimoyama, 2005)(Ye *et al.*, 2007). This metal admixture is one of the most commonly used material in the French concrete industry. Limestone as a filler, however, does not present hydraulic or pozzolanic characteristics. To improve durability and mechanical performances, ternary mixture cement/ pozzolanic /limestone filler can be used (Nepomuceno, Oliveira and Lopes, 2012)(Antoni *et al.*, 2012).

As a non-pozzolanic metal mixture, use of LP can improve the liquidity of concrete (Shi, Matsui and Feng, 2002) (Zhu and Gibbs, 2005). It was found that concrete had higher strength with 20% LP, 10% silica fume, and 20% GGBS than without LP after 28 days because of quickened hydration of silica fume and cement (Shi, Matsui and Feng, 2002)(Zhu and Gibbs, 2005), Further, it was noted that the use of VMA as a substitute filler for limestone produces SCC with lower drying shrinkage, being approximately 33% less than SCC produced with limestone filler without VMA (Valcuende *et al.*, 2012).

Most PC recommendations permit the use of up to 5% limestone, beyond which PLCs are classified depending on the ratio of limestone added to the cement. PLCs comprising limestone from 6–35% are created and used in several countries around the world. Therefore, depending on the PLC classification (e.g., PLC II/A-L), the amount of LP used in designing SCC mix can be optimised. The fresh properties of concrete are of great significance because of their influences on construction quality in the forming and casting processes, as well as the characteristics of hardened concrete (Jiao, D. Shi, C. Yuan, 2017). In order to reduce the artificial errors, it is important to characterize fresh and hardened properties of concrete using fundamental national standards. Although the performance of PLC has been generally explored in the past in terms of workability (flow and passing ability) and strength of SCC design mix, the obtainable information has remained fragmented and often unhelpful in further improving the use of PLC in concrete construction.

The use of PLC (or PC+LP) as a blended SCC, incorporating powder content as a cementitious supplementary (filler), such as FA, limestone, silica fume, and GGBS, is now widely promoted, and a great deal of research relating to it has been published in international journals. For practical reasons, the impact of using PLC as a blended cement in SCC is not completely understood, particularly in terms of the effects of incorporating LP on flow, passing ability, and compressive strength in the development of concrete. Apart from

technical effects, the broader associated impacts in terms of reduced carbon dioxide emissions remain unclear. These are difficult questions that have not been addressed by the construction industry. Once they are answered, broader and better-informed use of LP in the production of concrete can be enabled.

This chapter explores the rheological properties of SCC mixes containing limestone, with special emphasis on quantifying the influence of powder content additions for pastes with different compressive strength and varying limestone dosages (e.g., 6%, 10%, 15%, and 20% by volume). Experimental assessments of rheological properties are conducted for SCC mixes with various limestone content to investigate the effect of paste on flow and passing ability of the designed SCC mixes. In addition, cube compressive strength tests were performed on concrete produced to determine the influence of paste content on mechanical properties of SCC. For the above-mentioned tests, the SCC mixes with target compressive strength between 30 – 70 MPa were considered.

6.2 Materials

PLC of type CEM II/A-L/32.5R was used, conforming with (BS EN 197-1, 2011), with a specific gravity of 2.95. As a cement replacement material, GGBS with a specific gravity of 2.40 was used. A new generation of polycarboxylic-based ether hyper-plasticiser (SP) with specific gravity of 1.07 was used in all the trial mixes. Crushed limestone CA with (10 mm) nominal particle size and (20 mm) maximum size and a specific gravity of 2.80 was used, while the FA was river sand (less than 2 mm) with a specific gravity of 2.65. LP as a filler with (125 μm) of maximum particle size (specific gravity 2.40) was used. A part of the river sand (FA) was substituted by an equal quantity of the coarser fraction of LP in the size range between 125 μm – 2 mm. The results of sieve analysis for these two types of aggregate are shown in Figure 6.1.

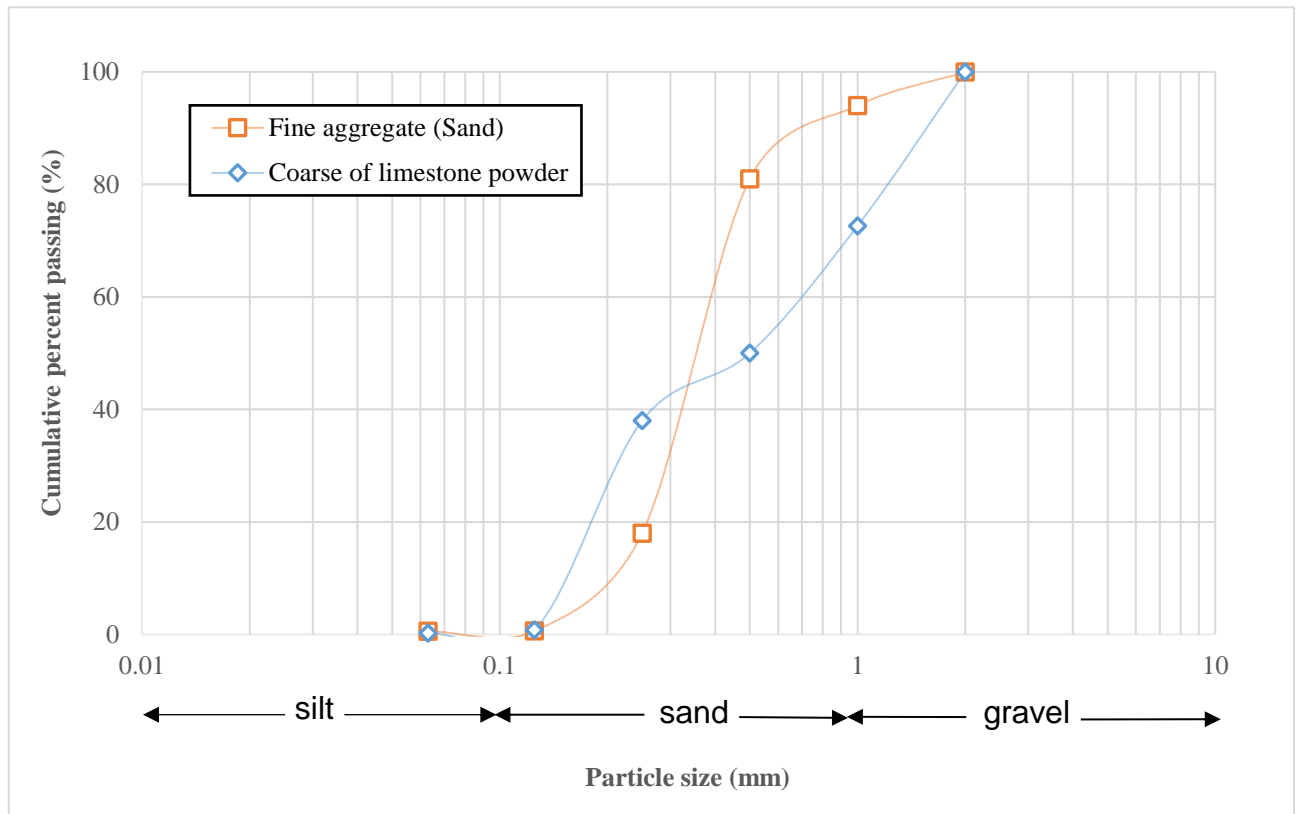


Figure 6.1: Particle size distribution curves for FA and coarser fraction of LP

6.3 Mix design method

The best proportioning of design mixes in SCC have been achieved through changing the percentage of filler materials in the mix. The fundamental materials and secondary materials for the mix in SCC are produced following the European Federation of Specialist Construction Chemicals and Concrete Systems (EFNARC) guidelines (EFNARC, 2005), where the specified typical ranges of primary constituent materials include powder (cementitious materials + filler), water, and aggregate as shown in Table 6.1. A rigorous process of proportioning materials for normal strength SCC is dependent on the plastic viscosity and compressive strength of the SCC mixes (Abo Dhaheer *et al.*, 2016c).

Table 6.1: Typical range of SCC mix compositions according to EFNARC (EFNARC, 2005)

Ingredients	Typical range by mass (kg/m³)	Typical range by volume (liters/m³)
Powder (cementitious materials + filler)	380–600	-
Water	150–210	150–210
Coarse aggregate	750–1000	270–360
Water to powder ratio by volume	0.85–1.10	
Fine aggregate	Typically, 48–55% of the total aggregate	

The mix design selected raw materials in optimal proportions to provide concrete with the required characteristics in fresh and hardened states for specific applications. Densely compacted cementitious matrix with good workability and strength can be achieved by targeted SCC design. (Abo Dhaheer *et al.*, 2016c) developed a rational mix design method for SCC based on the desired target plastic viscosity and compressive strength of the mix. In the present work, this mix design method proposed by (Abo Dhaheer *et al.*, 2016c) has been adopted.

The Table 6.2 present the mix proportions of test SCC mixes produced based on (Abo Dhaheer *et al.*, 2016c). It can be noted that the Table 6.2 contains mix proportions of the mixes with target compressive strength as indicated in the column ‘Mix designation’. For example, C30 implies that the target compressive strength of the mix is equal to 30 MPa. The Table 6.3 provide further details of mixes presented in Table 6.2. Next section summarises the experimental procedures used for evaluating the fresh and hardened properties of SCC mixes designed and tested in this study.

Table 6.2 :Mix proportions of test SCC mixes (kg / m³)

Mix designation	cm ^a		Water	SP ^b	w/cm	SP/cm	LP ^c	FA ^d		CA ^e
	Cement	ggbs						FA ^{**}	FA ^{***}	
C30	239	78	201	2.1	0.63	0.65	160	222	550	851
								772		
C40	288	95	219	2.5	0.57	0.78	130	200	544	770
								744		
C50	300	100	210	2.9	0.52	0.72	115	185	600	780
								785		
C60	314	105	197	2.6 (2.8) ¹	0.47	0.62	99	167	550	924
								717		
C70	348	116	186	2.8 (3.5) ²	0.40	0.60	117	230	501	843
								731		
Density	2950	2400	1000	1070	--	--	2400	2400	2650	2800

a Cementitious material.

b Super-plasticizer.

c Limestone powder <125 μm.

d Fine aggregate <2 mm (Note: a part of the fine aggregate is the coarser fraction of the limestone powder, FA^{**}125 μm–2 mm, whereas FA^{***} refers to natural river sand < 2 mm).

e Coarse aggregate < 20 mm.

Table 6.3 :Further details of test SCC mixes

Mix designation	Target plastic viscosity (Pa s)	Actual plastic* viscosity (Pa s)	Plastic Viscosity diff.	Paste vol. fraction	Solid vol. fraction	Paste/Solid (by vol.)
C30	5	4.92	-1.69	0.38	0.61	0.62
C40	5	4.91	-1.76	0.41	0.58	0.72
C50	7	6.76	-3.3	0.40	0.60	0.67
C60	8.5	8.69	+2.29	0.39	0.62	0.62
C70	9.5	9.55	-0.53	0.40	0.60	0.68

Actual plastic viscosity*: mix plastic viscosity that is calculated using equation 4.6.

6.4 Experimental program

The fresh and hardened characteristics of SCC mixes were analysed to verify whether the self-compacting ability and compressive strength of the prepared mixes met the design requirements. Different examinations were conducted to analyse SCC mix characteristics, for example, the slump flow test was performed to determine the flow behaviour and filling ability; this test provides an indication regarding the level of plastic viscosity (PV) of fresh SCC. The J-ring trial was performed to analyse the passing ability of SCC among reinforcement steel bars without producing segregation and blocking, according to (EFNARC, 2005). Table 6.4 presents the general acceptance criteria of fresh SCC mix. Additionally, visual inspection was performed to detect any bleeding and segregation of SCC flow. The compressive strength of SCC was determined in accordance with (BS EN 12390-3, 2009), using cubic samples with size $100 \times 100 \times 100 \text{ mm}^3$. Cube samples were demoulded and kept in water for curing until 7, 14, and 28 days respectively for testing at different curing ages. For these tests curing temperature is maintained between $20 - 24 \text{ }^\circ\text{C}$. The procedure used for testing and ensuring self-compacting ability of the designed mixes is summarized in Figure 6.2.

Table 6.4: General acceptance criteria of SCC

Slump-flow classes		Viscosity classes – t_{500}		Reference
Class	Slump flow (mm)	class	$t_{500} \text{ mm(S)}$	
SF ₁	550 to 650	VS ₁	< 2,0	(BS EN 206-9:2010, 2010)
SF ₂	660 to 750	VS ₂	$\geq 2,0$	
Passing ability classes – J-ring				
Class		J-ring step (mm)		
P _{J2}		≤ 10 with 16 rebars		
Blocking assessment (mm)				(ASTM:C1621/C1621M1, 2017)
Difference Between Slump flow and J-Ring flow		Blocking assessment (mm)		
≤ 25		No visible blocking		
> 25 to 50 mm		Minimal to noticeable blocking		
> 50 mm		Noticeable to extreme blocking		

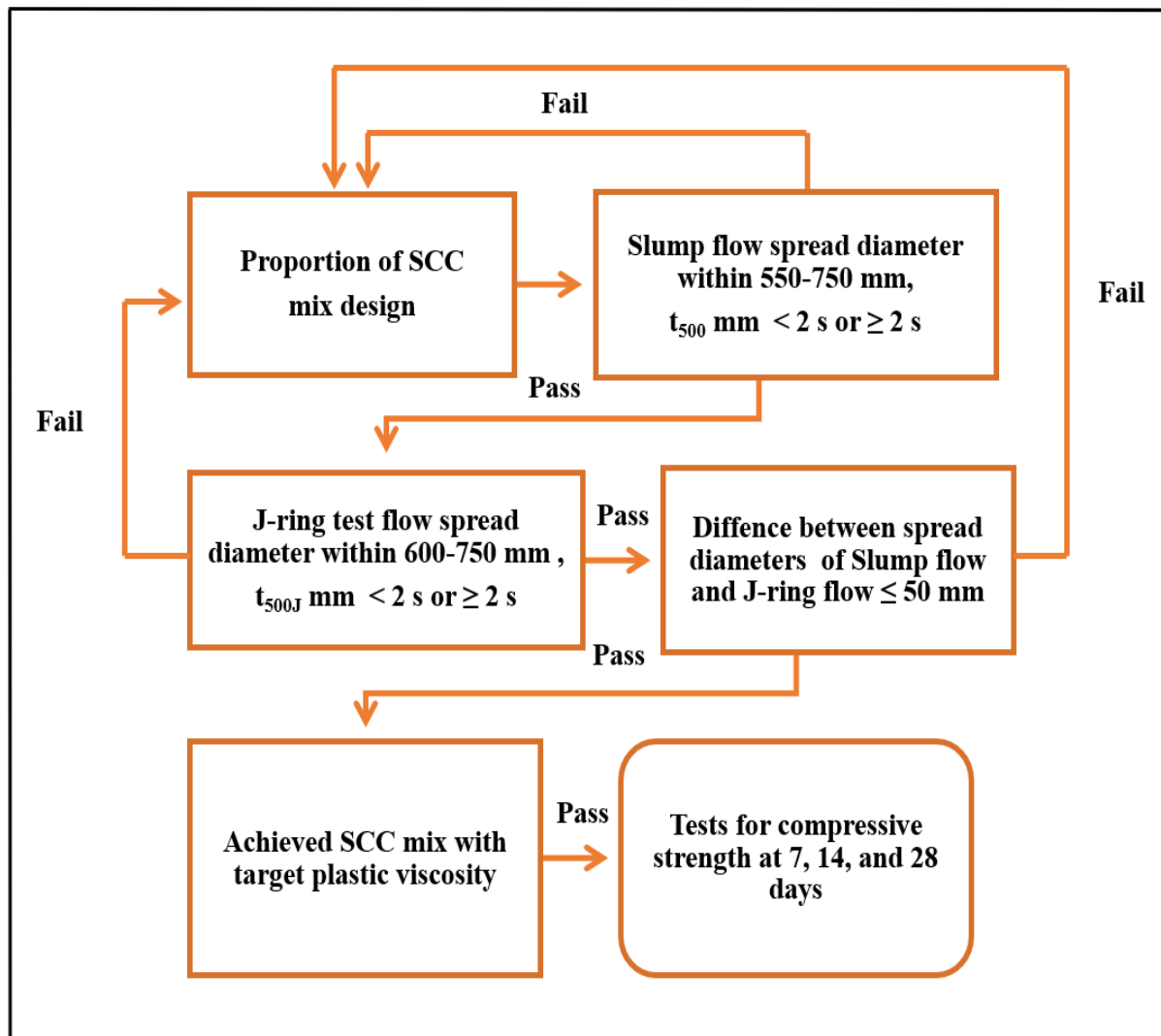


Figure 6.2: Schematic of experiments of study stages

6.5 Validation of mix design method

6.5.1 Tests on fresh SCC

Experiments were conducted to determine the t_{500} of the fresh mixtures, as shown in Table 6.5. The time taken for fresh SCC mixture to reach a 500 mm diameter spread in the slump flow test (i.e., t_{500}) was determined from time sequencing a video recording of the trial, with an accuracy of thousandth of a second. The range of flow spread diameters of all tested SCC mixes was from 600 to 750 mm (SF_1/SF_2), with t_{500} between 1.13 and 1.87 s, and the viscosity class based on t_{500} time is either VS_1 or VS_2 in accordance with (BS EN 206-9:2010, 2010). Figure 6.3 to Figure 6.5 displays the horizontal spread of various SCC

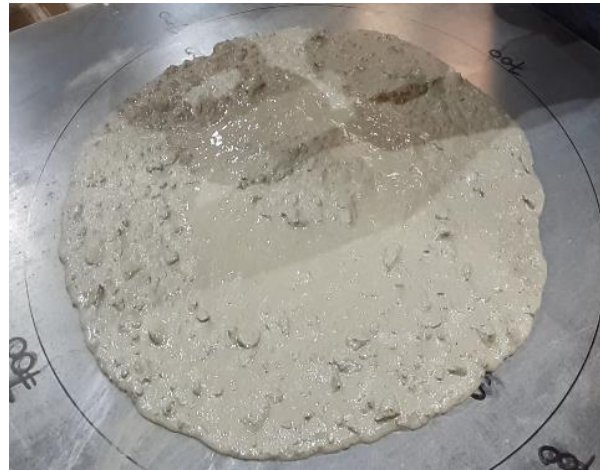
mixtures observed in the laboratory. A thorough visual inspection indicated that the self-compacting mixtures showed no signs of bleeding or segregation.

Table 6.5: Slump flow results for SCC mixes with various compressive strengths

Mix designation	Slump flow	Time for 500 mm dia. t_{500} in sec.	Viscosity class $t_{500} < 2$ s or ≥ 2 s
C30	610	1.13	VS ₁
C40	602.5	1.20	VS ₁
C50	637.5	1.35	VS ₁
C60	717.5	1.75	VS ₁
C70	690	1.87	VS ₁



(a)



(b)

Figure 6.3: Horizontal spread of SCC mixes (a) C30 (b) C40



(a)



(b)

Figure 6.4: Horizontal spread of SCC mixes (a) C50 (b) C60



Figure 6.5: Horizontal spread of SCC mix C70

Figure 6.6 illustrates the flow time of all the mixtures and the corresponding water to powder ratio (w/p) (powder consists of cement + GGBS+ LP < 125 μm). It can be clearly observed that a higher t_{500} of C70 corresponds to larger powder or reduced water content. It has been reported that the water to powder (w/p) proportion has a significant effect on both the fresh and hardened characteristics of SCC, and its impact on flow characteristics often limit the amount that can be used (Dhaheer, Alyhya and Karihaloo, 2016a). Moreover, the use of LP increases the liquidity of the SCC mix, but can negatively influences its stability. In other words, increasing the amount of LP reduces the PV of the mix (Derabla and Benmalek, 2014). Meanwhile, the use of LP in SCC increases the SP requirement to maintain a steady slump flow diameter (Gesoglu, Mehmet Güneyisi, Erhan Kocabağ, 2012). However, mixtures with low water content requires comparatively high doses of SP, specifically at low cement contents, to realize the accepted level of SCC deformability (H. Okamura and Ouchi, 2003).

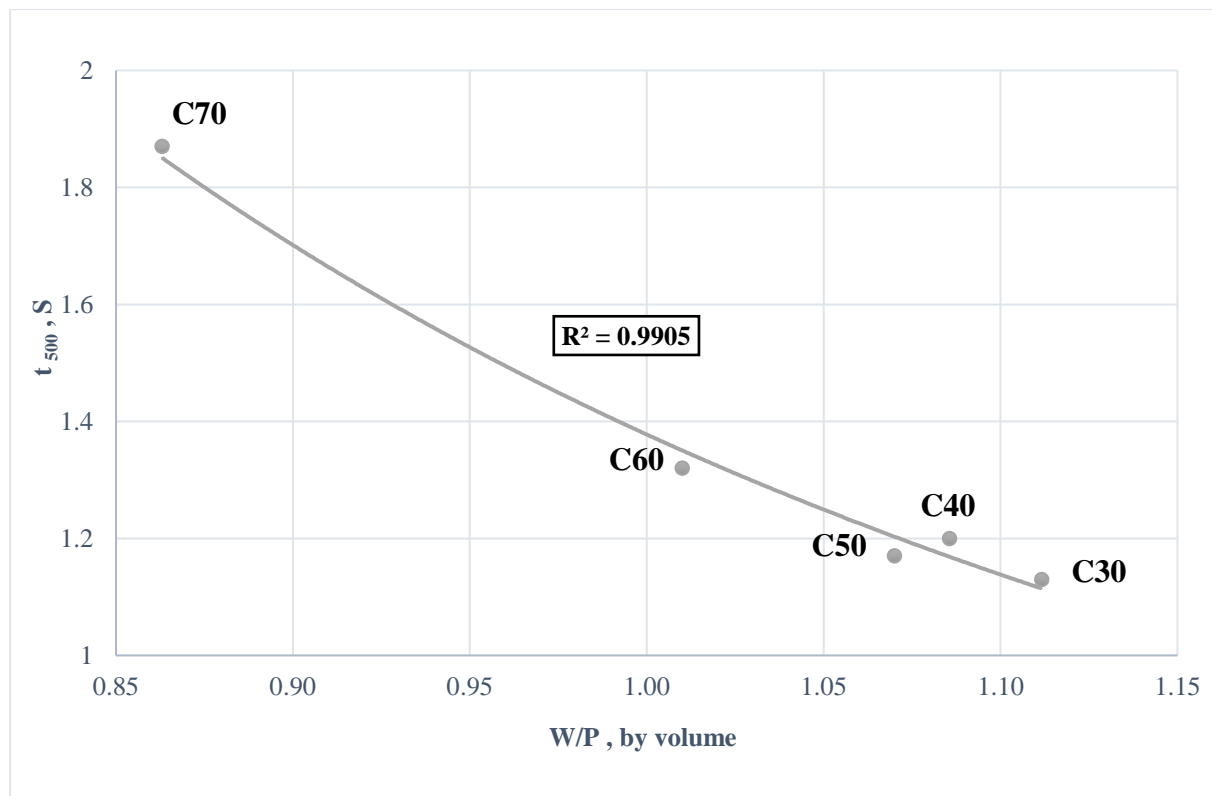


Figure 6.6: Relationship between t_{500} and water to powder volume ratio of SCC mix

Figure 6.7 shows the relationship between water-to-cement (w/cm) ratio of all the mixes and the corresponding amount of SP used. It can be clearly observed that a lower SP (e.g., C30) requirement corresponds to an increased w/cm ratio. When SP was added to increase the workability to the required level of slump flow, it was observed that a much higher SP was needed in the case of mix C70 which has very low w/c ratio. (Li and Kwan, 2015) observed that the SP amount required changed from 1.80 to 12.72 kg/m^3 and increased quite significantly with the limestone fine aggregate. Therefore, the SP required would significantly increase when limestone fine aggregate is added to substitute an equal quantity of cementitious paste, as a result of reduced water content and increased powder content.

Furthermore, it was reported in (Chen, Kwan and Jiang, 2014) that the increase in SP dose was proportionally greater than the increase in content of powder. The increase in SP requirement may be contributed by decrease in workability due to the addition of fine aggregate limestone as a cementitious paste replacement.

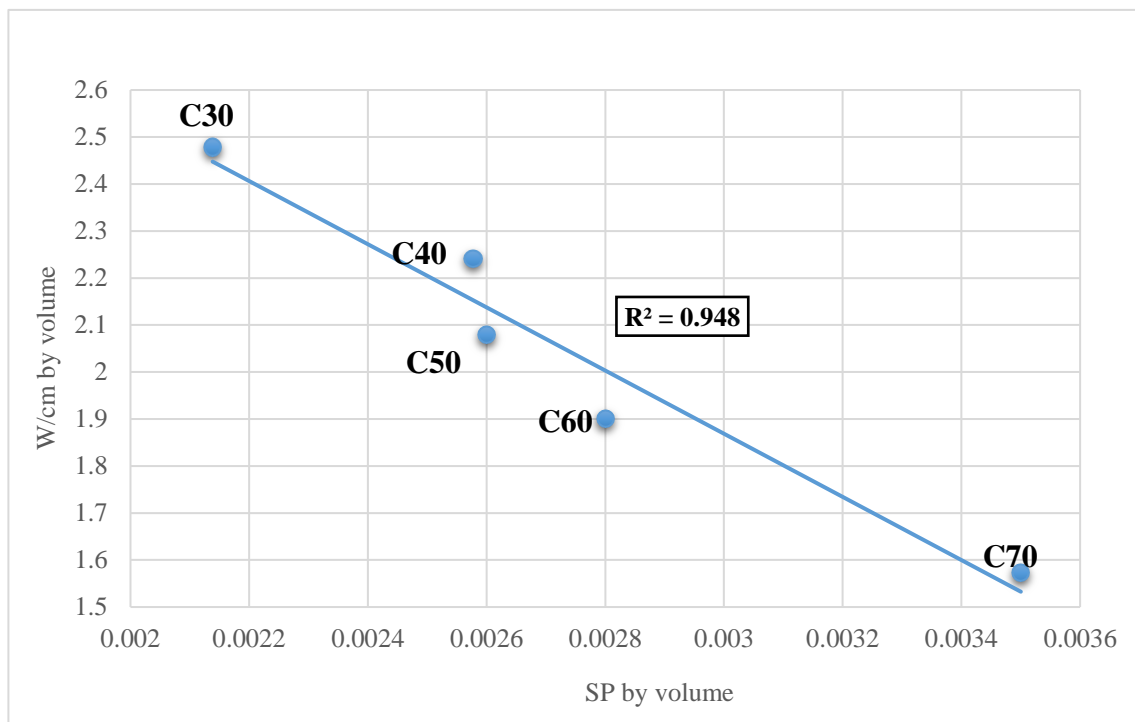


Figure 6.7: Relationship between amount of SP and water-to-cement (w/cm) volume ratio of SCC

The time taken to reach spread diameter of 500 mm is related to the PV of the mixture as shown in Figure 6.8. PV of the mixes with the final spread range of 650 ± 50 mm cannot be measured experimentally with high accuracy (Abo Dhaheer *et al.*, 2016b). Instead PV was used as the monitoring parameter, assuming that the mixtures had approximately the same yield stress, associated with t_{500} in Figure 6.8. (Hodges and Richardson, 1996)(Nehdi, Mindess and Aïtcin, 2012) described that the LP as a filler substitution of cement slightly augments the yield stress of cement paste and reduces its PV, which caused improved flowing ability and stability in cement paste. However, increasing the LP content causes bleeding of cement paste in case of high water-to-binder ratios (w/b), although it does not cause any significant influence at low w/b ratios. A sufficient volume of powder guarantees adequate flowing ability and deformability of fresh SCC, while an excess amount of powder can be counter-productive by increasing the viscosity or yield strength of a mix (Girish, Ranganath and Vengala, 2010).

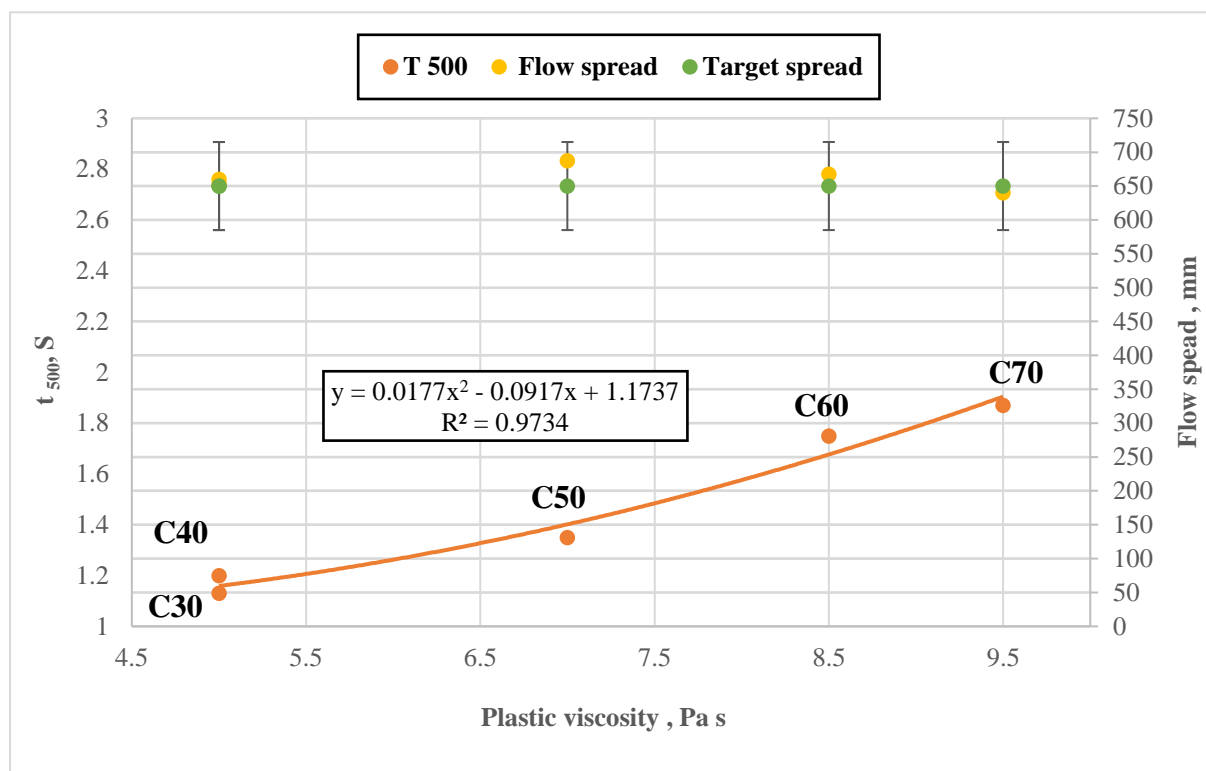


Figure 6.8: Relationship between PV, t_{500} and target flow spread (650 ± 50 mm)

All the trial mixes that fulfilled the flowing ability standard and presented no signs of segregation were subjected to filling and passing ability trial using J-ring tests to ensure that they were able to pass through narrow gaps among reinforcing bars in structural elements produced by reinforced concrete. For this objective, 300 mm diameter J-ring equipment with 16 steel rods (each of diameter 16 mm and 100 mm height) was utilized, as recommended by (BS EN 12350-8, 2010). In J-ring tests, values for final spread ranged from 590 to 695 mm, which indicated variation in viscosity class and t_{500J} (i.e., time taken for reaching 500mm diameter in J-ring test) values were between 1.97 and 2.59 s (VS₁ or VS₂). Table 6.6 presents the results of the J-ring experiment for the fresh SCC mixes. SCC mixes passed the flowing ability test and passing ability standard, and all mixtures showed no blockage or signs of segregation (Figure 6.9 to Figure 6.11). The results obtained here are in good agreement with the results reported in (Dhaheer, Alyhya and Karihaloo, 2016a). Figure 6.12 displays t_{500J} time against plastic viscosity of the SCC mixes. In addition, the Figure 6.13 compares t_{500} for both slump flow and J-ring flow of SCC mixes against their plastic viscosities. The variation among these times is minimum for the mixes with higher PV (i.e., 9.5 Pa s for C70).

Table 6.6: J-ring resulting of SCC concordance with mix

Mix designation	J-ring	Time for 500 mm dia. t_{500J} in sec.	Viscosity class t_{500} < 2 s or \geq 2 s
C30	600	1.97	VS ₁
C40	600	2.02	VS ₂
C50	592.5	2.59	VS ₂
C60	695	2.55	VS ₁
C70	685	2.24	VS ₂



(a)



(b)

Figure 6.9: Flow and passing ability of SCC mix (a) C30 (b) C40



(a)



(b)

Figure 6.10: Flow and passing ability of SCC mix (a) C50 (b) C60

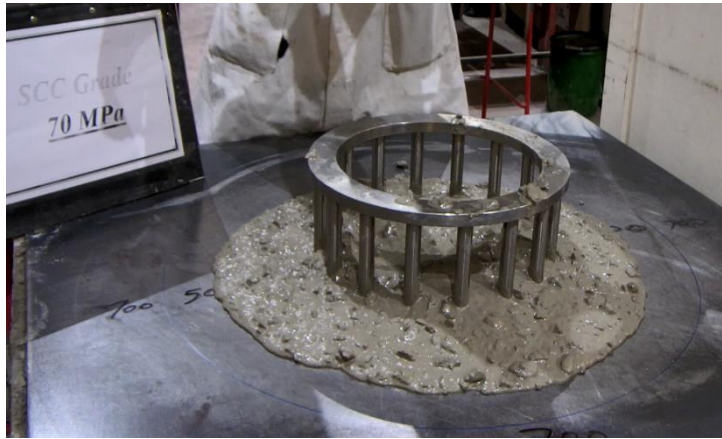
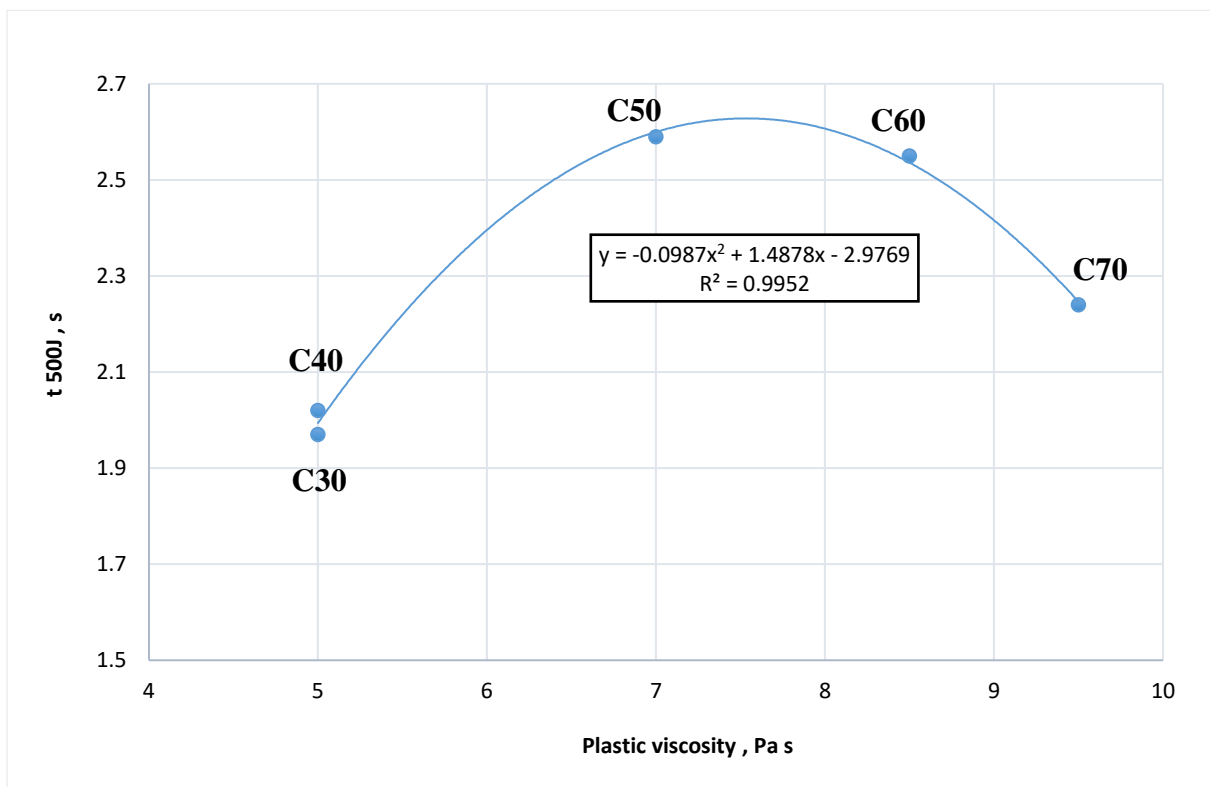


Figure 6.11:Flow and passing ability of SCC mix (C70)

Figure 6.12:t_{500J} time. plastic viscosity

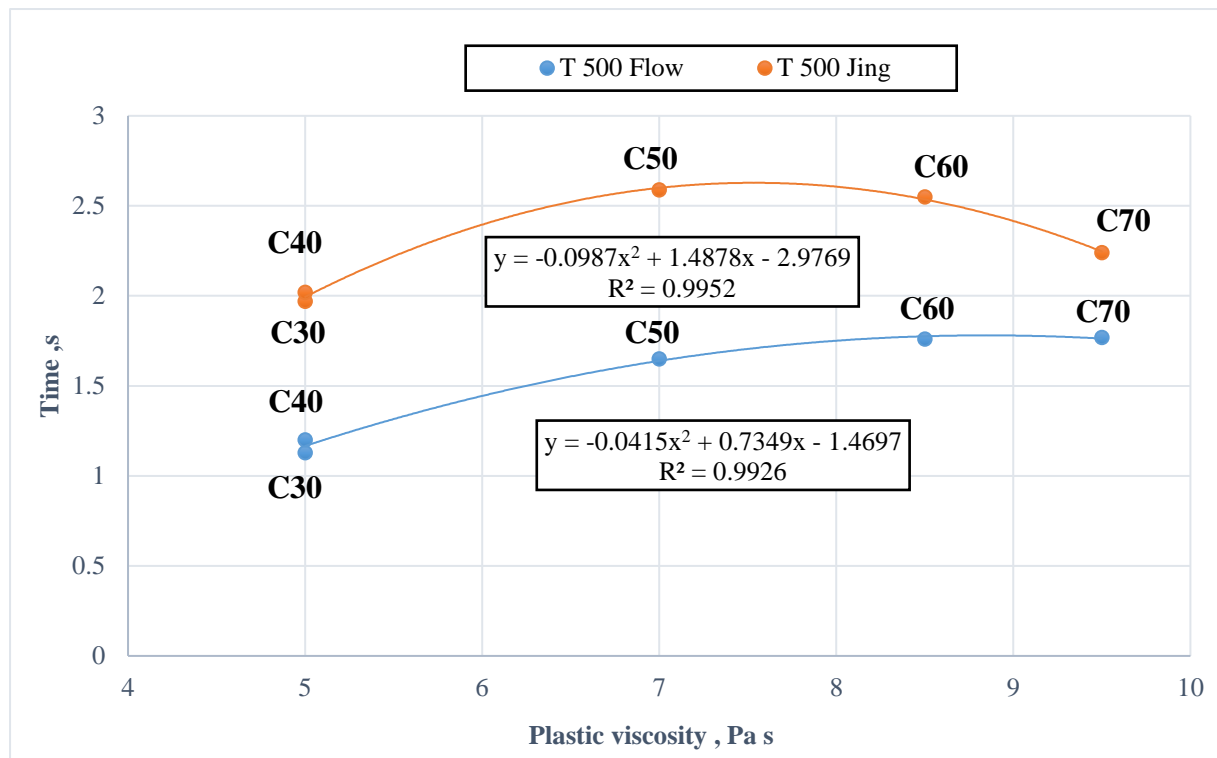


Figure 6.13: Plastic viscosity versus t_{500} and t_{500J} of SCC mixes

The passing ability of SCC can also be judged by measuring height variation between the concrete mix outside and inside steel bars of the J-ring, as shown in Figure 6.14. According to (BS EN 206-9:2010, 2010) the blocking step (P_J) should be less than 10 mm for an SCC mix to satisfy the passing ability. The blocking step height (P_J) obtained during the J-ring test is also presented in Table 6.7. It is clear from the results that all SCC mixes satisfy the passing ability criteria.

Table 6.7 :J-ring test (blocking step) resulting of SCC concordance with mix

Mix designation	$P_J = \frac{\Delta h_{x1} + \Delta h_{x2} + \Delta h_{y1} + \Delta h_{y2}}{4} - \Delta h_0$	That it could be ≤ 10 mm
C30	10	= 10 mm
C40	9.5	< 10 mm
C50	8.25	< 10 mm
C60	9.25	< 10 mm
C70	9.75	< 10 mm



Figure 6.14: J-ring test (blocking step) SCC mix

In accordance with (ASTM:C1621/C 1621M1, 2017), the slump flow test can be used with the J-ring test to measure the passing ability of SCC. If the difference in spread diameters of the two tests ($D_{\text{flow}} - D_{\text{J-ring}}$) is minimal (less than 25 mm), there is no visual blockage. If it is from 25 to 50 mm, there is minimum to noticeable blockage. Table 6.8 displays the difference from slump flow and J-ring trial, clearly showing that for most of the mixtures there is minimum or no blockage.

Table 6.8: Difference between flow and J-ring spread diameter

Mix designation	D_{FLOW} , mm	D_{J} , mm	$D_{\text{FLOW}} - D_{\text{J}}$ (mm)
C30	610	600	10
C40	602.5	600	2.5
C50	637.5	592.5	45
C60	717.5	695	22.5
C70	690	685	5

6.5.2 Tests on hardened SCC

The compressive strength test was performed in this experimental study on the cube specimens (three per mixture and curing age) with size $100 \times 100 \times 100$ mm³ from each mix. These compressive strength tests were conducted on specimen following under water curing regimes at 7, 14, and 28 days. The results of the compressive strength tests are shown in Table 6.9 and Figure 6.15.

Table 6.9: Compressive strength of samples water cured at 7, 14 and 28 days

Mix designation	Compressive strength (7 days) MPa	Compressive strength (14 days) MPa	Compressive strength (28 days) MPa
C30	26.21	32.18	39.51
C40	29.13	34.71	40.64
C50	33.57	40.75	50.45
C60	40.94	45.92	56.32
C70	45.35	55.01	63.01

It can be noted that increase in compressive strength can be described through decreased water or powder content, corresponding to w/cm ratios decreasing, as shows in Figure 6.16. This outcome is in agreement with results stated by Appa Rao (Rao, 2001) and Fernandes et al. (Fernandes et al., 2005).

Increase of w/c ratio from 0.35 to 0.7 results in 66% decreased compressive strength. This trend has also been stated by Felekoglu et al. (Felekoğlu, Türkel and Baradan, 2007) , while Domone (Domone, 2007) stated that in SCC the type and content of powder affect the compressive strength much more than the w/c ratio.

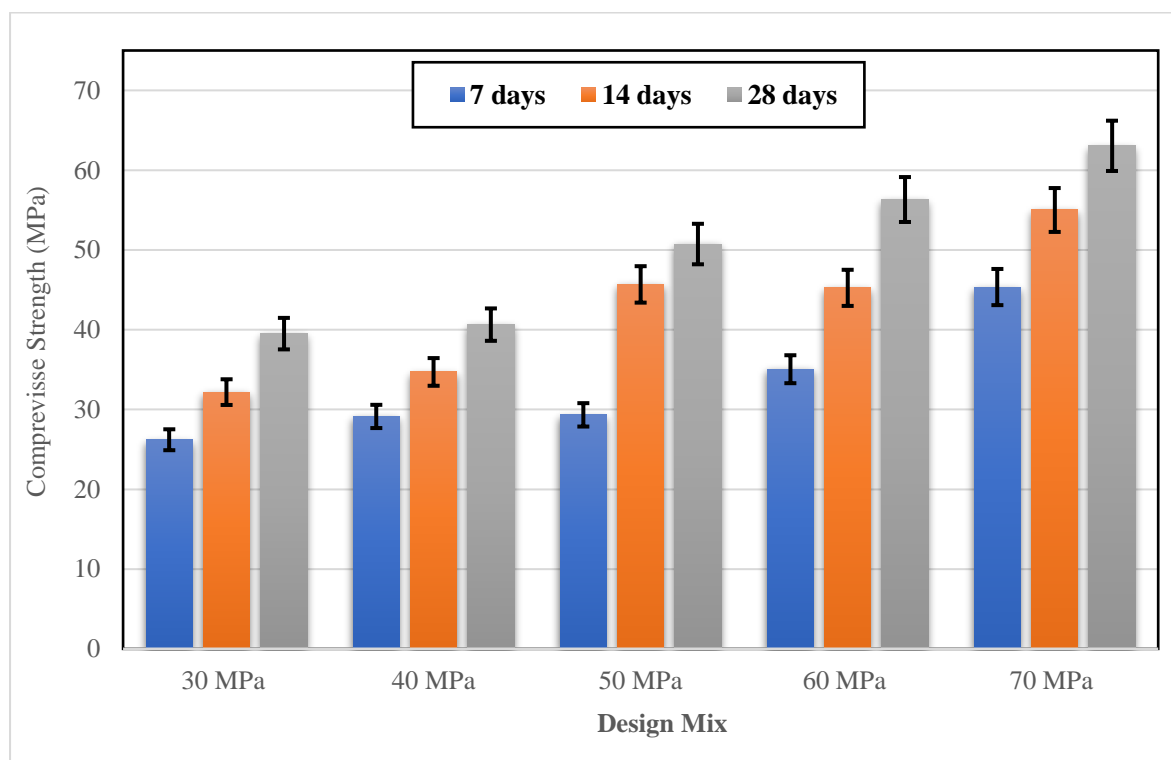


Figure 6.15: Improvement in compressive strength of SCC mixes

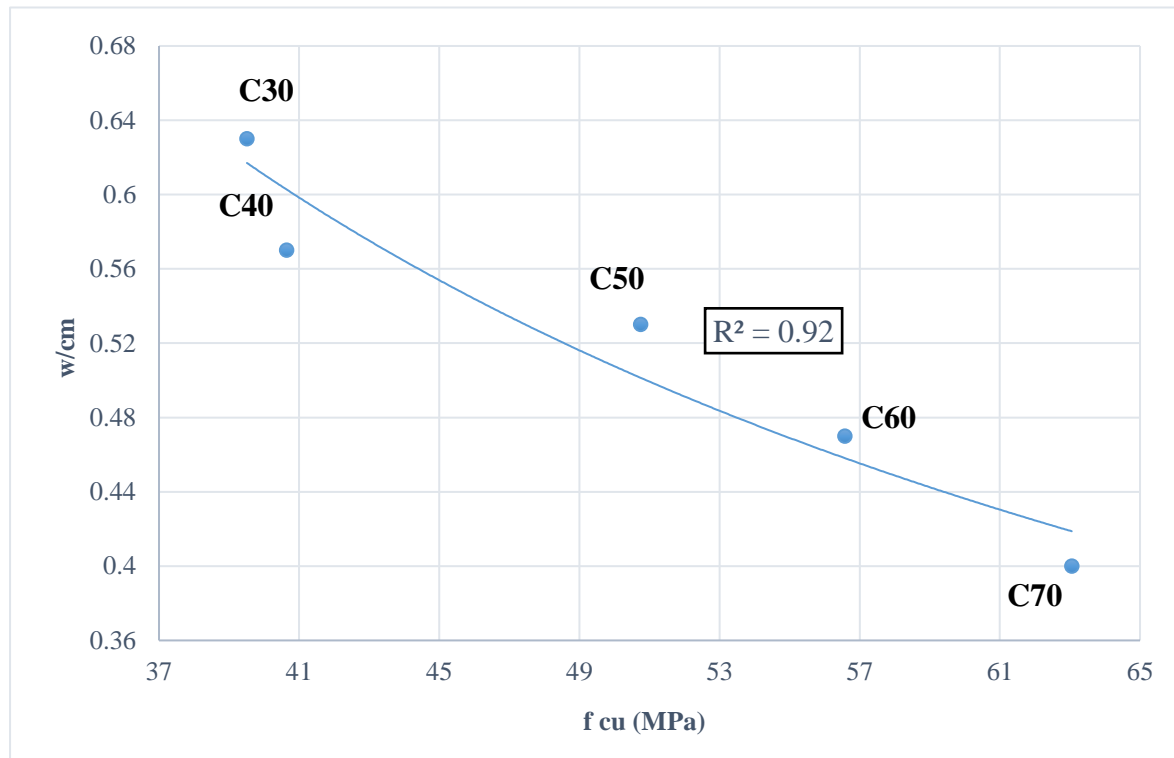


Figure 6.16: Relationship between compressive strength (MPa) after 28 days and w/cm ratios

6.6 Further analysis of SCC mix with target compressive strength of 50 MPa , 60 MPa and 70 MPa

It can be noted from Table 6.9 that the compressive strengths of mixes C60 and C70 did not reach their target compressive strengths (i.e., 60 and 70 MPa respectively) in 28 days. Although these mixes satisfied the SCC criteria for fresh state tests, they are not able to reach the predicted compressive strengths. To further investigate this behaviour, additional tests were carried out on SCC mixes with target compressive strength of 60 MPa and 70 MPa. However, to ensure the consistency across further investigations, the same additional tests were also conducted on 50 MPa mix.

According to the specification of PLC (i.e., CEM II/A-L/32.5R) used in this work, this cement is likely to contain 6% to 20% of LP by weight. Therefore, it was assumed that the amount of LP already contained may impact on the amount of cement available to achieve the target compressive strengths in case of 60MPa and 70MPa. Hence, to investigate the influence of LP already in this cement, four different mixes for each target compressive strengths (i.e., 50MPa, 60MPa and 70MPa) were designed assuming that the cement already includes (i) 6%, (ii) 10%, (iii) 15% or (iv) 20% LP. And these new mixes are denoted, respectively, as C50⁽ⁱ⁾, C50⁽ⁱⁱ⁾, C50⁽ⁱⁱⁱ⁾, C50^(iv), C60⁽ⁱ⁾, C60⁽ⁱⁱ⁾, C60⁽ⁱⁱⁱ⁾ and C60^(iv), C70⁽ⁱ⁾, C70⁽ⁱⁱ⁾, C70⁽ⁱⁱⁱ⁾ and C70^(iv). For example, in mix C60⁽ⁱ⁾, the mix proportions of the constituents were estimated assuming that the PLC already contains 6% of LP by weight and accordingly adjustments were made in the amount of cement and LP used in the mix design. To be precise, compared with C60 mix in Table 6.2, 6% more PLC (CEM II/A-L/32.5R) was used in C60⁽ⁱ⁾ and, accordingly the corresponding amount of LP was reduced compared with C60. The same procedure was repeated in the case of the other three mixes according to 10, 15 and 20% LP content in the cement. All the mixes were designed according to mix proportioning method discussed in chapter 4.

Table 6.10 presents mix proportions of amended mixes and the original mixes with target compressive strengths 50 MPa, 60 MPa and 70 MPa. Additional details of these SCC test mixes are presented in Table 6.11.

Table 6.10: Mix proportions of test SCC mixes (kg / m³)

Mix designation	cm ^a		Water	SP ^b	w/cm	SP/cm	LP ^c	FA ^d		CA ^e
	Cement	ggs						FA ^{**}	FA ^{***}	
C50	300	100	210	2.9	0.52	0.72	115	185	600	780
								785		
C50⁽ⁱ⁾	293	98	207	2	0.53	0.51	113	229	550	868
								729		
C50⁽ⁱⁱ⁾	293	98	207	1.85	0.53	0.47	100	233	500	873
								733		
C50⁽ⁱⁱⁱ⁾	293	98	207	1.78	0.53	0.45	86	240	500	881
								740		
C50^(iv)	293	98	207	1.70 (2.6) ^f	0.53	0.43	69	248	500	890
								748		
C60	314	105	197	2.6 (2.8) ^g	0.47	0.62	99	167	550	924
								717		
C60⁽ⁱ⁾	315	105	198	2.9	0.47	0.69	151	283	410	856
								693		
C60⁽ⁱⁱ⁾	315	105	198	2.6	0.47	0.62	140	198	500	862
								698		
C60⁽ⁱⁱⁱ⁾	315	105	198	2.3	0.47	0.55	125	206	500	871
								706		
C60^(iv)	315	105	198	2	0.47	0.48	109	214	500	881
								714		
C70	348	116	186	2.8 (3.5) ^h	0.40	0.60	117	230	501	843
								731		
C70⁽ⁱ⁾	351	117	187	2.8 (3.8) ^h	0.40	0.59	96	238	500	851
								738		
C70⁽ⁱⁱ⁾	351	117	187	2.8 (3.8) ^h	0.40	0.59	85	224	520	858
								744		
C70⁽ⁱⁱⁱ⁾	351	117	187	2.8 (3.9) ^h	0.40	0.59	68	252	500	868
								752		
C70^(iv)	351	117	187	2.8 (3.9) ^h	0.40	0.59	49	261	500	879
								761		
Density	2950	2400	1000	1070	--	--	2400	2400	2650	2800

(i), (ii), (iii) and (iv) refer to the reduction in Limestone powder (LP) volume by 6 %, 10%, 15% and 20% respectively in the mix for the same strength grade.

a Cementitious material.

b Super-plasticizer.

c Limestone powder <125 μm .

d Fine aggregate <2 mm (Note: a part of the fine aggregate is the coarser fraction of the limestone powder, FA**125 μm –2 mm, whereas FA*** refers to natural river sand < 2 mm).

e Coarse aggregate < 20 mm.

f the number in parentheses indicates the amount of SP required during the experiment instead of the estimated amount of 1.7.

g the number in parentheses indicates the amount of SP required during the experiment instead of the estimated amount of 2.6.

h the number in parentheses indicates the amount of SP required during the experiment instead of the estimated amount of 2.8.

Table 6.11: Further details of test SCC mixes

Mix designation	Target plastic viscosity (Pa s)	Actual plastic* viscosity (Pa s)	Plastic Viscosity diff.	Paste vol. fraction	Solid vol. fraction	Paste/Solid (by vol.)
C50	7	6.76	-3.3	0.40	0.60	0.67
C50 ⁽ⁱ⁾	7	6.91	-1.21	0.39	0.61	0.65
C50 ⁽ⁱⁱ⁾	7	6.77	-3.19	0.39	0.61	0.64
C50 ⁽ⁱⁱⁱ⁾	7	6.75	-3.63	0.39	0.62	0.63
C50 ^(iv)	7	6.76	-3.42	0.38	0.62	0.61
C60	8.5	8.69	+2.29	0.39	0.62	0.62
C60 ⁽ⁱ⁾	8.5	8.39	-1.23	0.41	0.58	0.70
C60 ⁽ⁱⁱ⁾	8.5	8.32	-2.07	0.41	0.59	0.69
C60 ⁽ⁱⁱⁱ⁾	8.5	8.32	-2.06	0.40	0.59	0.67
C60 ^(iv)	8.5	8.32	-2.07	0.39	0.60	0.65
C70	9.5	9.55	-0.53	0.40	0.60	0.68
C70 ⁽ⁱ⁾	9.5	9.24	-2.73%	0.39	0.60	0.66
C70 ⁽ⁱⁱ⁾	9.5	9.34	-1.72%	0.39	0.61	0.65
C70 ⁽ⁱⁱⁱ⁾	9.5	9.38	-1.27%	0.38	0.61	0.63
C70 ^(iv)	9.5	9.42	-0.79%	0.37	0.60	0.61

Actual plastic viscosity*: mix plastic viscosity that is calculated using equation 4.6.

Table 6.12 and Table 6.13 present the experimental results obtained in slump flow and J-ring tests. The results show that all the mixes successfully fulfilled both flow tests and satisfied the recommended SCC properties in the fresh state. Furthermore, it can be noticed that the flow properties (e.g., flow spread) of the mixtures were not significantly affected by the changes made in the amount of PLC and LP (Figure 6.17 to Figure 6.20) and (Figure 6.21 to Figure 6.24).

Table 6.12: Slump flow and J-ring test results for corresponding SCC mixes

Mix design	Slump flow	Time 500 mm (sec)	Viscosity class $t_{500} < 2 \text{ s or } \geq 2 \text{ s}$	J-ring	Time 500 mm (sec)	Viscosity class $t_{500} < 2 \text{ s or } \geq 2 \text{ s}$
C50	637.5	1.35	VS ₁	592.5	2.59	VS ₂
C50⁽ⁱ⁾	605	1.60	VS ₁	600	1.86	VS ₁
C50⁽ⁱⁱ⁾	615	1.53	VS ₁	610	1.80	VS ₁
C50⁽ⁱⁱⁱ⁾	635	1.37	VS ₁	627.5	1.75	VS ₁
C50^(iv)	615	1.17	VS ₁	610	1.73	VS ₁
C60	717.5	1.75	VS ₁	695	2.55	VS ₂
C60⁽ⁱ⁾	675	1.67	VS ₁	665	1.75	VS ₁
C60⁽ⁱⁱ⁾	625	1.41	VS ₁	620	1.73	VS ₁
C60⁽ⁱⁱⁱ⁾	645	1.29	VS ₁	635	1.66	VS ₁
C60^(iv)	705	1.18	VS ₁	690	1.59	VS ₁
C70	690	1.87	VS ₁	685	2.24	VS ₂
C70⁽ⁱ⁾	625	2.36	VS ₂	602.5	2.80	VS ₂
C70⁽ⁱⁱ⁾	645	2.60	VS ₂	622.5	2.83	VS ₂
C70⁽ⁱⁱⁱ⁾	725	2.58	VS ₂	710	2.56	VS ₂
C70^(iv)	740	2.33	VS ₂	730	2.93	VS ₂

Table 6.13: J-ring test (blocking step) and difference between flow and J-ring spread diameter results of corresponding SCC mixes

Mix designation	P_J	That it could be ≤ 10 mm	D_{FLOW} , mm	D_J , mm	$D_{FLOW} - D_J$ (mm)
C50	8.25	< 10 mm	637.5	592.5	45
C50⁽ⁱ⁾	8.25	< 10 mm	605	600	5
C50⁽ⁱⁱ⁾	6.5	< 10 mm	615	610	5
C50⁽ⁱⁱⁱ⁾	7.75	< 10 mm	635	627.5	7.5
C50^(iv)	8	< 10 mm	615	610	5
C60	9.25	< 10 mm	717.5	695	22.5
C60⁽ⁱ⁾	7.5	< 10 mm	675	665	10
C60⁽ⁱⁱ⁾	7.75	< 10 mm	625	620	5
C60⁽ⁱⁱⁱ⁾	9.25	< 10 mm	645	640	5
C60^(iv)	8	< 10 mm	705	690	15
C70	9.75	< 10 mm	690	685	5
C70⁽ⁱ⁾	8	< 10 mm	625	602.5	22.5
C70⁽ⁱⁱ⁾	7.5	< 10 mm	645	622.5	22.5
C70⁽ⁱⁱⁱ⁾	9	< 10 mm	725	710	15
C70^(iv)	9	< 10 mm	740	730	10



(a)



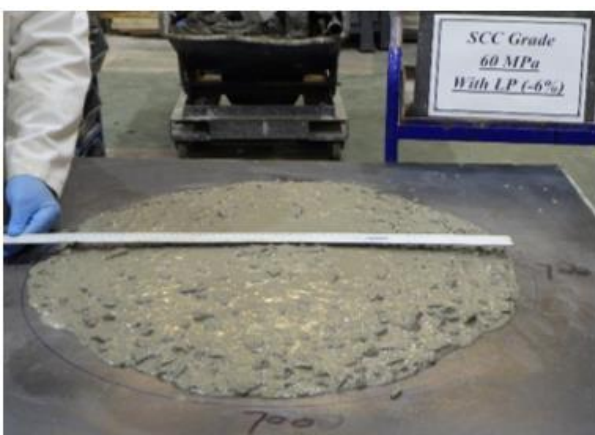
(b)

Figure 6.17: Horizontal spread of SCC mix (a)C50⁽ⁱ⁾ (b)C50⁽ⁱⁱ⁾

(a)



(b)

Figure 6.18: Horizontal spread of SCC mix (a)C50⁽ⁱⁱⁱ⁾ (b)C50^(iv)

(a)



(b)

Figure 6.19: Horizontal spread of SCC mix (a)C60⁽ⁱ⁾ (b)C60⁽ⁱⁱ⁾



(a)



(b)

Figure 6.20: Horizontal spread of SCC mix (a)C60⁽ⁱⁱⁱ⁾ (b)C60^(iv)



(a)



(b)

Figure 6.21: Flow and passing ability of SCC mix (a)C50⁽ⁱ⁾ (b)C50⁽ⁱⁱ⁾



(a)



(b)

Figure 6.22: Flow and passing ability of SCC mix (a)C50⁽ⁱⁱⁱ⁾ (b)C50^(iv)



Figure 6.23: Flow and passing ability of SCC mix (a)C60⁽ⁱ⁾ (b)C60⁽ⁱⁱ⁾



Figure 6.24: Flow and passing ability of SCC mix (a)C60⁽ⁱⁱⁱ⁾ (b)C60^(iv)

Table 6.14 summarises the experimental results obtained during cube compression tests. It can be seen from Table 6.14 that the new mixes (i.e., denoted by i, ii, iii, iv) were able to achieve compressive strengths closer to target compressive strength compared to the corresponding original mixes C60 and C70. Figure 6.25 provides additional information on the range of compressive strengths reached at 28 days of age compared with the original SCC mix with a target compressive strength 50 MPa (i.e., C50). It can also be noted from the above results that the difference in compressive strength achieved by the new mixes at the end of 28 days was not significant.

Table 6.14: Compressive strength of samples water cured at 7, 14 and 28 days

Mix designation	Compressive strength (7 days) MPa	Compressive strength (14 days) MPa	Compressive strength (28 days) MPa
C50	33.57	40.75	50.45
C50⁽ⁱ⁾	30.82	47.17	53.35
C50⁽ⁱⁱ⁾	31.73	46.05	52.42
C50⁽ⁱⁱⁱ⁾	31.47	46.83	59.51
C50^(iv)	29.33	45.68	50.74
C60	40.94	45.92	56.32
C60⁽ⁱ⁾	39.44	51.86	58.33
C60⁽ⁱⁱ⁾	38.12	51.44	60.98
C60⁽ⁱⁱⁱ⁾	37.81	55.01	58.38
C60^(iv)	37.77	50.83	59.79
C70	45.35	55.01	63.01
C70⁽ⁱ⁾	55.79	58.97	72.89
C70⁽ⁱⁱ⁾	55.36	60.61	66.57
C70⁽ⁱⁱⁱ⁾	55.30	62.68	70.72
C70^(iv)	56.06	63.32	65.81

All the new mixes satisfied the fresh-state requirements. Furthermore, it can be seen clearly from Figure 6.25 , Figure 6.26 and Figure 6.27 that the new mixes were able to achieve compressive strengths closer to the target value. These results indicate that amending the amount of PLC and accordingly adjusting the amount of LP as per the specification of CEM II/A-L/32.5R enable the recommended (Abo Dhaheer et al., 2016b) mix proportion to achieve a target compressive strength of 60 MPa or above. The investigations demonstrate that the mix proportions derived according to the method of (Abo Dhaheer et al., 2016b) may not always produce the desired SCC compressive strength unless PLC with a suitable specification is used. Therefore, when using the procedure proposed by (Abo Dhaheer et al., 2016b), it is important to consider the cement specification to be used for preparing the mix proportions, especially for higher target compressive strengths (i.e., for 60 MPa and above).

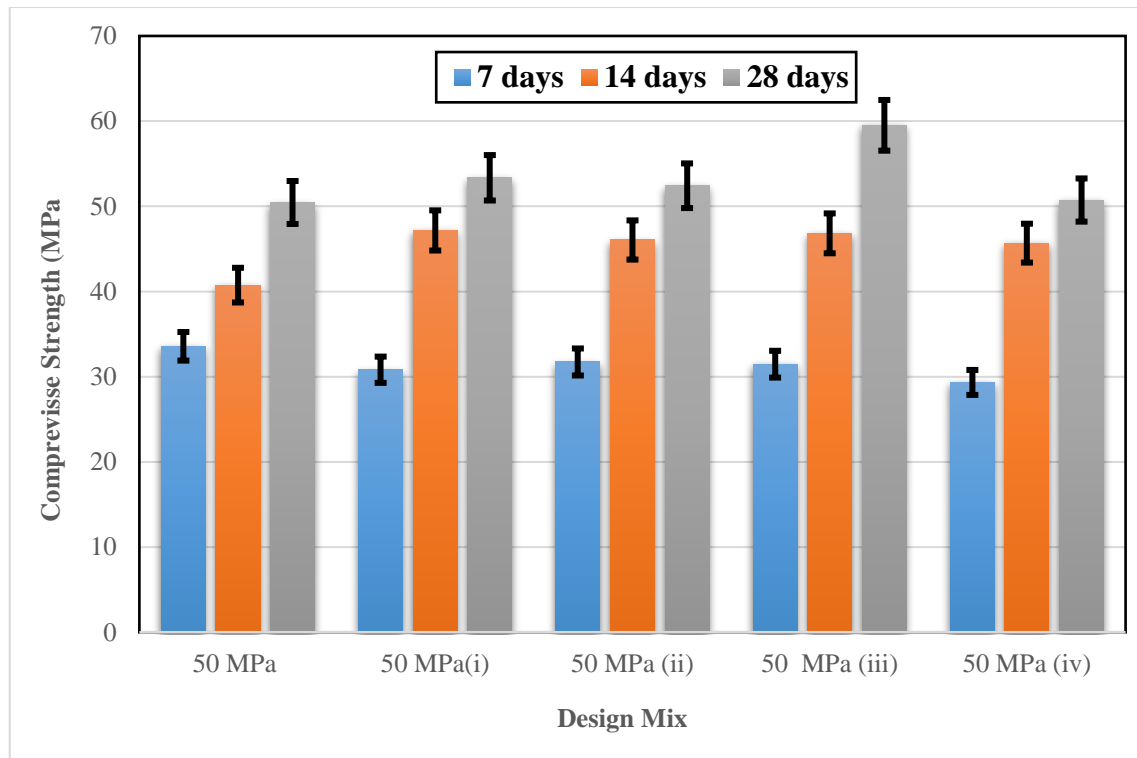


Figure 6.25: Variability of the compressive strength of each mix related to the control mix C50

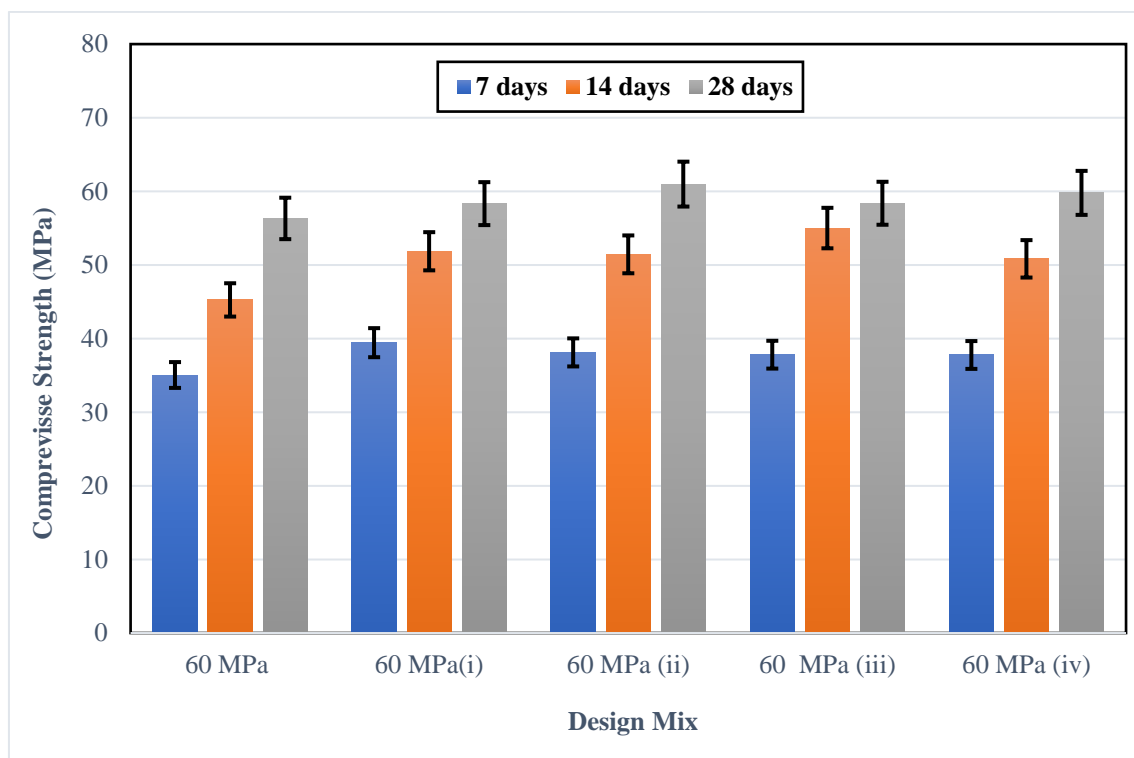


Figure 6.26: Variability of the compressive strength of each mix related to the control mix C60

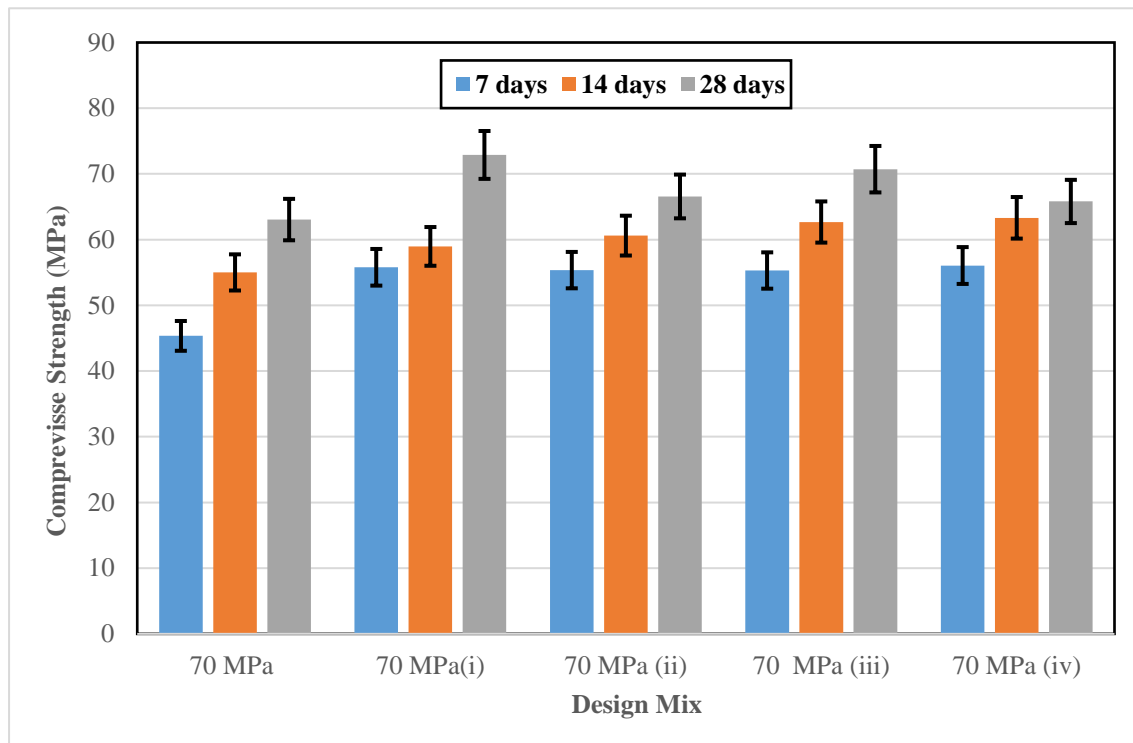


Figure 6.27: Comparison of compressive strength between new mixes and control mix C70

6.7 Concluding remarks

This study explored the influence of SCC design mix variables with various combinations of powder materials (in a ternary mix of Portland limestone cement (PLC) + GGBS + LP), water/binder ratios, and SP dose, in order to understand the impacts of Limestone powder on both fresh and hardened design mix SCC. Based on the experimental work and analysis presented above, the following salient conclusions can be drawn:

- Using LP as a filler with PLC did not significantly affect T_{500} time test values.
- Reducing w/cm proportions from 0.63 to 0.40 increased the value of compressive strength by 44%.
- The influence of powder content in increasing compressive strength is more remarkable (e.g. limestone and GGBS).
- With reduced LP content (from 6–20%) as a replacement with PLC of the SCC mix (with 50 MPa 60 MPa and 70 MPa), compressive strength increased by 15% , 7% and 14% at 28 days for w/cm ratios of 0.53 , 0.47 and 0.40 respectively.

- Incorporating LP to replace sand (fine aggregate) improves the characteristics of PLC-based materials, therefore it is recommended to replace fine aggregate or cement paste with a suitable quantity of LP.

Chapter 7

Developing self-compacting steel fibre reinforced concrete - an investigation of flow and mechanical properties: Experimental validation II

7.1 Introduction

The standard design of a self-compacting concrete (SCC) mix is a compromise between two conflicting goals. On the one hand, the SCC has to be as fluid as possible to ensure that it will fill the formwork under its own weight. On the other hand, the mixture has to be stable enough to prevent segregation of solids during the flow (Spangenberg J, Roussel N, Hattel JH, Thorborg J, Geiker MR, 2010)(Su, Hsu and Chai, 2001)(Roussel, 2007). The former criterion is ensured by using super-plasticiser and/or viscosity modifying admixtures, while the latter is achieved through the selection of an appropriate amount and type of powders, i.e., cement and additional cementitious materials (ACMs), and by striking an right balance between the solids and liquids in the mix. Therefore, viscosity-modifying agent, additional cementitious materials (e.g., ground granulated blast-furnace slag, natural pozzolans, and fly ash etc), and superplasticizer (SP) are necessary elements to decrease the water/binder proportion, to decrease the production cost of SCC and to ensure accurate viscosity level (Sahmaran and Yaman, 2007). The mix quality of SCC with steel fibres significantly depends on the composition and characteristics of its components both in its fresh and hardened properties. The prediction of its flowing and passing behaviour is very complicated particularly in the presence of congestion with reinforcing steel bars and in formworks of complex shapes. Nevertheless, an understanding of the behaviour, namely the flow and passing characteristics are crucial to achieving a high-quality of Self-compacting steel fibre reinforced concrete (SCSFRC). The most pragmatic and effective way to achieve such an understanding is by performing Laboratory experiments, which will enable us to fully understand the flow, passing and filling ability behaviour of SCSFRC and to reveal the distribution of steel fibres and their orientations inside the formworks.

Significant efforts have been devoted to understand the effect of steel fibres in concrete for decades, by testing the properties of both fresh and hardened SCC. Fibres are known to influence the workability and flow properties of fresh concrete relative to the content and type of fibres used, and matrix components in which they are embedded. A favourable fibre distribution is essential in order to obtain optimal advantages of any fibres. Applications of SCC aim to achieve satisfactory workability of fresh concrete characteristics with enhanced performance of hardened concrete characteristics. The addition of fibres tends to decrease workability, varying according to the amount, type, and shape of fibres used. The fibre content that can be used while the mixture is still workable depends completely on the mix composition and fibre type (El-dieb and Taha, 2012).

Self-compacting fibre reinforced concrete can enhance fibre dispersion, decrease the risk of inefficient workability, and assist placement and compaction, but the fibres are expected to decrease the flow and passing ability of fresh SCC, which is susceptible to mix design methods. This is usually addressed by using limits on fibre content and size, while increasing the use of chemical admixtures (Forgeron and Omer, 2010). While fibres considerably enhance the performance and load-bearing abilities, the addition of fibres in concrete fundamentally degrades the workability and passing ability (Wang, Aslani and Liu, 2020). SCC is a favourable material that can overcome these obstacles for some extent compare to conventional vibrated concrete (VC) (Abo Dhaheer, Kulasegaram and Karihaloo, 2016). SCC settles through gravity and there is no requirement for any external vibration or agitation, hence it is much easier to work with steel or other types of fibre.


The advantages of self-compacting concrete (SCC) are increased by fibres bridging cracks, delaying their spread and hence enhancing the hardened properties of concrete including, tensile strength, fracture toughness, and flexural strength. Consequently, the use of fibres may expand the potential scopes of application of SCC. Steel fibre reinforced concrete is widely used in sidewalks and roads, parking lots, airports, tunnels and bridges (Mohamed *et al.*, 2019)(Ghasemi, Ghasemi and Mousavi, 2018a). The addition of steel fibres improves the mechanical characteristics and the ductility of SCC in much the same manner as in vibrated concrete. However, the fibres greatly impair the workability of SCC because of their elongated shape and large surface area. The amount of fibre that can be added to a SCC mix is therefore limited and depends on the fibre type used and the composition of the SCC mix. The maximum amount of fibre needs to be determined in such a way as to cause the least impact on the workability, whilst maintaining good flowing, passing and filling ability. In order to make the best use of the fibres, they need to be homogeneously distributed in the mix without clustering. This chapter focuses on the development of self-compacting normal-performance concrete mixes with steel fibres. The aim is to investigate how the proportions of solids and liquids and the super-plasticiser need to be selected for a particular type of steel fibre in order to produce SCC mixes with the right flowing, passing and filling ability. The plastic viscosity of the SCC mixes so developed will then be assessed by the micromechanical procedure explained by (Ghanbari and Karihaloo, 2009). This plastic viscosity, together with the yield stress of the mix, is needed in the numerical simulation of SCC flow in moulds of different shapes and sizes (Kulasegaram, Karihaloo* and Ghanbari., 2010). In addition, it is the

objective to investigate in detail the role of several composition parameters (steel fibre volume, paste to solids and water to binder ratios) of SCC in their fracture behaviour.

7.2 Experimental programme

A laboratory study was conducted to produce various grade from normal strengths of SCC with and without steel fibres (the 30 mm long, 0.55 mm diameter, see Table 7.1). These mixes correspond to nominal 28 days cube compressive strengths of 30 MPa, 50 MPa and 70 MPa. The amounts and details of the components used in the SCC mixes are shown in Table 7.2. Portland limestone cement (PLC) (CEM II/A-L/32.5R) conforming to (BS EN 197-1, 2011) with a specific gravity of 2.95, the Ground granulated blast-furnace slag (GGBS) with a specific gravity of 2.40 and Micro-silica (MS) with a specific gravity of 2.20 were used as the main cement and cement replacement materials respectively. A new generation of polycarboxylic ether-based superplasticiser (SP) with specific gravity of 1.07 was used in all the test mixes. Crushed limestone coarse aggregate with maximum particle size of 20 mm and a specific gravity of 2.80 was used, while the fine aggregate was river sand (less than 2 mm) having a specific gravity of 2.65. Limestone powder (LP) as a filler with maximum particle size of 125 μm (specific gravity 2.40) was used. A part of the river sand was substituted by an equal amount of the coarser fraction of LP in the size range 125 μm – 2 mm. All mixes were subjected to the slump cone, J-ring and L-box tests to ensure that the fresh state properties met the prescribed criteria (BSi, 2010) (EFNARC, 2005).

Table 7.1: Characteristics of steel fibres

Fiber shape	Hooked end	
Length (mm)	30	
Wire diameter (mm)	0.55	
Aspect ratio	55	
Specific Gravity	7.85	
Tensile strength (MPa)	1.345	
Young's Modulus	± 210.000	

Better proportioning of design mixes in SCC are achieved through optimising the percentage of filler materials in the mix. The fundamental materials and secondary materials for the mix in SCC and SCSFRC are produced according to the mix design method proposed by (Karihaloo and Ghanbari, 2012a), (Deeb and Karihaloo, 2013a), (Abo Dhaheer *et al.*, 2016a) and (de la Rosa *et al.*, 2018b). The mixes were designed to achieve 28-day nominal cube compressive strengths of 30, 50 and 70 MPa with w/cm ratios of 0.63, 0.52 and 0.40

respectively. Here the specified typical ranges of primary constituent materials include powder (cementitious materials + filler), water, and aggregate as shown in Table 7.2. A rigorous process of proportioning materials for normal strength SCC is dependent on the plastic viscosity and compressive strength of the SCC mixes (Abo Dhaheer *et al.*, 2016a). The procedure followed for mix design and testing is summarized in Figure 7.1:

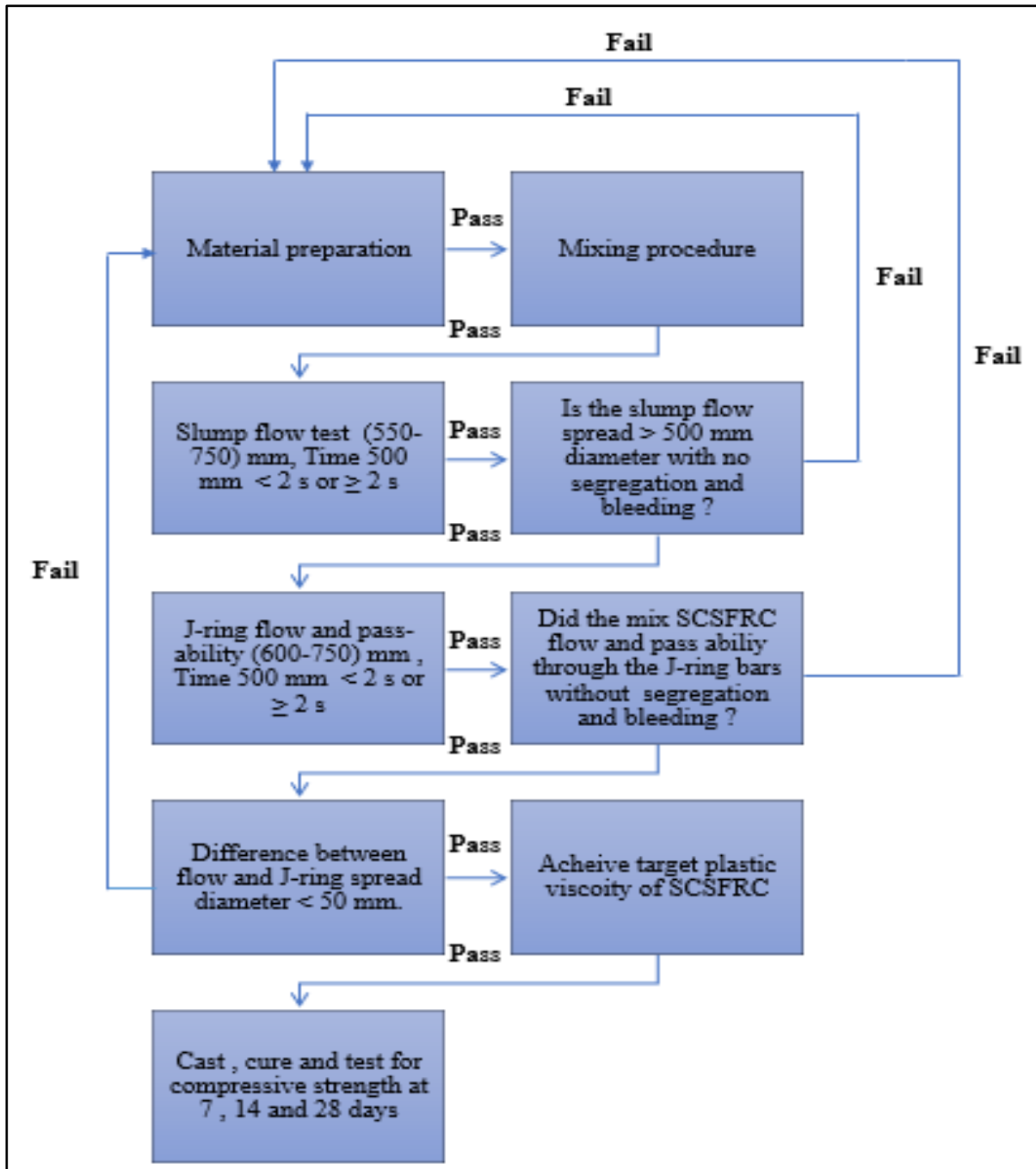


Figure 7.1: Schematic diagram detailing various stages of the experimental study

The mix design chose raw materials in optimal proportions to provide concrete with the required characteristics in fresh and hardened states for specific applications. Densely

compacted cementitious matrix with good workability and strength can be achieved by targeted SCC design. (Abo Dhaheer *et al.*, 2016a) developed a mix design method for SCC based on the desired target plastic-viscosity and compressive strength of the mix. In the present work, proportioning of SCC mixes were undertaken using the procedures described in (Abo Dhaheer *et al.*, 2016a). The mix proportions of SCC test mixes designed based on (Abo Dhaheer *et al.*, 2016a) (Karihaloo and Ghanbari, 2012a), (Deeb and Karihaloo, 2013a) are shown in Table 7.2. The plastic viscosity of each mix was calculated using the micro-mechanical procedure (Ghanbari and Karihaloo, 2009) and the plastic viscosity of the homogeneous paste was obtained from (Sun, Voigt and Shah, 2006). Additional details of the test SCC mixes without and with steel fibre are also given in Table 7.3. Results obtained for flow properties of SCC mixes with and without fibres are shown in Table 7.4.

Table 7.2: Mix proportions of test SCC and SCSFRC mixes (kg / m³)

Mix NO.	cm ^a			W ^d	SP ^e	w/cm	SP/cm %	LP ^f	SF ^g	FA ^h		CA ⁱ	SF ^g % ratio
	Cement	ggbs ^b	ms ^c							FA ^{**}	FA ^{***}		
Mix 1 30 MPa	239	78	--	201	1.8	0.63	0.56%	160	--	222	550	851	0
Mix 2 30 MPa	244	81	--	205	2.1	0.63	0.65%	158	40	218	550	827	0.5
Mix 3 30 MPa	328	--	58	243	4.75	0.63	1.23%	366	103	446	700	--	1.0
Mix 4 50 MPa	293	98	--	207	2.3	0.52	0.59%	86	--	240	500	881	0
Mix 5 50 MPa	275	92	--	195	2.8	0.52	0.76%	207	38	189	600	842	0.5
Mix 6 50 MPa	400	--	71	244	8.25	0.52	1.75%	376	115	346	700	--	1.0
Mix 7 70 MPa	351	117	--	187	2.8	0.40	0.70%	49	--	261	500	879	0
Mix 8 70 MPa	338	113	--	180	3.8	0.40	0.84%	164	38	216	500	819	0.5
Mix 9 70 MPa	473	--	84	223	11.5	0.40	2.1%	331	112	369	700	--	1.0

^a Cementitious material.

^b Ground granulated blast-furnace slag

^c Micro-silica

^d Water

^e Superplasticizer.

^f Limestone powder <125 μm .

^g Steel Fibre.

^h Fine aggregate <2 mm (Note: a part of the fine aggregate is the coarser fraction of the limestone powder, FA**125 μm –2 mm, whereas FA*** refers to natural river sand < 2 mm).

ⁱ Coarse aggregate < 20 mm and < 10 mm.

Table 7.3: Further details of test SCC and SCSFRC mixes

Mix designation	Compressive strength at 28 days (MPa)	Target plastic viscosity (Pa s)	Actual plastic viscosity * (Pa s)	Plastic Viscosity diff.	Paste vol. fraction	Solid vol. fraction	Paste/Solid (by vol.)
Mix 1	39.51	5	4.92	-1.69	0.38	0.62	0.61
Mix 2	41.77	20	19.78	-1.10	0.39	0.61	0.64
Mix 3	35.85	41	39.66	-3.27	0.54	0.46	1.15
Mix 4	59.51	7	6.75	-3.63	0.39	0.62	0.65
Mix 5	50.20	35	33.85	-3.28	0.41	0.59	0.71
Mix 6	52.35	62	63.53	+2.46	0.57	0.43	1.33
Mix 7	70.72	9.5	9.42	-0.79	0.38	0.62	0.71
Mix 8	78.43	45	44.76	-0.53	0.41	0.51	0.80
Mix 9	70.33	81	81.21	+0.26	0.56	0.41	1.38

Actual plastic viscosity*: mix plastic viscosity that is calculated using equation 4.6 & 4.8.

7.3 Development of SCC mixes with and without fibre

7.3.1 Fresh behaviour of SCC with or without fibre

7.3.1.1 Flow test

The flow test (Table 7.4) used a time-sequenced video recording, with a correctness of a thousandth of a second, to assess the time taken for fresh SCC and SCSFRC (with 0.5% and 1% of steel fibre mix) to reach a 500 mm diameter. For all the tested SCC and SCSFRC mixes, the range of final flow spread diameters was between 600 to 750 mm (SF₁ and SF₂), with t_{500} between 1.15 and 3.70 s. The viscosity classes based on the t_{500} time were VS₁ or VS₂, in accordance with (BS EN 206-9:2010, 2010) as shown in Figure 7.2 and Figure 7.3. It can be clearly observed that both the t_{500} and plastic viscosity (e.g., in case of Mix 9) increase with the steel fibre volume content. Figure 7.4 displays the horizontal spread of various SCC and SCSFRC mixtures. A thorough visual inspection indicated that the self-compacting mixtures showed no signs of bleeding or segregation. Moreover, all the values were within the limits of recommended standards (EFNARC, 2005). For both the SCC and SCSFRC mixes

(mixes 1–9 in Table 7.2), the water-to-binder ratio was reduced to 0.40, while the superplasticiser to water ratio (SP/water) was increased to ensure good workability. As expected, the flow characteristics of the SCC mix with use of steel fibres (mix 2 and mix 3) were somewhat slow compared with the mixes (e.g., mix 1), produced without the use of steel fibres. Comparing the SCSFRC mixes with steel fibre, meanwhile, as expected, it was found that the flowing ability was not significantly affected by the volume of steel fibre added. In other words, the addition of 0.5% by volume of 30 mm long steel fibre with coarse aggregate had similar flow characteristics as the mix with 1% by volume of 30 mm long steel fibre, without coarse aggregate.

Table 7.4: Flow, passing and filling ability test results SCC and SCSFRC concordance with mix

Mix designation	Slump flow		J-ring flow test			$D_{\text{FLOW}} - D_J$ (mm) ^a	L-box test		
	Spread (mm)	Time 500 mm (sec)	Spared (mm)	Time 500 mm (sec)	P_J (mm)		t_{200} (sec)	t_{400} (sec)	H_2/H_1
Mix 1	635	1.13	625	1.97	10	10	0.47	1.23	0.88
Mix 2	632.5	2.16	630	2.50	9.50	2.5	0.50	1.27	0.91
Mix 3	620	2.34	610	3.10	6.25	10	0.63	1.70	0.94
Mix 4	635	1.37	627.5	2.05	7.75	7.5	0.60	1.35	0.89
Mix 5	635	2.47	625	3.47	9.75	10	0.97	2.27	0.87
Mix 6	605	3.64	600	5.12	6	5	1.13	2.66	0.93
Mix 7	740	1.87	730	2.24	9	10	0.82	1.44	0.89
Mix 8	730	2.67	725	3.50	7	5	1.30	3.24	0.95
Mix 9	710	3.70	700	5.47	9.25	10	1.39	3.57	0.94

^a Difference between Slump flow and J-ring flow test.

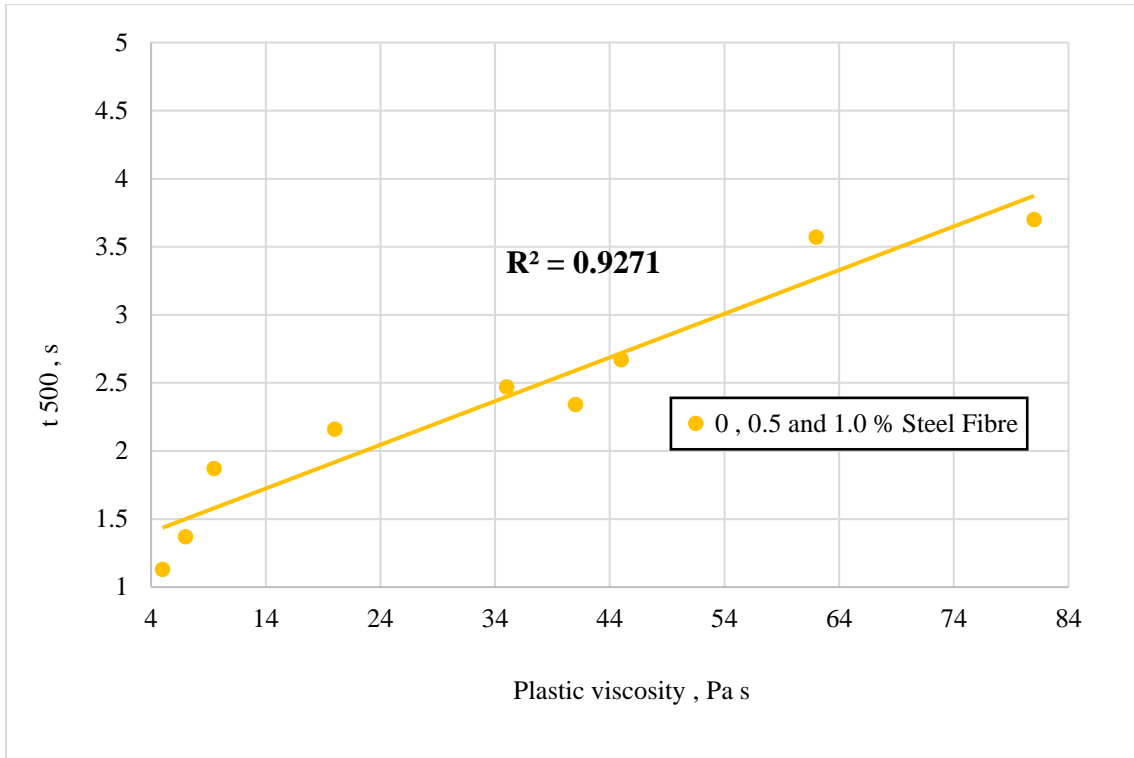


Figure 7.2: Relationship between the plastic viscosity and t_{500} of self-compacting concrete mixes

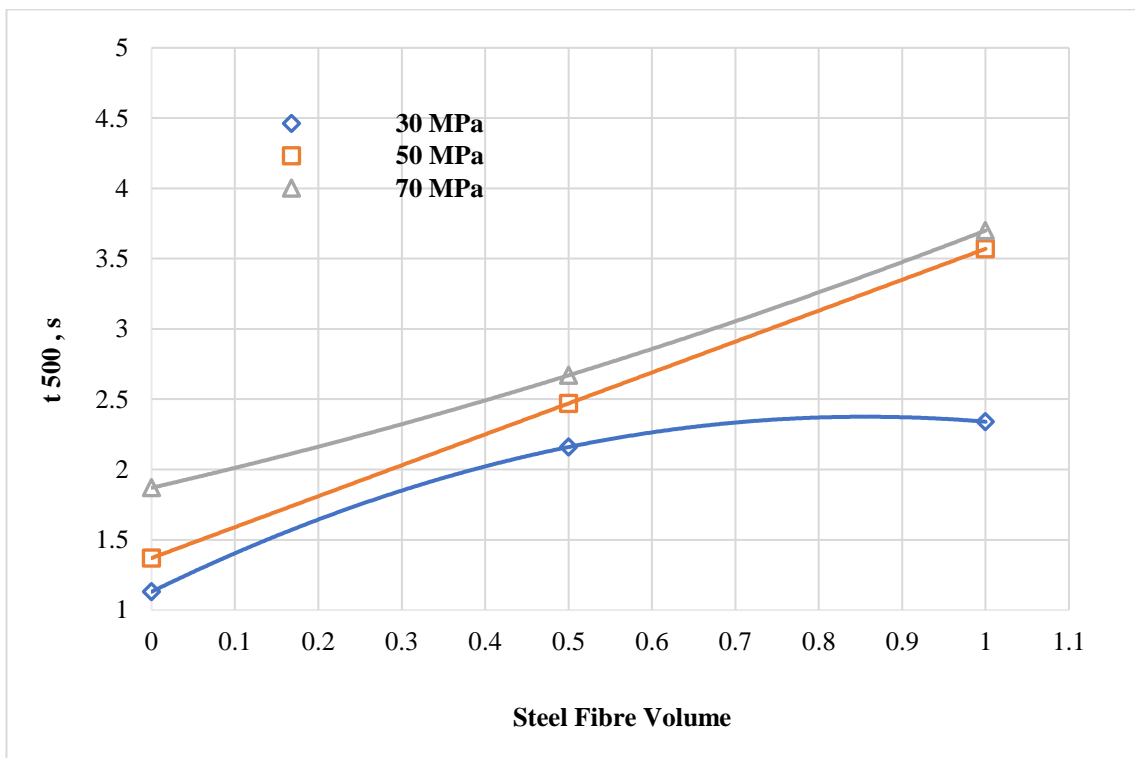


Figure 7.3: Relationship between the steel fibre volume and t_{500} for SCFRC mixes



Figure 7.4: Horizontal spread of SCC and SCSFRC mix: C30 (Mix 1) (Left), C50 (5) (Right)

7.3.1.2 Passing and filling test

This investigation followed the traditional trial-and-error approach, using J-ring and L-box tests on trial mixes, until the mix was found to meet the flowability, passing and filling ability criteria with no visible signs of segregation and blockage. All the above trial mixtures of SCC and SCSFRC (with 0, 0.5% and 1% of steel fibre) mixes (no. 1 to 9) that fulfilled the flowability standard and showed no signs of segregation were subjected to the filling and passing ability trial utilising the J-ring and L-box tests to ensure that they were able to pass through the narrow gaps that normally exist among reinforcing bars in structural elements produced with reinforced concrete.

For this objective, 300 mm diameter J-ring equipment with 12 steel rods (each of diameter 16 mm and 100 mm height as in Figure 7.5) was used, as recommended by (BS EN 12350-8, 2010). The viscosity values based on t_{500J} time (> 2 s) correspond to class VS₂, in accordance with (BS EN 206-9:2010, 2010). Figure 7.6 and Figure 7.7. illustrate the relationship between t_{500J} , plastic viscosity and fibre volume content respectively. It can be clearly observed that both the t_{500J} and plastic viscosity (Mix 9) increase with the steel fibre volume content.



Figure 7.5: Flow and pass-ability of SCSFRC mix: C50 (Mix 5) (Left), C70 (Mix 8) (Right)

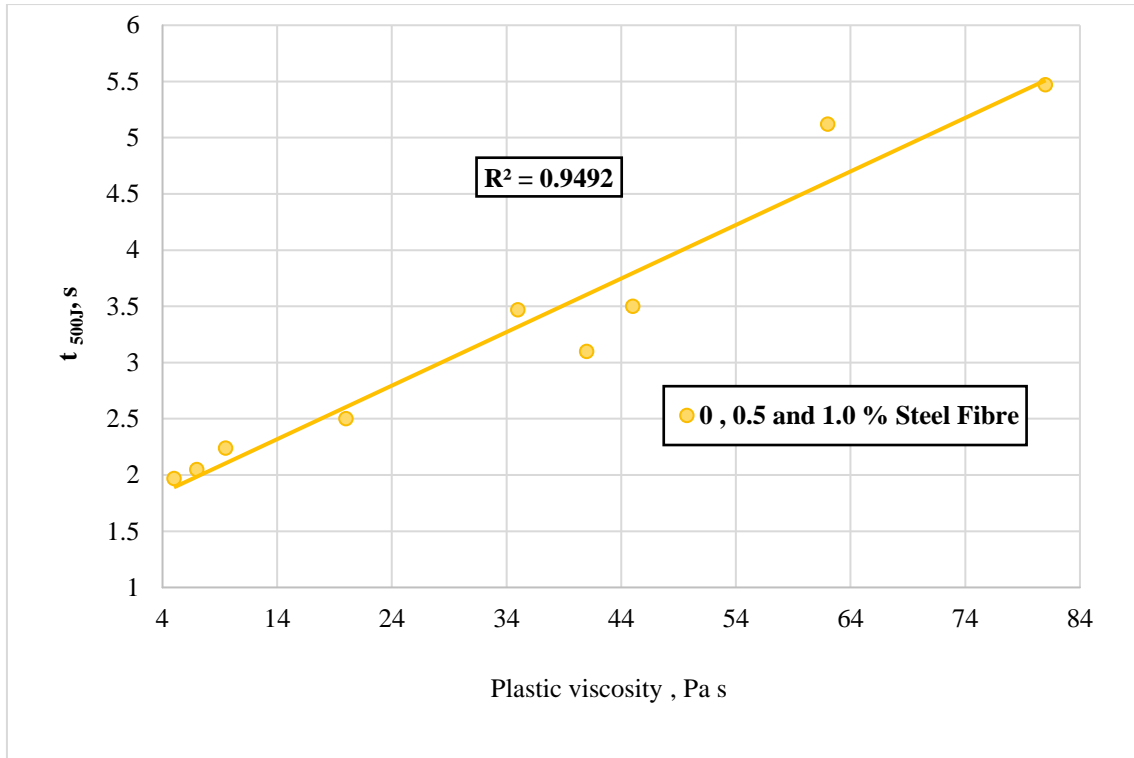


Figure 7.6: Relationship between the plastic viscosity and t_{500j} of self-compacting concrete mixes

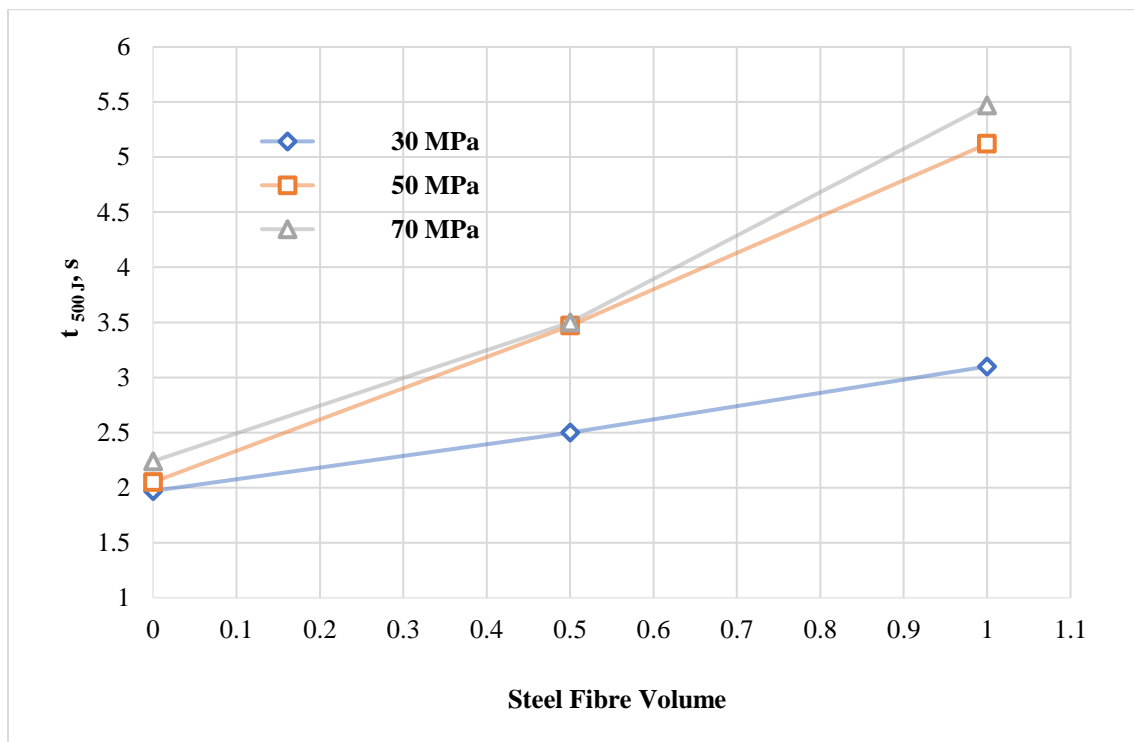


Figure 7.7: Steel fibre volume against t_{500j} for SCFRC mixes

For L-box test, the L-box apparatus with adjustable two steel rods of 12 mm diameter was used (BS EN12350-12:, 2010)(EFNARC, 2005)(Lanier *et al.*, 2003) as shown in Figure 7.10

and Figure 7.11. Table 7.4 presents the t_{200} and t_{400} obtained in L-box tests for all the mixes. Figure 7.8 and Figure 7.9 illustrate how t_{200} and t_{400} are influenced by plastic viscosity of the corresponding mixes.

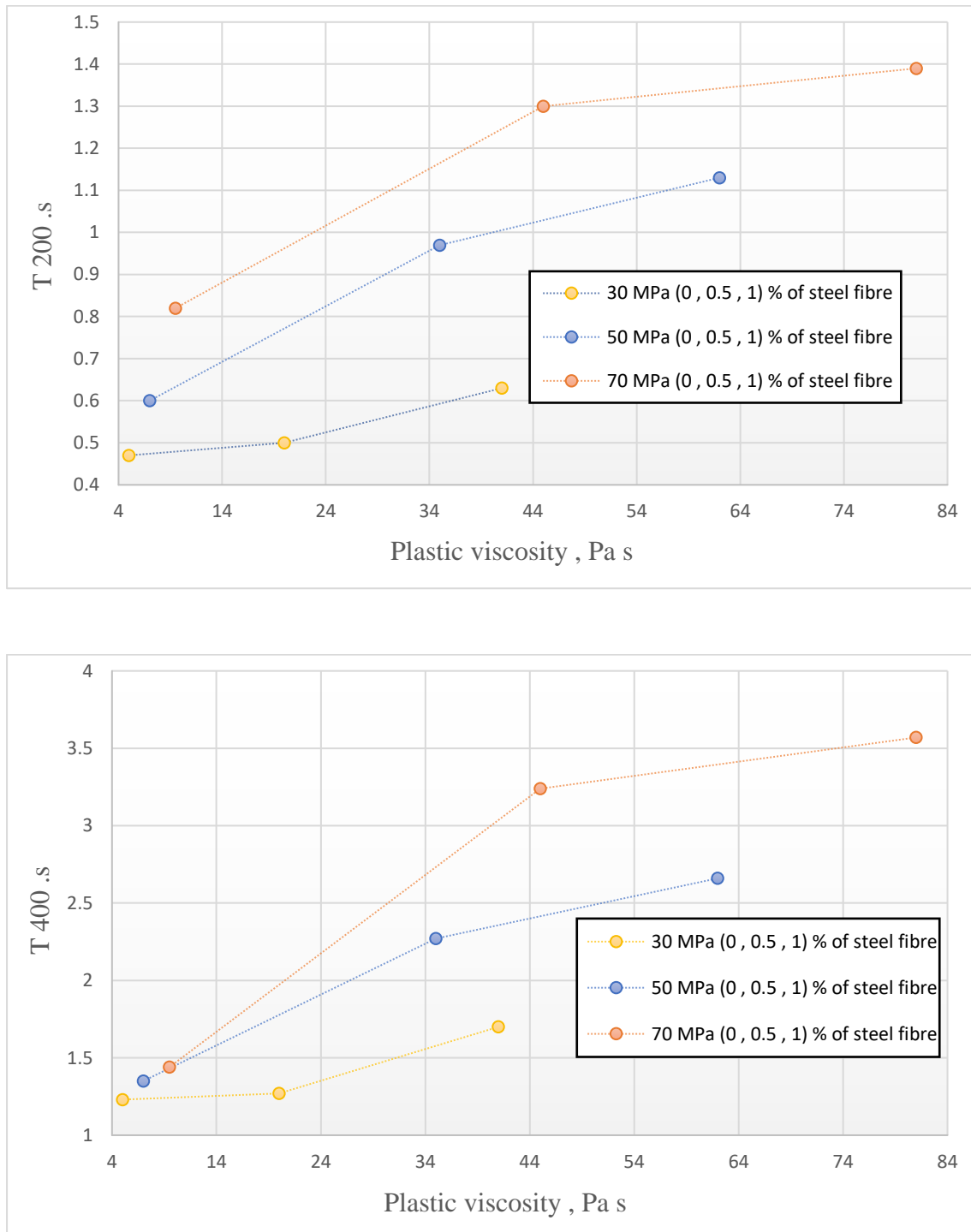


Figure 7.8: Relationship between the plastic viscosity and T₂₀₀, T₄₀₀ of self-compacting concrete mixes

Figure 7.9 shows that, it can be clearly observed that both the t_{200} and t_{400} increase with the steel fibre (1%) content based on the compressive strength (30MPa, 50MPa and 70MPa).

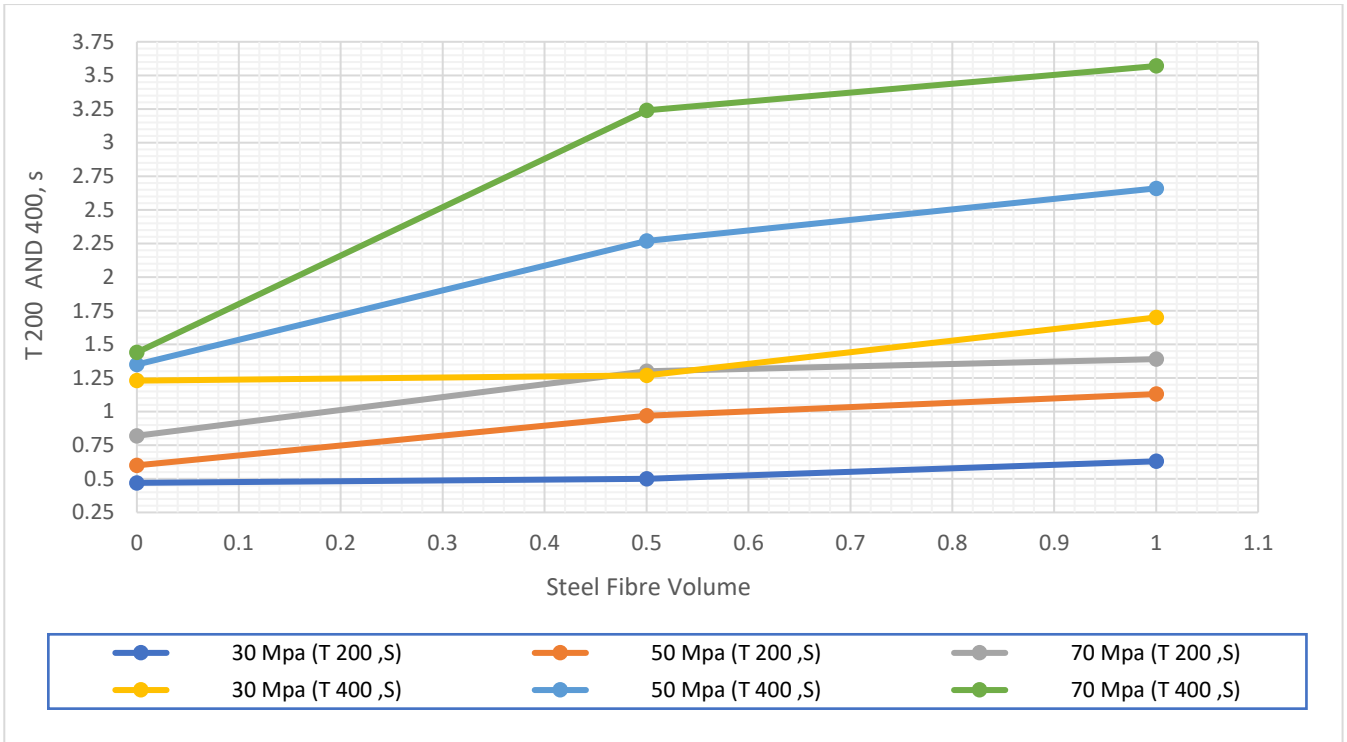


Figure 7.9: Relationship between the steel fibre volume and T₂₀₀, T₄₀₀ of self-compacting concrete mixes

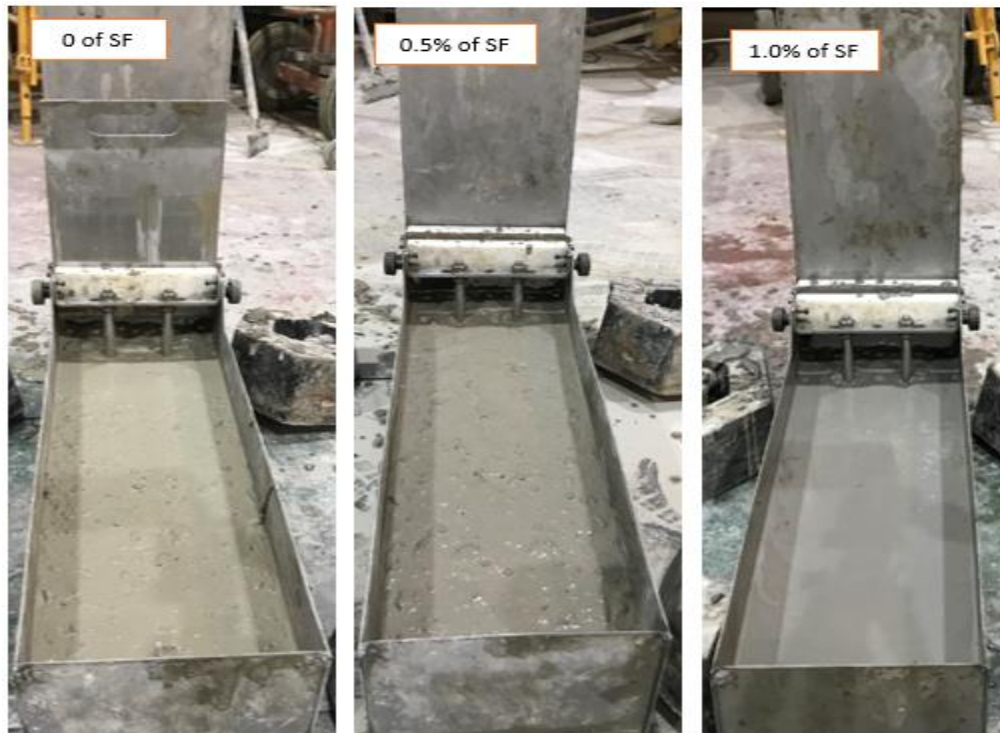


Figure 7.10: Passing and filling ability of SCSFRC mix with steel fibre (0, 0.5 and 1%) volume (C50) Mix 4, 5 and 6

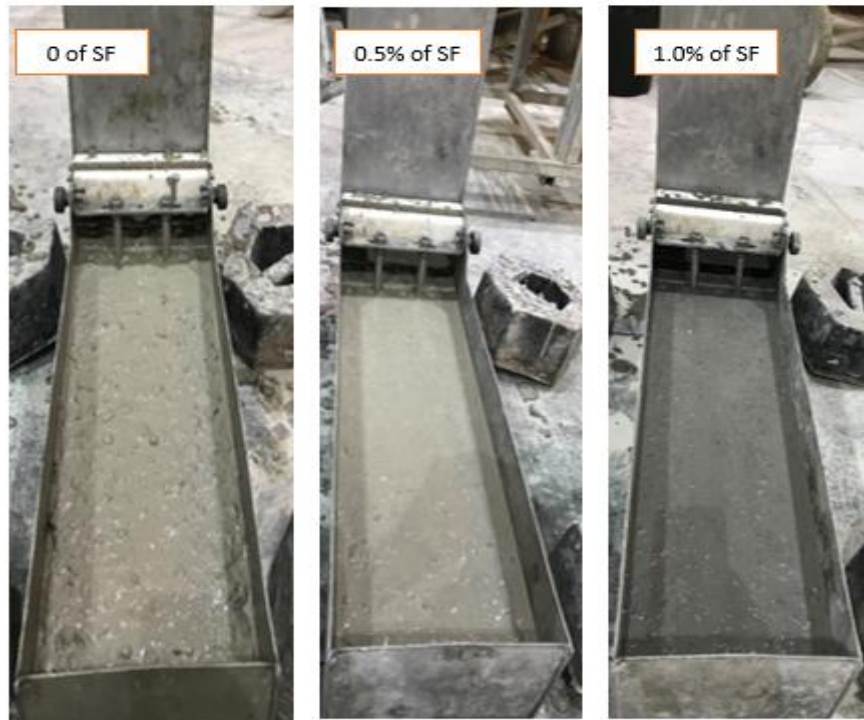


Figure 7.11: Passing and filling ability of SCSFRC mix with steel fibre (0, 0.5 and 1%) volume (C70) Mix 7, 8 and 9

To explore the effect of coarse aggregates on the performance of fibre reinforced SCC, the Mix 3 in Table 7.2 was further investigated by designing three variations of Mix 3 and denoting them as $3^{(1)}$, $3^{(2)}$ and $3^{(3)}$. These three mixes contained steel fibres of 1% volume fraction and coarse aggregates with various composition and sizes as detailed in Table 7.5. While Mix 3 fulfilled the passing and filling ability test, other mixes i.e., $3^{(1)}$, $3^{(2)}$ and $3^{(3)}$ failed to meet the fresh state test criteria as exemplified by Figure 7.12 and Figure 7.13. In such instances, the solid content i.e., the coarse aggregate was reduced, to meet flowing, passing and filling-ability tests. It can be noted from Figure 7.12 and Figure 7.13 that there was some blocking in the SCSFRC mixes $3^{(1)}$, $3^{(2)}$ and $3^{(3)}$ with the bulk of the fibres (1%) and coarse aggregates lumped in the centre of the flow spread. It was therefore necessary to adjust the mix proportions to ensure that the mix met the passing and filling ability requirements as demonstrated by Mix 3 in Figure 7.13 and Figure 7.14. Specifically, it can be noted from Table 7.2 that in Mix 3 (30 MPa), Mix 6 (50 MPa) and Mix 9 (70 MPa), the coarse aggregate was replaced with a corresponding increase in the fine aggregate (sand), as well as in the water and super-plasticiser contents.

Based on target of compressive strength of SCSFRC achieved by the traditional trial-and-error approach in mix 3, it is worth mentioning that the presence of steel fibres (1%) strongly increased the compressive strength of SCSFRC with various coarse aggregate sizes (10 mm (50%) and 20 mm (50%).

Table 7.5: Constituents and proportions for SCSFRC mixes (30 MPa) with steel fibres content (1%) and various coarse aggregate size (kg/m^3)

Mix designation	cma			Water	SP ^d	w/cm	SP/cm	LP ^e	SF ^f (1.0%) ratio	FA ^g		CA ^h
	Cement	ggbs ^b	ms ^c							FA ^{**}	FA ^{***}	
3 ⁽¹⁾	247	82	--	207	2.8	0.63	0.86%	278	76	205	500	364.5 (50%) 10 mm
												364.5 (50%) 20 mm
3 ⁽²⁾	247	82	--	207	2.8	0.63	0.86%	278	76	205	500	546.75 (75%) 10 mm
												182.25 (25%) 20 mm
3 ⁽³⁾	247	82	--	207	2.8	0.63	0.86%	278	76	205	500	729 (100%) 10 mm
												-- (0%)
3	328	--	58	243	4.75	0.63	1.23%	366	103	446	700	-- (0%)
												-- (0%)

^a Cementitious material.

^b Ground granulated blast-furnace slag

^c Micro-silica

^d Superplasticizer.

^e Limestone powder <125 μm .

^f Steel Fibre.

^g Fine aggregate <2 mm (Note: a part of the fine aggregate is the coarser fraction of the limestone powder,

FA^{**} 125 μm –2 mm, whereas FA^{***} refers to natural river sand < 2 mm).

^h Coarse aggregate < 20 mm and < 10 mm.

Table 7.6 : Results of flow, pass and fill-ability for SCSFRC mixes (30 MPa) with various coarse aggregate size

Mix designation	Slump flow		J-ring flow test			$D_{FLOW} - D_J$ (mm) ^a	L-box test			Target plastic viscosity (Pa s)	Compressive strength at 28 days (MPa)
	Spread (mm)	Time 500 mm (sec)	Spared (mm)	Time 500 mm (sec)	P_J (mm)		t_{200} (sec)	t_{400} (sec)	H_2/H_1		
3 ⁽¹⁾	630	1.97	615	3.50	24.5	15	1.17	2.33	0.88	41	34.38
3 ⁽²⁾	610	2.37	605	3.14	17	5	1.00	2.77	0.90	41	31.67
3 ⁽³⁾	605	1.99	600	3.05	12	5	1.01	2.50	0.89	41	30.05
3	620	2.34	610	3.10	6.25	10	0.63	1.70	0.94	41	35.85

^a Difference between Slump flow and J-ring flow test.

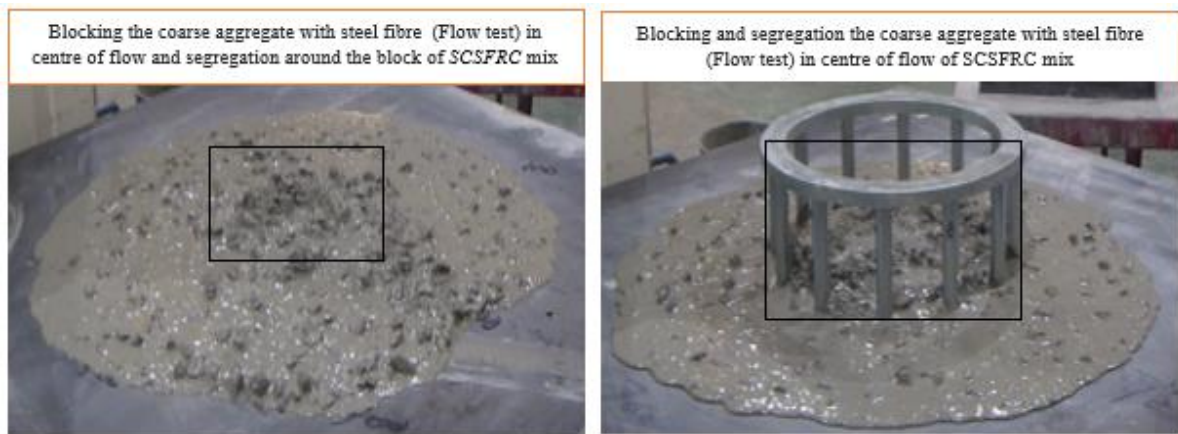


Figure 7.12:Flow and passing ability of SCSFRC mix (1%) volume (C30) Mix 3(1)

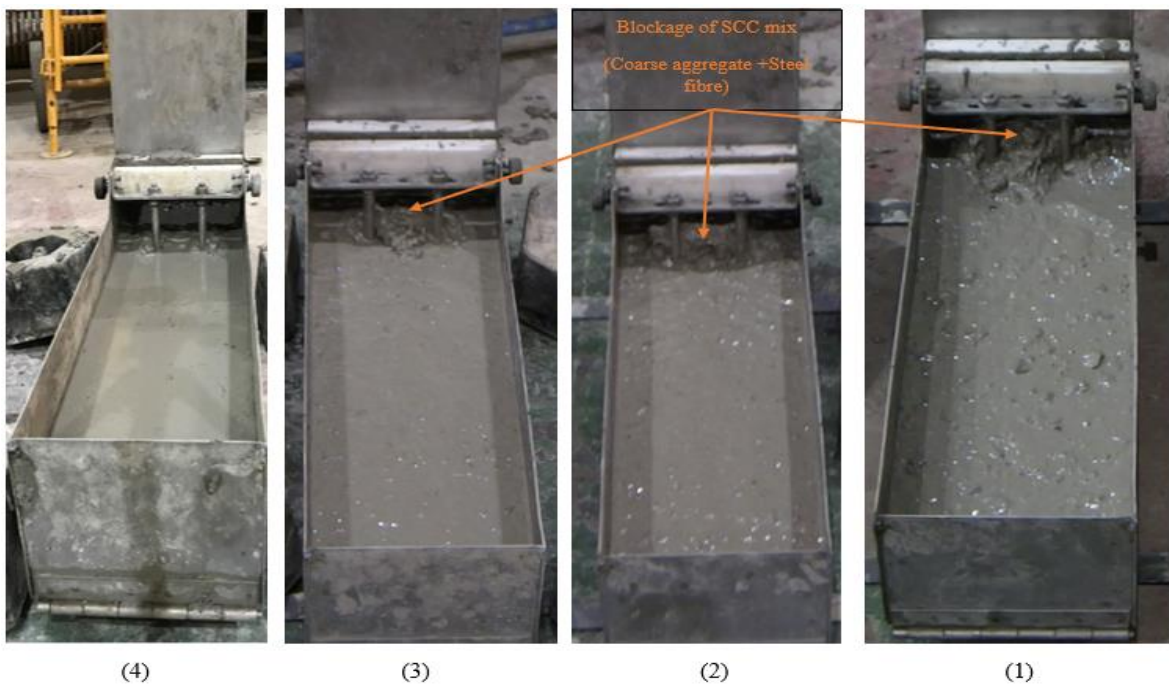


Figure 7.13:Passing and filling ability of SCSFRC mix (1%) volume (C30) Mix 3(1-2-3-4)



Figure 7.14: Flowing and Passing ability of SCSFRC mix (1%) volume (C30) Mix 3(4)

As observed in the above experiments, the flow criteria for SCSFRC can be achieved by increasing the content of cementitious paste and reducing volume of the large aggregate. It was also noted that the SCC mixes containing steel fibres with crimped ends were able to flow smoothly through gaps in the reinforcement bars, with the reasonable distribution of the fibres around the flow (Deeb, Ghanbari and Karihaloo, 2012a).

Previous findings (Khaloo *et al.*, 2014) also reported that the addition of steel fibres reduces the workability of the SCC; especially, when a 2% steel fibre content fraction is added to the mix, the workability falls below the lowest limits stated in (EFNARC, 2005). It was also noted that the addition of steel fibres to the SCC decreases the passing ability of the SCC, and therefore SCC with high volume fraction of fibre content cannot pass readily through the rebars. This is caused by increasing the interlocking and friction among aggregate and fibre. Both slump flow spread and J-ring spread were decreased due to the existence of growing fibre reinforcement. It is assumed that the existence of fibres produces a three-dimensional grid obstructing the flowability. In J-ring trials, all fibres are obstructed within J-ring, with no fibre spreading across the J-ring. The fibre length had further effect on the passing ability and dynamic stability of fresh SCSFRC. J-ring re-bar distance should be modified in relation to fibre length to rationally assess the passing ability. The fibre distribution standardization can be used to assess the constant segregation resistance of steel fibre in SCC (Ding *et al.*, 2018b).

Steel fibres (hooked ends) may also cause blocking of particles (e.g., aggregates) during the flow of concrete, and hence weaken the flowability (Sahmaran, Yurtseven and Ā, 2005). It could be said that factors significantly influence SCSFRC characteristics are paste content, maximum nominal aggregate size, steel fibre content, and concrete age.

It can be noted from Table 7.2, for the Mix 3, Mix 6 and Mix 9, when 1% volume fraction of steel fibres were used, the coarse aggregates were not used in the mixes to improve the flow properties. However, the absence of coarse aggregate may impact on the final compressive strength of the concrete. To overcome this issue, in place of GGBS, micro silica was added as a cement replacement material to the mixes to improve their corresponding compressive strengths. To demonstrate this behaviour of the SCSFRC, two variations of Mix 9 were designed and compared with the original mix. These mixes were denoted as Mix 9⁽¹⁾ and Mix 9⁽²⁾. Table 7.7 presents the composition of new mixes along with the original mix. It can be noted from Table 7.7, when micro-silica is used as cement replacement material, the mixes (9 and 9⁽²⁾) required higher SP doses to ensure flowability. When comparing 9 and 9⁽²⁾, it can be further establish that the more micro-silica is used the more SP is required. In addition, when GGBS is used as cement replacement material (in the absence of coarse aggregate), the compressive strength achieved by the mix (9⁽¹⁾) is 49.43 MPa (see Table 7.8) which is much lower than target compressive strength 70 MPa. However, in the case of Mixes 9 and 9⁽²⁾, the target compressive strength is achieved and the highest compressive strength of 75.02 MPa was achieved in case of Mixe 9⁽²⁾ due to the high content of micro-silica. This is why micro-silica was used to improve the compressive strength in the absence of coarse aggregates.

Table 7.7: Constituents and proportions for SCSFRC mixes (70 MPa) with steel fibres content (1%) and without coarse aggregate size (kg/m³)

Mix designation	cm ^a			Water	SP ^d	w/cm	SP/cm	LP ^e	SF ^f (1.0%) ratio	FA ^g	
	Cement	ggbs ^b	ms ^c							FA ^{**}	FA ^{***}
9 ⁽¹⁾	420	140 (25%)	--	224	4.8	0.40	0.90%	327	112	367	700
9 ⁽²⁾	415	--	138 (25%)	221	16.5	0.40	2.93%	329	112	362	700
9	473	--	84 (15%)	223	11.5	0.40	2.1%	369	112	369	700

^a Cementitious material.

^b Ground granulated blast-furnace slag

^c Micro-silica

^d Superplasticizer.

^e Limestone powder <125 μm .

^f Steel Fibre.

^g Fine aggregate <2 mm (Note: a part of the fine aggregate is the coarser fraction of the limestone powder,

FA**125 μm –2 mm, whereas FA*** refers to natural river sand < 2 mm).

Table 7.8: Results of flow, pass and fill-ability for SCSFRC mixes (70 MPa)

Mix designation	Slump flow		J-ring flow test			$D_{\text{FLOW}} - D_{\text{J}}$ (mm) ^a	L-box test			Target plastic viscosity (Pa s)	Compressive strength at 28 days (MPa)
	Spread (mm)	Time 500 mm (sec)	Spared (mm)	Time 500 mm (sec)	P_{J} (mm)		t_{200} (sec)	t_{400} (sec)	H_2/H_1		
9 ⁽¹⁾	730	3.06	705	3.86	8.25	25	1.31	2.98	0.91	81	49.43
9 ⁽²⁾	730	3.46	710	4.56	9.5	20	1.33	3.06	0.87	81	75.02
9	710	3.70	700	5.47	9.25	10	1.39	3.57	0.94	81	70.33

^a Difference between Slump flow and J-ring flow test.

7.3.1.3 Influence of super-plasticiser on SCC and SCSFRC mixes

The amount of SP used for preparing mixes consisting various strengths of SCC and SCSFRC mixes are analysed in this section. It was noted that the ratio of SP to cementitious material were within the limits specified (i.e., 0.56% to 2.1%). Figure 7.15, presents the set of SP to cementitious material ratio by volume used in preparing SCC and SCSFRC (with 0.5% and 1 % by volume steel fibres) mixes.

It was observed that the amount of ratio SP to cementitious material ratio is higher for SCSFRC mixes than SCC mixes for the same target strengths (i.e., C30, C50 and C70). For example, 70MPa SCC (Mix 7) required 0.70 % compared to 2.1% needed by 70MPa SCSFRC (Mix 9). As former studies revealed, the major role of SP is providing good dispersing influences on cementitious pastes or concrete and improving the workability. For a perfectly-dispersed cement paste, the cement particles are less aggregated or grouped together, and less viscous (Kristiawan and Tyas, 2017). Steel fibres negatively influences the workability of self-compacting reinforcement concrete, and adding admixtures, especially SP, can assist to overcome the decreased fresh properties (Aslani and Gedeon, 2019). Increasing the SP dose improves the workability of the fresh concrete without increasing the content of water, hence it is a necessary admixture for fibre reinforcement concrete (Yin et al.,

2015)(Khayat, 2015). Furthermore, higher SP dose in SCSFRC mixes makes the yield stress lower, which yet again increases their final spread (de la Rosa et al., 2018b).

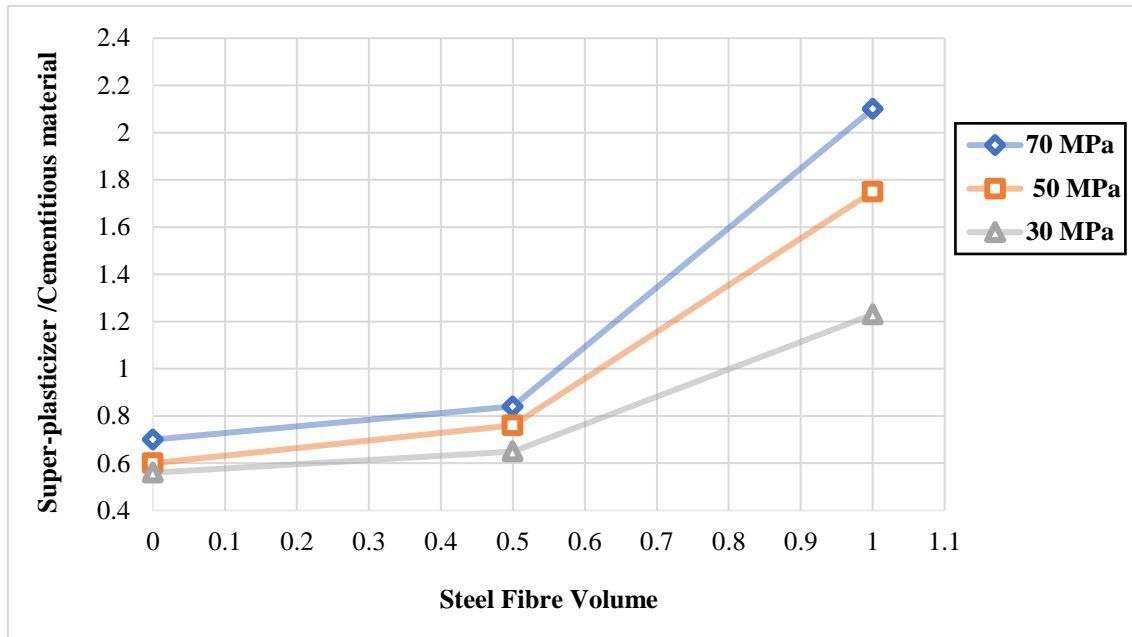


Figure 7.15:SP /Cementitious material ratio by volume in SCC and SCSFC mixes

7.3.1.4 Plastic viscosity of self-compacting concrete without and with steel fibre

The plastic viscosity (PV) predicted based on micromechanical approach revealed that the PV was higher in the self-compacting concrete with steel fibre than in the self-compacting concrete without steel fibre, as displayed in Figure 7.16. It is worth mentioning that the presence of steel fibres strongly increased the plastic viscosity of SCSFRC with various strengths (30 MPa, 50 MPa and 70 MPa) due to additional steel fibre content (Figure 7.17). According to micromechanics approach, the plastic viscosity of the viscous concrete comprising liquid and solid substances is additionally increased if steel fibres are added to it. The volume fraction of steel fibres used is typically small, so that the dilute approximation is adequate to predict the plastic viscosity (Ghanbari and Karihaloo, 2009).

Thus, the viscosity of SCC mixes can be correctly evaluated using a micromechanical method, depending on the measured viscosity of the cement paste. The 30 mm long, 0.55 mm diameter steel fibre with crimped ends considerably increased the viscosity of SCC with fibre mix as predicted following approach proposed in (Deeb, Ghanbari and Karihaloo, 2012a).

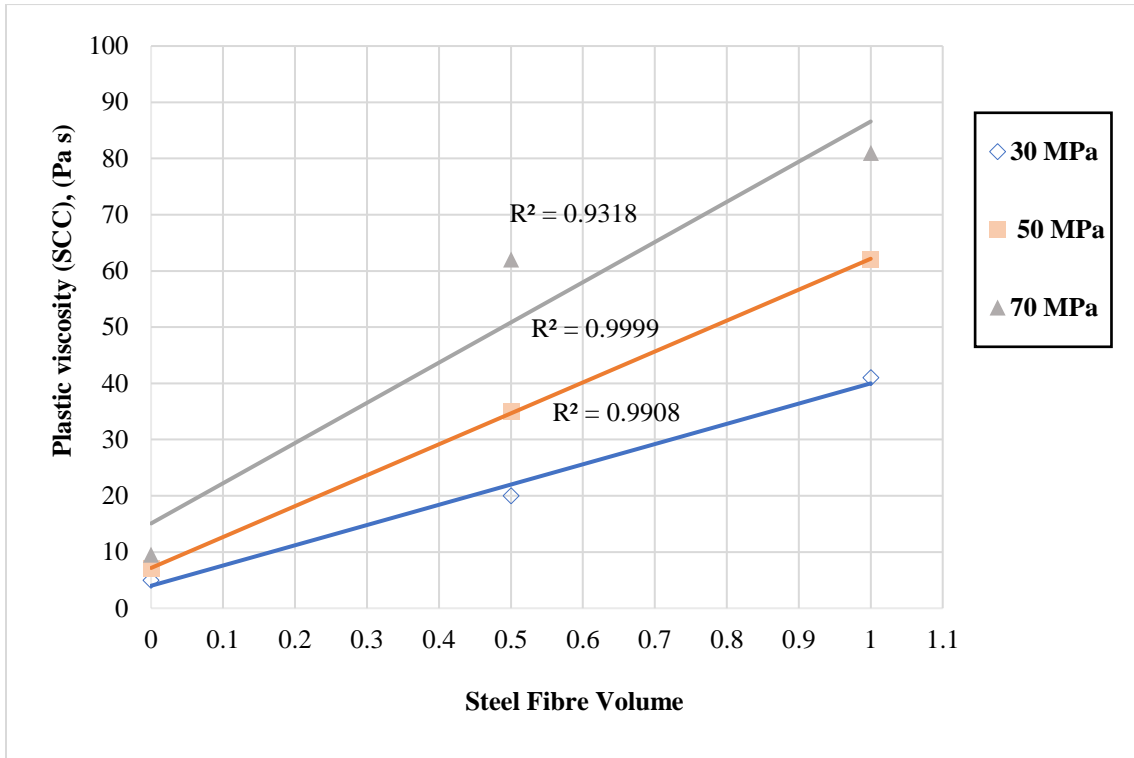


Figure 7.16: Plastic viscosity in SCC and SCSFC concrete mixes

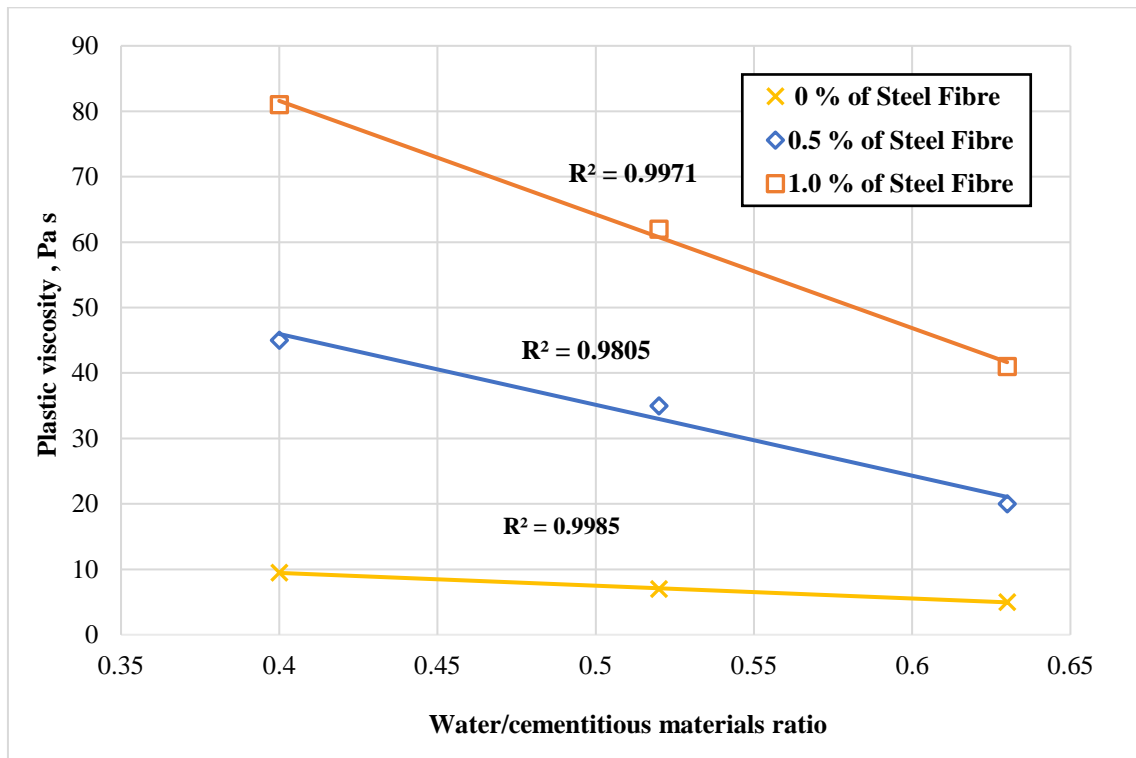


Figure 7.17: Relationship between the plastic viscosity and water/cementitious materials ratio of self-compacting concrete mixes

Figure 7.18 shows that, for the same compressive strength (or the same water to binder ratio), the paste to solids ratio in an SCSFRC mix is much higher than in its counterpart SCC mix. However, the difference parallels as the strength of the mix increases. This suggests that the solid content could be increasing while that of the paste content could be reducing in SCSFRC mixes.

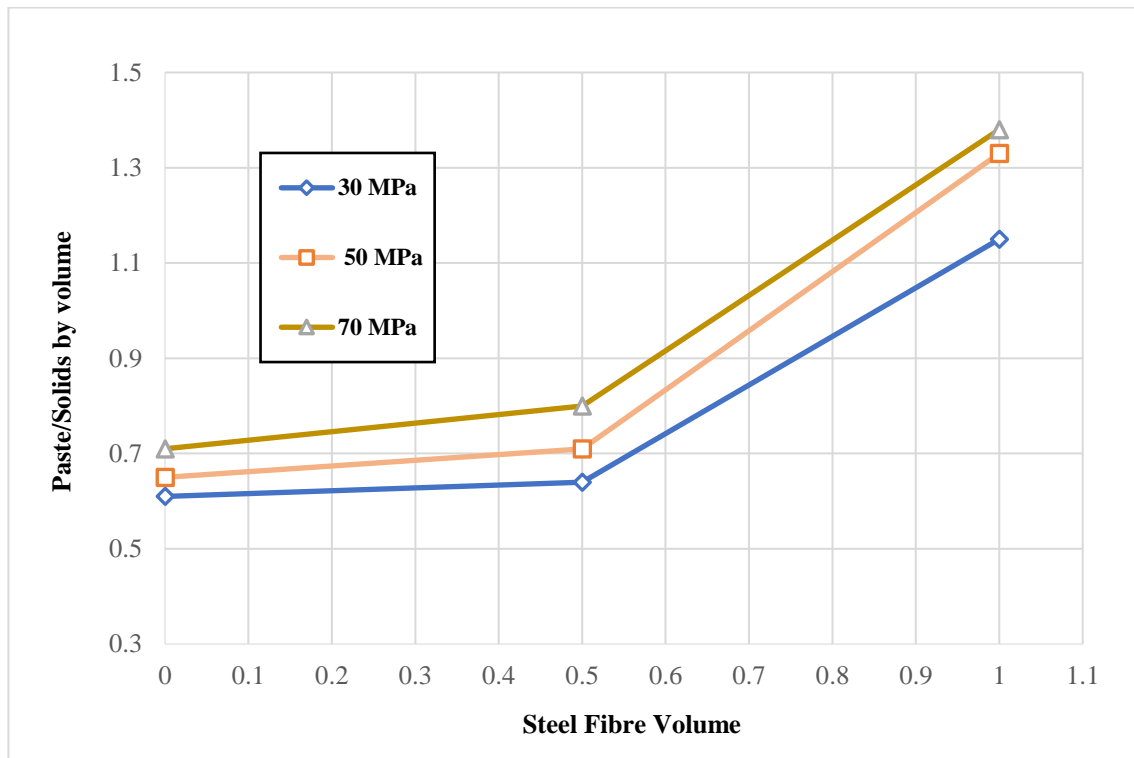


Figure 7.18: Paste to solids ratio by volume in SCC and SCSFRC concrete mixes

7.3.1.5 Further analysis of SCC and SCSFRC mix with target compressive strength 40 MPa and 60 MPa.

For both the SCC and SCSFRC mixes (mixes 10–13 in Table 7.9 and Table 7.10), the water-to-binder ratio was reduced to 0.57 and 0.47, while the superplasticiser to cementitious materials ratio (SP/cm) was increased in (Mix 10, Mix 11) and (Mix 12, Mix 13) to ensure good workability. The compressive strength achieved by SCSFRC mixes Mix 11 and Mix 13 is slightly increased (see Table 7.10).

Table 7.9: Constituents and proportions for SCC and SCSFRC mixes (40 MPa) and (60 MPa)

Mix designation	cma		SP ^c	w/cm	SP/cm	LP ^d	SF ^e (0.5%) ratio	FA ^f		CA ^g
	Cement	ggbs ^b						FA ^{**}	FA ^{***}	
Mix 10 (40 MPa)	288	95	2.5	0.57	0.78%	130	--	200	544	890
Mix 11 (40 MPa)	270	90	3	0.57	0.83%	143	40	240	500	839
Mix 12 (60 MPa)	315	105	2.6	0.47	0.62%	140	--	198	500	862
Mix 13 (60 MPa)	303	101	3.5	0.47	0.86%	129	39	210	700	887

^a Cementitious material.

^b Ground granulated blast-furnace slag

^c Superplasticizer.

^d Limestone powder <125 μ m.

^e Steel Fibre.

^f Fine aggregate <2 mm (Note: a part of the fine aggregate is the coarser fraction of the limestone powder, FA^{**}125 μ m–2 mm, whereas FA^{***} refers to natural river sand < 2 mm).

^g Coarse aggregate < 20 mm and < 10 mm.

Table 7.10 : Results of flow, pass and fill-ability for SCC and SCSFRC mixes (40 MPa) and (60 MPa)

Mix designation	Slump flow		J-ring flow test			D _{FLOW} - D _J (mm) ^a	L-box test			Target plastic viscosity (Pa s)	Compressive strength at 28 days (MPa)
	Spread (mm)	Time 500 mm (sec)	Spared (mm)	Time 500 mm (sec)	P _J (mm)		t ₂₀₀ (sec)	t ₄₀₀ (sec)	H ₂ /H ₁		
Mix 10	602.5	1.20	600	2.02	9.5	2.5	0.53	1.27	0.93	5	40.64
Mix 11	635	2.27	615	2.54	7.75	20	0.93	1.90	0.97	27	41.93
Mix 12	625	1.41	620	1.73	7.75	5	0.77	1.60	0.94	8.5	60.98
Mix 13	645	2.50	625	3.37	7	20	1.15	2.55	0.91	40	66.97

^a Difference between Slump flow and J-ring flow test.

For the above mixes flow and passing ability tests were conducted using J-ring test with 12 and 16 steel reinforcement bars and L-box with 2 and 3 steel reinforcement bars. In the case of SCSFRC mixes containing 0.5% volume fraction of fibre content, the coarse aggregate size from 10 mm to 20 mm with various compositions were used. According to (EN BS 206-9, 2010), J-ring test should be performed with 12 or 16 steel reinforcement bars. The J-ring flow test spread values are within the range of 600 mm to 650 mm for flow and passing ability of

SCSFRC. However, blocking of steel fibres and coarse aggregates (size from 10 mm to 20 mm) can be seen in Figure 7.19(a), where J-ring with 16 bars were used. In case of J-ring test with 12 bars the mixes showed no signs of blocking and bleeding or segregation, as shown in Figure 7.19(b).

L-box test with 3 or 2 steel reinforcement bars are used for testing passing and filling ability of SCSFRC. In the case of L-box test with 3 rebars, the blocking of steel fibres and coarse aggregates (size from 10 mm to 20 mm) can be seen in Figure 7.20 (a), while for L-box with 2 bars the mixes showed no signs of blocking and bleeding or segregation, as shown in Figure 7.20(b). Also, in the case of L-box test with 3 bars, the mixtures without steel fibre (containing equal compositions of coarse aggregates with sizes 10 mm and 20 mm) showed no signs of blocking and bleeding or segregation as illustrated in Figure 7.20(c). These experiments reveal that the optimum mix proportioning is vital for meeting the fresh state criteria and for obtaining high quality finish in the produced concrete structural elements.

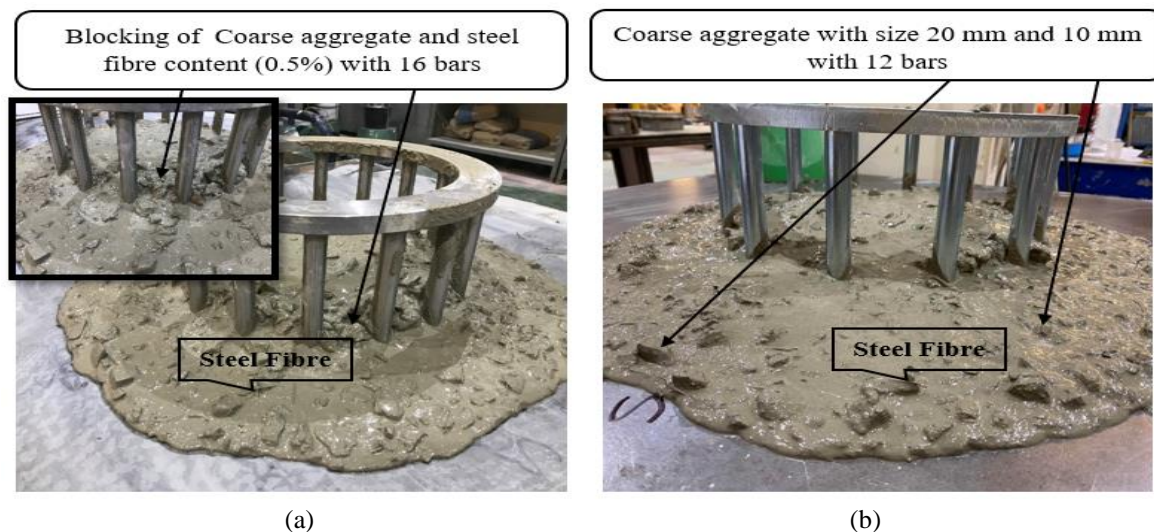


Figure 7.19: Flow and pass-ability of SCSFRC mix: C40 (a) with 16 bars, C40 (b) with 12 bars, (size of coarse aggregate with 50 % of 10mm and with 50 % of 20mm)



Figure 7.20: Flow, pass and fill-ability of SCSFRC mix: C40 (a) with 3 bars, C40 (b) with 2 bars, C60 (c) with 3 bars (size of coarse aggregate with 50 % of 10mm and with 50 % of 20mm)

7.3.1.6 Discussion of fresh behaviour of SCC with or without fibre

The development of self-compacting normal-performance concrete mixes with and without steel fibre is a complex process requiring the resolution of conflicting demands of flowing, passing, filling and non-segregation. These demands can be resolved by increasing the paste content and decreasing the solid content such as large aggregate volume. The addition of long steel fibres can compromise the ability of the mix to flow smoothly through gaps in the reinforcement causing the fibres to clump together. Our extensive investigations lead to the following major conclusions.

For SCC mixes without steel fibres the fulfilment of the flow and cohesiveness criteria, as measured by the slump cone flow test, are sufficient for the mix design. The resistance to segregation was checked visually. In the mixes with fibres (0.5% and 1.0% volume fractions), however, it was noticed that the fibres were uniformly distributed in the slump spread right up to the edge, but this does not ensure that the fibres will pass through narrow openings, especially when the steel fibre content is higher.

It is additionally necessary to check that the mixes meet the passing and filling ability criteria using the J-ring and L-box apparatus. Our investigations show that, even when the mixes with fibres meet the flow-ability criterion and are resistant to segregation, as judged by the slump flow test, they may not meet the passing or filling ability criteria. These mixes need to be more flowable than required by the slump flow test, in order to satisfy the passing and filling ability test. The viscosity of SCC mixes can be accurately estimated using a micromechanical procedure based on the measured viscosity of the cement paste and the mix proportions. The 30 mm long, 0.55 mm diameter steel fibres with crimped ends significantly increase the viscosity of SCC mixes with fibres.

7.3.2 Hardened behaviour of SCC with or without fibre

Self-compacting concrete (with and without steel fibres) has undergone extensive investigations that have led to confidence in its fresh and hardened characteristics, yet its composition variations raise concerns as to its fracture behaviour. This section presents the results of an experimental study on fracture behaviour of SCC with or without fibre mixes varying by the steel fibre volume (SF), paste to solids ratio (p/s) and water to binder (or cementitious material (w/cm)) ratio. The size-dependent fracture energy (G_f) has been determined using the RILEM work-of-fracture test on three-point bend specimens of a single size, which contained a shallow starter notch (notch to depth ratio = 0.1).

The non-linear theory of fracture process depend on the fictitious crack model commonly employed for the evaluation of cracked concrete structures (Ramachandra Murthy *et al.*, 2013a). Specific fracture energy and the tension softening diagram of a concrete mix are the most significant parameters describing its fracture behaviour. They form a basis for the evaluation of the load carrying capacity of cracked concrete structures (Alyhya *et al.*, 2016). Accordance to RILEM recommendation (RILEM 50FMC, 1985), the specific fracture energy (or toughness) can be achieved by the work-of-fracture procedure involving experiments on notched three-point bend (TPB) samples of various sizes and notch to depth percentages.

(Ghasemi, Ghasemi and Mousavi, 2018b) demonstrated that a change in the maximum aggregate size will cause the fracture behaviour of the SCSFRC to be various from that of the without fibre. Then, considering insufficient research in this regard, effort has been made in this study to add new variables and research the influences of the fibre volume of fraction, maximum aggregate size and w/c on the fracture parameters of SCC utilizing size effect method (SEM) and work fracture method (WFM). Some notched beams were made in an investigational plan and subjected to three-point bending (TPB) tests with a strain control device.

The steel fibre reinforced concrete (SFRC) has moderate tensile strength (Şahin and Köksal, 2011), high ductility, and effective strength (Guo *et al.*, 2019)(Cruz, 2001) (Caggiano *et al.*, 2016), high fracture energy (Vairagade and Kene, 2012). In normal steel fibre reinforced compounds (SFRC), short steel fibres have a random orientation and only steel fibres volume are efficient to resist external loads. The reinforcement adequacy based on the orientation and location of steel fibres which highly affected the performance of SFRC has been stated academically and empirically by many investigators (Villar *et al.*, 2019) (González *et al.*, 2018). In other words, the alignment of steel fibre comparative to main tensile stresses dictates the performance of cementitious compounds (Ahmad *et al.*, 2021). A change in any concrete component material at mix (aggregate volume, maximum aggregate size, cement, and w/c) or adding such materials as Nano-silica, fly ash, and fibres to concrete can impact its rheological characteristics, specifically, its fracture behaviour. (Mihashi, Nomura and Niiseki, 1991) have shown that in normal vibrated concrete (NVC), the fracture energy would increase with an increase in the aggregate size. (Beygi, Kazemi, Nikbin, *et al.*, 2014) have described that in SCC, the fracture energy would increase with an increase in the aggregate volume and maximum aggregate size. In this report, they changed the aggregate volume from 30 to 60%, and the maximum aggregate size in the range (9.5–19 mm). In another research (Beygi *et al.*, 2013), they studied the effect of w/c on the fracture energy of the SCC and presented that an increase in w/cm decreased the fracture energy and the concrete had a more ductile behaviour. (Köksal *et al.*, 2013) conducted research on the effects of w/cm in steel fibre-reinforced high-strength concrete. They used varying w/cm (0.35, 0.45, and 0.55) and two categories of fibres with different tensile strengths (1050 and 2000 N/mm²). Results of their study revealed that in steel fibre high-strength reinforced concrete, the fracture energy and the characteristic length parameter changed with a change in the fibre type and the w/cm.

Elices and co-workers (G.V.Guinea, J. Planas, 1992)(Guinea, Planas and Elices, 1992) recognized the sources of investigational error in the RILEM process and suggested a methodology for eliminating the main source of error, namely by comprising the work-of-fracture that is not measured in the RILEM method because of practical difficulties in capturing the tail section of the load–deflection plot. The second approach suggested by (Hu and Wittmann, 2000) identified that the local specific energy varied through the propagation of a crack, the difference becoming more than pronounced as the crack approached the stress-free back face boundary of the sample.

(Karihaloo, Abdalla and Imjai, 2003) and (Abdalla and B. L. Karihaloo, 2003) expanded the free boundary impact concept of (Hu and Wittmann, 2000) and demonstrated that the same size-independent specific fracture energy can as well be attained by experimentation just two samples of the same size but with notches which are well separated, Such as the notch to depth percentages in three-point bend (TPB) samples should be 0.1 and 0.6 or 0.05 and 0.5. Their approach significantly decreases the number of test samples and simplifies the determination of specific fracture energy (G_F) (Ramachandra Murthy *et al.*, 2013b). The fracture behaviour and the dilatant crack opening in the shear response of self-consolidating concrete with discrete steel fibre reinforcement were studied. The volume fraction of steel fibres (hooked end) in concrete was 0.75%. The fracture behaviour of SCSFRC was studied utilizing notched beams examined in flexure. In SCSFRC, there was a significant increase in fracture energy at a small crack opening. The significant post cracking resistance to crack opening given by fibres in an SCC matrix resulted in a double increase in energy up to 0.1 mm crack opening (Gali, Sharma and Subramaniam, 2018).

The most significant phase in concrete which have an efficient role in establishing the concrete properties is the interfacial transition zone (ITZ) of cement paste and aggregate. Various factors influence the value of this area, in which water to cementitious materials ratio (w/cm) is considered as one of the most significant factors. (Carpinteri and Brighenti, 2010) studied the plain concrete with normal strength under various fracture modes and demonstrated that the concrete fracture energy maximized in the optimum water to cement ratio; afterwards, it reduced when this ratio decreased and increased. (Beygi *et al.*, 2013) investigated the behaviour of the self-compacting concrete (SCC) and indicated that when the w/cm ratio increased from 0.35 to 0.7, the fracture energy initially increased and then reduced. Some findings have indicated that by reducing water to cement ratio (w/cm), the

fracture energy increased (Jo and Tae, 2001). (Zhao, Kwon and Shah, 2008) also demonstrated that no clear correlation could be given between water to cementitious materials ratio (w/cm) and fracture energy.

It is the objective of this section to explore in detail the role of several composition parameters of SCC mixes in their fracture behaviour. In particular, the influence of paste to solids (p/s) and water to binder (w/cm) ratios on the size-independent fracture energy (G_f) suggested by (Abdalla and B. L. Karihaloo, 2003) and validated by (Karihaloo, Abdalla and Imjai, 2003).

7.3.2.1 Determination of fracture parameter

The specific fracture energy (G_f), as specified by RILEM technical committee, is the typical energy provided by dividing the total work of fracture by the projected fracture region (i.e., cross-section of initially un-cracked ligament) based on the load–displacement (P – d) curve. Therefore, for a sample of depth W , thickness B and initial notch depth a (as schematically shown in Figure 7.21) the specific fracture energy (G_f) can be stated as:

$$G_f = \frac{1}{(w-\alpha)B} \int P d\delta \quad (7.1)$$

The sample weight can be neglected for the small samples used in this research.

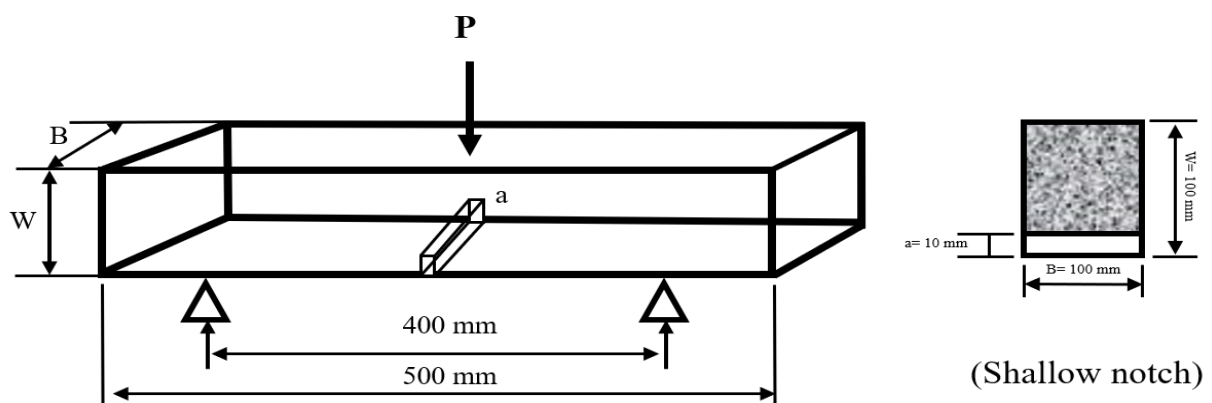


Figure 7.21: Schematic representation of the three-point bending test

7.3.2.2 Specimen preparation and test procedure

From each of the nine mixes (in Table 7.2) six beam specimens (Figure 7.22), three cubes (100 mm), and three cylinders (100 × 200 mm) were cast. The specimens were de-moulded

after 1 day and cured in water at ambient temperature (between 20-24°C) for 28 days. The compressive strength of SCC was estimated in accordance with (BS EN 12390-3, 2009), using concrete cube samples with size $100 \times 100 \times 100 \text{ mm}^3$. Beams were notched to a depth of 10 mm (notch to depth ratio $a/W= 0.1$) with a thin (2 mm) (Figure 7.22). The modulus of elasticity (E), and the split cylinder strength (f_{st}) were measured on cylinders according to (BS EN 12390-6, 2009) and (BS EN 1881-121, 1993) respectively.



Figure 7.22: Shallow notch to depth ratio (0.1 mm)

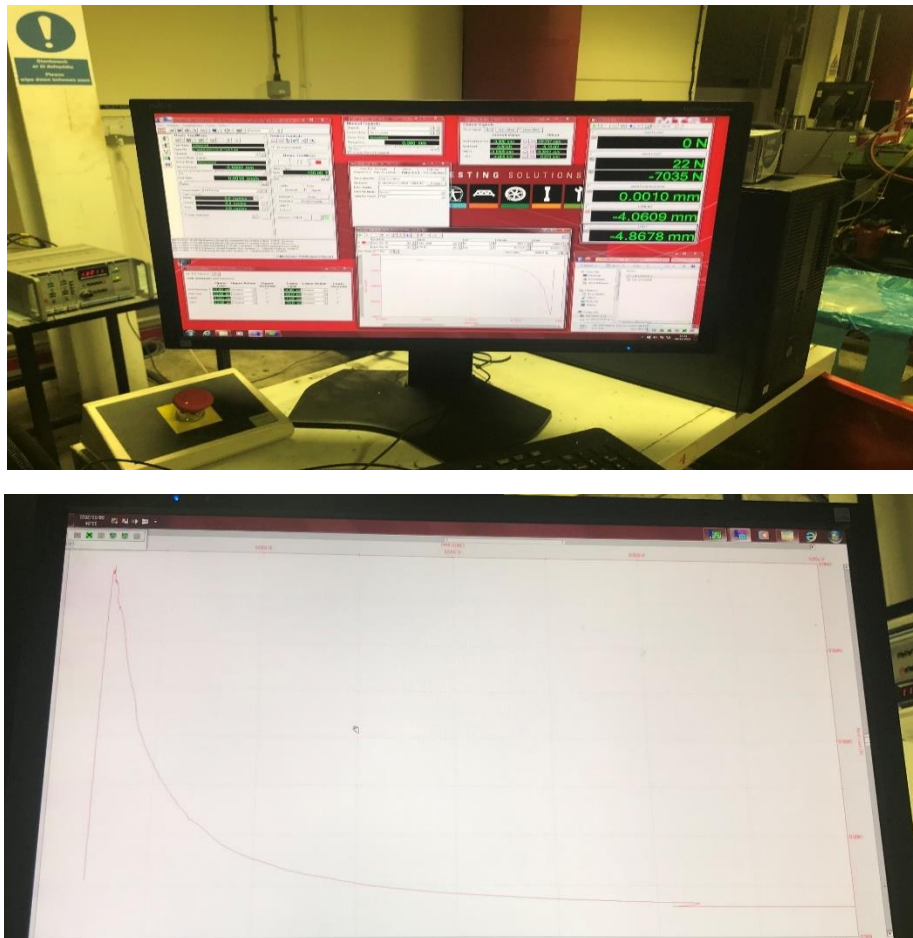


Figure 7.23: X-Y plotters for the load-deflection curve



Figure 7.24: Beam specimen used for TPB test

As schematically demonstrated in Figure 7.23, the tests for the determination of the fracture energy were performed according to the RILEM work-of-fracture method (RILEM 50FMC, 1985). The load-point deflection was measured simultaneously by means of a linearly variable displacement transducer (LVDT) (Figure 7.24). The experiments were performed in a stiff Dartec closed-loop universal testing machine with a maximum load capacity of 250 kN.

7.3.2.3 Discussion of Hardened behaviour of SCC with or without fibre

Typical recorded load–deflection drawings of one notched beam from the nine mixes are shown in Figure 7.25. The area under the load–deflection diagram was calculated from which the $G_f(a, W)$ was determined using Eq. (6.1). Table 7.11 shows the results of the measured fracture energy $G_f(a, W)$, with an indication of the mean value, standard deviation and the coefficient of variation (COV%).

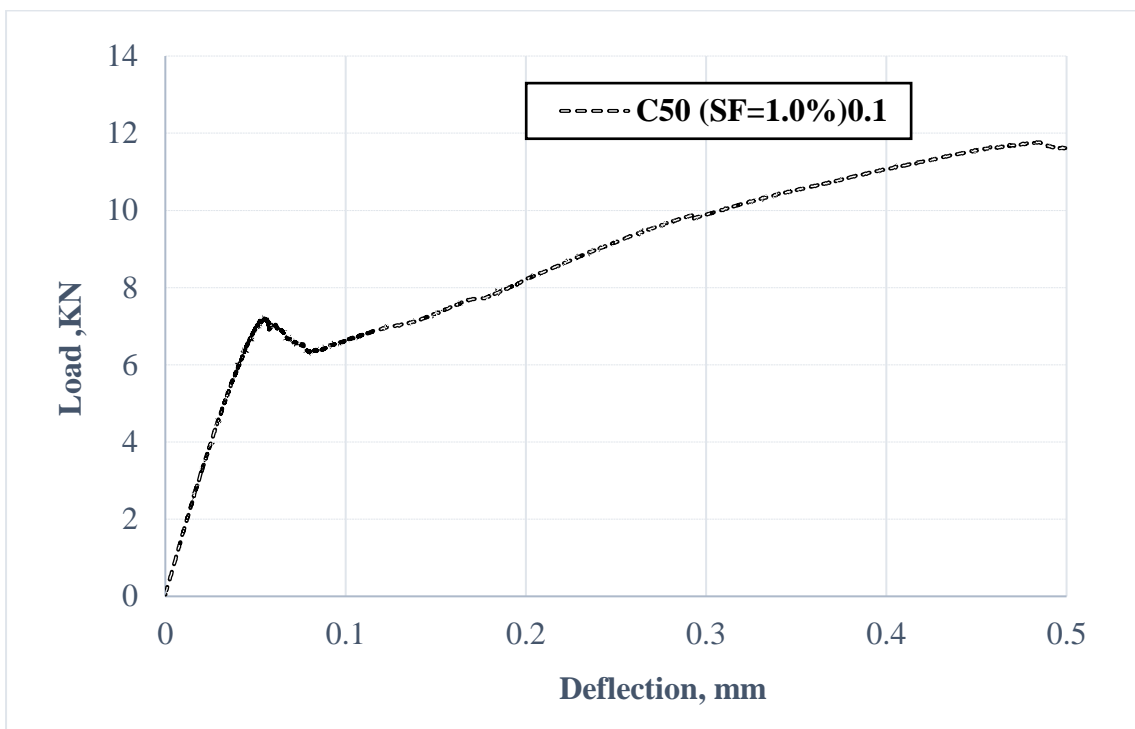
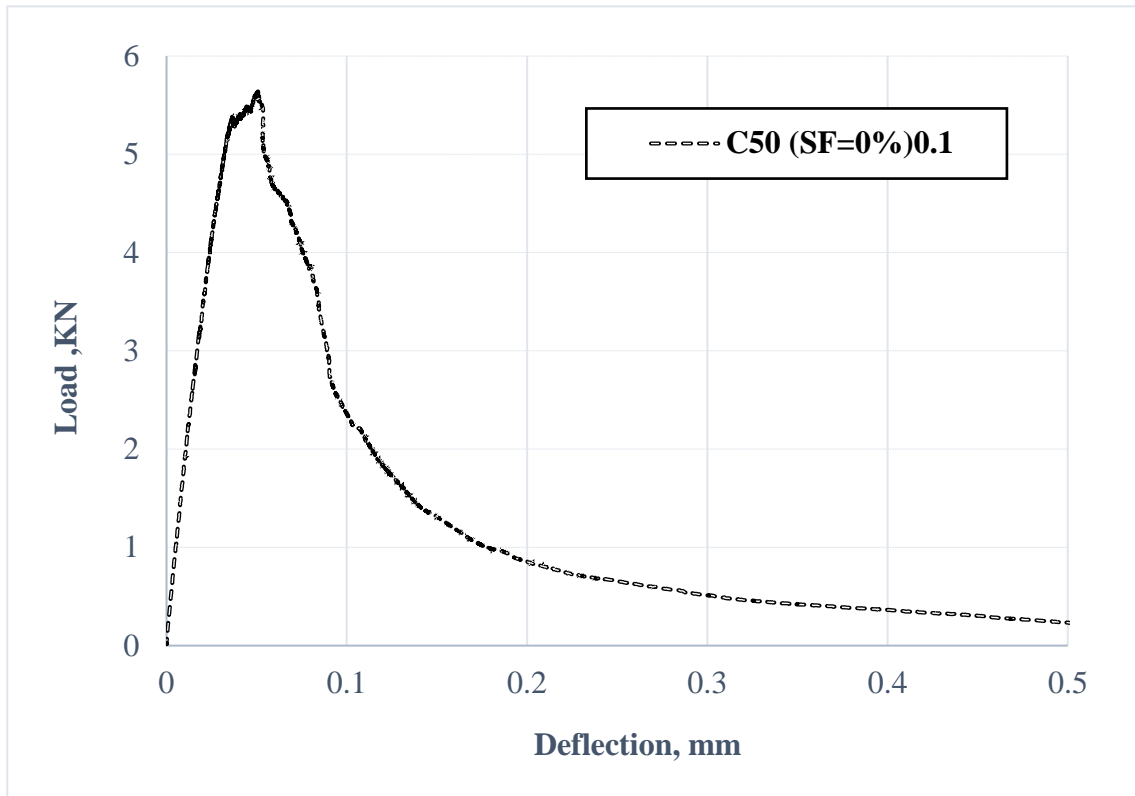


Figure 7.25: Typical load–displacement diagrams of one notched beam (0.1 mm) from SCC mixes without and with steel fibre.

Furthermore, it can be noticed from Figure 7.26 that the increase in G_F with the steel fibre volume fraction is more marked in the high strength mix (grade 70) than in mix grades 30 and 50. This may be attributed to the fact that the interfacial transition zone (ITZ) (Beygi, Kazemi, Vaseghi Amiri, et al., 2014) in (grade 70MPa) mixtures is much denser and then more susceptible to cracking because it includes a higher percentage of cementitious materials, as can be seen in Table 7.2.

Table 7.11: Measured fracture energy, G_f (a, W) for different SCC mixes from three-point bending test (TPB)

Mix Designation	W(mm)	a/W	Mean [St. dev.] G_f (a, W), N/m	COV (%)	SF (%)
Mix 1	100	0.1	64.44 [3.14]	4.87	0
Mix 2	100	0.1	252.29 [1.67]	0.66	0.5
Mix 3	100	0.1	359.33 [8.27]	2.30	1.0
Mix 4	100	0.1	75.83 [5.11]	6.73	0
Mix 5	100	0.1	273.88 [2.36]	0.86	0.5
Mix 5	100	0.1	368.33 [9.23]	2.51	1.0
Mix 7	100	0.1	80.83 [9.03]	11.17	0
Mix 8	100	0.1	310.00[1.57]	0.51	0.5
Mix 9	100	0.1	373.75 [8.05]	2.15	1.0

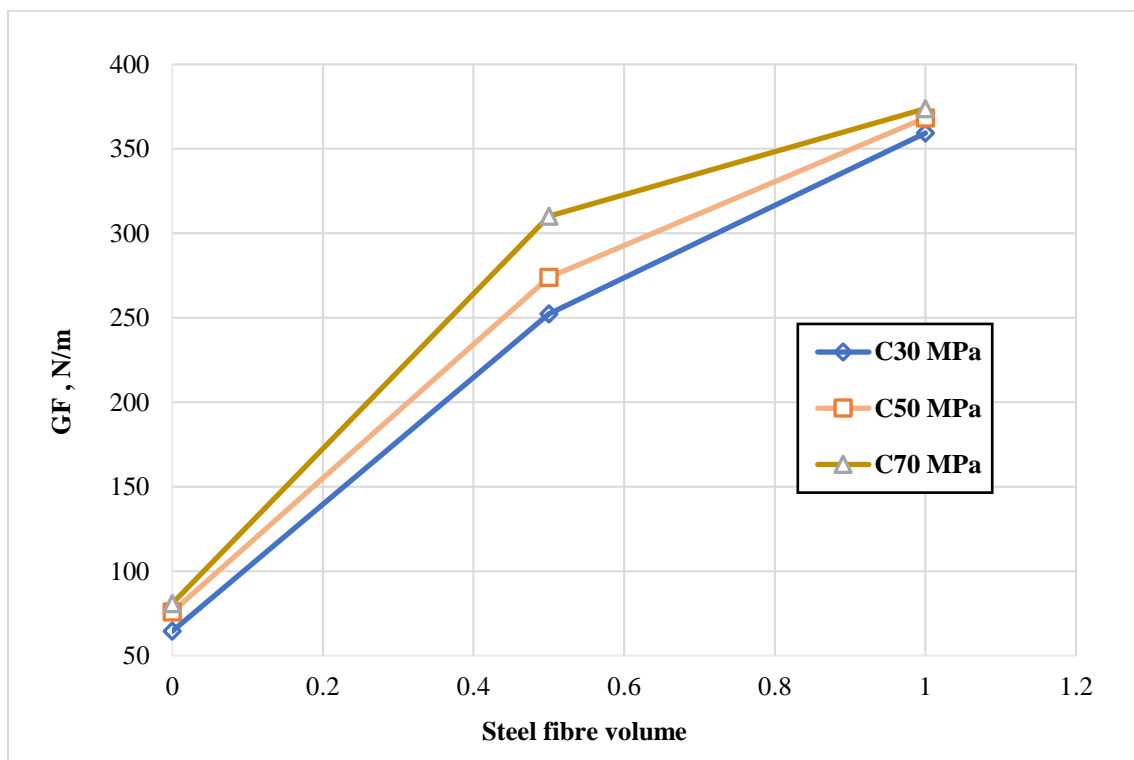


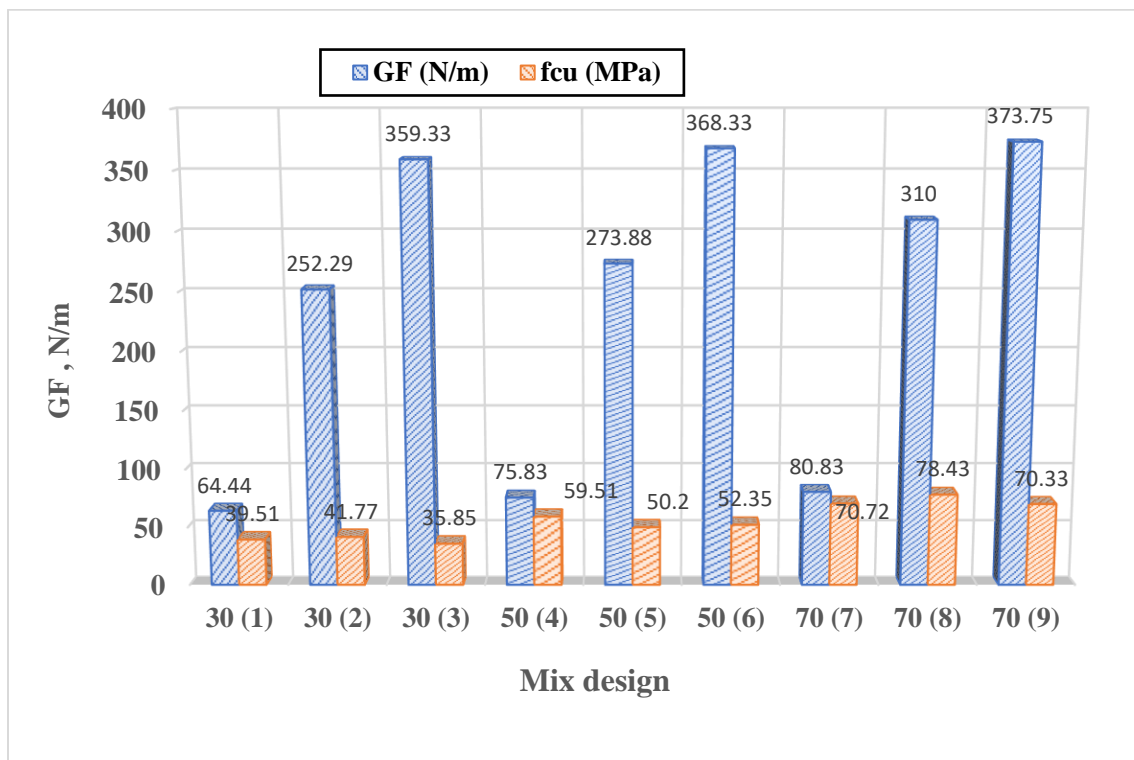
Figure 7.26: Variation of G_F of SCC mixes of grade with steel fibre volume fraction

An increase in the paste-to-solids (p/s) ratio in all mix grades, as expected, leads to increase in the G_F and tensile strength (f_{st}) with the steel fibre volume fraction (0 , 0.5, 1.0) % , but a noticeable no significant effect on cube compressive strength (f_{cu}) for 30 MPa (mixes 1,2,3) , 50 MPa (mixes 4,5,6) and 70 MPa (mixes 7,8,9) , as shown in Figure 7.27. The outcome is consistent with those of previous results (Noaman *et al.*, 2017) (Şahin and Köksal, 2011). According to (Mo *et al.*, 2014), enhanced fracture energy can be obtained by adding steel fibres. The steel fibre tries to elongate the path of cracking and the route of the crack, therefore preventing their propagation, and possibly improving the fracture capacity. This impact was as well observed by (Alyhya *et al.*, 2016) , as they obtained a noticeable decrease in G_F with an increase in the p/s ratio for different SCC without fibre mixes with compressive strength varying from 30MPa to 80 MPa.

The tensile strength of all SCC with fibre were higher compared with that of the SCC. The enhanced compressive/tensile strength of the concrete mixes with fibres can be attributed to the decreased growth of cracks, which is dependent on the bond strength (confinement influence) of the steel fibre with the concrete matrix (Li *et al.*, 2018) (Abbass, Khan and Mourad, 2018). The findings suggest that the fibres can improve the splitting tensile strength beyond 19.38%. Fibre content can improve the tensile strength properties for the reason that it hinders and bridges the cracks of the concrete matrix, and the bridging force specifically depends on the chosen fibre category (Abbass, Khan and Mourad, 2018)(E. A. H. Alwesabi *et al.*, 2020) (E. A. Alwesabi *et al.*, 2020).

Table 7.12: Results of f_{cu} , f_{st} , E , G_f of test SCC without and with steel fibre mixes

Mixture codes	Compressive strength (MPa) at 28 days	Tensile strength (MPa) at 28 days	E, 28 days (GPa)	G_f N/m
Mix 1	39.51	3.04	36.91	64.44
Mix 2	41.77	4.32	35.66	252.29
Mix 3	35.85	5.69	23.71	359.33
Mix 4	59.51	4.28	35.88	75.83
Mix 5	50.20	4.44	40.89	273.88
Mix 6	52.35	5.92	31.19	368.33
Mix 7	70.72	4.62	39.52	80.83
Mix 8	78.43	5.74	45.50	310
Mix 9	70.33	8.78	33.66	373.75

Figure 7.27: Variation of the G_f and f_{cu} with different p/s ratios

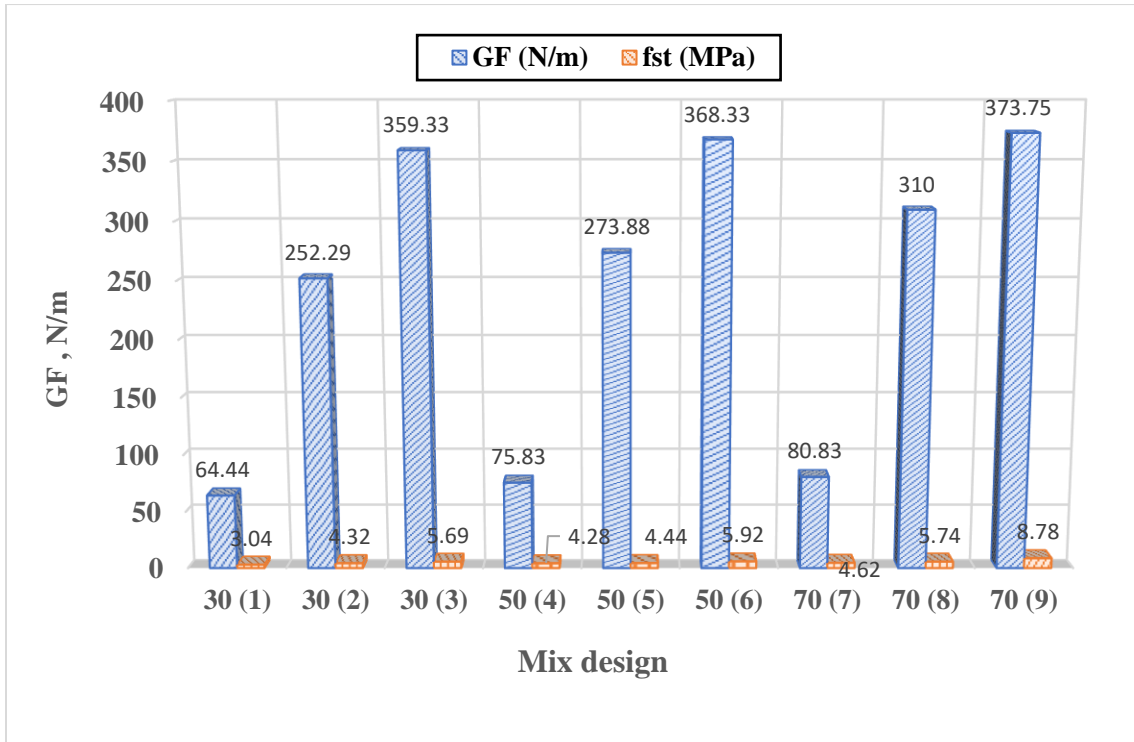


Figure 7.28: Variation of the G_f and f_{st} with different p/s ratios

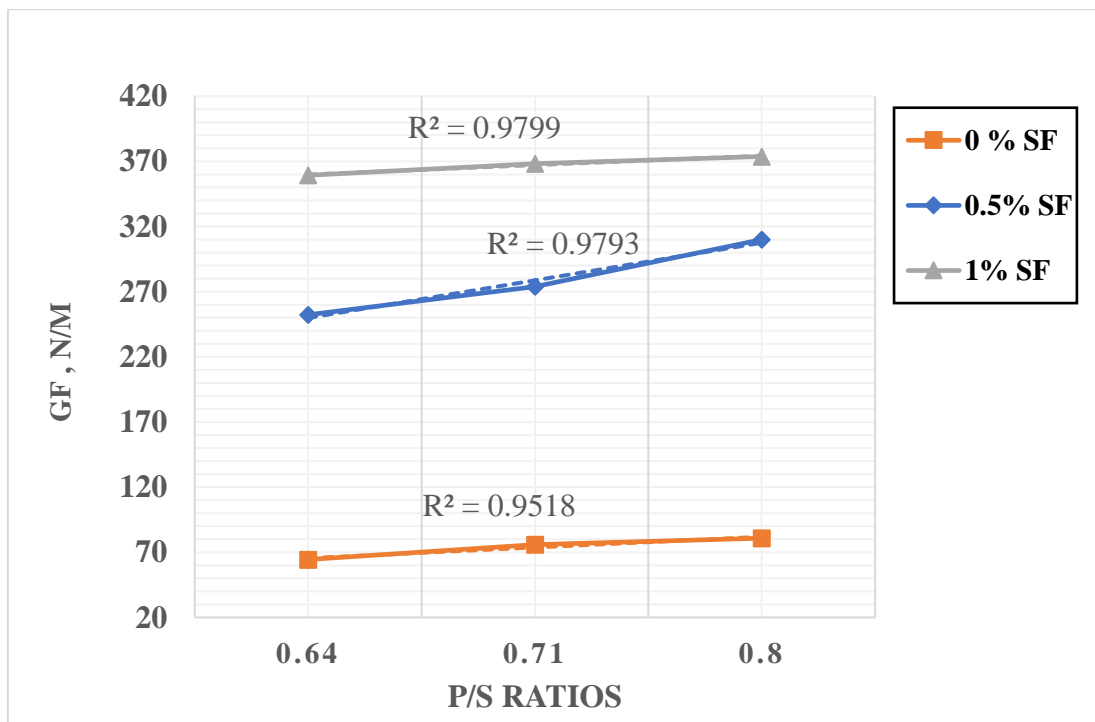


Figure 7.29: Variation of the G_f and p/s ratios

As expected, G_f decreases with increasing water to binder (w/cm) ratio, in much the same manner as in VC (Prokopski and Langier, 2000) as shown in Figure 7.30. This outcome is consistent with the recent analysis on normal-strength (NS) SCC attained by (Beygi et al., 2013) who observed that fracture energy reduces by 38% as w/cm percentage is increased from 0.4 to 0.7. G_f of high-strength (HS) SCC mixes ($f_{cu} \sim 100$ MPa), in contrast has been stated by (Cifuentes and Karihaloo, 2013) to be just 90 N/m for (w/cm = 0.23). This is a result of the densification of ITZ as a result of using a fairly high micro-silica volume fraction. When the volumetric content of steel fibre in the high-strength (HS) steel fibre reinforced SCC increases from 0 to 1%, the amount of G_f in w/cm = 0.35 and w/cm = 0.24 increases by 23.17 and 30.85 times compared to plain HSC, respectively. Additionally the increase in total fracture energy is significantly further than the initial fracture energy (Mousavi, Ranjbar and Madandoust, 2019). However, if the amounts achieved for the high-strength (HS) SCC mixes are compared with the similar amounts for normal-strength (NS) SCC mixes it is noted that there is no increase in the values of G_f with a decrease in the w/cm percentage, as might have been anticipated. This is because the decrease in G_f generated by an increase in the p/s percentage exceeds the increase given in it by a reduce in w/cm. Furthermore, in case of high-strength (HS) SCC mixes silica fume was employed instead of GGBS (Cifuentes, Ríos and Gómez, 2018). The use of silica fume in SCC generates a densification in the ITZ that leads to a tougher cementitious matrix (Akçaoğlu, Tokyay and Çelik, 2004) so that the frictional part of the P- δ curve is shorter in comparison with normal-strength (NS) SCC mixes. This impact was previously observed by (Cifuentes and Karihaloo, 2013) who observed that fracture energy decreased from 151.8 N/m for a w/cm ratio of 0.48 (normal strength SCC with $f_{cu} = 41.0$ MPa) to 88.7 N/m for a w/cm ratio of 0.23 (high-strength SCC with $f_{cu} = 97.7$ MPa).

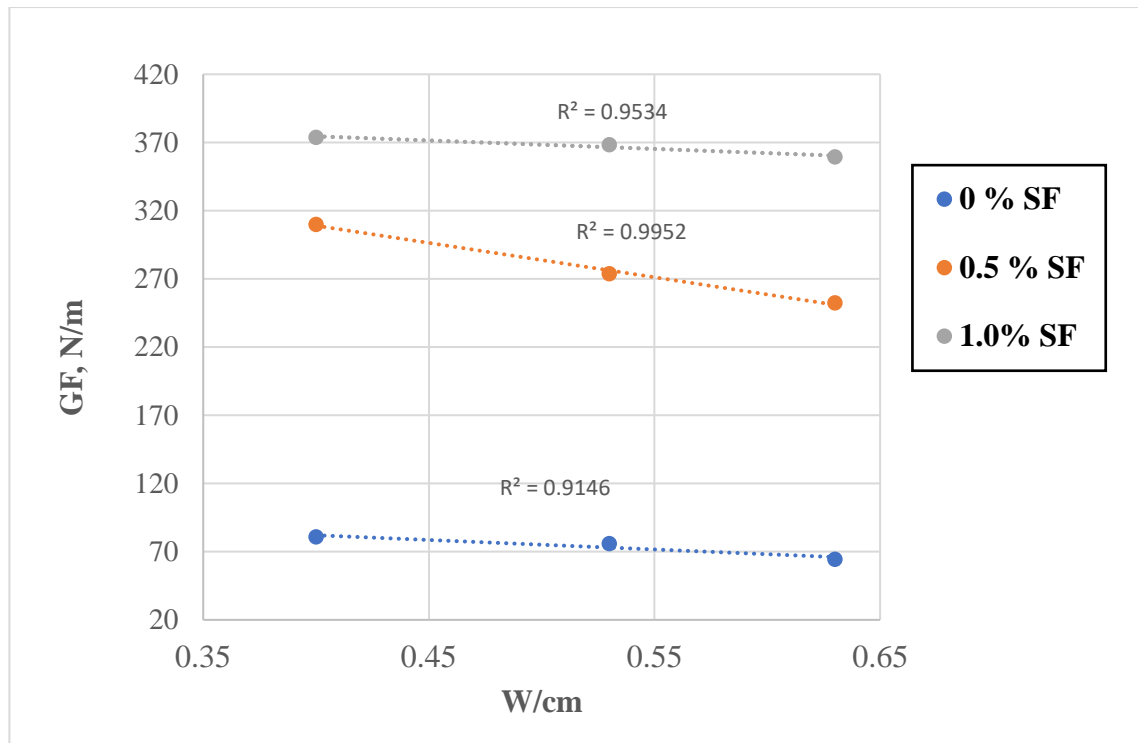


Figure 7.30: Variation in G_f with w/cm ratio for different steel fibre (SF) volume fractions

7.4 Concluding remarks

This chapter investigates what proportions of solids, liquids and super-plasticiser need to be selected for a particular type of steel fibre in order to produce self-compacting normal-performance concrete (SCC) mixes with the right flowing, passing and filling ability. To that end, a wide range of normal SCC mixes were prepared in the laboratory: with steel fibre proportions of 0, 0.5% with maximum coarse aggregate sizes (g) of 10 mm and 20 mm and 1% without coarse aggregate, and with compressive strength ranging between 30 and 70 MPa. The study finds that, for the SCC mixes without steel fibres, the fulfilment of flow and cohesiveness criteria are sufficient for the mix design. For the SCC mixes with steel fibres, however, it is found that passing and filling ability criteria are also important. In addition, the results of an experimental study on fracture behaviour of SCC mixes without and with fibre differing by the steel fibre volume, paste to solids ratio and water to binder ratio were presented in this chapter. This study compared SCSFRC to SCC mixes, and the experimental work and analysis presented above supports the following salient conclusions:

- Our studies indicate that the mixtures of steel fibres (0.5%) and various sizes of coarse aggregate (10 mm and 20 mm) meet the flow and pass-ability criterion, and are resistant to segregation, as judged by the slump flow and J-ring test with 12 bars. However, J-ring test

with 16 bars may not meet the passing ability criterion. These mixtures must be more flowable than needed by the slump flow test, in order to meet the passing ability test.

- Using steel fibre (0.0% and 0.5%) with various sizes of coarse aggregate (10 mm and 20 mm) as an addition to SCC and SCSFRC did not significantly affect t_{500} time test values.
- Using steel fibre (0.5%) with the size of coarse aggregate (10 mm) as an addition to SCC (40 MPa) did not affect t_{500} time test values. There was a remarkable regular distribution of coarse aggregate and steel fibre in the mix.
- Using steel fibre (1.0%) and various sizes of coarse aggregate (10 mm and 20 mm) as an addition to SCC that showed signs of bleeding and segregation of mix with (30 MPa), while increasing the SP of the mix.
- Using steel fibre (1.0%) without coarse aggregate as an addition to SCC that showed no signs of bleeding and segregation of mix with (30 MPa, 50 MPa and 70 MPa), while increasing the SP of the mix.
- With reduced w/c proportions from 0.63 to 0.40 of SCSFRC mixes, the value of compressive strength increased by 44%.
- SP content was increased in SCSFRC compared to the SCC mixes as a result of adding steel fibre with SCC. while w/c proportions (i.e., water content) were constant for both SCSFRC and SCC mixes.
- The plastic viscosity of SCC increases with additional steel fibre in mixes.
- The specific fracture energy (G_f) increases with an increase in the steel fibre volume fraction, irrespective of the SCC mix grade, although the increase is less pronounced in higher strength mix (grade 70 MPa) than in grades 30 MPa and 50 MPa of SCC.
- Within the same nominal strength grade, an increase in the paste to solids (p/s) ratio results in a marginal increase in the G_f , but noticeably no significant on cube compressive strength (f_{cu}).
- An increase in the w/cm ratio reduces G_f . The decrease becomes more pronounced with decreasing steel fibre volume fraction.
- An increase in the steel fibre volume fraction with the same nominal strength grade increases tensile strength.

The next Chapter will investigate the simulation of the flow of SCSFRC in the slump flow and L-box tests using SPH strategy.

Chapter 8

**Simulation of SCC flow with fibre Modelling
and validation**

8.1 General Instructions

Self-compacting steel fibre reinforced concrete (SCSFRC) may contribute to significant development of high quality complex concrete structures and open new applications for concrete. The addition of fibres makes the fresh concrete stiffer and reduces its workability. This also limits the number of fibres that can be uniformly orientated and distributed in the presence of heavy reinforcement, complex formwork shapes and large aggregates. As the orientation of fibres alter throughout the production of the concrete, it is essential to understand these changes in the fibre orientation. In particular, the orientation and distribution of fibres may be significantly affected, especially when the concrete is cast in the presence of heavy reinforcements. In the past, most of the study focused on visual inspection of fibres in hardened concrete parts cut after casting (Zak, Park and Benhabib, 2001)(Bernasconi, Cosmi and Hine, 2012)(Lee *et al.*, 2002) and the prediction of typical orientation factor of fibres from the cut sections (Martinie and Roussel, 2011).

The prediction of SCSFRC flow and its passing and filling behaviour is very challenging particularly within the congestion of reinforced formwork geometry and in the presence of reinforcing steels. However, an understanding of the flow behaviour and its properties is important for producing high-quality SCC. The most cost-effective way to gain such an understanding is by performing computational simulations, which will enable one to fully characterize the flow behaviour of SCSFRC and to reveal the orientation of fibres inside the complex formwork shapes. The rheological behaviour of fresh concrete mix must be consistent with the formworks of complex shapes to ensure the production of complete and high-quality casting of structural elements. In this work, a three-dimensional Lagrangian smooth particle hydrodynamics (SPH) method is used to simulate and predict the flow of SCSFRC. SPH method is ideal for simulating the flow, passing ability and filling ability of SCSFRC mixes, irrespective of their characteristic compressive strength. These simulations will provide information about the distribution and orientation of fibres throughout the entire process of casting SCSFRC into the formworks of complex shapes to ensure that the mixture flows as a homogeneous mass without any sign of segregation or blockage. In this chapter, a simple method has been established to predict the distribution and orientation of steel fibres in self-compacting concrete mixes during flow-ability (Slump Flow test), passing and filling ability (L-box test) tests.

8.2 Development of the self-compacting normal-strength performance steel fibre reinforced concrete mixes

A laboratory study was conducted to produce various grades of SCSFRC mixes (with nominal 28 days cube compressive strengths of 30 MPa, 40 MPa, 50 MPa, 60 MPa and 70 MPa). The fundamental materials and secondary materials for the SCC mix are produced following the European Federation of Specialist Construction Chemicals and Concrete Systems (EFNARC) guidelines (EFNARC, 2005). These mixes were developed using a mix design method for SCC based on the desired target plastic-viscosity and compressive strength in accordance with mix design method proposed by (Abo Dhaheer, M. S. Al-Rubaye, M. M. Alyhya, 2016)(Abo Dhaheer *et al.*, 2016b), which rationalized and simplified the method recommended previously by (Karihaloo and Ghanbari, 2012b) and (Deeb and Karihaloo, 2013a). As an example, the amounts and specifications of the components used in the SCC design mix with target compressive strength 40MPa are shown in Table 8.1. Portland limestone cement (PLC) (CEM II/A-L/32.5R) conforming to (BS EN 197-1, 2011) with a specific gravity of 2.95 and Ground granulated blast-furnace slag (GGBS) with a specific gravity of 2.40 were used as the main cement and cement replacement materials respectively. A new generation of polycarboxylic ether-based superplasticiser (SP) with specific gravity of 1.07 was used in all the test mixes. Crushed limestone coarse aggregate with maximum particle size of 20 mm and a specific gravity of 2.80 was used, while the fine aggregate was river sand (less than 2 mm) having a specific gravity of 2.65. Limestone powder (LP) as a filler with maximum particle size of 125 μm (specific gravity 2.40) was used. A part of the river sand was substituted by an equal amount of the coarser fraction of LP in the size range 125 μm – 2 mm. As shown in Table 8.2, further details of test SCSFRC mix. The mix was tested in the fresh state utilizing slump cone and L-box tests. The plastic viscosity of each mix was calculated using the micro-mechanical procedure described by (Ghanbari and Karihaloo, 2009).

Table 8.1: Constituents and proportions for SCSFRC mix (kg/m^3)

Mix designation	cm ^a		Water	SP ^b	w/cm	SP/cm	LP ^c	SF ^e (0.5%) ratio	FA ^d		CA ^e
	Cement	ggbfs							FA**	FA***	
40 MPa	270	90	205	2.3	0.57	0.64	143	40	740		839
									240	550	

^a Cementitious material.

^b Super-plasticizer.

^c Limestone powder <125 μm .

^d Fine aggregate <2 mm (Note: a part of the fine aggregate is the coarser fraction of the limestone powder,

FA**125 μm –2 mm, whereas FA*** refers to natural river sand < 2 mm).

^e Coarse aggregate < 10 mm.

Table 8.2 : Further details of test SCSFRC mix

Mix designation	Estimate plastic viscosity (Pa s)	Paste vol. fraction	Solid vol. fraction	Paste/Solid (by vol.)
40 MPa	27	0.40	0.60	0.66

8.3 Modelling the flow-ability , pass—ability and fill—ability of steel fibre suspended self-compacting based on experiment

In the rheological studies to characterize fresh concrete, SCSFRC is understood as a suspension of solid particles (coarse aggregate and steel fiber) in a fluid phase (cement paste), in which various of particle size distribution and fluid stage are typically enhanced to meet the three main properties of SCSFRC in the fresh state: flowing ability, filling ability, passing ability, and segregation resistance.

SCSFRC mixtures are designed to meet flowability and cohesiveness (i.e., resistance to segregation) standards utilizing the slump cone test. In this test, the time for the SCSFRC mix to spread to a diameter of 500 mm (t_{500}) after the cone filled with the mixture has been suddenly lifted is recorded, as well as the diameter of the spread when the flow stops (EFNARC, 2005). The resistance to segregation and blockage is checked visually between the coarse aggregate and steel fibre (Figure 8.1).

To test the ability of a SCSFRC mix to pass and fill the formwork containing reinforcement under its own weight, the L-box apparatus is used (EFNARC, 2005). The vertical leg of the L-box is filled with the SCSFRC mix. At the bottom of this leg is a gate with two or three rods in front of it. When the gate is lifted, the mix flows into the horizontal part of the L-box through the gaps between the rods. The times for the mix to reach 200 mm (T200) and 400 mm (T400) from the gate are recorded, as well as the time it takes the mix to level off in the horizontal leg of the L-box. Again, it is required that no coarse large aggregate particles or steel fibres be blocked by the rods (Figure 8.2).

The addition of steel fibres enhances the mechanical characteristics and the ductility of SCC in much the same approach as in vibrated concrete (VC). Nevertheless, the fibres significantly impair the workability of SCC due to their elongated shape and large surface area. The volume of fibre added to a SCC mixture is therefore limited and depends on the fibre type

used and the composition of the SCC mixture. Therefore, the maximum volume of fibres is decided in such a way to manage the workability, whilst maintaining excellent flowing and passing ability. For the optimum results, the fibres require to be homogeneously distributed in the mixture without clustering or segregation and blockage.

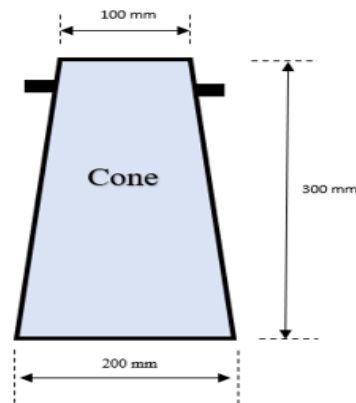


Figure 8.1: Dimension of Flow test of SCSFRC

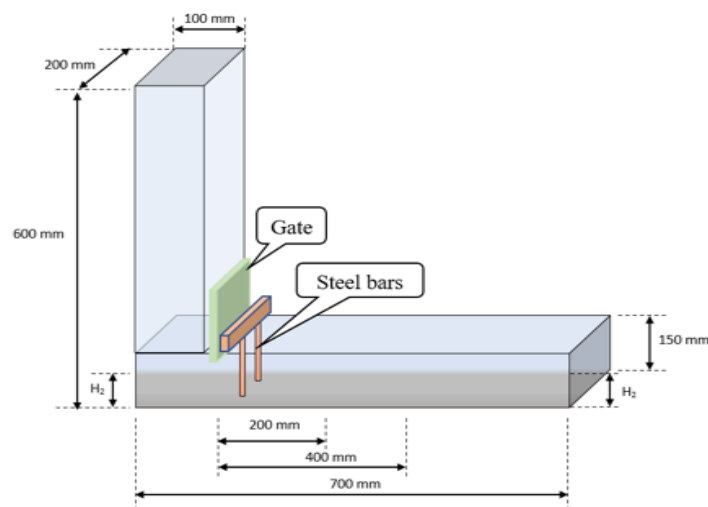


Figure 8.2: Dimension of L-box test of SCSFRC

8.4 Modelling simulation the flowing, passing and filling ability of SCSFRC

Since fresh SCSFRC flow in slump and L-box test configurations is a gravitational flow with large deformations, a three-dimensional smooth particle hydrodynamic (SPH) mesh-less numerical methodology is chosen here to simulate the fresh state. This section briefly introduces the fundamental governing equations, numerical model and the boundary conditions required for modelling SCSFRC flow in slump flow and L-box of tests with 3D-

Lagrangian SPH method.

8.4.1 Governing equations

Fresh SCSFRC mix is a non-Newtonian incompressible fluid which can be described by a bilinear Bingham-type model with relation between the shear stress and shear strain rate which includes two material parameters: the yield stress (τ_y) (Badry, Kulasegaram and Karihaloo, 2016) and the plastic viscosity (η) (Ghanbari and Karihaloo, 2009) (Papanastasiou, 1987).

$$\tau = \eta \dot{\gamma} + \tau_y (1 - e^{-m\dot{\gamma}}) \quad (8.1)$$

Where m is a very large number (e.g., $m > 1000$). There are two basic equations to be solved in the SPH method, together with the constitutive relation – the incompressible mass and momentum conservation equations.

$$\frac{1}{\rho} \frac{D\rho}{Dt} + \nabla \cdot \mathbf{v} = 0 \quad (8.2)$$

To include the effect of immersed boundary, the momentum conservation equation is modified:

$$\frac{D\mathbf{v}}{Dt} = -\frac{1}{\rho} \nabla P + \frac{1}{\rho} \nabla \cdot \boldsymbol{\tau} + \mathbf{g} + \mathbf{f} \quad (8.3)$$

where ρ , t , \mathbf{v} , P , \mathbf{g} and $\boldsymbol{\tau}$ represent the fluid particle density, time, particle velocity, pressure, gravitational acceleration, and shear stress tensor, respectively. Here, \mathbf{f} represents the effective reaction force of the fibres on the fluid at any chosen location. However, the reaction force \mathbf{f} will not be acting on the fluid particles which do not fall within the radius of influence (or smoothing length) of any boundary particles of a given fibre. In the proposed numerical procedure, fibres are described by immersed boundaries.

8.4.2 Numerical implementation

A projection method based on the predictor–corrector time stepping scheme was adopted to track the Lagrangian non-Newtonian flow. The prediction step is an explicit integration in time without enforcing incompressibility as shown in Figure 8.3. Only the viscous stress and gravity terms are considered in the momentum equation (Equation 8.3) and an intermediate particle velocity is obtained as:

$$v_{n+1}^* = v_n + \left(g + f + \frac{1}{\rho} \nabla \cdot \tau \right) \Delta t \quad (8.4)$$

in which v_n and v_{n+1}^* are the particle velocity and intermediate particle velocity at time t_n and t_{n+1} , respectively. Then the correction step is performed by considering the pressure term in Equation 8.3

$$\frac{v_{n+1} - v_{n+1}^*}{\Delta t} = - \left(\frac{1}{\rho} \nabla P_{n+1} \right) \quad (8.5)$$

Rearranging Equation 8.5 gives,

$$\frac{v_{n+1} - v_{n+1}^*}{\Delta t} = - \left(\frac{1}{\rho} \nabla P_{n+1} \right) \quad (8.6)$$

where v_{n+1} is the corrected particle velocity at time step t_{n+1} . By imposing the incompressibility condition in the mass conservation equation (Equation 8.2), the pressure P_{n+1} in Equation 8.6 will be obtained. As the particle density remains constant during the flow, the velocity v_{n+1} is divergence-free so that Equation 8.2 can be simplified as.

$$\nabla \cdot v_{n+1} = 0 \quad (8.7)$$

Substitution into Equation 8.6 gives,

$$\nabla \left(\frac{1}{\rho} \nabla P_{n+1} \right) = \frac{\nabla \cdot v_{n+1}^*}{\Delta t} \quad (8.8)$$

which can be rewritten as

$$\nabla^2 P_{n+1} = \frac{\rho}{\Delta t} \nabla \cdot v_{n+1}^* \quad (8.9)$$

where ∇^2 is the Laplacian. Solution of the second-order Poisson equation (Equation 8.9) gives the pressure from which the particle velocity is updated (see Equation 8.6). Finally, the instantaneous particle position is updated using the corrected velocity.

$$x_{n+1} = x_n + v_{n+1} \Delta t \quad (8.10)$$

where x_{n+1} and x_n are the particle positions at time t_{n+1} and t_n , respectively.

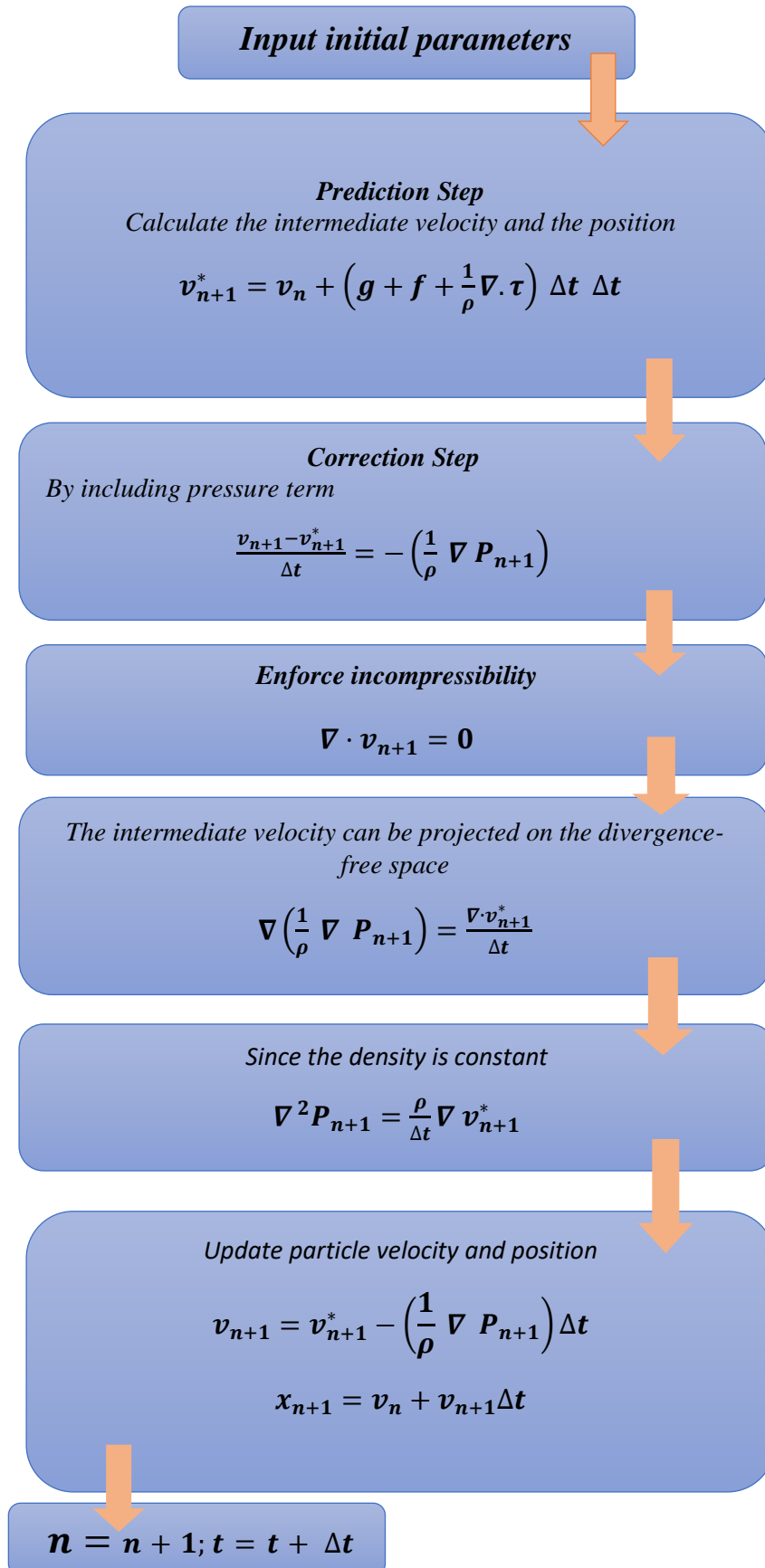


Figure 8.3: Flow chart of truly compressible solution of the governing equations of the fluid flow

The interaction between SPH fluid particles surrounding the rigid fibres can be modelled by treating fibres as immersed boundaries (Figure 8.4). This would offer a simple and efficient methodology to determine fibre orientations and distribution during the flow.

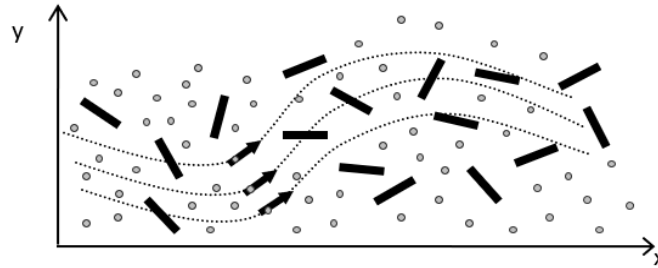


Figure 8.4: Schematic diagram of the flow of SCSFRC with rigid steel fibres

8.5 Initial configuration and boundary conditions

When solving the Navier-Stokes and continuity equations, appropriate initial and boundary conditions need to be applied. Three types of boundary conditions need to be considered in the simulation of slump cone test; a zero-pressure condition on the free surface, Dirichlet boundary condition at the wall of the cone, and Neumann conditions on the pressure gradient as illustrated in Figure 8.5.

Four arrays of rigid dummy particles placed outside the wall of the cone were used to implement the wall boundary conditions with space r_0 between the arrays, where r_0 is the initial particle spacing. To represent the non-slip boundary conditions along the cone wall, the velocity of both the wall and dummy particles must be zero. Friction between SCC flow and boundaries was also considered and imposed on the cone wall and the bottom plate with a dynamic coefficient of friction between the SCC mix and steel equal to 0.55 Ns/m.

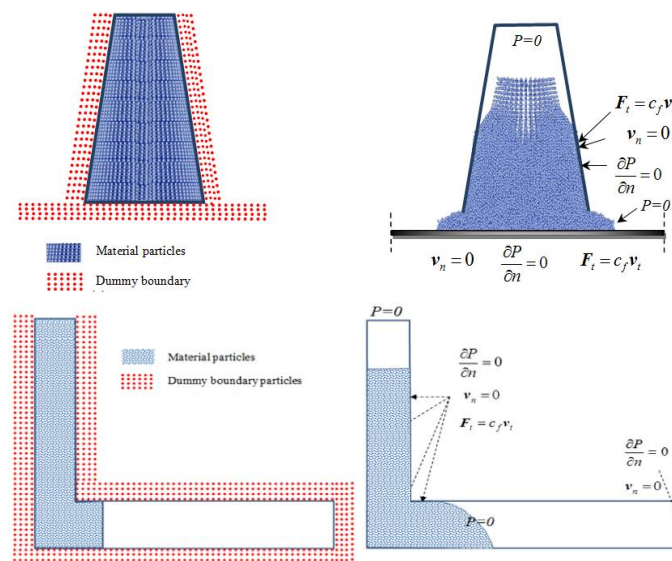


Figure 8.5: Slump flow and L-box test initial condition

8.6 Three-dimension simulation results

To examine how the steel fibres will distribute and orient themselves throughout the filling process, flow (slump flow) and pass/fill (L-box) tests were conducted for SCC mix with steel fibre (Mix 40MPa, Table 8.1). The steel fibres were treated as described above. The plastic viscosity (i.e., 27 Pas) of the mix was estimated analytically using micro-mechanics-based formulations as shown in Table 8.2. The yield stress and the dynamic coefficient of friction with the steel wall of the cone and the base plate were assumed to be 200 Pa and 0.55 Ns/m respectively.

Table 8.3: Comparison of experimental and simulations results for slump flow and L-box tests

	Mix strength grade: 40 MPa	
	Simulation	Experiment
t_{500 mm in Flow}: s	1.45	1.40
Flow spread: mm	615	600
T₂₀₀ in L-box: s	0.75	0.93
T₄₀₀ mm in L-box: s	1.70	1.90

Figure 8.6 and Figure 8.8 displays the distribution of fibres and their orientation during the numerical simulation of slump flow and L-box tests. During the simulation of slump flow, the time for the mixtures to spread to a diameter of 500 mm ($T_{500} = 1.45$ sec) matches closely with the time measured in the laboratory (Table 8.3)(Figure 8.7). The surface of the spread is smooth, and the fibres stay homogeneously distributed at all times during the flow. Similarly, the L-box tests also produced comparable results with experimental observations as shown in Figure 8.7 and Figure 8.9.

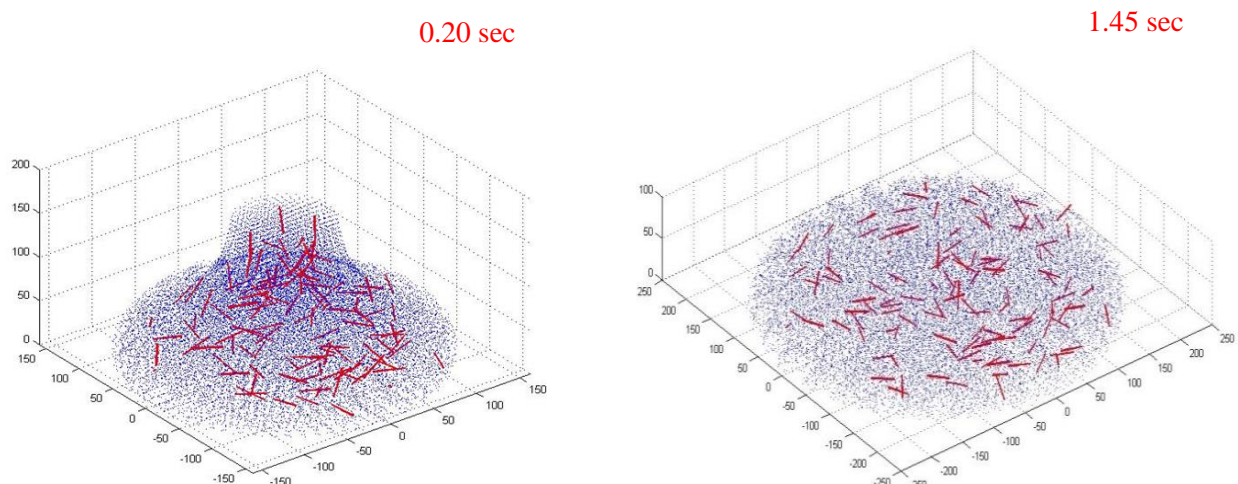


Figure 8.6: 3D numerical simulation of slump flow test for SCSFRC (0.5% vol fibre)



Figure 8.7: Experiment of slump flow test for SCSFRC (0.5% vol fibre)

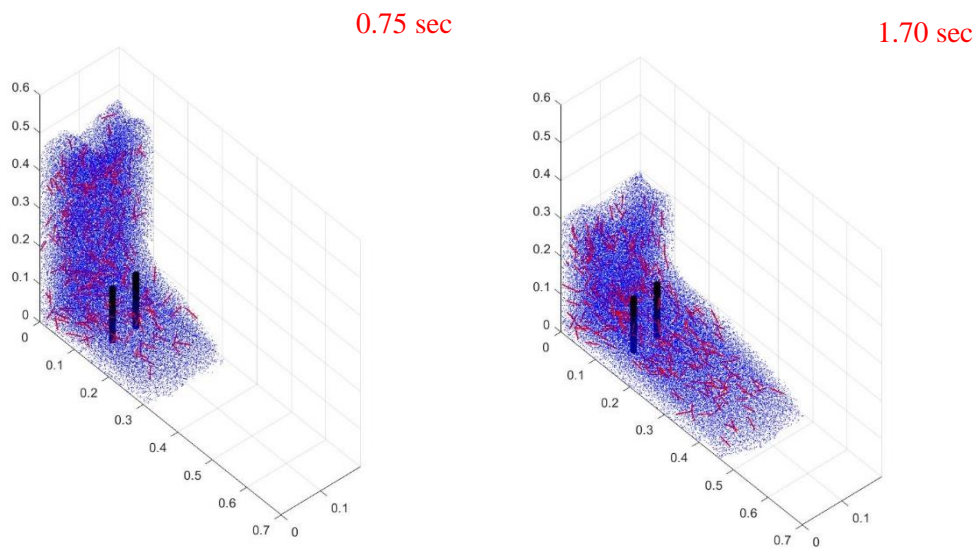


Figure 8.8:3D numerical simulation of L-box test for SCSFRC (0.5% vol fibre).

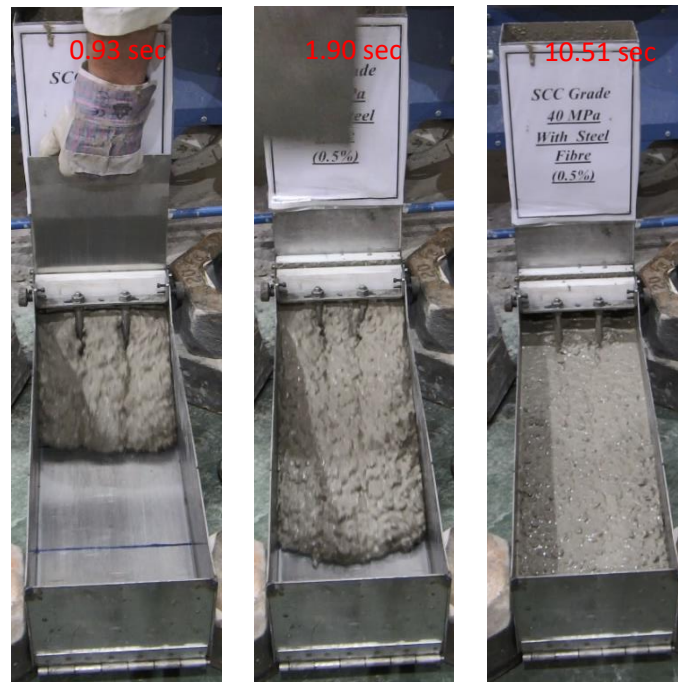


Figure 8.9: Experiment of L-box test for SCSFRC (0.5% vol fibre)

The proposed method can be successfully applied in the numerical simulation of SCSFRC flow to analyse the flow, passing and filling behaviour of these highly viscous fluids. The numerical results are in excellent agreement with experimental results and validate that the 3D SPH methodology can predict the flow of fresh SCSFRC mix with reasonable accuracy.

8.7 Concluding remarks

A Lagrangian SPH method has been used to simulate the flow of self-compacting normal performance concrete with steel fibre during the slump flow and L-box tests in 3-dimensional configurations. An appropriate Bingham model (Ghanbari and Karihaloo, 2009) has been coupled with the Lagrangian Navier-Stokes and continuity equations to model this flow. The mixture characteristics of the SCSFRC mix have been fully incorporated implicitly through the plastic viscosity, which has been assessed exploiting the micromechanical model described in (Ghanbari and Karihaloo, 2009).

The simulation of SCSFRC mixes focused on the orientations of fibres and their distributions during the flow, passing, and filling phases of the slump flow and L-box tests. The established numerical methodology is able to capture the flow, passing, and filling behaviour of SCSFRC mixes and to provide insight into the distribution of fibres and their orientations during these phases. The comparison of the experimental and the simulation results is very encouraging. More flow simulations and validations of SCSFRC mixes (with nominal 28 days cube compressive strengths between 30 to 70 MPa) needs to be carried out to perform additional parametric studies and to further establish the accuracy of the numerical model. Due to the time restrictions and the large simulation time involved, these simulations could not be completed for the purpose of this thesis.

The next Chapter will give a brief and succinct outline of the main conclusions and recommendations for future work.

Chapter 9

**Conclusions and recommendations for
further study**

9.1 Conclusions

From the main achievements of the study presented in this thesis, the following conclusions can be drawn:

- Self-compacting concrete (SCC) without and with steel fibre (SCSFRC) has undergone extensive investigations that have led to confidence in its fresh and hardened properties. Nevertheless, its mix proportioning methods have not kept pace with their production techniques. An easy-to-use rational method for designing an SCC mix with and without steel fibre mix based on the desired target plastic viscosity and compressive strength of the mix was investigated in the present study. The systematic steps taken to develop this rational method were described in Chapter 4 & 5, based on a recently developed micromechanical procedure to determine SCC with and without steel fibre mix plastic viscosity. It should not be forgotten that the developed micromechanical procedure has enriched this research work far beyond the scope of its original intended use for the determination of SCC mix plastic viscosity; it forms the backbone of this rational mix design method. The simplicity and usefulness of this mix proportioning method are enhanced by the provision of design charts as a guide for mix proportioning. The characteristic cube strength of SCC mixes without steel fibres varied between 30 and 70 MPa at 28 days of age, and the target plastic viscosity was between 3 and 15 Pa s: the upper bound of all mix grades was 15 Pa s, whereas the lower bound varied between 3 – 8 Pa s in mix grade range 30 to 70 MPa. In addition, the characteristic cube strength of SCC mixes with steel fibres varied between 30 and 70 MPa at 28 days age, and the target plastic viscosity between 20 and 80 Pa s.
- The experimental work establishing the validity of the proposed mix design procedure was performed via a series of SCC mixes in both fresh and hardened states (Chapter 6). The test mixes were found to meet the necessary SCC and the compressive strength standards, thus fully validating the proposed mix proportioning method. This method considerably reduces the extent of laboratory work, testing time, and materials used to achieve the required level of consistency in these mixes. The sustainability of the designed SCC mixes were enhanced by incorporating LP to replace sand (i.e, fine aggregates) which improves the characteristics of PLC-based materials. Therefore, appropriate quantity of LP can be used to replace fine aggregate or cement content in the paste. Such a replacement is more environmentally friendly and cost-efficient.

- The experimental work demonstrating the validity of the proposed mix design procedure was performed via a series of SCC without and with steel fibre mixes in both fresh and hardened states (Chapter 7). The test mixes were found to meet the necessary self-compacting and the compressive strength criteria, thus fully validating the proposed mix proportioning method. A wide range of normal SCC mixes were prepared in the laboratory: with steel fibre proportions of 0% and 0.5%, with maximum coarse aggregate sizes of 10 mm and 20 mm; and steel fibre proportion of 1% without coarse aggregate; with compressive strength values of 30, 40, 50, 60, and 70 MPa. The study found that SCC mixes without steel fibre had sufficiently fulfilled flow and cohesiveness criteria for the mix design. For the SCC mixes with steel fibre, however, it was found that fulfilment of passing and filling ability criteria was dependent on fibre volume fraction, maximum size of coarse aggregates and their composition.
- Although SCC without and with steel fibre has now become an industrial product, the variations in its composition compared to vibrated concrete still raise concerns about its fracture behaviour. In this study, the role of several composition parameters of SCC mixes' i.e., steel fibre volume , paste-to-solids ratio (p/s) and water-to-binder ratio (w/cm) in their fracture behaviour was investigated (Chapter 7). The results showed that the specific fracture energy (G_f) increases with an increase in the steel fibre volume fraction, irrespective of the SCC mix grade, although the increase is less pronounced in higher strength than in low-strength SCC mixes. Within the same nominal strength grade, an increase in the p/s results in an increase in the G_f . Furthermore, an increase in the w/cm ratio reduces G_f , and the decrease becomes more pronounced with decreasing steel fibre volume fraction.
- An incompressible mesh-less smooth particle hydrodynamics (SPH) methodology was employed to simulate the flow of SCC using in the both tests of the flow and L-box (through gaps in reinforcing bars). A suitable Bingham-type constitutive model was coupled with the Lagrangian momentum and continuity equations to simulate the flow. The numerical simulation results were compared with the actual slump flow and L-box tests carried out on SCC mix with fibre mixes, and the comparison revealed that this

methodology is well suited for predicting the flow behaviour of fibre reinforced SCC in terms of passing and filling abilities (Chapter 8).

- The findings demonstrated that demonstrated that all the simulated mix met required flowing, passing, and filling ability through the gaps in the L-box without blockage, as it did in the laboratory tests. In conditions of segregation evaluation, SPH permits tagging of the fibre particles in order to track their locations during the flowing, passing, and filling phases, and after it has stopped. This allows the distribution of fibre in the mixes to be assessed in order to ensure that they have not segregated from the mortar. The SPH simulation methodology can substitute time-consuming and expensive laboratory investigation for tests of slump flow and L-box, thereby saving time, effort, and materials.

9.2 Recommendations

The improvement of (SCC) with or without fibres (SCSFRC) has revolutionised construction methods by offering superior economic and technical advantages over VC. Being one of the future's environmentally friendly materials for buildings and various construction applications, further research into SCC with or without fibres particularly, is worthwhile, and the following particular areas of investigation are recommended:

- Depending on the findings observed from the present experimental study, using limestone powder as a supplementary cementitious material with PLC to strengthen concrete and improve its fresh and mechanical characteristics should be explored. Limestone powder may be used with other supplementary cementitious materials, such as silica fume and GGBS, and fly ash which can be tested as a replacement for cement by specific percentages in concrete (Chapter 6&7).
- All the design charts of the proposed mixture design method, as described in Chapter 4, were established for proportioning SCC mixes without and with steel fibres, and with characteristic cube strength between 30 and 70 MPa. This procedure can be generalized, and the design charts can be further enhanced if using different types of fibers with various percentages, such as polypropylene, glass, carbon, Poly Vinyl Alcohol (PVA), and asbestos, in addition to steel, which would result in a range of characteristic cube strengths (Chapter 7).

- The maximum sizes of the coarse aggregate in all the SCC mixes reported in Chapters 5 and 6 were 10 mm and 20 mm. The procedure described in Chapter 6 for proportioning the SCC mixes with 1% volume fraction of steel fibre can not be employed if larger size coarse aggregates (e.g., 20 mm) are used. As observed in the case of J-ring and L-box tests, such mixes will lead to blockage between steel fibre and coarse aggregate within re-bars. It is therefore necessary to develop an enhanced mix design procedure for SCSFRC to address these scenarios.
- J-ring and L-box tests used 12 and 2 re-bars respectively for SCC mixes with fibre volume content of 0.5% and 1%. For complete understanding of the passing and filling ability of SCC with or without fibres (at various percentages) in unconfined spaces, SCC mixes should be tested using J-ring and L-box with respectively 16 and 3 bars (Chapter 7).
- In the L-box laboratory test, the gate was manually lifted to release the mix with a little fluctuation of L-box, thus increasing the measured times, especially for mixes with larger content of coarse aggregate and/or fibres. This problem needs to be solved by providing an alternative method for controlling the test procedure (Chapter 7).
- The passing and filling ability of SCC mixes with or without fibres are tested using J-ring, L-box and V-funnel tests. In this thesis, only the simulation of slump flow and L-box test were implemented in 3D configuration. For a full understanding of the passing and filling ability of SCC with or without fibres in unconfined spaces, a 3D simulation of SCC mixes in J-ring and V-funnel tests are needed.
- To take advantage of the full potential of SPH methodology, it is useful to simulate the flow of SCC mixtures and monitor their coarse aggregate or fibre with different percentages within practical size formworks, with the presence of various sizes and densities of reinforcement. To gain this advantage, it is essential to accelerate the SPH simulation method, as the time taken to simulate the flow will be longer than that in the specification tests (Chapter 8).
- Ideal design approaches involve characterization of fibre distribution and orientation in the structural application. Further development of detection methods to assess the fibre configuration in multiple structural applications would help. Study in this field is already ongoing to evaluate fibre distribution, but further investigations should address increasing

their availability for industrial usage. It is equally essential to further develop the numerical tools that simulate the casting process and predict the most likely fibre configuration. Further development is needed to include the fibre segregation effect, and to overcome the limits required by computational time on the size of the structures or the number of fibres that can be simulated(Chapter 8).

References

- Abbass, W., Khan, M.I. and Mourad, S. (2018) 'Evaluation of mechanical properties of steel fiber reinforced concrete with different strengths of concrete', *Construction and Building Materials*, 168, pp. 556–569. Available at: <https://doi.org/10.1016/j.conbuildmat.2018.02.164>.
- Abdalla, H.M. and B. L. Karihaloo (2003) 'Determination of size-independent specific fracture energy of normal- and high-strength self-compacting concrete from wedge splitting tests', *Magazine of Concrete Research*, 55(2), pp. 133–141. Available at: <https://doi.org/10.1016/j.conbuildmat.2013.07.062>.
- AbdelAleem, B.H. and Hassan, A.A.A. (2019) 'Influence of synthetic fibers' type, length, and volume on enhancing the structural performance of rubberized concrete', *Construction and Building Materials*, 229, p. 116861. Available at: <https://doi.org/10.1016/j.conbuildmat.2019.116861>.
- Abdelrazik, A.T. and Khayat, K.H. (2020) 'Effect of fiber characteristics on fresh properties of fiber-reinforced concrete with adapted rheology', *Construction and Building Materials*, 230, p. 116852. Available at: <https://doi.org/10.1016/j.conbuildmat.2019.116852>.
- Abo Dhaheer, M. S. Al-Rubaye, M. M. Alyhya, W.S. et al. (2016) 'Proportioning of self-compacting concrete mixes based on target plastic viscosity and compressive strength: Part I - mix design procedure', *Journal of Sustainable Cement-Based Materials*, 5(4), pp. 199–216. Available at: <https://doi.org/10.1080/21650373.2015.1039625>.
- Abo Dhaheer, M.S. et al. (2016a) 'Proportioning of self-compacting concrete mixes based on target plastic viscosity and compressive strength: Part I - mix design procedure', *Journal of Sustainable Cement-Based Materials*, 5(4), pp. 217–232. Available at: <https://doi.org/10.1080/21650373.2015.1036952>.
- Abo Dhaheer, M.S. et al. (2016b) 'Proportioning of self-compacting concrete mixes based on target plastic viscosity and compressive strength: Part II - experimental validation', *Journal of Sustainable Cement-Based Materials*, 5(4), pp. 217–232. Available at: <https://doi.org/10.1080/21650373.2015.1036952>.
- Abo Dhaheer, M.S. et al. (2016c) 'Proportioning of self-compacting concrete mixes based on target plastic viscosity and compressive strength: Part I - mix design procedure', *Journal of Sustainable Cement-Based Materials*, 5(4), pp. 199–216. Available at: <https://doi.org/10.1080/21650373.2015.1039625>.

- Abo Dhaheer, M.S., Kulasegaram, S. and Karihaloo, B.L. (2016) ‘Simulation of self-compacting concrete flow in the J-ring test using smoothed particle hydrodynamics (SPH)’, *Cement and Concrete Research*, 89, pp. 27–34. Available at: <https://doi.org/10.1016/j.cemconres.2016.07.016>.
- Abrishambaf, A., Barros, J.A.O. and Cunha, V.M.C.F. (2013) ‘Relation between fibre distribution and post-cracking behaviour in steel fibre reinforced self-compacting concrete panels’, *Cement and Concrete Research*, 51, pp. 57–66. Available at: <https://doi.org/10.1016/j.cemconres.2013.04.009>.
- Ahmad, I. *et al.* (2021) ‘Experimental investigations on fracture parameters of random and aligned steel fiber reinforced cementitious composites’, *Construction and Building Materials*, 284. Available at: <https://doi.org/10.1016/j.conbuildmat.2021.122680>.
- Akçaoğlu, T., Tokyay, M. and Çelik, T. (2004) ‘Effect of coarse aggregate size and matrix quality on ITZ and failure behavior of concrete under uniaxial compression’, *Cement and Concrete Composites*, 26(6), pp. 633–638. Available at: [https://doi.org/10.1016/S0958-9465\(03\)00092-1](https://doi.org/10.1016/S0958-9465(03)00092-1).
- Akçay, B. and Tasdemir, M.A. (2012) ‘Mechanical behaviour and fibre dispersion of hybrid steel fibre reinforced self-compacting concrete’, *Construction and Building Materials*, 28(1), pp. 287–293. Available at: <https://doi.org/10.1016/j.conbuildmat.2011.08.044>.
- Al-Rubaye, M., Karihaloo, B.L. and Kulasegaram, S. (2017) ‘Simulation of self-compacting concrete in an L-box using smooth particle hydrodynamics’, *Magazine of Concrete Research*, 69(12), pp. 618–628. Available at: <https://doi.org/10.1680/jmacr.16.00408>.
- Alberti, M.G., Enfedaque, A. and Gálvez, J.C. (2019) ‘The effect of fibres in the rheology of self-compacting concrete’, *Construction and Building Materials*, 219, pp. 144–153. Available at: <https://doi.org/10.1016/j.conbuildmat.2019.05.173>.
- Alwesabi, E.A. *et al.* (2020) ‘Impact resistance of plain and rubberized concrete containing steel and polypropylene hybrid fiber’, *Materials Today Communications*, 25(August), p. 101640. Available at: <https://doi.org/10.1016/j.mtcomm.2020.101640>.
- Alwesabi, E.A.H. *et al.* (2020) ‘Experimental investigation on mechanical properties of plain and rubberised concretes with steel–polypropylene hybrid fibre’, *Construction and Building Materials*, 233, p. 117194. Available at: <https://doi.org/10.1016/j.conbuildmat.2019.117194>.
- Alyhya, W.S. *et al.* (2016) ‘Influence of mix composition and strength on the fracture

- properties of self-compacting concrete’, *Construction and Building Materials*, 110, pp. 312–322. Available at: <https://doi.org/10.1016/j.conbuildmat.2016.02.037>.
- Alyhya, W.S., Kulasegaram, S. and Karihaloo, B.L. (2017) ‘Simulation of the flow of self-compacting concrete in the V-funnel by SPH’, *Cement and Concrete Research*, 100(July 2016), pp. 47–59. Available at: <https://doi.org/10.1016/j.cemconres.2017.05.021>.
- Amini, Y., Emdad, H. and Farid, M. (2011) ‘A new model to solve fluidhypo-elastic solid interaction using the smoothed particle hydrodynamics (SPH) method’, *European Journal of Mechanics, B/Fluids*, 30(2), pp. 184–194. Available at: <https://doi.org/10.1016/j.euromechflu.2010.09.010>.
- Antoni, M. *et al.* (2012) ‘Cement substitution by a combination of metakaolin and limestone’, *Cement and Concrete Research*, 42(12), pp. 1579–1589. Available at: <https://doi.org/10.1016/j.cemconres.2012.09.006>.
- Ashish, D.K. (2018) ‘An overview on mixture design of self-compacting concrete’, (December 2017), pp. 371–395. Available at: <https://doi.org/10.1002/suco.201700279>.
- Ashish, D.K. and Verma, S.K. (2018) ‘An overview on mixture design of self-compacting concrete’, *Structural Concrete*, 20(1), pp. 371–395. Available at: <https://doi.org/10.1002/suco.201700279>.
- Aslani, F. and Gedeon, R. (2019) ‘Experimental investigation into the properties of self-compacting rubberised concrete incorporating polypropylene and steel fibers’, *Structural Concrete*, 20(1), pp. 267–281. Available at: <https://doi.org/10.1002/suco.201800182>.
- ASTM:C1621/C 1621M1 (2017) ‘Standard Test Method for Passing Ability of Self-Consolidating Concrete by J-Ring.’ Annual Book of ASTM Standards, pp. 1–8.
- Badogiannis, E.G. *et al.* (2015) ‘Durability of metakaolin Self-Compacting Concrete’, *Construction and Building Materials*, 82, pp. 133–141. Available at: <https://doi.org/10.1016/j.conbuildmat.2015.02.023>.
- Badry, F., Kulasegaram, S. and Karihaloo, B.L. (2016) ‘Estimation of the yield stress and distribution of large aggregates from slump flow test of self-compacting concrete mixes using smooth particle hydrodynamics simulation’, *Journal of Sustainable Cement-Based Materials*, 5(3), pp. 117–134. Available at: <https://doi.org/10.1080/21650373.2014.979266>.
- Bahrami, N. *et al.* (2020) ‘Optimum recycled concrete aggregate and micro-silica content in

- self-compacting concrete: Rheological, mechanical and microstructural properties’, *Journal of Building Engineering*, 31(September 2019), p. 101361. Available at: <https://doi.org/10.1016/j.job.2020.101361>.
- Bai, J. and Wild, S. (2002) ‘Investigation of the temperature change and heat evolution of mortar incorporating PFA and metakaolin’, *Cement and Concrete Composites*, 24(2), pp. 201–209. Available at: [https://doi.org/10.1016/S0958-9465\(01\)00042-7](https://doi.org/10.1016/S0958-9465(01)00042-7).
- Bai, J., Wild, S. and Sabir, B.B. (2002) ‘Sorptivity and strength of air-cured and water-cured PC-PFA-MK concrete and the influence of binder composition on carbonation depth’, *Cement and Concrete Research*, 32(11), pp. 1813–1821. Available at: [https://doi.org/10.1016/S0008-8846\(02\)00872-4](https://doi.org/10.1016/S0008-8846(02)00872-4).
- Bai, J., Wild, S. and Sabir, B.B. (2003) ‘Chloride ingress and strength loss in concrete with different PC-PFA-MK binder compositions exposed to synthetic seawater’, *Cement and Concrete Research*, 33(3), pp. 353–362. Available at: [https://doi.org/10.1016/S0008-8846\(02\)00961-4](https://doi.org/10.1016/S0008-8846(02)00961-4).
- Banfill, P.F.G. (2006) ‘Rheology of Fresh Cement and Concrete’, *Rheology of Fresh Cement and Concrete*, 2006, pp. 61–130. Available at: <https://doi.org/10.4324/9780203473290>.
- Banthia, N. and Dubey, A. (2000) ‘Measurement of flexural toughness of fiber-reinforced concrete using a novel technique-part 2: Performance of various composites’, *ACI Structural Journal*, 97(1), pp. 3–11. Available at: <https://doi.org/10.14359/799>.
- Bayasi, Z. and Kaiser, H. (2003) ‘Flexural Behavior of Composite Concrete Slabs Using Carbon Fiber Laminate Decks’, *ACI Materials Journal*, pp. 274–279. Available at: <https://doi.org/10.14359/12664>.
- Bažant, Z.P. and Planas, J. (1997) *Fracture and Size Effect in Concrete and Other Quasibrittle Materials*, *Fracture and Size Effect in Concrete and Other Quasibrittle Materials*. CRC press.
- Becker and Teschner (2007) ‘Weakly compressible SPH for free surface flows’, 1.
- Behfarnia, K. and Farshadfar, O. (2013) ‘The effects of pozzolanic binders and polypropylene fibers on durability of SCC to magnesium sulfate attack’, *Construction and Building Materials*, 38, pp. 64–71. Available at: <https://doi.org/10.1016/j.conbuildmat.2012.08.035>.
- Beigi, Morteza H. *et al.* (2013) ‘An experimental survey on combined effects of fibers and

nanosilica on the mechanical, rheological, and durability properties of self-compacting concrete’, *Materials and Design*, 50, pp. 1019–1029. Available at: <https://doi.org/10.1016/j.matdes.2013.03.046>.

Beigi, Morteza H *et al.* (2013) ‘An experimental survey on combined effects of fibers and nanosilica on the mechanical, rheological, and durability properties of self-compacting concrete’, *Materials and Design*, 50, pp. 1019–1029. Available at: <https://doi.org/10.1016/j.matdes.2013.03.046>.

Bencardino, F. *et al.* (2008) ‘Stress-Strain Behavior of Steel Fiber-Reinforced Concrete in Compression’, *Journal of Materials in Civil Engineering*, 20(3), pp. 255–263. Available at: [https://doi.org/10.1061/\(asce\)0899-1561\(2008\)20:3\(255\)](https://doi.org/10.1061/(asce)0899-1561(2008)20:3(255)).

Benson, S.D.P. and Karihaloo, B.L. (2005) ‘CARDIFRC® - Development and mechanical properties. Part I: Development and workability’, *Magazine of Concrete Research*, 57(6), pp. 347–352. Available at: <https://doi.org/10.1680/mac.2005.57.6.347>.

Bernasconi, A., Cosmi, F. and Hine, P.J. (2012) ‘Analysis of fibre orientation distribution in short fibre reinforced polymers: A comparison between optical and tomographic methods’, *Composites Science and Technology*, 72(16), pp. 2002–2008. Available at: <https://doi.org/10.1016/j.compscitech.2012.08.018>.

Beygi, M.H.A. *et al.* (2013) ‘The effect of water to cement ratio on fracture parameters and brittleness of self-compacting concrete’, *Materials and Design*, 50, pp. 267–276. Available at: <https://doi.org/10.1016/j.matdes.2013.02.018>.

Beygi, M.H.A., Kazemi, M.T., Vaseghi Amiri, J., *et al.* (2014) ‘Evaluation of the effect of maximum aggregate size on fracture behavior of self compacting concrete’, *Construction and Building Materials*, 55, pp. 202–211. Available at: <https://doi.org/10.1016/j.conbuildmat.2014.01.065>.

Beygi, M.H.A., Kazemi, M.T., Nikbin, I.M., *et al.* (2014) ‘The influence of coarse aggregate size and volume on the fracture behavior and brittleness of self-compacting concrete’, *Cement and Concrete Research*, 66, pp. 75–90. Available at: <https://doi.org/10.1016/j.cemconres.2014.06.008>.

Bezerra, E.M., Joaquim, A.P. and Savastano, H. (2004) ‘Some properties of fibre-cement composites with selected fibres’, *In Proceedings of the Conferencia Brasileira de Materiais e Tecnologias Não Convencionais: Habitações e Infra-Estrutura de Interesse Social Brasil-*

NOCMAT, pp. 34–43.

Bianchi, Q. (2014) *Application of nano-silica in concrete*. Available at: <https://doi.org/10.6100/IR780551>.

Bonavetti, V. *et al.* (2003) ‘Limestone filler cement in low w/c concrete: A rational use of energy’, *Cement and Concrete Research*, 33(6), pp. 865–871. Available at: [https://doi.org/10.1016/S0008-8846\(02\)01087-6](https://doi.org/10.1016/S0008-8846(02)01087-6).

Bonen, D. and Shah, S.P. (2005) ‘Fresh and hardened properties of self-consolidating concrete’, *Progress in Structural Engineering and Materials*, 7(1), pp. 14–26. Available at: <https://doi.org/10.1002/pse.186>.

Bonet, J. and Kulasegaram, S. (2000) ‘Correction and stabilization of smooth particle hydrodynamics methods with applications in metal forming simulations’, *International Journal for Numerical Methods in Engineering*, 47(6), pp. 1189–1214. Available at: [https://doi.org/10.1002/\(SICI\)1097-0207\(20000228\)47:6<1189::AID-NME830>3.0.CO;2-I](https://doi.org/10.1002/(SICI)1097-0207(20000228)47:6<1189::AID-NME830>3.0.CO;2-I).

Bonet, J. and Lok, T.S.L. (1999) ‘Variational and momentum preservation aspects of Smooth Particle Hydrodynamic formulations’, *Computer Methods in Applied Mechanics and Engineering*, 180(1–2), pp. 97–115. Available at: [https://doi.org/10.1016/S0045-7825\(99\)00051-1](https://doi.org/10.1016/S0045-7825(99)00051-1).

Boukendakdji, O., Kadri, E. and Kenai, S. (2012) ‘Cement & Concrete Composites Effects of granulated blast furnace slag and superplasticizer type on the fresh properties and compressive strength of self-compacting concrete’, *Cement and Concrete Composites*, 34(4), pp. 583–590. Available at: <https://doi.org/10.1016/j.cemconcomp.2011.08.013>.

Boulekbache, B. *et al.* (2010) ‘Flowability of fibre-reinforced concrete and its effect on the mechanical properties of the material’, *Construction and Building Materials*, 24(9), pp. 1664–1671. Available at: <https://doi.org/10.1016/j.conbuildmat.2010.02.025>.

Boulekbache, B. *et al.* (2012) ‘Influence of yield stress and compressive strength on direct shear behaviour of steel fibre-reinforced concrete’, *Construction and Building Materials*, 27(1), pp. 6–14. Available at: <https://doi.org/10.1016/j.conbuildmat.2011.07.015>.

Bouzoubaâ, N. and Lachemi, M. (2001) ‘Self-compacting concrete incorporating high volumes of class F fly ash: Preliminary results’, *Cement and Concrete Research*, 31(3), pp. 413–420. Available at: [https://doi.org/10.1016/S0008-8846\(00\)00504-4](https://doi.org/10.1016/S0008-8846(00)00504-4).

- Brandt, A.M. (2008) 'Fibre reinforced cement-based (FRC) composites after over 40 years of development in building and civil engineering', *Composite Structures*, 86(1–3), pp. 3–9. Available at: <https://doi.org/10.1016/j.compstruct.2008.03.006>.
- Brouwers, H.J.H. and Radix, H.J. (2005) 'Self-compacting concrete: Theoretical and experimental study', *Cement and Concrete Research*, 35(11), pp. 2116–2136. Available at: <https://doi.org/10.1016/j.cemconres.2005.06.002>.
- Brower, L.C.F.F. (2000) 'Workability of Self-Compacting Concrete', *International Symposium on High Performance Concrete*, pp. 398–407.
- BS EN 12350-8 (2010) 'BSI Standards Publication Testing fresh concrete'.
- BS EN 12390-13:2013 (2019) 'Testing hardened concrete , Part 13: Determination of secant modulus of elasticity in compression', *British Standard*, 3(July).
- BS EN 12390-3 (2009) 'Testing hardened concrete - Part 3:Compressive strength of test specimens', *British Standard*, 3(1), pp. 420–457.
- BS EN 12390-6 (2009) 'Testing hardened concrete - Part 6:Tensile splitting strength of test specimens', *British Standards Institution BSI*, 3(1), pp. 420–457.
- BS EN 12620:2002 +A1:2008 (2004) 'Aggregates for Concrete', *ACI Journal Proceedings*, 8(3). Available at: <https://doi.org/10.14359/16172>.
- 'BS EN 14651-2005' (no date).
- BS EN 1881-121 (1993) *Method for determination of static modulus of elasticity in compression*, London: BSI Standards Publication.
- BS EN 197-1:2000 (2007) 'Part 1: Composition, specifications and conformity criteria for common cements', *BSI*, 3.
- BS EN 197-1 (2011) 'Cemet: Composition, specifications and conformity criteria for common cements', *BSI* [Preprint].
- BS EN, 2008 (2008) '12620:2002 , Aggregates for concrete', 3(May 2004).
- BS EN 206-9:2010 (2010) 'Part 9: Additional Rules for Self- compacting Concrete (SCC)', *Bsi* [Preprint].
- BS EN 933-1:2012 (2012) 'Tests for geometrical properties of aggregates Part 1: Determination of particle size distribution — Sieving method', *British European Standard*

[Preprint].

BS EN12350-12:, 2010 (2010) ‘BSI Standards Publication Testing fresh concrete Part 12: Self-compacting concrete -- J ring test’, *BSI Standards Publication* [Preprint].

BSi (2010) ‘Concrete, Part 9: Additional Rules for Self- compacting Concrete (SCC). London: BSI’.

BSI Standards Publication (2011) ‘BSI Standards Publication Cement Part 1 : Composition , specifications and’, (November).

Btech, B.J. (2018) ‘Comparative study on self-compacting concrete reinforced with different chopped fibers’, 171.

Buratti, N., Mazzotti, C. and Savoia, M. (2011) ‘Post-cracking behaviour of steel and macro-synthetic fibre-reinforced concretes’, *Construction and Building Materials*, 25(5), pp. 2713–2722. Available at: <https://doi.org/10.1016/j.conbuildmat.2010.12.022>.

Caggiano, A. *et al.* (2016) ‘Experimental characterization of the post-cracking response in Hybrid Steel/Polypropylene Fiber-Reinforced Concrete’, *Construction and Building Materials*, 125, pp. 1035–1043. Available at: <https://doi.org/10.1016/j.conbuildmat.2016.08.068>.

Carpinteri, A. and Brighenti, R. (2010) ‘Fracture behaviour of plain and fiber-reinforced concrete with different water content under mixed mode loading’, *Materials and Design*, 31(4), pp. 2032–2042. Available at: <https://doi.org/10.1016/j.matdes.2009.10.021>.

Centonze, G. *et al.* (2016) ‘Concrete reinforced with recycled steel fibers from end of life tires: Mix-design and application’, *Key Engineering Materials*, 711, pp. 224–231. Available at: <https://doi.org/10.4028/www.scientific.net/KEM.711.224>.

Chan, K.D., Ong, K.C. and G, Tan, C.T. (2010) ‘Passing ability of SCC–improved method based on the P-Ring’, *In 35th Conference on our world in concrete and structures (OWICs), Singapore, Singapore Concrete Institute* [Preprint].

Chen, J.J., Kwan, A.K.H. and Jiang, Y. (2014) ‘Adding limestone fines as cement paste replacement to reduce water permeability and sorptivity of concrete’, *Construction and Building Materials*, 56, pp. 87–93. Available at: <https://doi.org/10.1016/j.conbuildmat.2014.01.066>.

Chidiac, S.E. and Mahmoodzadeh, F. (2009) ‘Plastic viscosity of fresh concrete - A critical

- review of predictions methods’, *Cement and Concrete Composites*, 31(8), pp. 535–544. Available at: <https://doi.org/10.1016/j.cemconcomp.2009.02.004>.
- Chui, Y.P. and Heng, P.A. (2010) ‘A meshless rheological model for blood-vessel interaction in endovascular simulation’, *Progress in Biophysics and Molecular Biology*, 103(2–3), pp. 252–261. Available at: <https://doi.org/10.1016/j.pbiomolbio.2010.09.003>.
- Cifuentes, H. and Karihaloo, B.L. (2013) ‘Determination of size-independent specific fracture energy of normal- and high-strength self-compacting concrete from wedge splitting tests’, 48, pp. 548–553. Available at: <https://doi.org/10.1016/j.conbuildmat.2013.07.062>.
- Cifuentes, H., Ríos, J.D. and Gómez, E.J. (2018) ‘Effect of mix design on the size-independent fracture energy of normal- And high-strength self-compacting concrete’, *Materiales de Construcción*, 68(329), pp. 1–11. Available at: <https://doi.org/10.3989/mc.2018.00717>.
- Colagrossi, A. and Landrini, M. (2003) ‘Numerical simulation of interfacial flows by smoothed particle hydrodynamics’, *Journal of Computational Physics*, 191(2), pp. 448–475. Available at: [https://doi.org/10.1016/S0021-9991\(03\)00324-3](https://doi.org/10.1016/S0021-9991(03)00324-3).
- Colleparidi, M. Colleparidi, S . Ogoumah Olagot, J.J. et al (2003) ‘Laboratory-tests and field-experiences of high-performance SCCs’, *In Proceedings of the Third International Symposium on “Self Compacting Concrete”*, p. Reykjavik, Iceland, (pp. 904-912).
- Corinaldesi, V. and Moriconi, G. (2004) ‘Durable fiber reinforced self-compacting concrete’, 34(December 2002), pp. 249–254. Available at: <https://doi.org/10.1016/j.cemconres.2003.07.005>.
- Corinaldesi, V., Moriconi, G. and Ash, F. (2011) ‘The role of industrial by-products in self-compacting concrete’, *Construction and Building Materials*, 25(8), pp. 3181–3186. Available at: <https://doi.org/10.1016/j.conbuildmat.2011.03.001>.
- Crofton, M. (1885) ‘in Encyclopedia Britannica’, *Probability*, pp. 768–788.
- Cruz, J.S. (2001) ‘Fracture energy of steel fibre reinforced concrete’, (1), pp. 1–24.
- Cummins, S.J. and Rudman, M. (1999) ‘An SPH Projection Method’, *Journal of Computational Physics*, 152(2), pp. 584–607. Available at: <https://doi.org/10.1006/jcph.1999.6246>.
- Cunha, V.M.C.F., Barros, J.A.O. and Sena-Cruz, J.M. (2011) ‘An integrated approach for

modelling the tensile behaviour of steel fibre reinforced self-compacting concrete', *Cement and Concrete Research*, 41(1), pp. 64–76. Available at: <https://doi.org/10.1016/j.cemconres.2010.09.007>.

Damtoft, J.S. *et al.* (2008) 'Sustainable development and climate change initiatives', *Cement and Concrete Research*, 38(2), pp. 115–127. Available at: <https://doi.org/10.1016/j.cemconres.2007.09.008>.

Deeb, R. (2013) 'Flow of Self-Compacting Flow of Self-Compacting'.

Deeb, R., Ghanbari, A. and Karihaloo, B.L. (2012a) 'Development of self-compacting high and ultra high performance concretes with and without steel fibres', *Cement and Concrete Composites*, 34(2), pp. 185–190. Available at: <https://doi.org/10.1016/j.cemconcomp.2011.11.001>.

Deeb, R., Ghanbari, A. and Karihaloo, B.L. (2012b) 'Development of self-compacting high and ultra high performance concretes with and without steel fibres', *Cement and Concrete Composites*, 34(2), pp. 185–190. Available at: <https://doi.org/10.1016/j.cemconcomp.2011.11.001>.

Deeb, R. and Karihaloo, B.L. (2013a) 'Mix proportioning of self-compacting normal and high-strength concretes', *Magazine of Concrete Research*, 65(9), pp. 546–556. Available at: <https://doi.org/10.1680/mac.12.00164>.

Deeb, R. and Karihaloo, B.L. (2013b) 'Mix proportioning of self-compacting normal and high-strength concretes', 65(9).

Deeb, R., Karihaloo, B.L. and Kulasegaram, S. (2014) 'Reorientation of short steel fibres during the flow of self-compacting concrete mix and determination of the fibre orientation factor', *Cement and Concrete Research*, 56, pp. 112–120. Available at: <https://doi.org/10.1016/j.cemconres.2013.10.002>.

Deeb, R., Kulasegaram, S. and Karihaloo, B.L. (2014a) '3D modelling of the flow of self-compacting concrete with or without steel fibres. Part I: slump flow test', *Computational Particle Mechanics*, 1(4), pp. 373–389. Available at: <https://doi.org/10.1007/s40571-014-0002-y>.

Deeb, R., Kulasegaram, S. and Karihaloo, B.L. (2014b) '3D modelling of the flow of self-compacting concrete with or without steel fibres . Part II : L-box test and the assessment of fibre reorientation during the flow', pp. 391–408. Available at:

<https://doi.org/10.1007/s40571-014-0003-x>.

Dehn, F., Holschemacher, K. and Weiße, D. (2000) ‘Self-Compacting Concrete (SCC) Time Development of the Material Properties and the Bond Behaviour’, *LACER No 5 2000*, pp. 115–124. Available at: <http://www.wilbertprecast.com/documents/scc.pdf>.

Derabla, R. and Benmalek, M.L. (2014) ‘Characterization of heat-treated self-compacting concrete containing mineral admixtures at early age and in the long term’, *Construction and Building Materials*, 66, pp. 787–794. Available at: <https://doi.org/10.1016/j.conbuildmat.2014.06.029>.

Desnerck, P. *et al.* (2016) ‘Mixture compositions and fresh properties of self- compacting concrete : analysis of 25 years of research’, *SCC 2016, 8th International RILEM Symposium on Self-Compacting Concrete, Flowing toward Sustainability*, pp. 1–10.

Dhaheer, M.S.A., Alyhya, W.S. and Karihaloo, B.L. (2016a) ‘Proportioning of self-compacting concrete mixes based on target plastic viscosity and compressive strength : Part II - experimental validation’, 0373. Available at: <https://doi.org/10.1080/21650373.2015.1036952>.

Dhaheer, M.S.A., Alyhya, W.S. and Karihaloo, B.L. (2016b) ‘Proportioning of self – compacting concrete mixes based on target plastic viscosity and compressive strength : Part I - mix design procedure’, *Journal of Sustainable Cement-Based Materials*, 0373(May 2015), pp. 1–18. Available at: <https://doi.org/10.1080/21650373.2015.1039625>.

Dinakar, P., Sethy, K.P. and Sahoo, U.C. (2013) ‘Design of self-compacting concrete with ground granulated blast furnace slag’, *Materials and Design*, 43, pp. 161–169. Available at: <https://doi.org/10.1016/j.matdes.2012.06.049>.

Ding, J.T. and Li, Z. (2002) ‘Effects of metakaolin and silica fume on properties of concrete’, *ACI Materials Journal*, 99(4), pp. 393–398.

Ding, X. *et al.* (2018a) ‘Effects of different deformed steel-fibers on preparation and fundamental properties of self-compacting SFRC’, *Construction and Building Materials*, 168, pp. 471–481. Available at: <https://doi.org/10.1016/j.conbuildmat.2018.02.162>.

Ding, X. *et al.* (2018b) ‘Effects of different deformed steel-fibers on preparation and fundamental properties of self-compacting SFRC’, *Construction and Building Materials*, 168, pp. 471–481. Available at: <https://doi.org/10.1016/j.conbuildmat.2018.02.162>.

- Domone, P.L. (2003) ‘Fresh concrete’, *Advanced Concrete Technology*, pp. 3–29. Available at: <https://doi.org/10.1016/B978-075065686-3/50248-2>.
- Domone, P.L. (2006) ‘Self-compacting concrete: An analysis of 11 years of case studies’, *Cement and Concrete Composites*, 28(2), pp. 197–208. Available at: <https://doi.org/10.1016/j.cemconcomp.2005.10.003>.
- Domone, P.L. (2007) ‘A review of the hardened mechanical properties of self-compacting concrete’, *Cement and Concrete Composites*, 29(1), pp. 1–12. Available at: <https://doi.org/10.1016/j.cemconcomp.2006.07.010>.
- Dransfield, J. (2003) ‘Admixtures for concrete, mortar and grout’, In: Newman J, Choo BS, editors. *Advanced Concrete Technology*, 2(Elsevier; 2003 [chapter 4]).
- Dransfield J (1967) ‘Advanced Concrete Technology’, *Angewandte Chemie International Edition*, 6(11), 951–952. [Preprint].
- Dufour, F. and Pijaudier-Cabot, G. (2005) ‘Numerical modelling of concrete flow: Homogenous approach’, *International Journal for Numerical and Analytical Methods in Geomechanics*, 29(4), pp. 395–416. Available at: <https://doi.org/10.1002/nag.419>.
- EFNARC (2005) ‘The European guidelines for self-compacting concrete—specification, production and use.’, *The European Guidelines for Self Compacting Concrete* [Preprint], (May).
- El-Dieb, A.S. and Reda Taha, M.M. (2012) ‘Flow characteristics and acceptance criteria of fiber-reinforced self-compacted concrete (FR-SCC)’, *Construction and Building Materials*, 27(1), pp. 585–596. Available at: <https://doi.org/10.1016/j.conbuildmat.2011.07.004>.
- El-dieb, A.S. and Taha, M.M.R. (2012) ‘Flow characteristics and acceptance criteria of fiber-reinforced self- compacted concrete (FR-SCC) Flow characteristics and acceptance criteria of fiber-reinforced self-compacted concrete (FR-SCC)’, *Construction and Building Materials*, 27(1), pp. 585–596. Available at: <https://doi.org/10.1016/j.conbuildmat.2011.07.004>.
- Elgalhud, A.A., Dhir, R.K. and Ghataora, G. (2018) ‘Chloride ingress in concrete: Limestone addition effects’, *Magazine of Concrete Research*, 70(6), pp. 292–313. Available at: <https://doi.org/10.1680/jmacr.17.00177>.
- Elgalhud, A.A., Dhir, R.K. and Ghataora, G.S. (2017) ‘Carbonation resistance of concrete:

- Limestone addition effect', *Magazine of Concrete Research*, 69(2), pp. 84–106. Available at: <https://doi.org/10.1680/jmacr.16.00371>.
- EN BS 206-9 (2010) 'Additional Rules for Self- compacting Concrete (SCC).', *BSI Standards Publication* [Preprint].
- Ezeldin, B.A.S., Member, A. and Balaguru, P.N. (1993) 'Normal- and high - strength fiber-reinforced concrete under compression', 4(170), pp. 415–429.
- Felekoglu, B. (2007) 'Utilisation of high volumes of limestone quarry wastes in concrete industry (self-compacting concrete case)', *Resources, Conservation and Recycling*, 51(4), pp. 770–791. Available at: <https://doi.org/10.1016/j.resconrec.2006.12.004>.
- Felekoğlu, B., Türkel, S. and Baradan, B. (2007) 'Effect of water/cement ratio on the fresh and hardened properties of self-compacting concrete', *Building and Environment*, 42(4), pp. 1795–1802. Available at: <https://doi.org/10.1016/j.buildenv.2006.01.012>.
- Fernandes, V. *et al.* (2005) 'Evaluation of mixing and application process parameters of single-coat mortars', *Cement and Concrete Research*, 35(5), pp. 836–841. Available at: <https://doi.org/10.1016/j.cemconres.2004.10.026>.
- Ferreira, J.P.J.G. and Branco, F.A.B. (2007) 'The use of glass fiber-reinforced concrete as a structural material', *Experimental Techniques*, 31(3), pp. 64–73. Available at: <https://doi.org/10.1111/j.1747-1567.2007.00153.x>.
- Figueiras, H. *et al.* (2014) 'Linking fresh and durability properties of paste to SCC mortar', *Cement and Concrete Composites*, 45, pp. 209–226. Available at: <https://doi.org/10.1016/j.cemconcomp.2013.09.020>.
- De Figueiredo, A.D. and Ceccato, M.R. (2015) 'Workability analysis of steel fiber reinforced concrete using slump and ve-be test', *Materials Research*, 18(6), pp. 1284–1290. Available at: <https://doi.org/10.1590/1516-1439.022915>.
- Flatt, R.J. (2004) 'Towards a prediction of superplasticized concrete rheology', *Materials and Structures*, 37(5), pp. 289–300. Available at: <https://doi.org/10.1007/bf02481674>.
- Forgeron, D. and Omer, A. (2010) 'Flow Characteristics of Macro-Synthetic Fiber-Reinforced Self-Consolidating Concrete'.
- G.Murali *et al.* (2012) 'Experimental Investigation on Fibre Reinforced Concrete using Waste Materials', *International Journal of Engineering Trends and Technology*, 34(3), pp. 100–105.

Available at: <https://doi.org/10.14445/22315381/ijett-v34p221>.

G.V.Guinea, J. Planas, M.E. (1992) ‘Measurement of the fracture energy using three-point bend tests: part 1—influence of experimental procedures’, *Mater. Struct.* 25, 25, pp. 212–218.

Gali, S., Sharma, D. and Subramaniam, K.V.L. (2018) ‘Influence of Steel Fibers on Fracture Energy and Shear Behavior of SCC’, *Journal of Materials in Civil Engineering*, 30(11). Available at: [https://doi.org/10.1061/\(asce\)mt.1943-5533.0002496](https://doi.org/10.1061/(asce)mt.1943-5533.0002496).

GÁLVEZ, V.S. (2015) *MECHANICAL BEHAVIOUR OF LAMINATED FUNCTIONALLY GRADED FIBRE-REINFORCED SELF-COMPACTING CEMENTITIOUS COMPOSITES*.

Gesoğlu, Mehmet Güneyisi, Erhan Kocabağ, M.E. (2012) ‘Fresh and hardened characteristics of self compacting concretes made with combined use of marble powder, limestone filler, and fly ash’, *Construction and Building Materials*, 37, pp. 160–170. Available at: <https://doi.org/10.1016/j.conbuildmat.2012.07.092>.

Gesoğlu, M., Güneyisi, E. and Özbay, E. (2009) ‘Properties of self-compacting concretes made with binary, ternary, and quaternary cementitious blends of fly ash, blast furnace slag, and silica fume’, *Construction and Building Materials*, 23(5), pp. 1847–1854. Available at: <https://doi.org/10.1016/j.conbuildmat.2008.09.015>.

Gesoğlu, M. and Özbay, E. (2007) ‘Effects of mineral admixtures on fresh and hardened properties of self-compacting concretes: Binary, ternary and quaternary systems’, *Materials and Structures/Materiaux et Constructions*, 40(9), pp. 923–937. Available at: <https://doi.org/10.1617/s11527-007-9242-0>.

Ghalehnovi, M. *et al.* (2019) ‘Effect of red mud (bauxite residue) as cement replacement on the properties of self-compacting concrete incorporating various fillers’, *Journal of Cleaner Production*, 240, p. 118213. Available at: <https://doi.org/10.1016/j.jclepro.2019.118213>.

Ghanbari, A. (2011) ‘High and Ultra High Performance’.

Ghanbari, A. and Karihaloo, B.L. (2009) ‘Prediction of the plastic viscosity of self-compacting steel fibre reinforced concrete’, *Cement and Concrete Research*, 39(12), pp. 1209–1216. Available at: <https://doi.org/10.1016/j.cemconres.2009.08.018>.

Ghanem, H. and Obeid, Y. (2015) ‘THE EFFECT OF STEEL FIBERS ON THE RHYOLOGICAL AND MECHANICAL PROPERTIES OF SELF COMPACTING’, 11(21), pp. 85–98.

- Ghasemi, M., Ghasemi, M.R. and Mousavi, S.R. (2018a) 'Investigating the effects of maximum aggregate size on self-compacting steel fiber reinforced concrete fracture parameters', *Construction and Building Materials*, 162, pp. 674–682. Available at: <https://doi.org/10.1016/j.conbuildmat.2017.11.141>.
- Ghasemi, M., Ghasemi, M.R. and Mousavi, S.R. (2018b) 'Investigating the effects of maximum aggregate size on self-compacting steel fiber reinforced concrete fracture parameters', *Construction and Building Materials*, 162, pp. 674–682. Available at: <https://doi.org/10.1016/j.conbuildmat.2017.11.141>.
- Giaccio, G., Tobes, J.M. and Zerbino, R. (2008) 'Use of small beams to obtain design parameters of fibre reinforced concrete', *Cement and Concrete Composites*, 30(4), pp. 297–306. Available at: <https://doi.org/10.1016/j.cemconcomp.2007.10.004>.
- Gingold and Monaghan (1977) 'Smooth particle hydrodynamics: theory and application to non-spherical stars', (*Mon. Not. R. Astron. Soc.* 181: 375).
- Girish, S., Ranganath, R. V. and Vengala, J. (2010) 'Influence of powder and paste on flow properties of SCC', *Construction and Building Materials*, 24(12), pp. 2481–2488. Available at: <https://doi.org/10.1016/j.conbuildmat.2010.06.008>.
- Glinicki, M.A. (2010) 'Beton ze zbrojeniem strukturalnym', *XXV Ogólnopolskie Warsztaty Pracy Projektanta Konstrukcji*, pp. 279–308.
- Gokulnath, V., Ramesh, B. and Raghuraman, R. (2019) 'Materials Today : Proceedings Study on the effect of M-sand in self compacting concrete with addition of steel fibers', *Materials Today: Proceedings* [Preprint], (xxxx). Available at: <https://doi.org/10.1016/j.matpr.2019.11.029>.
- González, D.C. *et al.* (2018) 'Study of the effect of the fibers' orientation on the post-cracking behavior of steel fiber reinforced concrete from wedge-splitting tests and computed tomography scanning', *Construction and Building Materials*, 192, pp. 110–122. Available at: <https://doi.org/10.1016/j.conbuildmat.2018.10.104>.
- Goodier, C.I. and Repository, I. (2003) 'Development of self-compacting concrete', *Proceedings of the ICE- Structures and Buildings*, 156(4), pp. 405–414.
- Grunewald, S. (2004) *Performance-based design of self-compacting fibre reinforced concrete, Technology*. Available at: <http://repository.tudelft.nl/view/ir/uuid:07a817aa-cba1-4c93-bbed-40a5645cf0f1/>.

- Grünewald, S. and Walraven, J.C. (2001) 'Parameter-study on the influence of steel fibers and coarse aggregate content on the fresh properties of self-compacting concrete', *Cement and Concrete Research*, 31(12), pp. 1793–1798. Available at: [https://doi.org/10.1016/S0008-8846\(01\)00555-5](https://doi.org/10.1016/S0008-8846(01)00555-5).
- Grünewald, S. and Walraven, J.C. (2020) *Properties of fibre reinforced SCC, Self-Compacting Concrete: Materials, Properties and Applications*. Available at: <https://doi.org/10.1016/b978-0-12-817369-5.00012-x>.
- Gueciouer, D., Youcef, G. and Tarek, N. (2019) 'Rheological and mechanical optimization of a steel fiber reinforced self-compacting concrete using the design of experiments method', *European Journal of Environmental and Civil Engineering*, 0(0), pp. 1–21. Available at: <https://doi.org/10.1080/19648189.2019.1697758>.
- Guinea, G. V., Planas, J. and Elices, M. (1992) 'Measurement of the fracture energy using three-point bend tests: Part 1-Influence of experimental procedures', *Materials and Structures*, 25(4), pp. 212–218. Available at: <https://doi.org/10.1007/BF02473065>.
- Güneyisi, E. (2010) 'Fresh properties of self-compacting rubberized concrete incorporated with fly ash', *Materials and Structures/Materiaux et Constructions*, 43(8), pp. 1037–1048. Available at: <https://doi.org/10.1617/s11527-009-9564-1>.
- Guo, H. *et al.* (2019) 'Effect of steel and polypropylene fibers on the quasi-static and dynamic splitting tensile properties of high-strength concrete', *Construction and Building Materials*, 224, pp. 504–514. Available at: <https://doi.org/10.1016/j.conbuildmat.2019.07.096>.
- H. Solomon (1978) 'Geometric probability', *Society for industrial and applied mathematics.*, 20(4), pp. 11–16. Available at: <https://doi.org/10.1007/BF03025223>.
- Han, B. and Zhang, L. (2017) *B. Han, L. Zhang, and J. Ou, Smart and Multifunctional Concrete Towards Sustainable Infrastructures, 2017: Springer Singapore*.
- Hazrina, A. *et al.* (2018) 'Effects of Steel Fibre Addition on the Mechanical Properties of Steel Fibre Reinforced Self-Compacting Concrete (Sccfibre)', *IOP Conference Series: Materials Science and Engineering*, 431(4). Available at: <https://doi.org/10.1088/1757-899X/431/4/042004>.
- Heirman, G. *et al.* (2008) 'Integration approach of the Couette inverse problem of powder type self-compacting concrete in a wide-gap concentric cylinder rheometer', *Journal of Non-*

- Newtonian Fluid Mechanics*, 150(2–3), pp. 93–103. Available at: <https://doi.org/10.1016/j.jnnfm.2007.10.003>.
- Ho, D. W.S., Shein, A. M.M., Ng, C.C. e. al. (2002) ‘The use of quarry dust for SCC applications’, *Cement and Concrete Research*, 32(4), pp. 505–511. Available at: [https://doi.org/10.1016/S0008-8846\(01\)00726-8](https://doi.org/10.1016/S0008-8846(01)00726-8).
- Hodges, P.W. and Richardson, C.A. (1996) ‘No Title список литературы’, *Spine (Phila Pa 1976)*, 21(6), pp. 2640–50. Available at: http://repository.upi.edu/1360/1/s_d5451_0604180_chapter1.pdf.
- Holschmacher, K. and Klug, Y. (2002) ‘A Database for the Evaluation of Hardened Properties of SCC .’, *Lacer*, 7, pp. 123–134.
- Hosseinpoor, M. (2016) ‘Numerical Simulation of Fresh Scc Flow in Wall and Beam Elements Using Flow’.
- Hu, X. and Wittmann, F. (2000) ‘Size effect on toughness induced by crack close to free surface’, *Engineering Fracture Mechanics*, 65(2–3), pp. 209–221. Available at: [https://doi.org/10.1016/s0013-7944\(99\)00123-x](https://doi.org/10.1016/s0013-7944(99)00123-x).
- Huang, H., Gao, X. and Zhang, A. (2019) ‘Numerical simulation and visualization of motion and orientation of steel fibers in UHPC under controlling flow condition’, *Construction and Building Materials*, 199, pp. 624–636. Available at: <https://doi.org/10.1016/j.conbuildmat.2018.12.055>.
- Jiao, D. Shi, C. Yuan, Q. et al. (2017) ‘Effect of constituents on rheological properties of fresh concrete-A review’, *Cement and Concrete Composites*, 83, pp. 146–159. Available at: <https://doi.org/10.1016/j.cemconcomp.2017.07.016>.
- Jo, B.W. and Tae, G.H. (2001) ‘Experimental study on fracture energy of low-heat concrete by three-point bend tets’, *Russian Journal of Nondestructive Testing*, 37(12), pp. 907–915. Available at: <https://doi.org/10.1023/A:1016829820077>.
- John, N. and Choo, B.S. (2013) ‘Advanced Concrete Technology’, *Journal of Chemical Information and Modeling*, 53(9), pp. 1689–1699. Available at: <https://doi.org/10.1017/CBO9781107415324.004>.
- Johnson, G.R., Stryk, R.A. and Beissel, S.R. (1996) ‘SPH for high velocity impact computations’, *Computer Methods in Applied Mechanics and Engineering*, 139(1–4), pp.

347–373. Available at: [https://doi.org/10.1016/S0045-7825\(96\)01089-4](https://doi.org/10.1016/S0045-7825(96)01089-4).

Johnston, C.D. (1996) ‘Proportioning, Mixing and Placement of Fibre-Reinforced Cements and Concretes’, *Production Methods and Workability of Concrete*, p. 26. Available at: <https://doi.org/10.1201/9781482271782-24>.

Karihaloo, B.L. (1995) *Fracture mechanics and structural concrete*. Addison Wesley Longman, UK.

Karihaloo, B.L., Abdalla, H.M. and Imjai, T. (2003) ‘A simple method for determining the true specific fracture energy of concrete’, *Magazine of Concrete Research*, 55(5), pp. 471–481. Available at: <https://doi.org/10.1680/mac.2003.55.5.471>.

Karihaloo, B.L. and Ghanbari, A. (2012a) ‘Mix proportioning of self- compacting high- and ultra- high-performance concretes with and without steel fibres’, 64(12).

Karihaloo, B.L. and Ghanbari, A. (2012b) ‘Mix proportioning of selfcompacting high-and ultrahigh-performance concretes with and without steel fibres’, *Magazine of Concrete Research*, 64(12), pp. 1089–1100. Available at: <https://doi.org/10.1680/mac.11.00190>.

Katzer, J. and Domski, J. (2012) ‘Quality and mechanical properties of engineered steel fibres used as reinforcement for concrete’, *Construction and Building Materials*, 34, pp. 243–248. Available at: <https://doi.org/10.1016/j.conbuildmat.2012.02.058>.

Khaloo, A. *et al.* (2014) ‘Mechanical performance of self-compacting concrete reinforced with steel fibers’, *Construction and Building Materials*, 51, pp. 179–186. Available at: <https://doi.org/10.1016/j.conbuildmat.2013.10.054>.

Khayat, K.H. (2000) ‘Optimization and performance of air-entrained, self-consolidating concrete’, *ACI Structural Journal*, 97(5), pp. 526–535. Available at: <https://doi.org/10.14359/9285>.

Khayat, K.H. (2015) ‘Workability , Testing , and Performance of Self-Consolidating’, (May 1999).

Khayat, K.H., Kassimi, F. and Ghoddousi, P. (2014) ‘Mixture design and testing of fiber-reinforced self-consolidating concrete’, *ACI Materials Journal*, 111(2), pp. 143–152. Available at: <https://doi.org/10.14359/51686722>.

Khayat, K.H. and Roussel, Y. (2000) ‘Testing and performance of fiber-reinforced , self-consolidating concrete’, 33(July), pp. 391–397.

- Köksal, F. *et al.* (2013) ‘Fracture energy-based optimisation of steel fibre reinforced concretes’, *Engineering Fracture Mechanics*, 107, pp. 29–37. Available at: <https://doi.org/10.1016/j.engfracmech.2013.04.018>.
- Kovler, K. and Roussel, N. (2011) ‘Properties of fresh and hardened concrete’, *Cement and Concrete Research*, 41(7), pp. 775–792. Available at: <https://doi.org/10.1016/j.cemconres.2011.03.009>.
- Krieger, D. (1959) ‘A mechanism for Non-Newtonian flow in suspensions of rigid spheres.pdf’, p. ;3:137–152.
- Kristiawan, S.A. and Tyas, G.P. (2017) ‘Statistical and Detailed Analysis on Fiber Reinforced Self-Compacting Concrete Containing Admixtures- A State of Art of Review Statistical and Detailed Analysis on Fiber Reinforced Self- Compacting Concrete Containing Admixtures - A State of Art of Review’. Available at: <https://doi.org/10.1088/1757-899X/263/3/032037>.
- De Kruif, C.G. *et al.* (1985) ‘Hard sphere colloidal dispersions: Viscosity as a function of shear rate and volume fraction’, *The Journal of Chemical Physics*, 83(9), pp. 4717–4725. Available at: <https://doi.org/10.1063/1.448997>.
- Kulasegaram, S. *et al.* (2004) ‘A variational formulation based contact algorithm for rigid boundaries in two-dimensional SPH applications’, *Computational Mechanics*, 33(4), pp. 316–325. Available at: <https://doi.org/10.1007/s00466-003-0534-0>.
- Kulasegaram, S. and Karihaloo, B.L. (2013) ‘Fibre-reinforced, self-compacting concrete flow modelled by smooth particle hydrodynamics’, 166.
- Kulasegaram, S., Karihaloo, B.L. and Ghanbari, A. (2011) ‘Modelling the flow of self-compacting concrete’, *INTERNATIONAL JOURNAL FOR NUMERICAL AND ANALYTICAL METHODS IN GEOMECHANICS Int. J. Numer. Anal. Meth. Geomech.*, 35(April 2010), pp. 713–723. Available at: <https://doi.org/10.1002/nag>.
- Kulasegaram, S., Karihaloo*, B.L. and Ghanbari., A. (2010) ‘Modelling the flow of self-compacting concrete’, *International Journal for Numerical and Analytical Methods in Geomechanics*, 30(13), pp. 1303–1336. Available at: <https://doi.org/10.1002/nag>.
- Kwan, A.K.H. and Ng, I.Y.T. (2010) ‘Improving performance and robustness of SCC by adding supplementary cementitious materials’, *Construction and Building Materials*, 24(11), pp. 2260–2266. Available at: <https://doi.org/10.1016/j.conbuildmat.2010.04.030>.

- de la Rosa, Á. *et al.* (2018a) ‘Proportioning of self-compacting steel-fiber reinforced concrete mixes based on target plastic viscosity and compressive strength: Mix-design procedure & experimental validation’, *Construction and Building Materials*, 189, pp. 409–419. Available at: <https://doi.org/10.1016/j.conbuildmat.2018.09.006>.
- de la Rosa, Á. *et al.* (2018b) ‘Proportioning of self-compacting steel-fiber reinforced concrete mixes based on target plastic viscosity and compressive strength: Mix-design procedure & experimental validation’, *Construction and Building Materials*, 189, pp. 409–419. Available at: <https://doi.org/10.1016/j.conbuildmat.2018.09.006>.
- Lanier, M. *et al.* (2003) ‘Interim guidelines for the use of self-consolidating concrete in PCI member plants’, *PCI Journal*, 48(3), pp. 14–18.
- Lashkarbolouk, H. *et al.* (2013) ‘Viscosity evaluation of SCC based on flowsimulation in the L-box test’, *Magazine of Concrete Research*, 65(6), pp. 365–376. Available at: <https://doi.org/10.1680/mac.12.00115>.
- Lashkarbolouk, H., Halabian, A.M. and Chamani, M.R. (2014) ‘Simulation of concrete flow in V-funnel test and the proper range of viscosity and yield stress for SCC’, *Materials and Structures/Materiaux et Constructions*, 47(10), pp. 1729–1743. Available at: <https://doi.org/10.1617/s11527-013-0147-9>.
- Le, H.T. *et al.* (2015) ‘The mix design for self-compacting high performance concrete containing various mineral admixtures’, *Materials and Design*, 72, pp. 51–62. Available at: <https://doi.org/10.1016/j.matdes.2015.01.006>.
- Lee, E.S. *et al.* (2008) ‘Comparisons of weakly compressible and truly incompressible algorithms for the SPH mesh free particle method’, *Journal of Computational Physics*, 227(18), pp. 8417–8436. Available at: <https://doi.org/10.1016/j.jcp.2008.06.005>.
- Lee, Y.H. *et al.* (2002) ‘Characterization of fiber orientation in short fiber reinforced composites with an image processing technique’, *Materials Research Innovations*, 6(2), pp. 65–72. Available at: <https://doi.org/10.1007/s10019-002-0180-8>.
- Li, B. *et al.* (2018) ‘Effects of fiber type, volume fraction and aspect ratio on the flexural and acoustic emission behaviors of steel fiber reinforced concrete’, *Construction and Building Materials*, 181, pp. 474–486. Available at: <https://doi.org/10.1016/j.conbuildmat.2018.06.065>.
- Li, L.G. and Kwan, A.K.H. (2011) ‘Mortar design based on water film thickness’,

- Construction and Building Materials*, 25(5), pp. 2381–2390. Available at: <https://doi.org/10.1016/j.conbuildmat.2010.11.038>.
- Li, L.G. and Kwan, A.K.H. (2015) ‘Adding limestone fines as cementitious paste replacement to improve tensile strength, stiffness and durability of concrete’, *Cement and Concrete Composites*, 60, pp. 17–24. Available at: <https://doi.org/10.1016/j.cemconcomp.2015.02.006>.
- Liao, W.C. *et al.* (2006) ‘Self-Consolidating High Performance Fiber Reinforced Concrete: SCHPFRC’, *High Performance Fiber ...*, (December), p. 76. Available at: [http://wweb.uta.edu/faculty/schao/download/Conference Papers/Liao-et-al-HPFRCC5-c-web.pdf](http://wweb.uta.edu/faculty/schao/download/Conference%20Papers/Liao-et-al-HPFRCC5-c-web.pdf).
- Liu, M. (2010) ‘Self-compacting concrete with different levels of pulverized fuel ash’, *Construction and Building Materials*, 24(7), pp. 1245–1252. Available at: <https://doi.org/10.1016/j.conbuildmat.2009.12.012>.
- Long, G., Gao, Y. and Xie, Y. (2015) ‘Designing more sustainable and greener self-compacting concrete’, *Construction and Building Materials*, 84, pp. 301–306. Available at: <https://doi.org/10.1016/j.conbuildmat.2015.02.072>.
- Lucy, L.B. (1977) ‘A numerical approach to the testing of the fission hypothesis’, *The Astronomical Journal*, 82(12), pp. 1013–1024.
- Majain, N. *et al.* (2019) ‘Effect of steel fibers on self-compacting concrete slump flow and compressive strength’, *IOP Conference Series: Materials Science and Engineering*, 513(1). Available at: <https://doi.org/10.1088/1757-899X/513/1/012007>.
- Martinie, L., Rossi, P. and Roussel, N. (2010) ‘Rheology of fiber reinforced cementitious materials: classification and prediction’, *Cement and Concrete Research*, 40(2), pp. 226–234. Available at: <https://doi.org/10.1016/j.cemconres.2009.08.032>.
- Martinie, L. and Roussel, N. (2011) ‘Simple tools for fiber orientation prediction in industrial practice’, *Cement and Concrete Research*, 41(10), pp. 993–1000. Available at: <https://doi.org/10.1016/j.cemconres.2011.05.008>.
- Mašin, D. *et al.* (2006) ‘Directional response of a reconstituted fine-grained soil - Part II: Performance of different constitutive models’, *International Journal for Numerical and Analytical Methods in Geomechanics*, 30(13), pp. 1303–1336. Available at: <https://doi.org/10.1002/nag>.

- Mazaheripour, H. *et al.* (2011) 'The effect of polypropylene fibers on the properties of fresh and hardened lightweight self-compacting concrete', *Construction and Building Materials*, 25(1), pp. 351–358. Available at: <https://doi.org/10.1016/j.conbuildmat.2010.06.018>.
- Mechtcherine, V. *et al.* (2014) 'Simulation of fresh concrete flow using Discrete Element Method (DEM): Theory and applications', *Materials and Structures/Materiaux et Constructions*, 47(4), pp. 615–630. Available at: <https://doi.org/10.1617/s11527-013-0084-7>.
- Mihashi, H., Nomura, N. and Niiseki, S. (1991) 'Influence of aggregate size on fracture process zone of concrete detected with three dimensional acoustic emission technique', *Cement and Concrete Research*, 21(5), pp. 737–744. Available at: [https://doi.org/10.1016/0008-8846\(91\)90168-H](https://doi.org/10.1016/0008-8846(91)90168-H).
- Mo, K.H. *et al.* (2014) 'The effect of steel fibres on the enhancement of flexural and compressive toughness and fracture characteristics of oil palm shell concrete', *Construction and Building Materials*, 55, pp. 20–28. Available at: <https://doi.org/10.1016/j.conbuildmat.2013.12.103>.
- Mobasher, B., Stang, H., & Shah, S.P. (1990) '(Communicated by A.J. Majumdar) (Received Jan. 12, 1990)', *Cement and Concrete Research*, 20(5), pp. 665–676.
- Mohamed, R.N. *et al.* (2019) 'Steel fibre self-compacting concrete under biaxial loading', *Construction and Building Materials*, 224, pp. 255–265. Available at: <https://doi.org/10.1016/j.conbuildmat.2019.07.076>.
- Monaghan, J.J. (1994) 'Simulating Free Surface Flow with SPH', *Journal of Computational Physics*, pp. 399–406.
- Mousavi, S.M., Ranjbar, M.M. and Madandoust, R. (2019) 'Combined effects of steel fibers and water to cementitious materials ratio on the fracture behavior and brittleness of high strength concrete', *Engineering Fracture Mechanics*, 216(May), p. 106517. Available at: <https://doi.org/10.1016/j.engfracmech.2019.106517>.
- Naaman, A.E. (2009) 'High Performance Fiber Reinforced Cement Composites: Classification and Applications', *CBM-CI International Workshop, Karachi, Pakistan*, 1(1), pp. 389–401.
- Nataraja, M.C., Dhang, N. and Gupta, A.P. (2000) 'Toughness characterization of steel fiber-reinforced concrete by JSCE approach', *Cement and Concrete Research*, 30(4), pp. 593–597. Available at: [https://doi.org/10.1016/S0008-8846\(00\)00212-X](https://doi.org/10.1016/S0008-8846(00)00212-X).

- Nehdi, M., Mindess, S. and Aïtcin, P.-C. (2012) ‘Statistical modelling of the microfiller effect on the rheology of composite cement pastes’, *Advances in Cement Research*, 9(33), pp. 37–46. Available at: <https://doi.org/10.1680/adcr.1997.9.33.37>.
- Nehdi, M. and Rahman, M.A. (2004) ‘Estimating rheological properties of cement pastes using various rheological models for different test geometry, gap and surface friction’, *Cement and Concrete Research*, 34(11), pp. 1993–2007. Available at: <https://doi.org/10.1016/j.cemconres.2004.02.020>.
- Nepomuceno, M., Oliveira, L. and Lopes, S.M.R. (2012) ‘Methodology for mix design of the mortar phase of self-compacting concrete using different mineral additions in binary blends of powders’, *Construction and Building Materials*, 26(1), pp. 317–326. Available at: <https://doi.org/10.1016/j.conbuildmat.2011.06.027>.
- Neville, A.M. (1995) *Properties of Concrete*. 4th ed. UK: Longman Scientific Group Ltd.
- Nikbin, I.M. *et al.* (2014) ‘A comprehensive investigation into the effect of aging and coarse aggregate size and volume on mechanical properties of self-compacting concrete’, *Materials and Design*, 59, pp. 199–210. Available at: <https://doi.org/10.1016/j.matdes.2014.02.054>.
- Nitesh, K.J.N.S., Rao, S.V. and Kumar, P.R. (2019) ‘An experimental investigation on torsional behaviour of recycled aggregate based steel fiber reinforced self compacting concrete’, *Journal of Building Engineering*, 22(June 2018), pp. 242–251. Available at: <https://doi.org/10.1016/j.jobe.2018.12.011>.
- Noaman, A.T. *et al.* (2017) ‘Fracture characteristics of plain and steel fibre reinforced rubberized concrete’, *Construction and Building Materials*, 152, pp. 414–423. Available at: <https://doi.org/10.1016/j.conbuildmat.2017.06.127>.
- Okamura, H. and Ouchi, K. (1996) ‘Self-compacting high performance concrete’, *Structural Engineering International: Journal of the International Association for Bridge and Structural Engineering (IABSE)*, 6(4), pp. 269–270. Available at: <https://doi.org/10.2749/101686696780496292>.
- Okamura, H. and Ouchi, M. (2003) ‘Self-Compacting Concrete’, *Journal of Advanced Concrete Technology*, 1(1), pp. 5–15. Available at: <https://doi.org/10.3151/jact.1.5>.
- Okamura and Ouchi (2003) ‘Self Compacting Concrete - research paper’, *Journal of Advanced Concrete Technology*, pp. 5–15.

- Okeh, C.A.O. *et al.* (2019) 'Behaviour of hybrid steel fibre reinforced self compacting concrete using innovative hooked-end steel fibres under tensile stress', *Construction and Building Materials*, 202, pp. 753–761. Available at: <https://doi.org/10.1016/j.conbuildmat.2018.12.067>.
- Omran, A. and Khayat, K. (2016) 'Models to predict form pressure exerted by SCC – results of six field campaigns', *In: 8th International RILEM Symposium on Self-Compacting Concrete*, (Washington DC, USA), pp. 599–612. Available at: <https://doi.org/10.1617/2912143624.005>.
- Ozyurt, N., Mason, T.O. and Shah, S.P. (2007) 'Correlation of fiber dispersion, rheology and mechanical performance of FRCs', *Cement and Concrete Composites*, 29(2), pp. 70–79. Available at: <https://doi.org/10.1016/j.cemconcomp.2006.08.006>.
- Painuly, P. and Uniyal, I. (2016) 'LITERATURE REVIEW ON SELF-COMPACTING', 4(2), pp. 178–180.
- Paja, M. and Ponikiewski, T. (2013) 'Flexural behavior of self-compacting concrete reinforced with different types of steel fibers', 47, pp. 397–408. Available at: <https://doi.org/10.1016/j.conbuildmat.2013.05.072>.
- Pajak, M. and Ponikiewski, T. (2013) 'Flexural behavior of self-compacting concrete reinforced with different types of steel fibers', *Construction and Building Materials*, 47, pp. 397–408. Available at: <https://doi.org/10.1016/j.conbuildmat.2013.05.072>.
- Papanastasiou, T. (1987) 'Flows of Materials with Yield', *Journal of Rheology*, 31(5), pp. 385–404. Available at: <https://doi.org/10.1122/1.549926>.
- Parra, C., Valcuende, M. and Gómez, F. (2011) 'Splitting tensile strength and modulus of elasticity of self-compacting concrete', *Construction and Building Materials*, 25(1), pp. 201–207. Available at: <https://doi.org/10.1016/j.conbuildmat.2010.06.037>.
- PD 6682-1:2009+A1:2013 (2013) 'BS EN 12620', *Part 1: Aggregates for concrete – Guidance on the use of BS EN 12620* [Preprint].
- Persson, B. (2001) 'A comparison between mechanical properties of self-compacting concrete and the corresponding properties of normal concrete', *Cement and Concrete Research*, 31(2), pp. 193–198. Available at: [https://doi.org/10.1016/S0008-8846\(00\)00497-X](https://doi.org/10.1016/S0008-8846(00)00497-X).
- Ponikiewski, T. and Go, J. (2014) 'The influence of high-calcium fly ash on the properties

of fresh and hardened self-compacting concrete and high performance self-compacting concrete', 72, pp. 212–221. Available at: <https://doi.org/10.1016/j.jclepro.2014.02.058>.

Ponikiewski, T. and Katzer, J. (2014) 'Properties of fresh SCC mix reinforced by different types of steel and polymer fibre', *Construction and Building Materials*, 62, pp. 96–101. Available at: <https://doi.org/10.1016/j.conbuildmat.2014.03.037>.

Poveda, E. *et al.* (2017) 'Influence of the fiber content on the compressive low-cycle fatigue behavior of self-compacting SFRC', *International Journal of Fatigue*, 101, pp. 9–17. Available at: <https://doi.org/10.1016/j.ijfatigue.2017.04.005>.

Di Prisco, M., Plizzari, G. and Vandewalle, L. (2009) 'Fibre reinforced concrete: New design perspectives', *Materials and Structures/Materiaux et Constructions*, 42(9), pp. 1261–1281. Available at: <https://doi.org/10.1617/s11527-009-9529-4>.

Prokopski, G. and Langier, B. (2000) 'Effect of water/cement ratio and silica fume addition on the fracture toughness and morphology of fractured surfaces of gravel concretes', *Cement and Concrete Research*, 30(9), pp. 1427–1433. Available at: [https://doi.org/10.1016/S0008-8846\(00\)00332-X](https://doi.org/10.1016/S0008-8846(00)00332-X).

Qiu, L.C. and Han, Y. (2018) '3D Simulation of Self-Compacting Concrete Flow Based on MRT-LBM', *Advances in Materials Science and Engineering*, 2018. Available at: <https://doi.org/10.1155/2018/5436020>.

R. A. Gingold and J. J. Monaghan (1977) 'Smoothed particle hydrodynamics: theory and application to non-spherical stars', *Monthly Notices of the Royal Astronomical Society*, 181(3), pp. 375–389.

Ramachandra Murthy, A. *et al.* (2013a) 'Bilinear tension softening diagrams of concrete mixes corresponding to their size-independent specific fracture energy', *Construction and Building Materials*, 47, pp. 1160–1166. Available at: <https://doi.org/10.1016/j.conbuildmat.2013.06.004>.

Ramachandra Murthy, A. *et al.* (2013b) 'Determination of size-independent specific fracture energy of concrete mixes by two methods', *Cement and Concrete Research*, 50, pp. 19–25. Available at: <https://doi.org/10.1016/j.cemconres.2013.03.015>.

Rambo, D.A.S., Silva, F.D.A. and Toledo Filho, R.D. (2014) 'Effect of steel fiber hybridization on the fracture behavior of self-consolidating concretes', *Cement and Concrete Composites*, 54, pp. 100–109. Available at:

<https://doi.org/10.1016/j.cemconcomp.2014.02.004>.

Ramezaniapour, A.A. *et al.* (2009) 'Influence of various amounts of limestone powder on performance of Portland limestone cement concretes', *Cement and Concrete Composites*, 31(10), pp. 715–720. Available at: <https://doi.org/10.1016/j.cemconcomp.2009.08.003>.

Ramezaniapour, A.A. and Bahrami Jovein, H. (2012) 'Influence of metakaolin as supplementary cementing material on strength and durability of concretes', *Construction and Building Materials*, 30, pp. 470–479. Available at: <https://doi.org/10.1016/j.conbuildmat.2011.12.050>.

Randles, P.W. and Libersky, L.D. (1996) 'Smoothed particle hydrodynamics: Some recent improvements and applications', *Computer Methods in Applied Mechanics and Engineering*, 139(1–4), pp. 375–408. Available at: [https://doi.org/10.1016/S0045-7825\(96\)01090-0](https://doi.org/10.1016/S0045-7825(96)01090-0).

Rao, G.A. (2001) 'Generalization of Abrams' law for cement mortars', *Cement and Concrete Research*, 31(3), pp. 495–502. Available at: [https://doi.org/10.1016/S0008-8846\(00\)00473-7](https://doi.org/10.1016/S0008-8846(00)00473-7).

Repository, I. (2003) 'Development of self-compacting concrete'.

Richardson, A. and Dave, U. V. (2008) 'The effect of polypropylene fibres within concrete with regard to fire performance in structures', *Structural Survey*, 26(5), pp. 435–444. Available at: <https://doi.org/10.1108/02630800810922775>.

RILEM 50FMC (1985) 'Determination of the fracture energy of mortar and concrete by means of three-point bend tests on notched beams"', *Materials and Structures*, 18(106), pp. 285–290. Available at: <https://doi.org/10.1007/BF02498757>.

Roussel, N. (2006) 'A theoretical frame to study stability of fresh concrete', *Materials and Structures/Materiaux et Constructions*, 39(1), pp. 81–91. Available at: <https://doi.org/10.1617/s11527-005-9036-1>.

Roussel, N. *et al.* (2007) 'Computational modeling of concrete flow: General overview', *Cement and Concrete Research*, 37(9), pp. 1298–1307. Available at: <https://doi.org/10.1016/j.cemconres.2007.06.007>.

Roussel, N. (2007) 'Rheology of fresh concrete: From measurements to predictions of casting processes', *Materials and Structures/Materiaux et Constructions*, 40(10), pp. 1001–1012. Available at: <https://doi.org/10.1617/s11527-007-9313-2>.

Roussel, N. (2018) 'Rheological requirements for printable concretes', *Cement and Concrete*

- Research*, 112(January), pp. 76–85. Available at: <https://doi.org/10.1016/j.cemconres.2018.04.005>.
- Roussel, N. and Gram, A. (2014) *Simulation of Fresh Concrete Flow, RILEM State-of-the-Art Reports*. Available at: https://doi.org/10.1007/978-94-017-8884-7_1.
- Şahin, Y. and Köksal, F. (2011) ‘The influences of matrix and steel fibre tensile strengths on the fracture energy of high-strength concrete’, *Construction and Building Materials*, 25(4), pp. 1801–1806. Available at: <https://doi.org/10.1016/j.conbuildmat.2010.11.084>.
- Sahmaran, et al. (2005) ‘Workability of hybrid fiber reinforced self-compacting concrete’, *Building and Environment*, 40(12), pp. 1672–1677.
- Şahmaran, M., Christianto, H.A. and Yaman, I.O. (2006) ‘The effect of chemical admixtures and mineral additives on the properties of self-compacting mortars’, *Cement and Concrete Composites*, 28(5), pp. 432–440. Available at: <https://doi.org/10.1016/j.cemconcomp.2005.12.003>.
- Sahmaran, M. and Yaman, I.O. (2007) ‘Hybrid fiber reinforced self-compacting concrete with a high-volume coarse fly ash’, 21, pp. 150–156. Available at: <https://doi.org/10.1016/j.conbuildmat.2005.06.032>.
- Sahmaran, M., Yurtseven, A. and Ą, I.O.Y. (2005) ‘Workability of hybrid fiber reinforced self-compacting concrete’, 40, pp. 1672–1677. Available at: <https://doi.org/10.1016/j.buildenv.2004.12.014>.
- Sandbakk, S. (2011) ‘Fibre reinforced concrete’, *Angewandte Chemie International Edition*, 6(11), pp. 951–952.
- Sarmiento, E.V. (2015) *Flowable fibre-reinforced concrete for structural applications*.
- Schachinger, I., Schubert, J. and Mazanec, O. (2004) *Effect of mixing and placement methods on fresh and hardened ultra-high performance concrete, Proceedings of the International Symposium on Ultra High Performance Concrete*. Available at: <http://www.upress.uni-kassel.de/katalog/abstract.php?978-3-89958-376-2>.
- Schutter, P.G.D.E. (2005) ‘guidelines for testing fresh Self-Compacting Concrete’, *Concrete* [Preprint], (September).
- Shao, S. and Lo, E.Y.M. (2003) ‘Incompressible SPH method for simulating Newtonian and non-Newtonian flows with a free surface’, *Advances in Water Resources*, 26(7), pp. 787–800.

Available at: [https://doi.org/10.1016/S0309-1708\(03\)00030-7](https://doi.org/10.1016/S0309-1708(03)00030-7).

Sheinn, A.M.M., Ho, D.W.S. and Tam, C.T. (ed.) (2003) *Effect of particle shape on paste rheology of SCC*.

Shi, C., Wu, Z., Lv, K., *et al.* (2015) 'A review on mixture design methods for self-compacting concrete', *Construction and Building Materials*, 84, pp. 387–398. Available at: <https://doi.org/10.1016/j.conbuildmat.2015.03.079>.

Shi, C., Wu, Z., Xiao, J., *et al.* (2015) 'A review on ultra high performance concrete: Part I. Raw materials and mixture design', *Construction and Building Materials*, 101, pp. 741–751. Available at: <https://doi.org/10.1016/j.conbuildmat.2015.10.088>.

Shi, C. and Wu, Y. (2005) 'Mixture proportioning and properties of self-consolidating lightweight concrete containing glass powder', *ACI Materials Journal*, 102(5), pp. 355–363.

Shi, Y., Matsui, I. and Feng, N. (2002) 'Effect of compound mineral powders on workability and rheological property of HPC', *Cement and Concrete Research*, 32(1), pp. 71–78. Available at: [https://doi.org/10.1016/S0008-8846\(01\)00631-7](https://doi.org/10.1016/S0008-8846(01)00631-7).

Shibani, A. *et al.* (2021) 'Investigate the Effect of Ground Granulated Blast Slag on Self Compacting Concrete', *International Journal of Civil Engineering*, 8(12), pp. 13–18. Available at: <https://doi.org/10.14445/23488352/ijce-v8i12p102>.

Siddique, R., Kaur, G. and Kunal (2016) 'Strength and permeation properties of self-compacting concrete containing fly ash and hooked steel fibres', *Construction and Building Materials*, 103, pp. 15–22. Available at: <https://doi.org/10.1016/j.conbuildmat.2015.11.044>.

Siddique, R. and Klaus, J. (2009) 'Influence of metakaolin on the properties of mortar and concrete: A review', *Applied Clay Science*, 43(3–4), pp. 392–400. Available at: <https://doi.org/10.1016/j.clay.2008.11.007>.

Siddiquea, R., Aggarwalb, P. and Aggarwalb, Y. (2012) 'Mechanical and durability properties of self-compacting concrete containing fly ash and bottom ash', *Journal of Sustainable Cement-Based Materials*, 1(3), pp. 67–82. Available at: <https://doi.org/10.1080/21650373.2012.726820>.

da Silva, M.A. *et al.* (2017) 'Rheological and mechanical behavior of High Strength Steel Fiber-River Gravel Self Compacting Concrete', *Construction and Building Materials*, 150, pp. 606–618. Available at: <https://doi.org/10.1016/j.conbuildmat.2017.06.030>.

- Solutions, M.B. (2016) ‘MasterGlenium ACE 474’, (3), pp. 2–5.
- Sonebi, M. and Bartos, P.J.M. (2002) ‘Filling ability and plastic settlement of self-compacting concrete’, *Materials and Structures/Materiaux et Constructions*, 35(8), pp. 462–469. Available at: <https://doi.org/10.1007/bf02483133>.
- Sonebi, M. and Yahia, A. (2020) *Mix design procedure, tests, and standards, Self-Compacting Concrete: Materials, Properties and Applications*. Elsevier Inc. Available at: <https://doi.org/10.1016/b978-0-12-817369-5.00001-5>.
- Spangenberg J, Roussel N, Hattel JH, Thorborg J, Geiker MR, S.H. (2010) ‘Prediction of the impact of flow-induced inhomogeneities in self-compacting concrete (SCC)’, in *In: Khayat KH, Feys D, editors. Proceedings of the 2010 international RILEM symposium on self-compacting concrete. Design, production and placement of self-consolidating concreteeds, Canada*, pp. 209–14.
- Su, N., Hsu, K.C. and Chai, H.W. (2001) ‘A simple mix design method for self-compacting concrete’, *Cement and Concrete Research*, 31(12), pp. 1799–1807. Available at: [https://doi.org/10.1016/S0008-8846\(01\)00566-X](https://doi.org/10.1016/S0008-8846(01)00566-X).
- Sua-iam, G. and Makul, N. (2013) ‘Utilization of limestone powder to improve the properties of self-compacting concrete incorporating high volumes of untreated rice husk ash as fine aggregate’, 38, pp. 455–464. Available at: <https://doi.org/10.1016/j.conbuildmat.2012.08.016>.
- Sun, Z., Voigt, T. and Shah, S.P. (2006) ‘Rheometric and ultrasonic investigations of viscoelastic properties of fresh Portland cement pastes’, *Cement and Concrete Research*, 36(2), pp. 278–287. Available at: <https://doi.org/10.1016/j.cemconres.2005.08.007>.
- Svec, O. (2013) *Flow modelling of steel fibre reinforced self-compacting concrete Simulating fibre orientation and mechanical properties*.
- Švec, O. *et al.* (2011) ‘Flow simulation of fiber reinforced self compacting concrete using Lattice Boltzmann method’, *Proceedings of ICCC*, (8th International Congress on the Chemistry of Cement), pp. 1–7.
- Švec, O. *et al.* (2014) ‘Influence of formwork surface on the orientation of steel fibres within self-compacting concrete and on the mechanical properties of cast structural elements’, *Cement and Concrete Composites*, 50, pp. 60–72. Available at: <https://doi.org/10.1016/j.cemconcomp.2013.12.002>.

- Svermova, L., Sonebi, M. and Bartos, P.J.M. (2003) 'Influence of mix proportions on rheology of cement grouts containing limestone powder', *Cement and Concrete Composites*, 25(7), pp. 737–749. Available at: [https://doi.org/10.1016/S0958-9465\(02\)00115-4](https://doi.org/10.1016/S0958-9465(02)00115-4).
- Takeda, H., Miyama, S.M. and Sekiya, M. (1994) 'Numerical Simulation of Viscous Flow by Smoothed Particle Hydrodynamics', *Progress of Theoretical Physics*, 92(5), pp. 939–960. Available at: <https://doi.org/10.1143/ptp/92.5.939>.
- Tattersall, G.H. (1991) 'Workability and Quality Control of Concrete', (UK: E and FN Spon Ltd).
- Thanh.Ha, Kraus. M, S.K. et al (2015) 'Effect of macro-mesoporous rice husk ash on rheological properties of mortar formulated from self-compacting high performance concrete', *Construction and Building Materials*, 80, pp. 225–235. Available at: <https://doi.org/https://doi.org/10.1016/j.conbuildmat.2015.01.079>.
- Thanh, H.T., Li, J. and Zhang, Y.X. (2020) 'Numerical simulation of self-consolidating engineered cementitious composite flow with the V-funnel and U-box', *Construction and Building Materials*, 236, p. 117467. Available at: <https://doi.org/10.1016/j.conbuildmat.2019.117467>.
- Thrane, L.N. (2007) *Form Filling with Self-Compacting Concrete, (Doctoral dissertation)*.
- Topçu, I.B. and Uygunoğlu, T. (2010) 'Effect of aggregate type on properties of hardened self-consolidating lightweight concrete (SCLC)', *Construction and Building Materials*, 24(7), pp. 1286–1295. Available at: <https://doi.org/10.1016/j.conbuildmat.2009.12.007>.
- Tregger, N. et al. (2012) 'Correlating dynamic segregation of self-consolidating concrete to the slump-flow test', *Construction and Building Materials*, 28(1), pp. 499–505. Available at: <https://doi.org/10.1016/j.conbuildmat.2011.08.052>.
- Tsivilis, S., Voglis, N. and Photou, J. (1999) 'Study on the intergrinding of clinker and limestone', *Minerals Engineering*, 12(7), pp. 837–840. Available at: [https://doi.org/10.1016/S0892-6875\(99\)00068-0](https://doi.org/10.1016/S0892-6875(99)00068-0).
- Vairagade, V.S. and Kene, K.S. (2012) 'Introduction to Steel Fiber Reinforced Concrete on Engineering Performance of Concrete', *International journal of scientific & technology research*, 1(4), pp. 4–6.
- Valcuende, M. et al. (2012) 'Influence of limestone filler and viscosity-modifying admixture

- on the shrinkage of self-compacting concrete’, *Cement and Concrete Research*, 42(4), pp. 583–592. Available at: <https://doi.org/10.1016/j.cemconres.2012.01.001>.
- Vandewalle, L. (1993) ‘Vezelversterkt Beton, Studiedag Speciale Betonsoorten en Toepassingen.pdf’, *Universiteit Leuven, Departement Burgerlijke Bouwkunde*, pp. 77–98.
- Vasilić, K. (2015) *A Numerical Model for Self-Compacting Concrete Flow through Reinforced Sections : a Porous Medium Analogy*, PhD thesis, Berlin, Germany.
- Vesjenjak, M. and Ren, Z. (2007) ‘Application aspects of the meshless SPH method’, *Journal of the Serbian Society for Computational Mechanics*, 1(1), pp. 74–86.
- Vignesh Kumar, V., Venkateswarlu, D. and Naidu, D.A. (2019) ‘Numerical modelling of self-compacting concrete flow’, *International Journal of Engineering and Advanced Technology*, 8(6), pp. 5192–5199. Available at: <https://doi.org/10.35940/ijeat.F95406.088619>.
- Villar, V.P. *et al.* (2019) ‘Assessment of parameters governing the steel fiber alignment in fresh cement-based composites’, *Construction and Building Materials*, 207, pp. 548–562. Available at: <https://doi.org/10.1016/j.conbuildmat.2019.02.036>.
- Vurst, F.V.D. S, Grünewald, S, Feys, D, *et al.* (2017) ‘Effect of the mix design on the robustness of fresh self-compacting concrete’, *Cement and Concrete Composites*, 82, pp. 190–201. Available at: <https://doi.org/http://dx.doi.org/10.1016/j.cemconcomp.2017.06.005>.
- Wallevik, O.H. *et al.* (2015) ‘Avoiding inaccurate interpretations of rheological measurements for cement-based materials’, *Cement and Concrete Research*, 78, pp. 100–109. Available at: <https://doi.org/10.1016/j.cemconres.2015.05.003>.
- Wallevik, O.H. and Wallevik, J.E. (2011) ‘Rheology as a tool in concrete science: The use of rheographs and workability boxes’, *Cement and Concrete Research*, 41(12), pp. 1279–1288. Available at: <https://doi.org/10.1016/j.cemconres.2011.01.009>.
- Wang, R. *et al.* (2017) ‘Influence of rheological properties of cement mortar on steel fiber distribution in UHPC’, *Construction and Building Materials*, 144, pp. 65–73. Available at: <https://doi.org/10.1016/j.conbuildmat.2017.03.173>.
- Wang, Y., Aslani, F. and Liu, Y. (2020) ‘The effect of tensile and bond characteristics of NiTi shape memory alloy, steel and polypropylene fibres on FRSCC beams under three-point flexural test’, *Construction and Building Materials*, 233, p. 117333. Available at: <https://doi.org/10.1016/j.conbuildmat.2019.117333>.

- Wetzstein, M. *et al.* (2005) 'Reports on Progress in Physics Related content Smoothed particle hydrodynamics'. Available at: <https://doi.org/10.1088/0034-4885/68/8/R01>.
- Woolfson, M.M. (2004) 'Smoothed particle hydrodynamics', *The Origin and Evolution of the Solar System* [Preprint]. Available at: <https://doi.org/10.1887/0750304588/b485b3>.
- Wu, Q. and An, X. (2014) 'Development of a mix design method for SCC based on the rheological characteristics of paste', *Construction and Building Materials*, 53, pp. 642–651. Available at: <https://doi.org/10.1016/j.conbuildmat.2013.12.008>.
- Xu, X. *et al.* (2013) 'SPH simulations of three-dimensional non-Newtonian free surface flows', *Computer Methods in Applied Mechanics and Engineering*, 256, pp. 101–116. Available at: <https://doi.org/10.1016/j.cma.2012.12.017>.
- Yahia, A., Tanimura, M. and Shimoyama, Y. (2005) 'Rheological properties of highly flowable mortar containing limestone filler-effect of powder content and W/C ratio', *Cement and Concrete Research*, 35(3), pp. 532–539. Available at: <https://doi.org/10.1016/j.cemconres.2004.05.008>.
- Yazici, H. *et al.* (2010) 'Mechanical properties of reactive powder concrete containing high volumes of ground granulated blast furnace slag', *Cement and Concrete Composites*, 32(8), pp. 639–648. Available at: <https://doi.org/10.1016/j.cemconcomp.2010.07.005>.
- Ye, G. *et al.* (2007) 'Influence of limestone powder used as filler in SCC on hydration and microstructure of cement pastes', *Cement and Concrete Composites*, 29(2), pp. 94–102. Available at: <https://doi.org/10.1016/j.cemconcomp.2006.09.003>.
- Yin, S. *et al.* (2015) 'Use of macro plastic fibres in concrete: A review', *Construction and Building Materials*, 93, pp. 180–188. Available at: <https://doi.org/10.1016/j.conbuildmat.2015.05.105>.
- Yu, R. (2015) *Development of sustainable protective ultra-high performance fibre reinforced concrete (UHPRFC): design, assessment and modeling*.
- Zainali, A. *et al.* (2013) 'Numerical investigation of Newtonian and non-Newtonian multiphase flows using ISPH method', *Computer Methods in Applied Mechanics and Engineering*, 254, pp. 99–113. Available at: <https://doi.org/10.1016/j.cma.2012.10.005>.
- Zak, G., Park, C.B. and Benhabib, B. (2001) 'Estimation of three-dimensional fibre-orientation distribution in short-fibre composites by a two-section method', *Journal of*

Composite Materials, 35(4), pp. 316–339. Available at: <https://doi.org/10.1106/65LQ-1UK7-WJ9H-K2FH>.

Zhao, Z., Kwon, S.H. and Shah, S.P. (2008) ‘Effect of specimen size on fracture energy and softening curve of concrete: Part I. Experiments and fracture energy’, *Cement and Concrete Research*, 38(8–9), pp. 1049–1060. Available at: <https://doi.org/10.1016/j.cemconres.2008.03.017>.

Zhou, G., Ge, W. and Li, J. (2010) ‘Smoothed particles as a non-Newtonian fluid: A case study in Couette flow’, *Chemical Engineering Science*, 65(6), pp. 2258–2262. Available at: <https://doi.org/10.1016/j.ces.2009.12.020>.

Zhu, H. *et al.* (2010) ‘A numerical study of the flow of Bingham-like fluids in two-dimensional vane and cylinder rheometers using a smoothed particle hydrodynamics (SPH) based method’, *Journal of Non-Newtonian Fluid Mechanics*, 165(7–8), pp. 362–375. Available at: <https://doi.org/10.1016/j.jnnfm.2010.01.012>.

Zhu, W. and Gibbs, J.C. (2005) ‘Use of different limestone and chalk powders in self-compacting concrete’, *Cement and Concrete Research*, 35(8), pp. 1457–1462. Available at: <https://doi.org/10.1016/j.cemconres.2004.07.001>.

Zhu, W., Sonebi, M. and Bartos, P.J.M. (2004) ‘Bond and interfacial properties of reinforcement in self-compacting concrete’, *Materials and Structures*, 37(7), pp. 442–448. Available at: <https://doi.org/10.1007/bf02481580>.

Žirgulis, G. (2015) ‘Fibre Orientation in Steel-Fibre- Reinforced Concrete: Quantification methods and influence of formwork surface and reinforcement bars in structural elements’. Available at: <https://ntnuopen.ntnu.no/ntnu-xmlui/handle/11250/2359720>.

Appendix A

Literatures Review of SCC

This study is based on research publications gathered from these previous researchers of SCC (without and with steel fibre) with different sources published from 2010 to 2018, as listed in Table A-1. On the base of different principles and parameters of design mix, the methods of these research are different process in term of properties of flowing, passing, and filling abilities of SCC, without steel fibre and with steel fibre, based on the volume and different type of fibre.

Table A-1:outline of show to usage of SCC in the literatures

Classification	Main features	Title article	Refs.
The results indicate that the flow properties of SCC increase with an increase in the paste volume.	The passing ability as indicated by J-ring improves as the paste content increases. However, an overall assessment from the experimental work has not indicated a clear limiting value of paste, but it could be just above 0.43 for the materials used in this work.	Influence of powder and paste on flow properties of SCC	(Girish, Ranganath and Vengala, 2010)
self-compacting high and ultra-high-performance concretes	It is additionally necessary to check that the mixes meet the passing ability criterion using the J-ring apparatus. Our investigations show that although the mixes with fibres meet the flow-ability criterion and are resistant to segregation, as judged by the slump flow test, they may not meet the passing ability criterion	Development of self-compacting high and ultra-high-performance concretes with and without steel fibres	(Deeb, Ghanbari and Karihaloo, 2012b)

Following

Classification	Main features	Title article	Refs.
Self-compacting ultra-high performance concrete mixes with and without steel fibres (with characteristic cube. strength between 140 and 160 MPa).	The maximum size of the coarse aggregate in all the SCC mixes reported above was 10 mm. This was the same as in the corresponding VC mixes prepared in the same laboratory. The procedure described above for proportioning the SCC mixes can, of course, also be applied if larger size coarse aggregate (say, 20 mm) is used, especially in mixes with compressive strength up to 60 MPa.	Mix proportioning of self-compacting normal and high-strength concretes	(Deeb and Karihaloo, 2013a)
Investigates the production of self-compacting concrete (SCC) more affordable for construction industry with various percentages of fly ash as part of the total powder content and bottom ash as replacement of fine aggregates.	Based on the materials used in this study, the results suggested that it is technically feasible to utilize bottom ash as a part of paste content in the production of SCC. Besides environmental benefits, there could be some technical and economic advantages as well.	Mechanical and durability properties of self-compacting concrete containing fly ash and bottom ash	(Siddiquea, Aggarwalb and Aggarwalb, 2012)
Addition of steel fibers decreases the workability of the SCC	The effect of steel fibers on rheological properties, compressive strength, splitting tensile strength, flexural strength, and flexural toughness of SCC specimens, using four different steel fiber volume fractions (0.5%, 1%, 1.5%, and 2%), were investigated.	Mechanical performance of self-compacting concrete reinforced with steel fibers	(Khaloo et al., 2014)

Following

Classification	Main features	Title article	Refs.
Mechanical Properties of Steel Fibre Reinforced Self-Compacting Concrete	In this research, normal strength steel fibre reinforced self-compacting concrete (SCC Fibre) of grade C30 was produced with the addition of Stahlcon HE 0.55/35 steel fibres at volume fraction of 1% (80 kg/m ³). The effect of the steel fibre addition on the SCC Fibre mix was investigated in terms of its rheological properties (slump flow diameter and time, J-ring) and mechanical properties (compressive strength, splitting tensile strength, flexural strengths and moduli of elasticity).	Effects of Steel Fibre Addition on the Mechanical Properties of Steel Fibre Reinforced Self-Compacting Concrete	(Hazrina et al., 2018)

Table A-2: Summary of mixture design methods for SCC with steel fibre

Categories	Additives	Compressive strength (MPa)	Main findings	Refs.
Strength based mixture design method	With hooked end of steel fibre 0.5% Dosage	20-80	Inclusion of steel fibers in both concretes will marginally decrease the fresh concrete properties and slightly enhance the compressive strength. Split tensile strength of both concretes has increased with significantly by addition of steel fibres compared to plain concrete irrespective of aspect ratio.	(Nitesh, Rao and Kumar, 2019)
Empirical mixture design method	Single and double hooked ends steel fibre at 0.75% and 1% fibre content respectively, Micro-steel fibre at 0.25%, 0.5%, 0.75% and 1% fibre content)	85-97.5	There is no significant increase in the density and compressive strength with steel fibre hybridisation in both conditions.	(Okeh <i>et al.</i> , 2019)
--	Steel fibre	--	The comparison of the hardened concrete specimens' tests have been done at curing age of 7 and 28 days. By adding steel fiber and other reinforced materials in self-compacting concrete with increasing the percentage the flexural, compressive, tensile and split-tensile strength of concrete.	(Gokulnath, Ramesh and Raghuraman, 2019)
Strength based mixture design method	Steel fibre of 0.5% and 1.0% Dosage	75	Additionally, the inclusion of steel fibers in SCC have slightly increased the compressive strength of concrete and changes the failure modes.	(Majain <i>et al.</i> , 2019)

Empirical mixture design method	0.1, 0.3, and 0.5% steel fiber and three aggregate sizes (9.5, 12.5, and 19 mm) were considered in each fiber series	30	Results have shown that in both methods, the largest aggregate size of 12.5 mm can be appropriate for self-compacting steel fiber-reinforced concrete (SCSFRC), although it is more significant in work fracture method.	(Ghasemi, Ghasemi and Mousavi, 2018a)
Empirical mixture design method	Crimped, Indentation Hooked-end, Large-end of steel fibre	---	The relationships of cubic compressive strengths at 7 days and 28 days, and the modulus of elasticity with cubic compressive strength of self-compacting SFRC are similar to VCC.	(Ding <i>et al.</i> , 2018b)
Empirical mixture design method	Steel Fibre of Hooked end $V_f = 0.5\%$	65-85	The addition of steel fibers in the SCC mixtures improves the compressive strength. This increase ranges from 11% to 26% depending on the aspect ratio and type of steel fibers.	(Ghanem and Obeid, 2015)
Empirical mixture design method	Steel fibre volume fractions (0.5%, 1%, 1.5%, and 2%),	40-60	Splitting tensile strength, flexural strength, and flexural toughness are increased by increasing the percentage of fibers; however compressive strength is decreased by increasing the percentage of fibers	(Khaloo <i>et al.</i> , 2014)
Empirical mixture design method	Steel fibre : 0.2, 0.3 and 0.5 volume percent (v%)	65-85	In case of metal fiber-reinforced concrete, increasing the fiber up to 3 v%, initially increased compressive strength to reach a peak value and then decreased	(Morteza H Beigi <i>et al.</i> , 2013)

Table A-3: Influence the plastic viscosity (Pas) and yield stress (Pas) on properties of mixes with and without fibres used in SCC

Reference No.	Type of fibre	Dosage in concrete	Length (mm)	Diameter (mm)	Aspect ratio	Specific gravity	plastic viscosity (Pas)	yield stress (Pas)	Other properties
(Sahmaran, Yurtseven and Ā, 2005)	Steel fibres	60 kg/m ³	6,30	0.16,0.55	37.5,55	7.17,7.85	--	--	SH: straight and hooked end
(Ozyurt, Mason and Shah, 2007)	Steel fibres	1% by volume	6, 40	0.16, 0.62	37.5,64.5	--	7.22	19.48	--
(AbdelAleem and Hassan, 2019)	Steel fibres	30 kg/m ³	25,40,60	0.38, 0.62, 0.92	65	--	--	--	--
(El-Dieb and Reda Taha, 2012)	Steel fibres	0.5–3.0% by volume	8, 13, 30	0.16, 0.5	50, 60, 80	7.85	--	--	SH: straight
(Ponikiewski and Katzer, 2014)	Steel fibres	15–30 kg/m ³	60	0.75	80	7.85	--	--	SH: hooked end
(Morteza H. Beigi <i>et al.</i> , 2013)	Steel fibres	0.2, 0.3, 0.5% by volume	36	0.7	50	7.8	--	--	SH: hooked end
(da Silva <i>et al.</i> , 2017)	--	--	--	--	--	--	104-69-146	237-133-43	SH: hooked end
(da Silva <i>et al.</i> , 2017)	Steel fibres	0.5, 0.75, 1.0% by volume	35	0.55	63.6	--	173-199-270 127-134-197 137-171-214	114-258-326 168-63-226 47-96-310	SH: hooked end
(Gueciouer, Youcef and Tarek, 2019)	--	--	30	0.55	55	7.8	16.21	38.17	SH: hooked end
(Gueciouer, Youcef and Tarek, 2019)	Steel fibres	16, 39 kg/m ³	30	0.55	55	7.8	19.83-8.48-14.67- 7.27-14.61-9.5- 17.39-3.28	48.1-32.91- 34.65-36.43- 54.91-40.15- 44.83-47.61	SH: hooked end
(Deeb, Ghanbari and	Steel fibres	(0.5% and	30	00.55		7.85	42.1 /54.3		SH: hooked end

Karihaloo, 2012a)		2.5% by volume)							
(Abdelrazik and Khayat, 2020)	(macro steel) , polypropylene and steel)	(0.5% and 0.75 % by volume)	--	--	--	--	24/45	23/128	--
(Deeb and Karihaloo, 2013b)	--	--	--	--	--	--	3.1/12.42	--	--
(Badry, Kulasegaram and Karihaloo, 2016)	--	--	--	--	--	--	6.57/10.62	150/200	--
(Abo Dhaheer <i>et al.</i> , 2016b)	--	--	--	--	--	--	4.5/11.5	--	--

Table A-4: Numerical simulations of SCC flow using SPH method

Researcher	Flow problem simulated by SPH
(Zhu et al., 2010)	2D simulation of vane and cylinder rheometers
(Deeb, Kulasegaram and Karihaloo, 2014a)	3D modelling of Slump flow, with or without steel fibers
(Badry, Kulasegaram and Karihaloo, 2016)	3D simulation of slump flow, for four different size of particles
(Deeb, Karihaloo and Kulasegaram, 2014)	3D modeling fiber orientation in slump flow test
(Abo Dhaheer, Kulasegaram and Karihaloo, 2014)	3D modeling of J-ring flow, considering four different size of particles
(Deeb, Kulasegaram and Karihaloo, 2014b)	3D modeling of L-Box test, considering four different size of particles
(Lashkarbolouk et al., 2013)	2D simulation of L-Box test
(Mašín et al., 2006)	2D simulations of slump flow and L-box, with and without presence of fibers
(Alyhya, Kulasegaram and Karihaloo, 2017)	3D simulation of V-funnel test
(Lashkarbolouk, Halabian and Chamani, 2014)	2D simulation of V-funnel test
(Al-Rubaye, Karihaloo and Kulasegaram, 2017)	3D simulation of L-Box test

Appendix B

Typical SCC without and with steel fibre mixes of different strength grades, plastic viscosities and paste/solid ratios designed using the proposed mix design method

Table B-1: Mix constituents (kg/m³) for SCC mixes grade 40

	Mix strength grade: MPa	
	40 MPa	40 MPa
Cement: kg/m ³	262.5	288
GGBS: kg/m ³	87.5	95
Micro-silica (MS): kg/m ³	--	--
Cementitious materials (cement + GGBS or MS): kg/m ³	350	383
Water: kg/m ³	199.5	219
Superplasticiser: kg/m ³	2.5	3.0 (2.5)
Water/cementitious materials ratio	0.57	0.57
Superplasticiser /cementitious materials ratio	0.71	0.78
Limestone powder: kg/m ³	194	130
Fine aggregate (<2 mm)	770	744
FA ^a : kg/m ³	291	200
FA ^b : kg/m ³	479	544
Coarse aggregate: kg/m ³	756	770
Plastic viscosity : P as	5	5
t ₅₀₀ in flow: s	2.03	1.20
Flow spread mm	785	602.5
t ₅₀₀ in J-ring: s	3.00	2.02
Flow, Pass-ability spread (J-ring test): mm	645(16Bars)	600(16Bars)
Blocking step (P_J) < 10 mm	--	9.5
Difference between flow and J-ring spread diameter	140	2.5
t ₂₀₀ in L-box: s	--	0.53
t ₄₀₀ in L-box: s	--	1.27
Levelling-off ratio, H ₂ /H ₁	--	0.93
Compressive strength: MPa	--	40.64
NOTES	Not achieve it	Achieve it

Table B-2: Mix constituents (kg/m³) for SCC mixes grade 50

	Mix strength grade: MPa		
	50 MPa	50 MPa	50 MPa
Cement: kg/m ³	294	303.6	300
GGBS: kg/m ³	98	98	100
Micro-silica (MS): kg/m ³	--	--	--
Cementitious materials (cement + GGBS or MS): kg/m ³	392	401.6	400
Water: kg/m ³	208	208	210
Superplasticiser: kg/m ³	2.9 (3.5)	2.9	2.9
Water/cementitious materials ratio	0.52	0.52	0.52
Superplasticiser /cementitious materials ratio	0.74	0.72	0.72
Limestone powder: kg/m ³	96	86.4	115
Fine aggregate (<2 mm)	749	749	785
FA ^a : kg/m ³	149	149	185
FA ^b : kg/m ³	600	600	600
Coarse aggregate: kg/m ³	859	859	780
Plastic viscosity : P as	7	7	7
t ₅₀₀ in flow: s	2.43	1.50	1.35
Flow spread mm	615	582.5	637.5
t ₅₀₀ in J-ring: s	2.15	3.02	2.59
Flow, Pass-ability spread (J-ring test): mm	612.5(16Bars)	537.5(16Bars)	592.5 (16Bars)
Blocking step (P_J) < 10 mm	9.75	8.25	8.25
Difference between flow and J-ring spread diameter	2.5	45	45
t ₂₀₀ in L-box: s	--	--	--
t ₄₀₀ in L-box: s	--	--	--
Levelling-off ratio, H ₂ /H ₁	--	--	--
Compressive strength: MPa	51.81	49.64	50.45
NOTES	Achieve it	Not achieve it	Achieve it

Table B-3: Mix constituents (kg/m³) for SCC mixes grade 60

	Mix strength grade: MPa		
	60 MPa	60 MPa	60 MPa
Cement: kg/m ³	305	308	314
GGBS: kg/m ³	105	102	105
Micro-silica (MS): kg/m ³	--	--	--
Cementitious materials (cement + GGBS or MS): kg/m ³	410	410	419
Water: kg/m ³	195	194	197
Superplasticiser: kg/m ³	3.0	3.0 (2.7)	2.6
Water/cementitious materials ratio	0.47	0.47	0.47
Superplasticiser /cementitious materials ratio	0.73	0.73	0.62
Limestone powder: kg/m ³	132	92	99
Fine aggregate (<2 mm)	780	777	717
FA ^a : kg/m ³	200	200	167
FA ^b : kg/m ³	580	577	550
Coarse aggregate: kg/m ³	812	823	924
Plastic viscosity : P as	10	9	8.5
t ₅₀₀ in flow: s	697.5	650	717.5
Flow spread mm	2.00	1.09	1.75
t ₅₀₀ in J-ring: s	2.35	1.03	2.55
Flow, Pass-ability spread (J-ring test): mm	715	637.5	695
Blocking step (P_J) < 10 mm	9.25	8	9.25
Difference between flow and J-ring spread diameter	17.5	12.5	22.5
t ₂₀₀ in L-box: s	1.17	--	0.80
t ₄₀₀ in L-box: s	2.30	--	1.70
Levelling-off ratio, H ₂ /H ₁	0.78	--	0.95
Compressive strength: MPa	55.34	53.28	56.32
NOTES	Not Achieve it	Not Achieve it	Not Achieve it

Table B-4: Mix constituents (kg/m³) for SCSFRC mixes grade 40

	Mix strength grade: MPa					
	40 MPa *	40 MPa **	40 MPa ***	40 MPa ****	40 MPa ****	40 MPa ****
Cement: kg/m ³	370	368	368	270	270	270
GGBS: kg/m ³	--	--	--	90	90	90
Cementitious materials (cement + GGBS): kg/m ³	370	368	368	360	360	360
Water: kg/m ³	211	210	210	205	205	205
Superplasticiser: kg/m ³	3.7	2.4	2.4	2.3	2.3	2.3
Water/cementitious materials ratio	0.57	0.57	0.57	0.57	0.57	0.57
Superplasticiser /cementitious materials ratio	1.00	0.65	0.65	0.64	0.64	0.64
Limestone powder: kg/m ³	151	149	137	143	143	143
steel fibre volume (SF) (0.5%): kg/m ³	47	42	40	40	40	40
steel fibre volume (SF) (1.0%): kg/m ³	--	--	--	--	--	--
Fine aggregate (<2 mm)	751	735	742	740	740	740
FA ^a : kg/m ³	375.5	235	242	240	240	240
FA ^b : kg/m ³	375.5	500	500	500	500	500
Coarse aggregate: kg/m ³	908	833	842	839	839	839
Coarse aggregate (10 mm): kg/m ³	454 (50%)	416.5 (50%)	421 (50%)	419.5 (50%)	839 (100%)	419.5 (50%)
Coarse aggregate (20 mm): kg/m ³	454 (50%)	416.5 (50%)	421 (50%)	419.5 (50%)	-- (0%)	419.5 (50%)
Plastic viscosity: P as	27	27	27	27	27	27
t ₅₀₀ in flow: s	642.5	1.13	0.96	1.74	1.40	2.27
Flow spread mm	1.46	620	645	630	600	635
t ₅₀₀ in J-ring: s	552.5	2.50	2.10	1.98	2.20	2.54
Flow, Pass-ability spread (J-ring test): mm	2.98	580 (16 Bars)	625 (16 Bars)	625 (16 Bars)	600 (12Bars)	615 (12 Bars)
Blocking step (P_f) < 10 mm	12	22.75	17	11	9.75	7.75
Difference between flow and J-ring spread diameter	90	40	20	5	0	20
t ₂₀₀ in L-box: s	--	0.92	0.87	--	0.90	0.93
t ₄₀₀ in L-box: s	--	1.91	1.96	--	1.93	1.90
Levelling-off ratio, H ₂ /H ₁	--	0.92 (three bars)	0.87 (three bars)	--	0.94 (two bars)	0.97 (two bars)
Compressive strength: MPa	--	--	--	--	39.51	41.93
NOTES	Not achieve it	Not achieve it	Not achieve it	Not achieve it	achieve it	achieve it

Appendix C

Typical SCC Fresh (Flowing, Passing and filling ability) without and with steel fibre mixes of different strength grades.



Figure C-1:Flowing and passing ability of SCC mix: C30

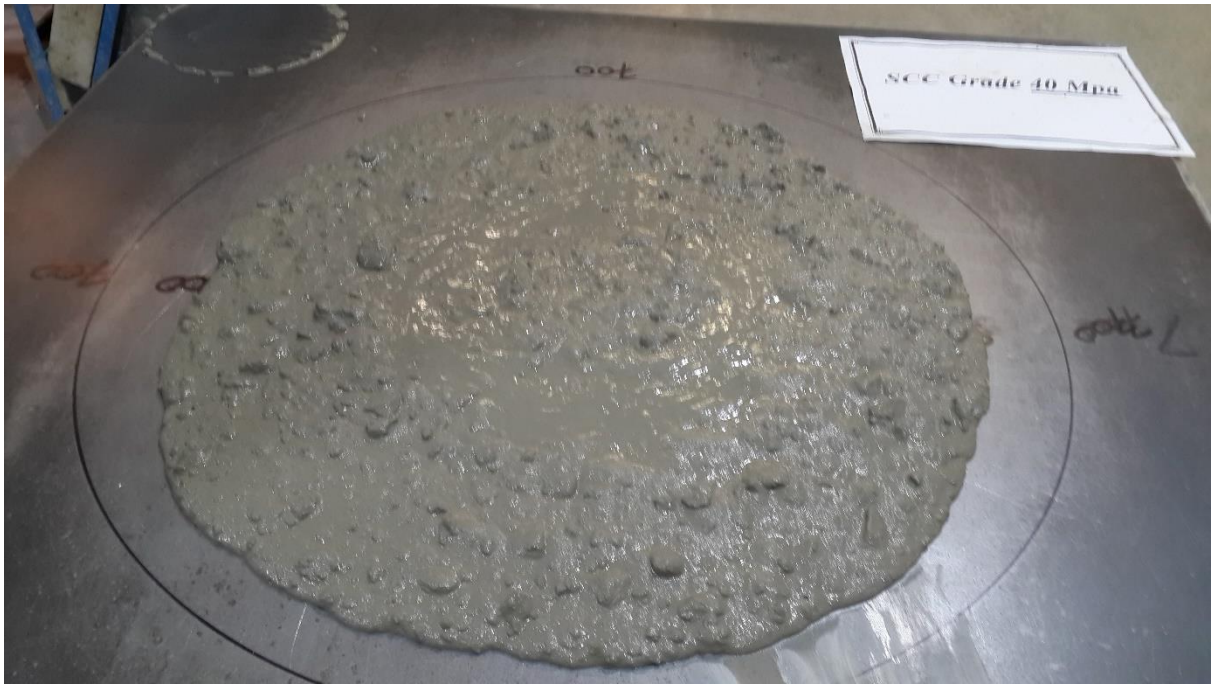


Figure C-2:Flowing and passing ability of SCC mix: C40

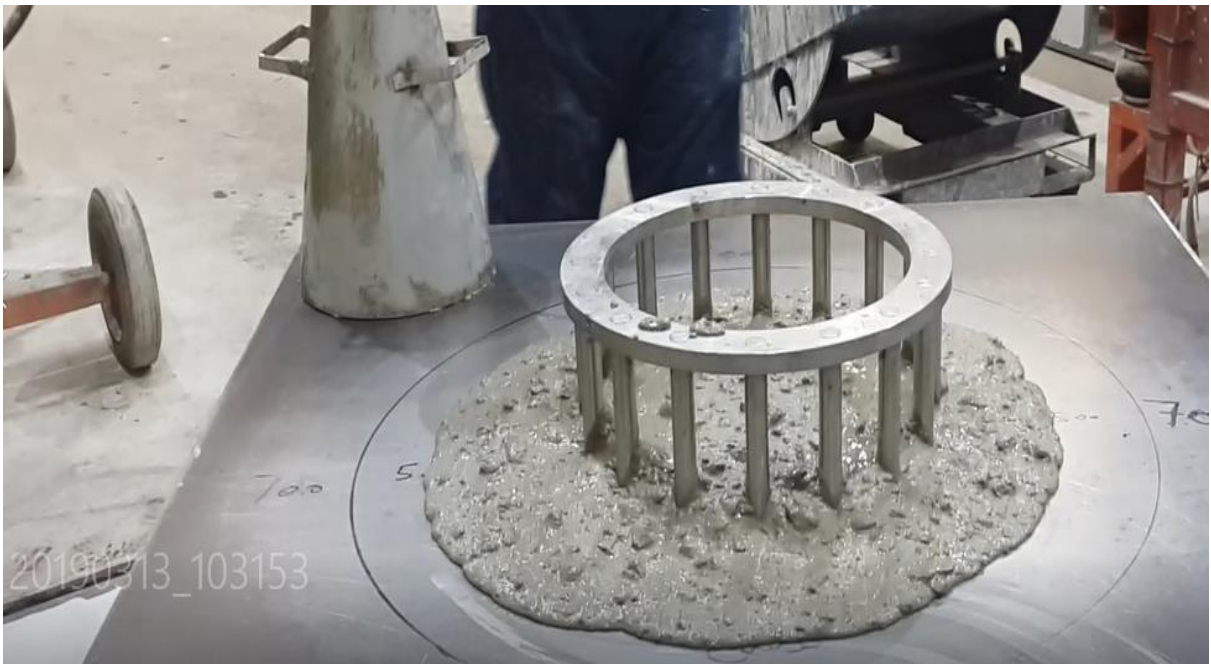


Figure C-3:Flowing and passing ability of SCC mix: C50



Figure C-4:Flowing and passing ability of SCC mix: C60



Figure C-5: Flowing ability of SCC mix: C70

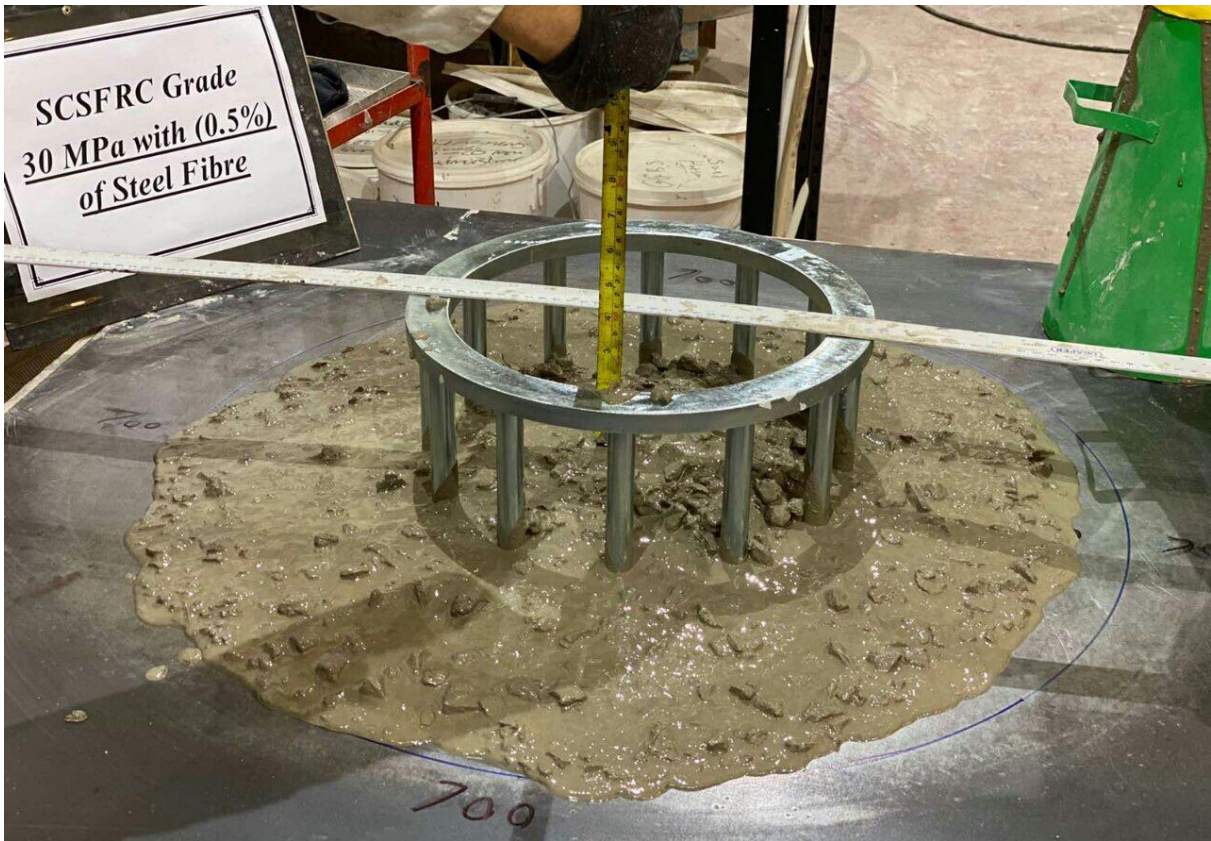


Figure C-6: Flowing and passing ability of SCSFRC mix: C30



Figure C-7: Flowing , passing and filling ability of SCSFRC mix: C40





Figure C-8: Flowing , passing and filling ability of SCSFRC mix: C40





Figure C-9:Flowing and passing ability of SCSFRC mix: C40



Figure C-10:Flowing and passing ability of SCSFRC mix: C40 *



Figure C-11: Flowing and passing ability of SCSFRC mix: C50





Figure C-12:Flowing and passing ability of SCSFRC mix: C60





Figure C-13:Flowing and passing ability of SCSFRC mix: C70

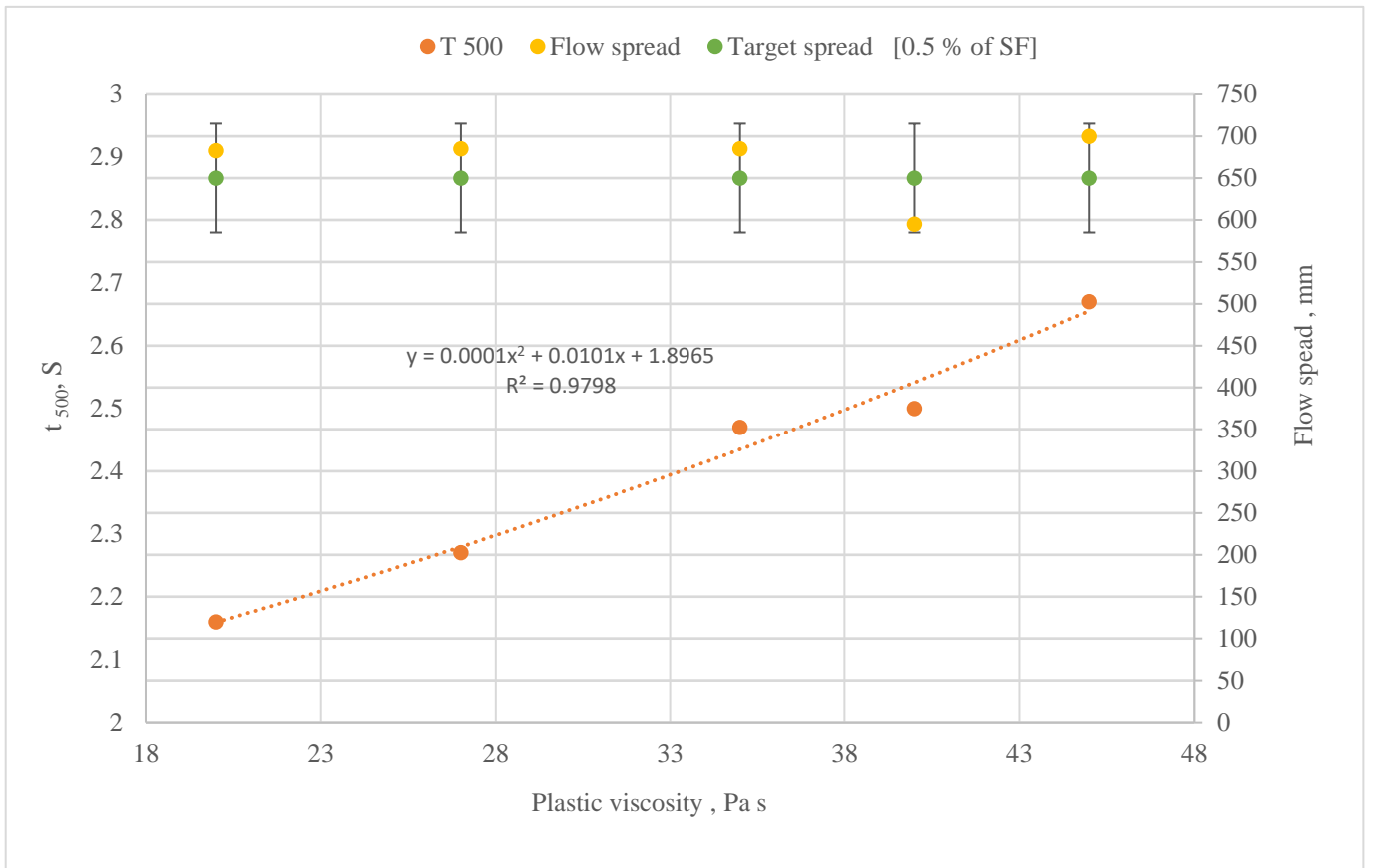


Figure C-14: Relationship between Plastic viscosity flow times (t_{500}) for target flow spread 650 \pm 50 mm [C30, C40, C50, C60 and C70].

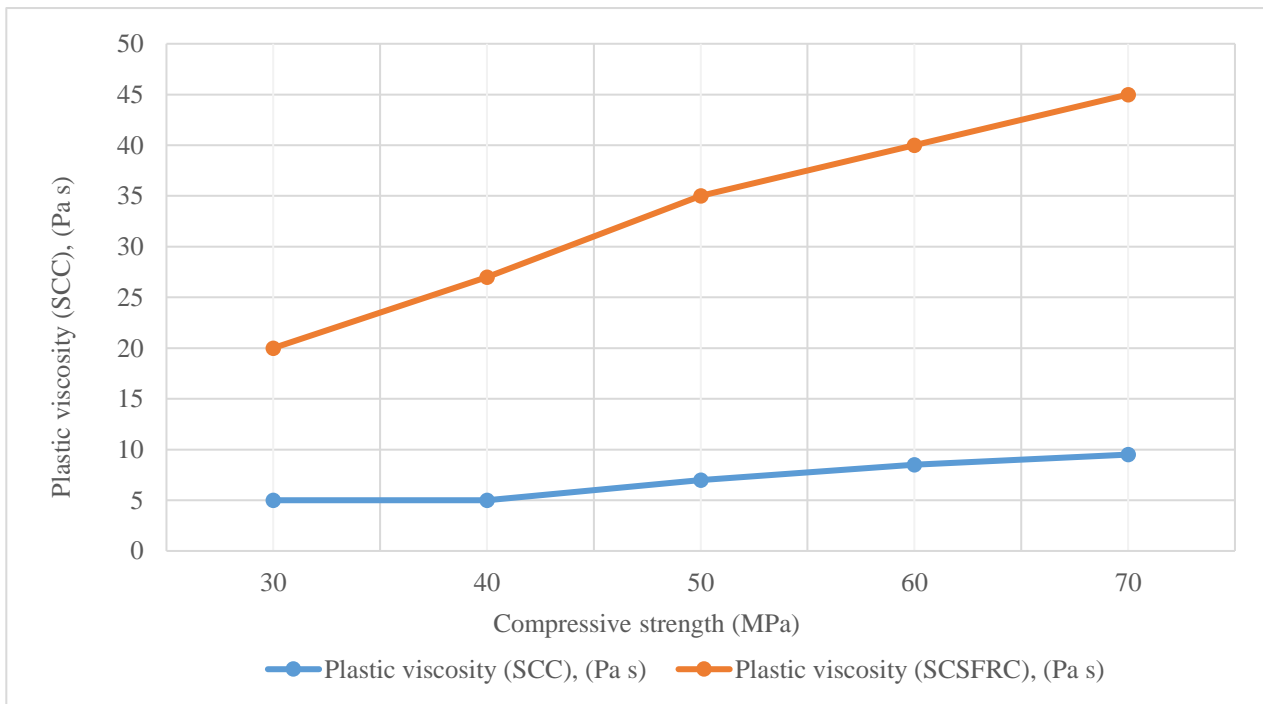


Figure C-15: Plastic viscosity in SCC and SCSFRC concrete mixes

Appendix D

Assessment of the distribution of steel fibre during the fresh and hardened of self-compacting concrete mixes

- Estimation of the distribution of Steel fibre in the flow test



Figure D-1:Hardened of SCSFRC in the flow test

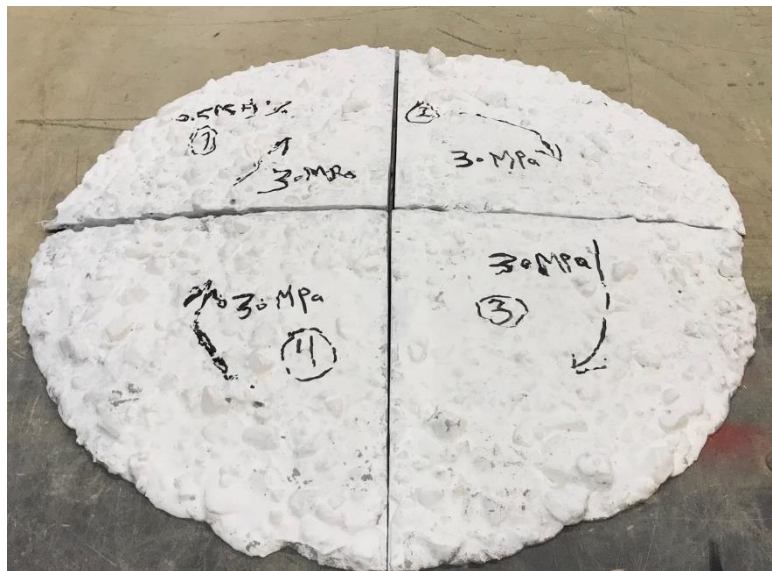


Figure D-2:Cut the hardened of SCSFRC in the flow test



Figure D-3:Section of Cut the hardened of SCSFRC in the flow test

- **Estimation of the distribution of Steel fibre in the beam of fracture test**

The steel fibre must be homogeneously distributed in the SCSFRC mixes, because a non-homogenous distribution through transport or placement can have an adverse influence on the characteristics of hardened concrete. Nevertheless, tracking the steel fibre particles inside hardened structure of SCSFRC is big challenge and difficult to achieve it. An idea was implemented in this paper to track the movement of steel fibre (the 30 mm long, 0.55 mm diameter) during the hardened concrete (see below in Figure D-4).



Figure D-4:Color-coded steel fibre; (the 30 mm long, 0.55 mm diameter)

In order to be able to show the random distribution of steel fibre in the structure beam of fracture test utilizing beam sample with size 500 * 100 * 100 mm³ (Figure D-5) in the cut section of the cured test beam of fracture, the steel fibre in one test mix were color coded with non-toxic non-water-soluble paints but it is not succeeded while that will be able to account random distribution of steel fibre of the cut section as is given in Figure D-6 (A-B-C).

Colored fibres steel fibre was used in the test mix 30MPa with 0.5% of steel fibre. The beam of fracture was hardened in water for 7 days, after which it was cut along one perpendicular section with a diamond saw (Figure D-6-A) and the number of steel fibre was counted (Table D-1). From the cut sections, it was evident that the steel fibre was evenly distributed in beam; the particles were suspended in the paste but had some paste in top without suspend aggregate and steel fibre (Figure D-6-B-C).

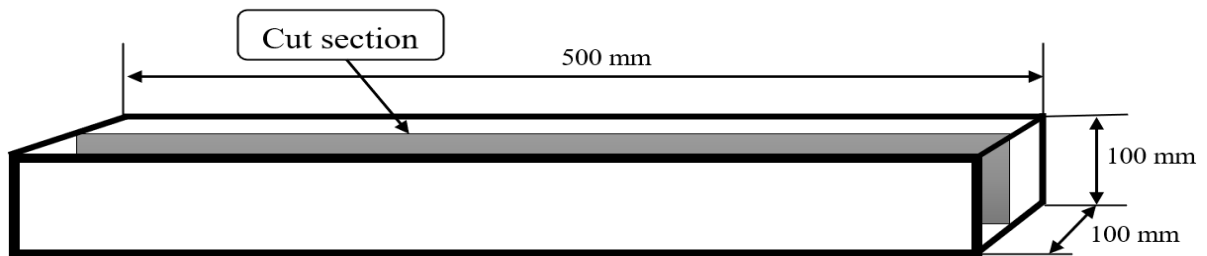
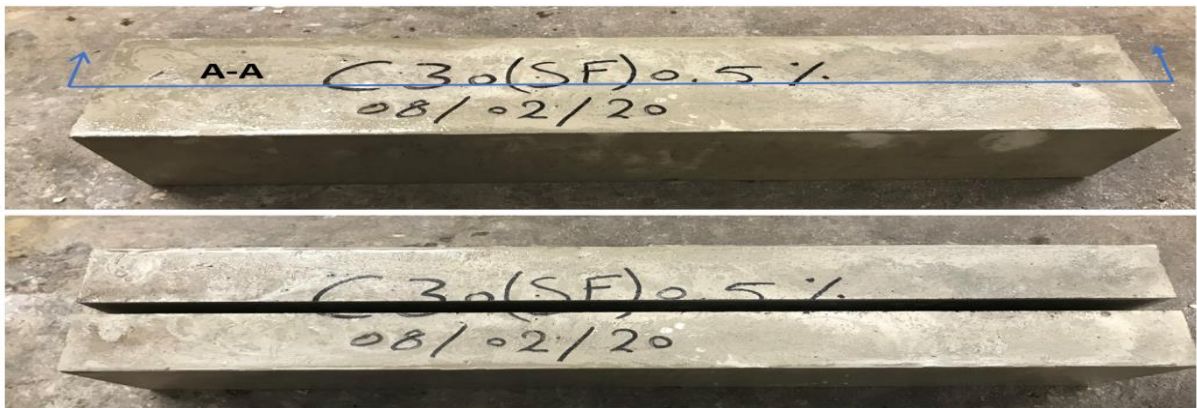


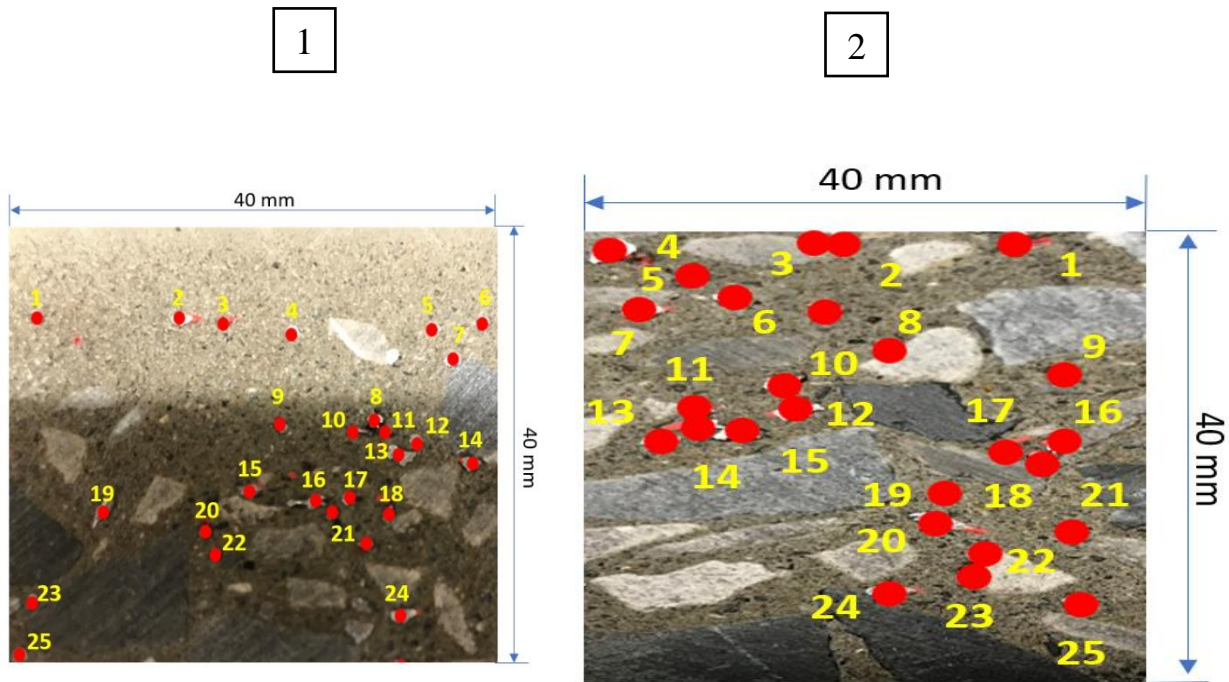
Figure D-5:Dimensions of specimen of the cast



(A)



(B)



(C)

Figure D-6:(a) Beam of fracture test in section (A-A). (b) One longitudinal sections of hardened slab with mix 30 MPa of SF (0.5%). (c) Red colour of account and distribution of the steel fibre clearly visible in the cut surface in two parts

It can be seen from Figure D-6 (C) that the number of fibres lying in the cut section surface. For a random distribution of steel fibres in an amount, the number of fibres lying in section of a certain zone or cut by it can be calculated accurately utilizing the theory of geometric probability, or more precisely from the solution of the so-called Buffon problem (H. Solomon, 1978)(Crofton, 1885). The solution is.

$$1- l \frac{E(h)}{E(c)} = 4 \frac{\sum \text{volumes}}{\sum \text{surface areas}}$$

The solution is obtained by dividing the volume of the cone into smaller cells larger in size than the longest ingredient in the SCC mix (i.e., the 30 mm steel fibre), say 40 mm cubes and then calculating the number of fibres of equal length that either fall into interior of the cells or are cut by one of its surfaces.

For Mix 30 MPa containing 0.5% volume fraction of 30mm long steel fibres with 0.55mm diameter, the total number of fibres in the volume of truncated beam $N_f = \frac{V_c}{V_f} * 0.5 \% =$

$\frac{5,000,000}{7.127} * 0.5 \% = 3508$. By dividing the cone volume into 40 mm cubical cells (there are nearly 78 such cells in the cone) we have from (5) that $\frac{E(h)}{E(c)} = \frac{200}{225}$.

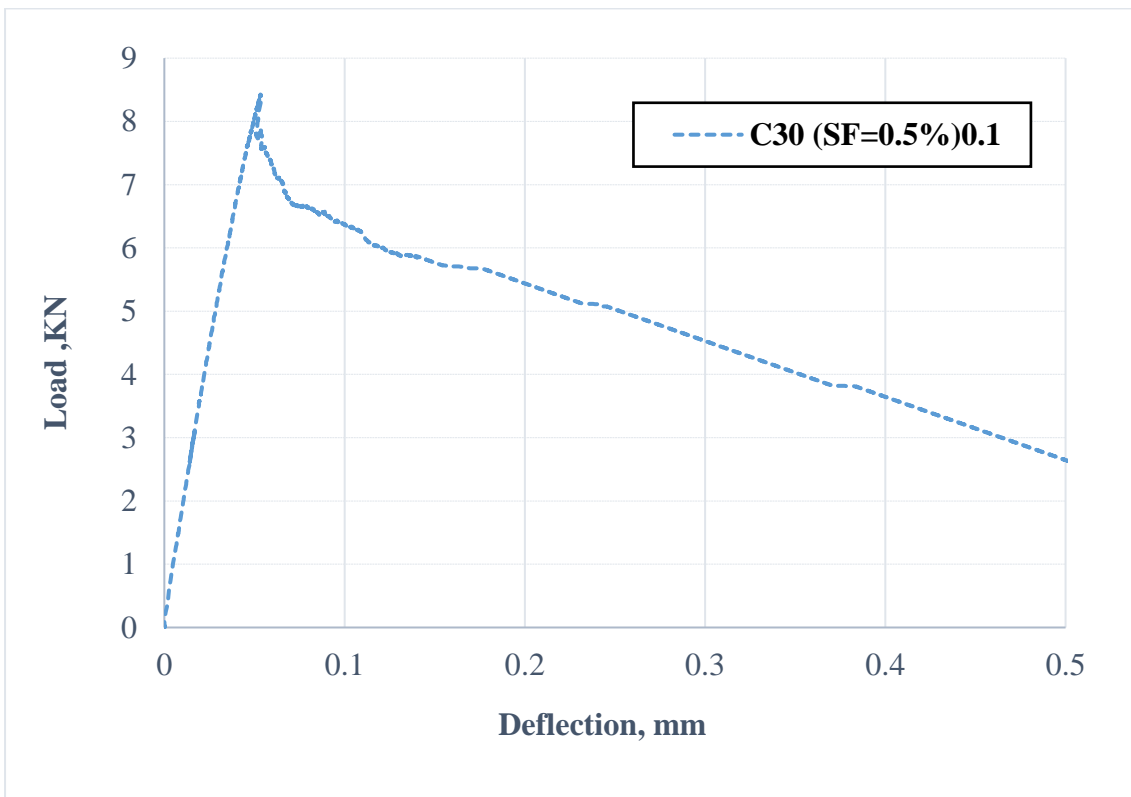
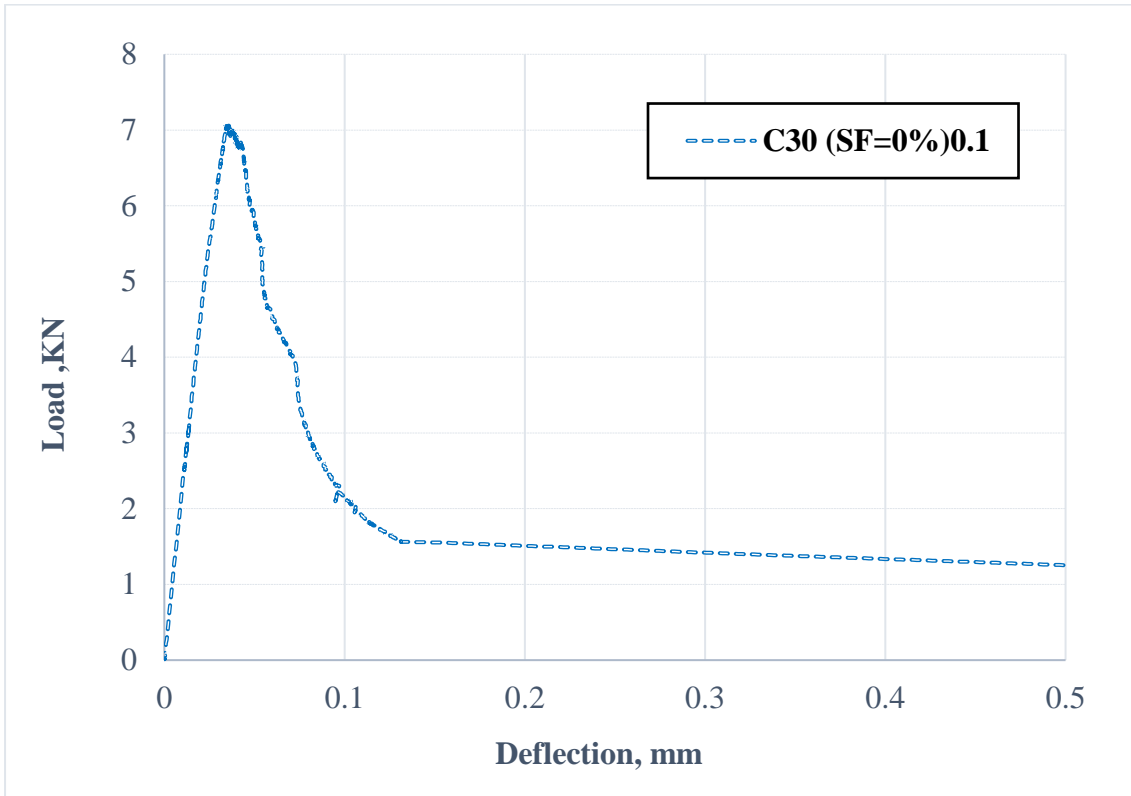
The total number of fibres in the interior of each cell or cut by one of its surfaces is $E(h) + E(c) = \frac{V_{\text{cube}}}{V_f} * 0.5 \% = \frac{40*40*40}{7.127} * 0.5 \% = 45$, whence it follows that the number of fibres cut by a 40×40 mm² side of the cube is $E(c) = 24$. The diametrical vertical section of the slump cone at the start of the test Figure D-6 (C) has a surface area equal to 45,000mm², thus that the total number of fibres cut by this section is $\frac{24}{40*40} * 45000 = 675$ out of a total of 3508. Though, as only 24 fibres represent the number of fibres section cut (1) in the Laboratory experiment (Table D-1). The differences between the theoretical and experimental numbers are because of the small volume and it cannot be seen the fibre distribution in the Laboratory experiment. since some of the defect in the SCSFRC mix is suppressed to take the degrees of freedom, it happens during mixer and casting of SCSFRC mix.

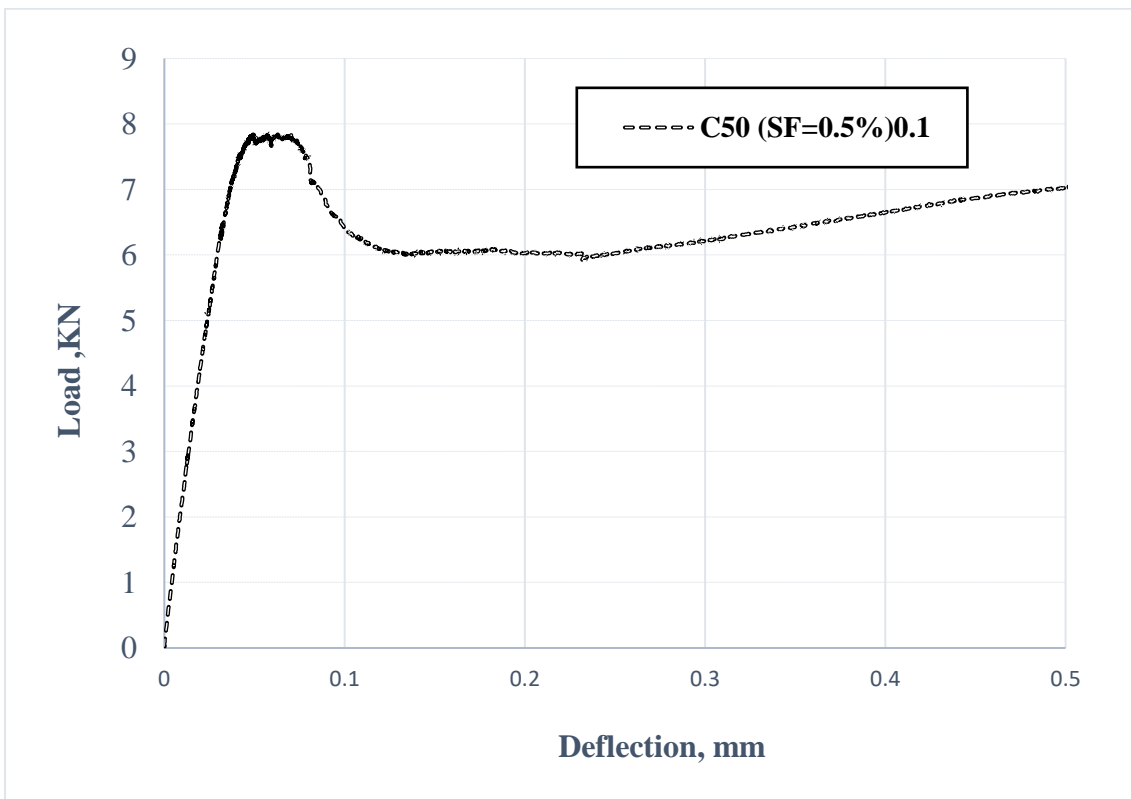
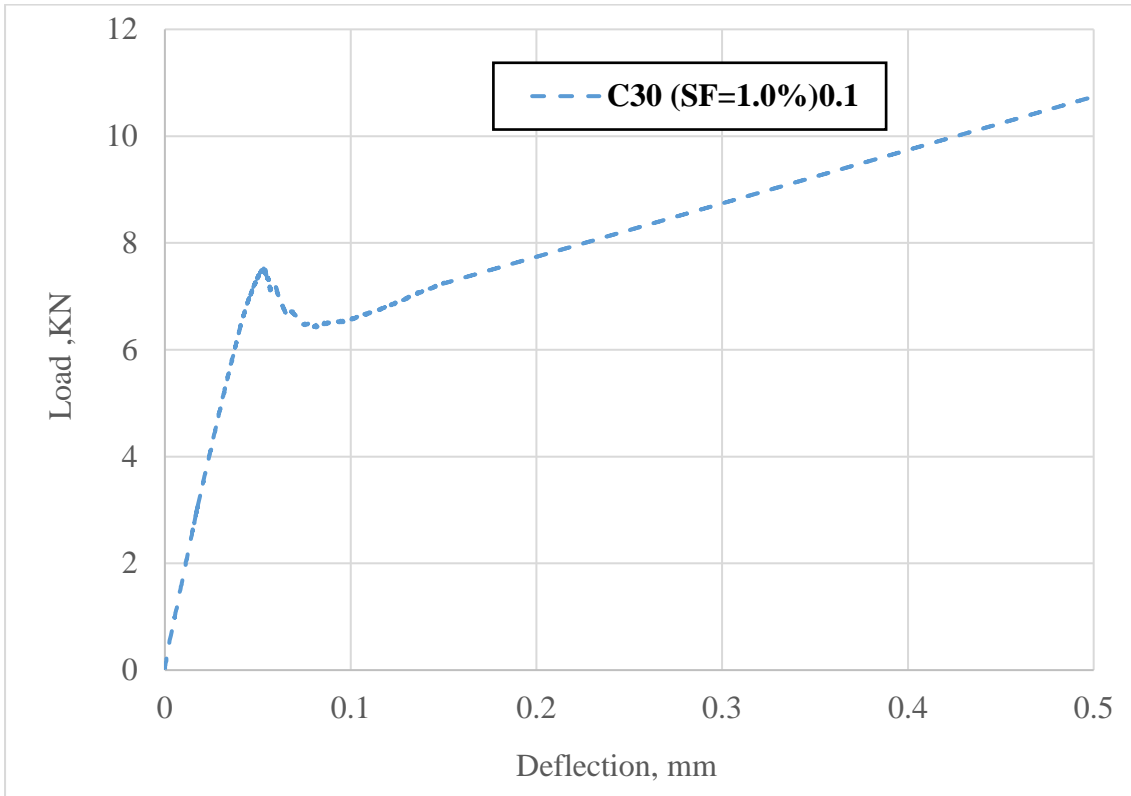
Table D-1: Number of fibres in a vertical cross-section of 30 MPa (0.5 % of SF) based on the Lab experiment and Buffon problem

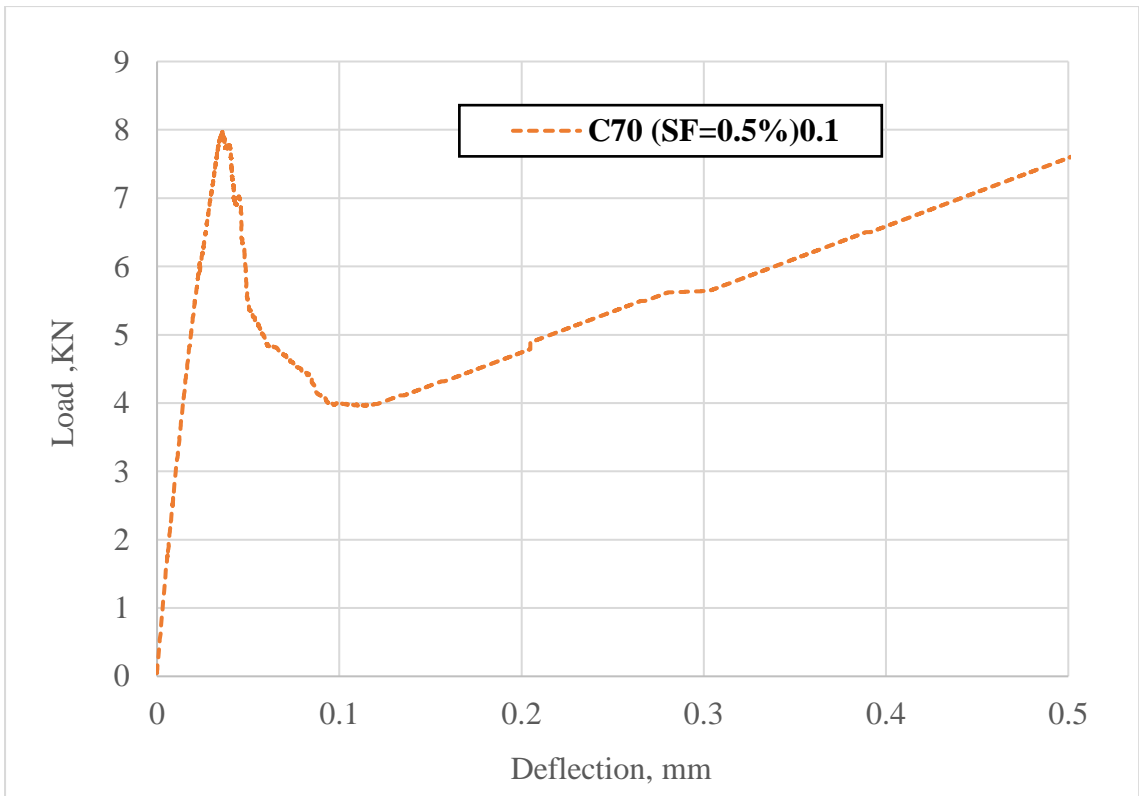
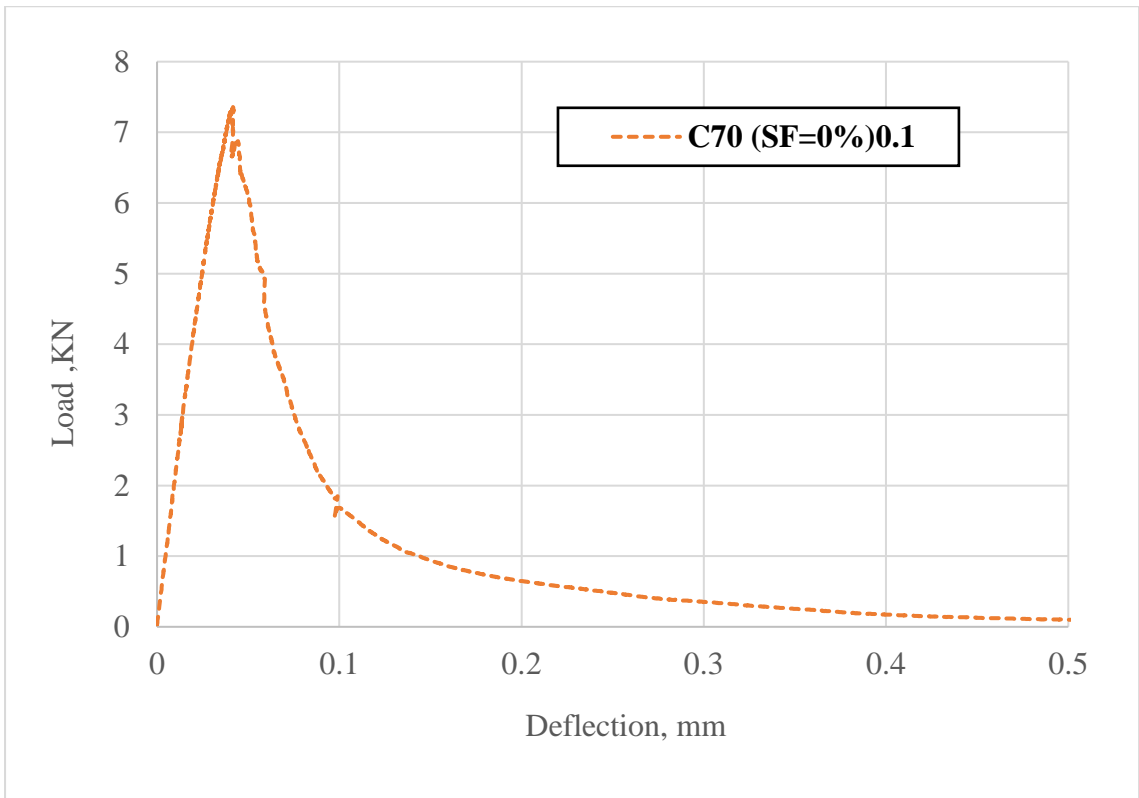
NO.	Design Mix	No. of fibres in the Lab	No. of fibres based on Buffon problem
1	30 MPa (0.5 % of SF)	25	24
2		25	24

Appendix E

Experimental load-deflection diagrams for shallow notched specimens of SCC and SCSFRC subjected to TPB test.







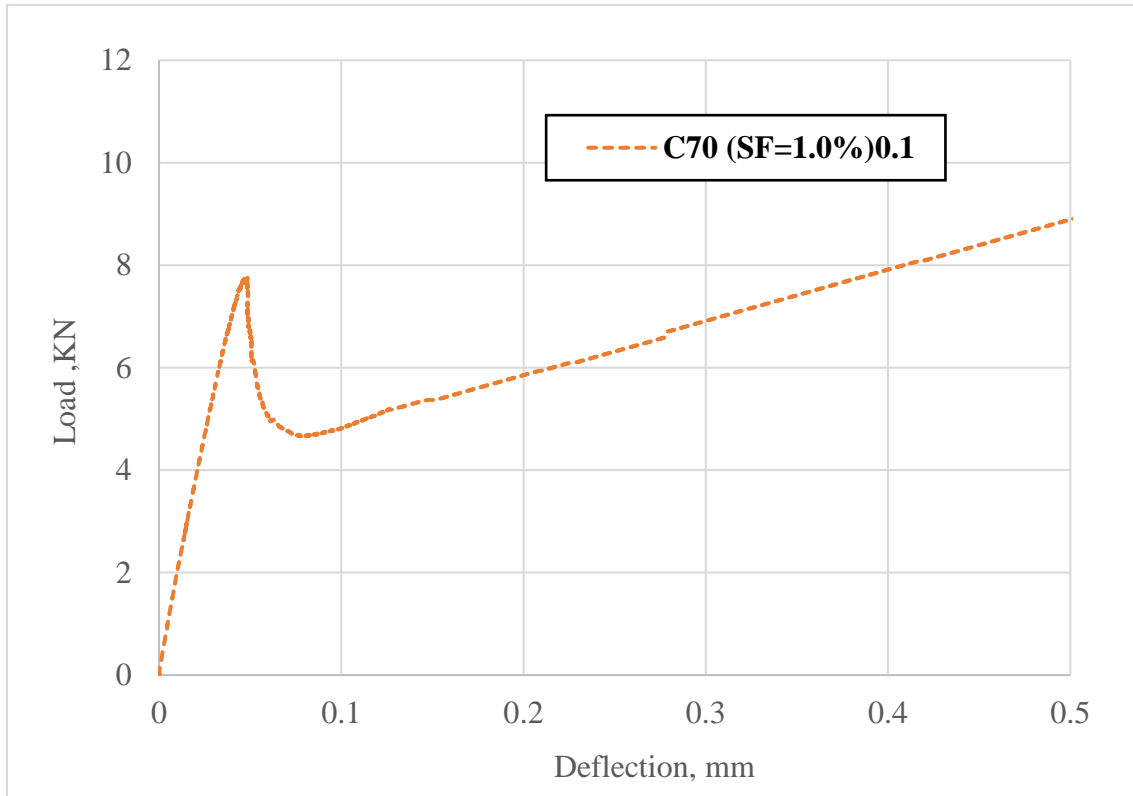


Figure E-1: Typical load–displacement diagrams of one notched beam (0.1 mm) from SCC mixes without and with steel fibre

Appendix F

Training and Development

The list below (Table F-1) the Research Skills training courses/events (e.g., conferences/seminars) that you have attended during the PhD research.

Table F-1: Training courses

Completed Courses	Source of Training
Technical Writing	School of Engineering
PGR student Induction	School of Engineering
Library sessions 1, 2	School of Engineering
PhD in Three	School of Engineering
Research Methods 3	School of Engineering
Project Management	School of Engineering
Research Methods 2	School of Engineering
Excel: Using Graphs and Charts to Present Your Data, Microsoft	Doctoral Academy
MATLAB: An Introduction	Doctoral Academy
ARC: An Introduction to Parallel Programming using OpenMP	Doctoral Academy
Mendeley: An Introduction	Doctoral Academy
ARC: An Introduction to Linux with Command Line (& Windows 101)	Doctoral Academy
ARC: Advanced Research Computing at Cardiff University	Doctoral Academy
EndNote: Further Techniques for Managing your References	Doctoral Academy
Inkscape for Easy Illustrations	Doctoral Academy
Starting Out: Induction Event for New Research Students	Doctoral Academy
Word: Working with Long Documents, Microsoft	Doctoral Academy
ARC: Supercomputing for Beginners	Doctoral Academy
What Next? Career Planning for PhD Students - (Sciences)	Doctoral Academy
Seven Secrets of Highly Successful Researchers	Doctoral Academy
The Second Year: Making Effective Progress	Doctoral Academy
Improving your Interaction with Others	Doctoral Academy
Planning and Writing Your Thesis (Sciences)	Doctoral Academy
Managing Stress in the PhD	Doctoral Academy
Finishing Your PhD	Doctoral Academy
PGR Festival – Day 6: The High Potential Researcher - Nutritional Workshop: Increase Energy	Doctoral Academy
Application Forms: Making your Answers Count	Doctoral Academy
How to use the Research Professional Funding Database	Doctoral Academy
Researching Companies and Industries In The Private Sector	Doctoral Academy
Overcoming Perfectionism	Doctoral Academy
Practical Project Management for Your Research	Doctoral Academy
Managing Research Data: Key Aspects of Legal Compliance and Record Management	Doctoral Academy
Turbocharge Your Writing	Doctoral Academy
English for Research Writing (Non-native Speakers)	Doctoral Academy
Examination and the Viva (Sciences)	Doctoral Academy
Run Your Own Conference	Doctoral Academy

Completed Courses	Source of Training
Lecturing Skills	Doctoral Academy
Writing and Publishing Your Research (Sciences)	Doctoral Academy
PowerPoint: Enhancing Your Presentation, Microsoft	Doctoral Academy
Practise your Presentation Skills	Doctoral Academy
Enhance Academic Writing in Your PhD Thesis	Doctoral Academy
Writing a Literature Review in the Sciences	Doctoral Academy
Assessing Student Learning in the Sciences	Doctoral Academy
Public Speaking for Researchers	Doctoral Academy
Be a Better Writer (Sciences)	Doctoral Academy
Using Technology to Teach	Doctoral Academy
Abstracts: How to Write them in the Sciences	Doctoral Academy
Demonstrating/Laboratory Based Teaching in the Sciences	Doctoral Academy
Qualitative Interviewing (Module 2)	External Training
On the Job: Securing a First Academic Post (Module 3)	External Training
Preparing Impactful Research Proposals & Grant Applications (Module 3)	External Training
Academic Publishing (Module 1)	External Training
Preparing & Delivering Lectures (Module 4)	External Training
Writing & Structuring an Effective Thesis (Module 1)	External Training
Assessment, Feedback, & Module Design (Module 4)	External Training
Preparing for your Viva (Module 3)	External Training
What Should a Literature Review Do? (Module 1)	External Training
Preparing & Delivering Seminars (Module 4)	External Training
How to Develop a Professional and Engaging Online Profile	Doctoral Academy
Imposter Syndrome: Why Successful People Often Feel Like Frauds	Doctoral Academy
Academic Writing: Reduce Anxiety	Doctoral Academy
Seven Secrets of Highly Successful Researchers	Doctoral Academy
Mindfulness: An Introduction	Doctoral Academy
Project Management for Researchers	Doctoral Academy
IEEE Authorship and Open Access Symposium: Best Practices to Get Published to Increase the Exposure and Impact of Your Research	External Training

Thesis output

The thesis concludes with an alphabetical list of references to the works in the literature, cited in the text, and several appendices. Some of the work described in this thesis has been published or is in the process of publication and has been presented at conferences. For easy reference, these publications are listed below:

- 1- **Mimoun, A.** Kulasegaram, S. and Davies, R. 2019. Development of self-compacting concrete mixes based on target plastic viscosity and compressive strength, In 11th ENGIN Postgraduate Conference, Gregynog, Cardiff, UK., 19-21 June 2019.
- 2- Kulasegaram, S. and **Mimoun, A.** 2019. An efficient computational procedure for modelling the flow of fibre suspended self-compacting concrete. Presented at: PARTICLES 2019, *Proceedings of VI International Conference on Particle-Based Methods. Fundamentals and Applications*, Barcelona, Spain., 28-30 October 2019. <https://orca.cardiff.ac.uk/id/eprint/128072>.
- 3- **Mimoun, A.** Kulasegaram, S. and Davies, R., 2020. Design of self-compacting concrete mixes with steel fibre based on target plastic viscosity and compressive strength, In 74th RILEM Annual Week and 40th Cement and Concrete Science Conference, Online, University of Sheffield, UK., 31 August - 4 September 2020. <https://orca.cardiff.ac.uk/id/eprint/149222>.
- 4- Kulasegaram, S. and **Mimoun, A.** 2021. A smoothed particle hydrodynamics study on modelling the flowability, pass-ability and fill-ability of steel fibre suspended self-compacting concrete. Presented at: PARTICLES 2021, *Proceedings of VI International Conference on Particle-Based Methods. Fundamentals and Applications*, Online, Hamburg, Germany, 4-6 October 2021. <https://orca.cardiff.ac.uk/id/eprint/145212>
- 5- **Mimoun, A.** Kulasegaram, S. and Davies, R., 2021. Development of Self-compacting steel fibre reinforced concrete mixes based on target plastic viscosity and compressive strength, In Speaking of Science Conference, Online, University of Cardiff, UK., 17 – 21 May 2021.

- 6- **Mimoun, A.** Kulasegaram, S. 2021. Design of self-compacting concrete mixes with steel fibre based on target plastic viscosity and compressive strength, In:11th ENGIN Postgraduate Conference, Gregynog Online 2021, Cardiff, UK. 11 June 2021.
- 7- **Mimoun, A.** and Kulasegaram, S., 2022. Plastic-viscosity based mix design and the effect of limestone powder on material performance of self-compacting concrete, *Proceedings of the ICE-Construction Materials*. <https://doi.org/10.1680/jcoma.21.00038>.
- 8- **Mimoun, A.** and Kulasegaram, S. 2022. Developing self-compacting steel fibre reinforced concrete (SCSFRC) mixes based on target plastic viscosity and compressive strength. Presented at: CSEE'22, *Proceedings of the 7h World Congress on Civil, Structural, and Environmental Engineering*, Online, Lisbon, Portugal – April 10 – 12, 2022. https://avestia.com/CSEE2022_Proceedings/files/paper/ICSECT/ICSECT_177.pdf
- 9- **Mimoun, A.** Kulasegaram, S. 2022. Simulation of self-compacting steel fibre reinforced concrete using an enhanced SPH methodology. Presented at: EURO-C 2022, *Proceedings of Computational Modelling of Concrete and Concrete Structures*, Vienna, Austria. May 23-26, 2022.
- 10- **Mimoun, A.** and Kulasegaram, S. 2022. Assessing the Effect of Coarse Aggregate Size on Self-Compacting Fibre Reinforced Concrete Mix, *International Journal of Civil Infrastructure (IJCI)*. <https://ijci.avestia.com/2022/inprogress/010.html>.

Scientific lectures

- The PhD position included academic years (2019/2020) and (2020/2021) of teaching assistance support at the Department of Civil Engineering.
- All courses and skills were undertaken during this PhD project that started in October 2018 until the thesis was submitted in March 2023 (Appendix F).